

**AFRL-VA-WP-TR-2000-3024**

**EQUIVALENT INITIAL FLAW SIZE  
TESTING AND ANALYSIS**



**SCOTT A. FAWAZ**

**AIR VEHICLES DIRECTORATE  
2790 D STREET, STE 504  
AIR FORCE RESEARCH LABORATORY  
WRIGHT-PATTERSON AFB, OH 45433-7542**

**JUNE 2000**

**FINAL REPORT FOR 10/01/1997 – 06/15/2000**

**APPROVED FOR PUBLIC RELEASE; DISTRIBUTION UNLIMITED**

**AIR VEHICLES DIRECTORATE  
AIR FORCE RESEARCH LABORATORY  
AIR FORCE MATERIEL COMMAND  
WRIGHT-PATTERSON AIR FORCE BASE OH 45433-7542**

## REPORT DOCUMENTATION PAGE

<b>1. REPORT DATE (DD-MM-YYYY)</b> 01-06-2000	<b>2. REPORT TYPE</b> Final Report	<b>3. DATES COVERED (FROM - TO)</b> 01-10-1997 to 15-06-2000
<b>4. TITLE AND SUBTITLE</b> Equivalent Initial Flaw Size Testing and Analysis  Unclassified		<b>5a. CONTRACT NUMBER</b>
		<b>5b. GRANT NUMBER</b>
		<b>5c. PROGRAM ELEMENT NUMBER</b>
<b>6. AUTHOR(S)</b> Fawaz, Scott A. ;		<b>5d. PROJECT NUMBER</b>
		<b>5e. TASK NUMBER</b>
		<b>5f. WORK UNIT NUMBER</b>
<b>7. PERFORMING ORGANIZATION NAME AND ADDRESS</b> Air Vehicles Directorate 2790 D. Street, Ste. 504 Air Force Research Laboratory Wright-Patterson AFB , OH 45433-7542		<b>8. PERFORMING ORGANIZATION REPORT NUMBER</b>
<b>9. SPONSORING/MONITORING AGENCY NAME AND ADDRESS</b> Air Vehicles Directorate Air Force Research Laboratory Air Force Materiel Command Wright-Patterson AFB , OH 45433-7542		<b>10. SPONSOR/MONITOR'S ACRONYM(S)</b> AFRL/VASM
		<b>11. SPONSOR/MONITOR'S REPORT NUMBER(S)</b>
<b>12. DISTRIBUTION/AVAILABILITY STATEMENT</b> A PUBLIC RELEASE  Air Vehicles Directorate Air Force Research Laboratory Air Force Materiel Command Wright-Patterson AFB , OH 45433-7542		



**13. SUPPLEMENTARY NOTES****14. ABSTRACT**

The Equivalent Initial Flaw Size (EIFS) concept was developed nearly 30 years ago in an attempt to account for the initial quality, both manufacturing and bulk material properties, of the structural detail prone to fatigue cracking. Widespread use of this concept has not been realized due to the large amount of test data required to develop a reliable EIFS distribution.

**15. SUBJECT TERMS**

EIFS; through crack; AFGROW; fuselage; fatigue; striations; corner crack; oblique; FASTRAN; joints; LEFM; marker loads

<b>16. SECURITY CLASSIFICATION OF:</b>			<b>17. LIMITATION OF ABSTRACT</b> Public Release	<b>18. NUMBER OF PAGES</b> 188	<b>19a. NAME OF RESPONSIBLE PERSON</b> Fenster, Lynn lfenster@dtic.mil
<b>a. REPORT</b> Unclassified	<b>b. ABSTRACT</b> Unclassified	<b>c. THIS PAGE</b> Unclassified			<b>19b. TELEPHONE NUMBER</b> <b>International Area Code</b>  <b>Area Code Telephone Number</b> 703 767-9007 <b>DSN</b> 427-9007

## NOTICE

*Using Government drawings, specifications, or other data included in this document for any purpose other than Government procurement does not in any way obligate the U.S. Government. The fact that the Government formulated or supplied the drawings, specifications, or other data does not license the holder or any other person or corporation; or convey any rights or permission to manufacture, use, or sell any patented invention that may relate to them.*

*This report is releasable to the National Technical Information Service (NTIS). At NTIS, it will be available to the general public, including foreign nations.*

**THIS TECHNICAL REPORT HAS BEEN REVIEWED AND IS APPROVED FOR PUBLICATION.**



JAMES A. HARTER  
Project Engineer  
Analytical Structural Mechanics Branch



DAVID M. AGINS, Maj, USAF  
Branch Chief  
Analytical Structural Mechanics Branch



JEFFREY S. TURCOTTE, LTC, USAF  
Deputy Chief  
Structures Division

*Do not return copies of this report unless contractual obligations or notice on a specific document requires its return.*

REPORT DOCUMENTATION PAGE			Form Approved OMB No. 0704-0188	
Public reporting burden for this collection of information is estimated to average 1 hour per response, including the time for reviewing instructions, searching existing data sources, gathering and maintaining the data needed, and completing and reviewing the collection of information. Send comments regarding this burden estimate or any other aspect of this collection of information, including suggestions for reducing this burden, to Washington Headquarters Services, Directorate for Information Operations and Reports, 1215 Jefferson Davis Highway, Suite 1204, Arlington, VA 22202-4302, and to the Office of Management and Budget, Paperwork Reduction Project (0704-0188), Washington, DC 20503.				
1. AGENCY USE ONLY (Leave blank)		2. REPORT DATE JUNE 2000		3. REPORT TYPE AND DATES COVERED FINAL REPORT FOR 10/01/1997 - 06/15/2000
4. TITLE AND SUBTITLE EQUIVALENT INITIAL FLAW SIZE TESTING AND ANALYSIS			5. FUNDING NUMBERS C IN-HOUSE PE 62201 PR 2401 TA 0H WU RD	
6. AUTHOR(S)  SCOTT A. FAWAZ				
7. PERFORMING ORGANIZATION NAME(S) AND ADDRESS(ES) AIR VEHICLES DIRECTORATE 2790 D STREET, STE 504 AIR FORCE RESEARCH LABORATORY WRIGHT-PATTERSON AFB, OH 45433-7542			8. PERFORMING ORGANIZATION REPORT NUMBER	
9. SPONSORING/MONITORING AGENCY NAME(S) AND ADDRESS(ES) AIR VEHICLES DIRECTORATE AIR FORCE RESEARCH LABORATORY AIR FORCE MATERIEL COMMAND WRIGHT-PATTERSON AFB, OH 45433-7542 POC: MAJOR DAVID AGINS, AFRL/VASM, 937-255-6104 EXT 244			10. SPONSORING/MONITORING AGENCY REPORT NUMBER  AFRL-VA-WP-TR-2000-3024	
11. SUPPLEMENTARY NOTES				
12a. DISTRIBUTION AVAILABILITY STATEMENT  APPROVED FOR PUBLIC RELEASE, DISTRIBUTION UNLIMITED.			12b. DISTRIBUTION CODE	
13. ABSTRACT (Maximum 200 words) The Equivalent Initial Flaw Size (EIFS) concept was developed nearly 30 years ago in an attempt to account for the initial quality, both manufacturing and bulk material properties, of the structural detail prone to fatigue cracking. Widespread use of this concept has not been realized due to the large amount of test data required to develop a reliable EIFS distribution. Four types of flat, production like joints were fatigue tested with crack detection and measurement via the traveling optical microscope, eddy current rotating probe system, and scanning electron microscope. Novel techniques were employed to avoid edge cracking of the joints and MSD developed in all but two joints. A programmed loading spectrum was used to mark the fracture surface to aid in post-test crack history reconstruction using an optical and scanning electron microscope. As seen in the post-test fractographic evaluation, many of the crack nucleation sites were damaged by large scale plastic deformation of the rivet hole edge during fatigue or final fracture of the joint. In addition, crack face contact resulted in marring the fracture surface and in some cases obliterating the marker bands used for crack history reconstruction. The mean EIFS for 48 cracks for which EIFS calculations were made was 21.0 mm with a standard deviation of 11.1 mm. However, the EIFS calculations are prone to compounding errors in the crack growth analysis due to the changing stress intensity factor solutions and stress fields as the crack gets longer. Therefore, only including EIFS calculations for crack length measurements less than 1.27 mm results in a mean EIFS of 12.7 mm with a standard deviation of 2.4 mm.				
14. SUBJECT TERMS EIFS, Through crack, AFGROW, Fuselage, Fatigue, Striations, Corner Crack, Oblique, FASTRAN, Joints, LEFM, Marker Loads			15. NUMBER OF PAGES 188	
			16. PRICE CODE	
17. SECURITY CLASSIFICATION OF REPORT  UNCLASSIFIED	18. SECURITY CLASSIFICATION OF THIS PAGE  UNCLASSIFIED	19. SECURITY CLASSIFICATION OF ABSTRACT  UNCLASSIFIED	20. LIMITATION OF ABSTRACT  SAR	



# Table of Contents

LIST OF FIGURES .....	iv
LIST OF TABLES .....	x
EQUIVALENT INITIAL FLAW SIZE TESTING AND ANALYSIS .....	xi
1. INTRODUCTION .....	1
2. BACKGROUND .....	2
3. EXPERIMENTAL INVESTIGATION .....	3
3.1. TEST ARTICLES .....	3
3.2. FINITE WIDTH EFFECT .....	4
3.3. TEST PROCEDURE .....	4
4. ANALYTICAL INVESTIGATION .....	6
4.1. FASTRAN .....	6
4.2. AFGROW .....	6
5. RESULTS AND DISCUSSION .....	7
5.1. STRAIN SURVEY .....	7
5.1.1. MECHANICAL PROPERTY TESTING .....	10
5.2. FRACTOGRAPHIC ANALYSIS .....	10
5.2.1. CRACK GROWTH HISTORIES .....	12
5.2.2. CRACK GROWTH RATES .....	13
5.2.3. EVALUATION OF ROTATING SELF-NULLING EDDY CURRENT PROBE SYSTEM .....	16
5.3. FATIGUE CRACK GROWTH PREDICTIONS .....	17
5.4. COMPARISON BETWEEN AFGROW AND FASTRAN .....	20
6. CONCLUSION .....	22
6.1. TESTING .....	22
6.2. ANALYSIS .....	22
7. RECOMMENDATION .....	24
8. REFERENCES .....	25
APPENDIX A: TEST HISTORY .....	93
APPENDIX B: TEST ARTICLE DIMENSIONS AND STRAIN GAGE LOCATIONS .....	96
APPENDIX C: RECONSTRUCTED CRACK HISTORY DATA .....	112
APPENDIX D: SEM FRACTORGRAPHS OF FRACTURE SURFACES .....	128
APPENDIX E: ROTATING SELF-NULLING EDDY CURRENT PROBE SYSTEM DATA .....	160
APPENDIX F: EIFS ITERATION ROUTINE, VISUAL BASIC FOR APPLICATIONS .....	169

## List of Figures

Figure 1 Air Force Research Laboratory Wide Panel Test Facility .....	34
Figure 2 Overload Spectrum .....	35
Figure 3 10-4-6 Marker Spectrum .....	35
Figure 4 Joint Type IV Spectrum .....	36
Figure 5 EIFS Joint Types .....	36
Figure 6 Joint Type I Configuration .....	37
Figure 7 Joint Type II Configuration .....	37
Figure 8 Joint Type III Configuration .....	37
Figure 9 Joint Type IV Configuration .....	38
Figure 10 Strain Gage Locations for EIFS Type I .....	38
Figure 11 Strain Gage Locations for EIFS Type II .....	39
Figure 12 Strain Gage Locations for EIFS Type III .....	39
Figure 13 Strain Gage Locations for EIFS Type IV .....	40
Figure 14 Generic Single Shear Lap Splice Joint .....	40
Figure 15 Methods of Reducing the Edge Effect .....	41
Figure 16 EIFS Type I and II Edge Blocks .....	42
Figure 17 Joint Type III with Dogboned Skins .....	42
Figure 18 Tensile Strain Variation Through the Panel Width .....	43
Figure 19 Bending Strain Variation Through the Panel Width .....	43
Figure 20 Parameter Definition for Generic Riveted Joint .....	44
Figure 21 Effect of Rivet Row Pitch on Bending Factor, $k$ .....	44
Figure 22 Effect of Sheet Length on Bending Factor, $k$ .....	45
Figure 23 EIFS-1 Top Sheet, Left Side Normal Strains .....	45
Figure 24 EIFS-1 Top Sheet, Right Side Normal Strains .....	46
Figure 25 EIFS-1 Top Sheet, Critical Rivet Row Normal Strains .....	46
Figure 26 EIFS-1 Bottom Sheet Normal Strains .....	46
Figure 27 EIFS-2 Top Sheet Normal Strains .....	47
Figure 28 EIFS-2 Bottom Sheet Normal Strains .....	47
Figure 29 EIFS-3 Top Sheet Normal Strains .....	48
Figure 30 EIFS-3 Bottom Sheet Normal Strains .....	48
Figure 31 EIFS-4 Top Sheet Normal Strains .....	49
Figure 32 EIFS-4 Bottom Sheet Normal Strains .....	49
Figure 33 EIFS-5 Top Sheet, Left Side Normal Strains .....	50
Figure 34 EIFS-5 Top Sheet, Right Side Normal Strains .....	51
Figure 35 EIFS-5 Top Sheet Critical Rivet Row Normal Strains .....	51
Figure 36 EIFS-5 Bottom Sheet Normal Strains .....	52
Figure 37 EIFS-6 Top Sheet Normal Strains .....	52
Figure 38 EIFS-6 Bottom Sheet Normal Strains .....	53
Figure 39 EIFS-7 Top Sheet Normal Strains .....	53
Figure 40 EIFS-7 Bottom Sheet Normal Strains .....	54
Figure 41 EIFS-8 Top Sheet Normal Strains .....	54
Figure 42 EIFS-8 Bottom Sheet Normal Strains .....	55
Figure 43 EIFS-9 Top Sheet, Left Side Normal Strains .....	55
Figure 44 EIFS-9 Top Sheet, Right Side Normal Strains .....	56
Figure 45 EIFS-9 Top Sheet, Critical Rivet Row Normal Strains .....	56
Figure 46 EIFS-9 Bottom Sheet Normal Strains .....	57
Figure 47 EIFS-10 Top Sheet Normal Strains .....	57
Figure 48 EIFS-10 Bottom Sheet Normal Strains .....	58
Figure 49 EIFS-10 Bottom Sheet Normal Strains after Dogbone Shape Cut into Top and Bottom Sheets and Applied Load Adjusted to Maintain Constant Remote Tensile Stress .....	58
Figure 50 EIFS-11 Top Sheet Normal Strains .....	59
Figure 51 EIFS-11 Bottom Sheet Normal Strains .....	59

Figure 52 EIFS-11 Top Sheet Normal Strains after Dogbone and Load Adjustment .....	59
Figure 53 EIFS-11 Bottom Sheet Normal Strains after Dogbone and Load Adjustment .....	60
Figure 54 EIFS-12 Top Sheet Normal Strains after Dogbone and Load Adjustment .....	60
Figure 55 EIFS-12 Bottom Sheet Normal Strains after Dogbone and Load Adjustment .....	61
Figure 56 EIFS-13 Top Sheet, Left Side Normal Strains .....	61
Figure 57 EIFS-13 Top Sheet, Right Side Normal Strains .....	62
Figure 58 EIFS-13 Top Sheet, Critical Rivet Row Normal Strains .....	62
Figure 59 EIFS-13 Bottom Sheet Normal Strains .....	63
Figure 60 EIFS-14 Top Sheet Normal Strains .....	63
Figure 61 EIFS-14 Bottom Sheet Normal Strains .....	64
Figure 62 EIFS-15 Top Sheet Normal Strains .....	64
Figure 63 EIFS-15 Bottom Sheet Normal Strains .....	65
Figure 64 EIFS-16 Top Sheet Normal Strains .....	65
Figure 65 EIFS-16 Bottom Sheet Normal Strains .....	66
Figure 66 Strain Variation Through the Width of the Joint, EIFS-1 .....	66
Figure 67 Strain Variation Through the Width of the Joint, EIFS-2 .....	67
Figure 68 Strain Variation Through the Width of the Joint, EIFS-3 .....	67
Figure 69 Strain Variation Through the Width of the Joint, EIFS-4 .....	68
Figure 70 Strain Variation Through the Width of the Joint, EIFS-5 .....	68
Figure 71 Strain Variation Through the Width of the Joint, EIFS-6 .....	69
Figure 72 Strain Variation Through the Width of the Joint, EIFS-7 .....	69
Figure 73 Strain Variation Through the Width of the Joint, EIFS-8 .....	70
Figure 74 Strain Variation Through the Width of the Joint, EIFS-9 .....	70
Figure 75 Strain Variation Through the Width of the Joint, EIFS-10 .....	71
Figure 76 Strain Variation Through the Width of the Joint, EIFS-11 .....	71
Figure 77 Strain Variation Through the Width of the Joint, EIFS-12 .....	72
Figure 78 Strain Variation Through the Width of the Joint, EIFS-13 .....	72
Figure 79 Strain Variation Through the Width of the Joint, EIFS-14 .....	73
Figure 80 Strain Variation Through the Width of the Joint, EIFS-15 .....	73
Figure 81 Strain Variation Through the Width of the Joint, EIFS-16 .....	74
Figure 82 2024-T3 Stress-Strain Curve, LT-Direction .....	74
Figure 83 2024-T3 Stress-Strain Curve, TL-Direction .....	75
Figure 84 Marker Bands on Fracture Surface .....	75
Figure 85 Fracture Surface Showing Hole Edge and Fretting Damage .....	76
Figure 86 Fatigue Striations from 15E20L, Low Magnification .....	76
Figure 87 Fatigue Striations from 15E20L, High Magnification .....	77
Figure 88 EIFS-7 Reconstructed Crack Histories .....	77
Figure 89 EIFS-3 Reconstructed Crack Histories .....	78
Figure 90 EIFS-4 Reconstructed Crack Histories .....	78
Figure 91 EIFS-8 Reconstructed Crack Histories .....	79
Figure 92 EIFS-9 Reconstructed Crack Histories .....	79
Figure 93 EIFS-10 Reconstructed Crack Histories .....	80
Figure 94 EIFS-11 Reconstructed Crack Histories .....	80
Figure 95 EIFS-15 Reconstructed Crack Histories .....	81
Figure 96 EIFS-5 Crack Histories Measured using the RPS and TOM .....	81
Figure 97 EIFS-6 Crack Histories Measured using the RPS and TOM .....	82
Figure 98 EIFS-3 Crack Growth Rates .....	82
Figure 99 EIFS-4 Crack Growth Rates .....	83
Figure 100 EIFS-7 Crack Growth Rates .....	83
Figure 101 EIFS-8 Crack Growth Rates .....	84
Figure 102 EIFS-9 Crack Growth Rates .....	84
Figure 103 EIFS-10 Crack Growth Rates .....	85
Figure 104 EIFS-11 Crack Growth Rates .....	85
Figure 105 EIFS-15 Crack Growth Rates .....	86
Figure 106 EIFS-5 Crack Growth Rates .....	86
Figure 107 EIFS-6 Crack Growth Rates .....	87

Figure 108 Comparison of Small Crack Data.....	87
Figure 109 2024-T3 Bare Crack Growth Rate Curve from AFGROW Material Database.....	88
Figure 110 RPS Reference Standard for Joint Type I and II.....	88
Figure 111 RPS Reference Standard for Joint Type III and IV.....	89
Figure 112 Comparison of Crack Growth History Obtained using the RPS and SEM.....	90
Figure 113 Crack Model for EIFS Predictions.....	90
Figure 114 Boeing Correlation Factor.....	90
Figure 115 FASTRAN Fatigue Life Predictions for EIFS-720.....	91
Figure 116 AFGROW Fatigue Life Predictions for EIFS-7, Crack 7A6R.....	92
Figure 117 Variation in Mean EIFS with Final Crack Length for All Cracks.....	92
Figure 118 Variation in EIFS Standard Deviation with Final Crack Length for All Cracks.....	93
Figure 119 Comparison of Straight Shank and Countersunk Hole K Solutions.....	93
Figure 120 3C9R.....	129
Figure 121 3C12R.....	128
Figure 122 3C12R Nucleation Site.....	130
Figure 123 3C12R Nucleation Site.....	130
Figure 124 3C14L.....	130
Figure 125 3C14L Nucleation Site.....	130
Figure 126 3C17R.....	130
Figure 127 3C17R.....	130
Figure 128 3C17R Nucleation Site.....	131
Figure 129 3C18L.....	131
Figure 130 3C18L.....	131
Figure 131 3C18R.....	131
Figure 132 3D11R.....	131
Figure 133 3D11R.....	131
Figure 134 3D11R Nucleation Site.....	132
Figure 135 3D12L.....	132
Figure 136 3D12L.....	132
Figure 137 3D12L Nucleation Site.....	132
Figure 138 3D12R.....	132
Figure 139 3D12R.....	132
Figure 140 3D13L.....	133
Figure 141 3D13R.....	133
Figure 142 3D13R.....	133
Figure 143 3D13R Nucleation Site.....	133
Figure 144 3D14L.....	133
Figure 145 3D15L.....	133
Figure 146 3D15L.....	134
Figure 147 4A13L.....	134
Figure 148 4C2L.....	134
Figure 149 4C2L Nucleation Site.....	134
Figure 150 4C3L.....	134
Figure 151 4C3L Nucleation Site.....	134
Figure 152 4C3R.....	135
Figure 153 4C3R Nucleation Site.....	135
Figure 154 4C4L.....	135
Figure 155 4C4L Nucleation Site.....	135
Figure 156 4C4R.....	135
Figure 157 4C5L.....	135
Figure 158 4C5L Nucleation Site.....	136
Figure 159 4C5R.....	136
Figure 160 4C6L.....	136
Figure 161 4C6R.....	136
Figure 162 4C6R Nucleation Site.....	136
Figure 163 4C7L.....	136



Figure 164 4C7R .....	137
Figure 165 4C7R Nucleation Site .....	137
Figure 166 4C8L .....	137
Figure 167 4C8R .....	137
Figure 168 4C8R Nucleation Site .....	137
Figure 169 4C9L .....	137
Figure 170 4C9R .....	138
Figure 171 4C10R .....	138
Figure 172 4C11L .....	138
Figure 173 4C11L Nucleation Site .....	138
Figure 174 4C11R .....	138
Figure 175 4C11R Nucleation Site .....	138
Figure 176 4C12R .....	139
Figure 177 4C12R .....	139
Figure 178 Corrosion on 4C12R .....	139
Figure 179 Corrosion on 4C12R .....	139
Figure 180 7A4R .....	139
Figure 181 7A4R Marker Bands .....	138
Figure 182 7A6L .....	139
Figure 183 7A6R .....	139
Figure 184 7A6R Marker Bands .....	139
Figure 185 7A7L .....	139
Figure 186 7A7L Nucleation Site .....	140
Figure 187 7A7L Marker Bands .....	140
Figure 188 7A7R .....	140
Figure 189 7A7R Nucleation Site .....	140
Figure 190 7A8L .....	140
Figure 191 7A8L Nucleation Site .....	140
Figure 192 7A10L .....	141
Figure 193 7A10L .....	141
Figure 194 7A12R .....	141
Figure 195 7A12R Nucleation Site, Macro View .....	141
Figure 196 7A12R Nucleation Site .....	141
Figure 197 7A12R Marker Bands .....	141
Figure 198 7A12R Marker Bands .....	142
Figure 199 7A12R Marker Bands .....	142
Figure 200 7A13R .....	142
Figure 201 7A13R Nucleation Site, Macro View .....	142
Figure 202 7A13R Nucleation Site .....	142
Figure 203 7A13R Marker Bands .....	142
Figure 204 7A13R Marker Bands .....	143
Figure 205 7A13R Marker Bands .....	143
Figure 206 7A13R Marker Bands .....	143
Figure 207 7A13R Marker Bands .....	143
Figure 208 7A13R Marker Bands .....	143
Figure 209 7A13R Marker Bands .....	143
Figure 210 7A13R Marker Bands .....	144
Figure 211 7A14L .....	144
Figure 212 7A14L Nucleation Site .....	144
Figure 213 7A14L Marker Bands .....	144
Figure 214 7A14R .....	144
Figure 215 7A14R Nucleation Site .....	144
Figure 216 7A14R Marker Bands .....	145
Figure 217 7A15R .....	145
Figure 218 7A15R Nucleation Site .....	145
Figure 219 7A16L .....	145

Figure 220 7A16R .....	145
Figure 221 7A16R Nucleation Site .....	145
Figure 222 7A16R Marker Bands .....	146
Figure 223 7A17L .....	146
Figure 224 7A17L Nucleation Site .....	146
Figure 225 7A17L Marker Bands .....	146
Figure 226 7A17R .....	146
Figure 227 7A17R Nucleation Site .....	146
Figure 228 8A4L .....	147
Figure 229 8A4R .....	146
Figure 230 8A5L .....	147
Figure 231 8A5R .....	147
Figure 232 8A6L .....	147
Figure 233 8A6R .....	147
Figure 234 8A6R Close-up .....	148
Figure 235 8A7L .....	148
Figure 236 8A7R .....	148
Figure 237 8A10L .....	148
Figure 238 8A10L Nucleation Site .....	148
Figure 239 8A10R .....	149
Figure 240 8A10R Nucleation Site .....	149
Figure 241 9A5L .....	149
Figure 242 9A5L Nucleation Site .....	149
Figure 243 9A5R .....	149
Figure 244 9A5R Nucleation Site .....	149
Figure 245 10F6R .....	150
Figure 246 10F6R Nucleation Site .....	150
Figure 247 10F7R .....	150
Figure 248 10F7R Nucleation Site .....	150
Figure 249 10F8L .....	150
Figure 250 10F8L Nucleation Site .....	150
Figure 251 10F8R .....	151
Figure 252 10F8R .....	151
Figure 253 10F10R .....	151
Figure 254 10F10R Nucleation Site .....	151
Figure 255 11F6L .....	151
Figure 256 11F6L Nucleation Site .....	151
Figure 257 11F6R .....	152
Figure 258 11F6R Nucleation Site .....	152
Figure 259 11F7L .....	152
Figure 260 11F7L Nucleation Site .....	152
Figure 261 11F7R .....	152
Figure 262 11F7R Nucleation Site .....	152
Figure 263 11F8L .....	153
Figure 264 11F8L Nucleation Site .....	153
Figure 265 11F8R .....	153
Figure 266 11F8R Nucleation Site .....	153
Figure 267 11F9R .....	153
Figure 268 11F9R Nucleation Site .....	153
Figure 269 11F10R .....	154
Figure 270 11F10R Nucleation Site .....	154
Figure 271 15E2R .....	154
Figure 272 15E2R Nucleation Site .....	154
Figure 273 15E11R .....	155
Figure 274 15E11R Nucleation Site .....	155
Figure 275 15E16L .....	155

Figure 276 15E16L Nucleation Site.....	155
Figure 277 15E16R .....	155
Figure 278 15E16R Nucleation Site .....	155
Figure 279 15E20L .....	156
Figure 280 15E20L Nucleation Site.....	156
Figure 281 15E28R .....	156
Figure 282 15E28R Nucleation Site .....	156
Figure 283 15E20L Marker Bands .....	157
Figure 284 No Cleaning.....	157
Figure 285 1 Minute 2% MicroClean, Sonicate .....	157
Figure 286 5 Minute 2% MicroClean, Sonicate .....	158
Figure 287 25 Minute 2% MicroClean, Sonicate .....	158
Figure 288 No Cleaning.....	158
Figure 289 1 Minute 2% MicroClean, Sonicate .....	158
Figure 290 5 Minute 2% MicroClean, Sonicate .....	158
Figure 291 25 Minute 2% MicroClean, Sonicate .....	158
Figure 292 No Cleaning.....	159
Figure 293 1 Minute 2% MicroClean, Sonicate .....	159
Figure 294 5 Minute 2% MicroClean, Sonicate .....	159
Figure 295 25 Minute 2% MicroClean, Sonicate .....	159
Figure 296 1 Minute 2% MicroClean, Sonicate .....	159
Figure 297 5 Minute 2% MicroClean, Sonicate .....	159
Figure 298 25 Minute 2% MicroClean, Sonicate .....	160

## List of Tables

Table 1 Crack Growth Analysis Model Parameters.....	27
Table 2 Crack Locations.....	28
Table 3 MicroMeasurements® Strain Gage Type .....	29
Table 4 2024-T3 Clad Mechanical Properties.....	29
Table 5 EIFS-5 Eddy Current and Travel Optical Microscope Crack Growth Data.....	29
Table 6 EIFS-6 Eddy Current and Travel Optical Microscope Crack Growth Data.....	30
Table 7 Load Transfer Parameters .....	30
Table 8 EIFS Summary .....	31
Table 9 EIFS Summary Using Crack Lengths to 1.27 mm .....	32
Table 10 EIFS Comparison: AFGROW vs. FASTRAN.....	33

# Equivalent Initial Flaw Size Testing and Analysis

## Abstract

The Equivalent Initial Flaw Size (EIFS) concept was developed nearly 30 years ago in an attempt to account for the initial quality, both manufacturing and bulk material properties, of the structural detail prone to fatigue cracking. Widespread use of this concept has not been realized due to the large amount of test data required to develop a reliable EIFS distribution. Since calculation of the EIFS is dependent on the crack growth model and all inputs to the crack growth model, the EIFS must be determined for each structural detail in question and all load spectra this detail may experience. Fuselage lap splice joints for transport aircraft are very similar across aircraft types and the loading spectrum is predominately constant amplitude as a result of cabin pressurization cycles. Thus, using the EIFS concept is acceptable.

Four types of flat, production like joints were fatigue tested with crack detection and measurement via the traveling optical microscope, eddy current rotating probe system, and scanning electron microscope. Novel techniques were employed to avoid edge cracking of the joints and MSD developed in all but two joints. A programmed loading spectrum was used to mark the fracture surface to aid in post-test crack history reconstruction using an optical and scanning electron microscope. As seen in the post-test fractographic evaluation, many of the crack nucleation sites were damaged by large scale plastic deformation of the rivet hole edge during fatigue or final fracture of the joint. In addition, crack face contact resulted in marring the fracture surface and in some cases obliterating the marker bands used for crack history reconstruction.

The mean EIFS for 48 cracks for which EIFS calculations were made was 21.0  $\mu\text{m}$  with a standard deviation of 11.1  $\mu\text{m}$ . However, the EIFS calculations are prone to compounding errors in the crack growth analysis due to the changing stress intensity factor solutions and stress fields as the crack gets longer. Therefore, only including EIFS calculations for crack length measurements less than 1.27 mm results in a mean EIFS of 12.7  $\mu\text{m}$  with a standard deviation of 2.4  $\mu\text{m}$ .



# 1. Introduction

The Equivalent Initial Flaw Size Testing and Analysis program is one of six technology thrusts in the Federal Aviation Administration's (FAA) Widespread Fatigue Damage (WFD) Evaluation program. The prime contractor to the FAA is The Boeing-Long Beach Company. The Air Force Research Laboratory, Air Vehicles Directorate, Structures Division, Analytical Structural Mechanics Branch (AFRL/VASM) is participating in five of the six technology areas; WFD Initiation, Small Crack Study, EIFS, Multiple Site Damage (MSD) in Flat Panels, and MSD in an Aft Pressure Bulkhead. The MSD in Curved Panels program is an effort solely executed by Boeing and the FAA. The EIFS testing is a cost share between the FAA and AFRL/VASM. Via the FAA, Boeing fabricated 16 production like joints to be tested at AFRL/VASM, Wright-Patterson AFB, OH.

The crack initiation life and damage tolerance characteristic of splice joints with MSD may vary significantly depending upon the initial size and distribution of the MSD flaws. The statistical behavior of the MSD flaw size and distribution may help explain the scatter in fatigue life and can be used to quantify, in fracture mechanics terms, the quality of the countersunk holes under varying manufacturing techniques and service loading.

The objective of the EIFS study is to generate fractographic data for fatigue cracks nucleating and growing from countersunk fastener holes in the critical row of typical fuselage longitudinal and circumferential splice joints subject to operational loading spectra. The observed cracks from the test are then extrapolated backwards using two separate crack growth analysis programs, FASTRAN III and AFGROW; developed by the NASA Langley Research Center and Air Force Research Laboratory, respectively. In addition, a comparison is made between the two crack growth algorithms used in the respective codes. The extrapolation extends from the first observed crack length to the length of the crack at the beginning of the test, time equals zero. To minimize the extrapolation distance, the scanning electron microscope (SEM) is used for post-test fractographic investigation. The EIFS distribution is then assumed to exist in like aircraft structure prior to service and can be accounted for in subsequent damage tolerance analyses.

## 2. Background

The EIFS concept was first used during the McDonnell Douglas F-4C/D Aircraft Structural Integrity Program<sup>1</sup>. In using linear elastic fracture mechanics, the method for determining the EIFS is the same regardless of the crack growth prediction code used. For a given fatigue specimen cycled with a known load history, a portion of the crack growth life can be obtained by *in situ* and/or fractographic measurements. A series of crack growth predictions can then be made with varying initial flaw sizes. The prediction yielding the best correlation between the analysis and experimental data defines the EIFS. If the cracks nucleate and grow as three-dimensional cracks, the crack shape must also be established; thus two parameters must be varied in the predictions, initial flaw size and shape. For example, corner cracks at hole, which are commonly found in mechanically fastened structure, are analyzed by specifying the crack length,  $c$ , and the crack depth to crack length ratio,  $a/c$ .

The EIFS analyses to follow are a new application of the concept in that two different crack closure models are used. FASTRAN uses a two-parameter plasticity induced closure model where the crack closure is caused by residual plastic deformation remaining in the wake of a growing crack. AFGROW uses a single parameter closure model based on changes in the crack driving force due to the cyclic plastic zone ahead of the crack tip.



### 3. Experimental Investigation

The Air Force Research Laboratory's Wide Panel Test Facility, see Figure 1, was designed and constructed specifically for the EIFS and MSD test programs. A digital computer was used to control the closed loop, servo hydraulic load frames. The maximum specimen dimensions are 48" x 86" with a 100 kip load cell. Each frame is equipped with a 20X traveling optical microscope (TOM) mounted to a stage that can translate along the length or across the width of the specimen. A linear voltage displacement transducer (LVDT) is attached to the stage so quantities in the specimen width direction, crack length for example, can be measured. The resolution of the TOM/LVDT system is  $\pm 2.54 \mu\text{m}$ . The data recording system can sample at 10 data points per second with all data being stored electronically. In the current configuration, one data channel is connected to a strip recorder, which was used to verify the applied load spectrum.

Crack detection and measurement was accomplished using the rotating self-nulling eddy current probe system (RPS) for subsurface cracks, cracks growing under the countersunk rivet head.<sup>2</sup> The TOM was used to measure the cracks once they grew through the specimen thickness and beyond the countersunk rivet head. After specimen failure, the critical rivet row, the rivet row containing the cracks that ultimately caused specimen failure, was removed and each crack was cut out for fractographic investigation in the scanning electron microscope (SEM).

Two different load spectra were used in attempt to mark the fracture surface with marker bands to aid crack growth history reconstruction via fractographic analysis using the SEM. Marker bands are created by an instantaneous or short duration variation in the constant amplitude (CA) maximum stress or stress ratio, which perturb the fatigue striation spacing created by the CA loading. The first spectrum contained 2000 baseline CA cycles at  $S_{\text{max}}$  with an  $R = 0.1$  followed by 10 overload cycles at 130%  $S_{\text{max}}$  with an  $R = 0.3$ , see Figure 2 with applied stress magnitudes given in Table 1. The second spectrum, Figure 3, contains 1000 baseline CA cycles at  $S_{\text{max}}$  followed by periodic blocks of 100 CA cycles at 75%  $S_{\text{max}}$  then 10 baseline CA cycles all blocks using an  $R = 0.02$ , further details of this spectrum can be found in reference [3]. The third spectrum used is a transport aircraft fuselage spectrum shown in Figure 4, which is derived by The Boeing Company from flight loads and cabin pressurization.<sup>4</sup>

#### 3.1. Test Articles

The EIFS specimen panels are based on fuselage splice joint designs that have been used in commercial aircraft for many years. Four types were chosen, two longitudinal lap-splice joints, one longitudinal butt splice joint, and one circumferential butt splice joint, see Figure 5. Aluminum doublers were bonded with FM73<sup>®</sup> to the specimen ends to prevent failure in or near the grip area. The adhesive cures at 250°F. The specimen is heated from room temperature to 250°F in one hour, held for one hour at a pressure of 40 $\pm$ 5 psi, then cooled to room temperature. The overall specimen dimensions are 22" x 56" with 22" x 40" outside the grip area; thus the specimen length to width ratio (L/W) is 1.8. An L/W of 1.8 was chose to ensure a uniform stress distribution through the width of the specimen outside the joint overlap region. The type I longitudinal lap-splice joint skin is made of 0.063" thick 2024-T3 aluminum clad sheet with a 7075-T6 aluminum doubler and longeron. Similarly, the type II longitudinal lap-splice joint skin is made of 0.063" thick 2024-T3 aluminum clad sheet with a 7075-T6 longeron and no doubler. The type III longitudinal butt-splice joint skin is made of 0.09" thick 2024-T3 aluminum clad sheet with the doubler and splice plate being made of 0.071" thick 2024-T3 aluminum clad sheet. The longeron is a 7150-T61511 extrusion. The type IV circumferential butt-splice joint skin is made of 0.063" thick 2024-T3 aluminum clad sheet with 7075-T6 doubler and splice plate. For the longitudinal joints, the material orientation of the skin in relation to the applied load is the TL direction; whereas, for the circumferential joint, the material orientation is in the LT direction. The four joint configurations can be seen in Figure 6 - Figure 9.

Each of the four joint types was instrumented with strain gages, see Table 2 and Figure 10 - Figure 13, having a single linear grid with the loading axis parallel to the longitudinal axis of the strain gage grid. The smaller gages, EA-13-062AQ-350, were used at the anticipated location of maximum stress in the critical outer rivet row. The larger gages, EA-13-250AQ-350, were used to determine the global response of the panel.

### 3.2. Finite Width Effect

Wide panel testing not only offers a more realistic representation of the full-scale structure, but may also respond to static or dynamic loading differently than the full-scale structure. The joints tested here differ from the real structure in that the specimen edges are unconstrained while in a fuselage circumferential and longitudinal stiffeners, frames and stringers, restrain the skin. This lack of restraint allows for an increased rotation about the joint and longitudinal axes of the specimen resulting in higher secondary bending stresses at the edges. Furthermore, the increased stiffness of the specimen in the joint overlap area, boxed area in Figure 5, constricts the amount of Poisson contraction in the overlap area compared to the skin. Thus, rivet loads at the specimen edge, rivets A1, A19, C1, and C19 in Figure 14, are larger than those of the interior rivets in the same row. Rivets B1 and B19 in the same figure are not susceptible to higher loads since the lateral contraction in the joint should not vary between rivet rows and the Poisson restriction is primarily occurring at rivet rows A and C. To study the finite width effect, Müller conducted several finite element analyses of single shear lap joints with varying sheet lengths and widths.<sup>5</sup> He found that for L/W ratios less than 1.25, the outer rivets, again rivets A1, A19, C1, and C19 in Figure 14, only see a slightly elevated rivet force. For the joints tested in this effort, the L/W = 1.8; thus, higher edge rivet loads should be expected. The larger secondary bending stresses and rivet loads cause edge cracking, cracks that nucleate and grow at the rivet holes in the outer rivet rows closest to the specimen edge. Due to the high crack driving force of an edge cracked rivet hole, MSD cannot develop in the remaining rivets of the same row. Several researchers have prevented edge cracking by stop drilling,<sup>6</sup> use of oversized rivets,<sup>6</sup> ball indentation at the crack tip,<sup>7</sup> use of protruding head rivets,<sup>8,9</sup> and application of doublers at the specimen edge.<sup>8,9</sup> Four different methods were used in this study as shown in Figure 15. One, from the specimen edge to the first column of rivets for all specimens, the skins were bonded together using FM73<sup>®</sup>. By bonding the sheets together at this location, the load transmission at the outer column rivets is slightly reduced due to the load transfer occurring through the adhesive. Although the joint stiffness will also be slightly increased, the increased secondary bending at the edge is not significantly reduced. Two, edge clamps were placed over the first (and last) column of rivets, see Figure 16. The edge clamps reduce the larger joint rotation at the free edge; thus, reducing the secondary bending. However, the Poisson restriction remains. Three, the skin material outside the joint was cut into a dog-bone shape. The dogboned sheet material outside the joint reduces the load transmission at the outer rivet columns. Four, the outer column of rivets at the specimen edges were oversized and heavily expanded. The larger rivets reduce the bearing stress. Large rivet hole expansion causes compressive residual stresses at the hole edge which inhibits crack nucleation and subsequent growth.

### 3.3. Test Procedure

The test procedure is typical of any increasing  $\Delta K$  fatigue test. The test article is mounted in the load frame and the strain gage wires are connected to the data collection system. Depending on the joint type, edge treatments in the joint overlap area were applied to decrease the likelihood of the finite width effect discussed previously. For joint types I and II, edge clamps were used as shown in Figure 16. Joint type III is by far the stiffest of all joints tested and it was anticipated that the edge clamps would not eliminate the finite width effect. Thus, the sheet material outside the joint overlap area was dogboned to reduce the load transmission at the outer columns of rivets, see Figure 17. In addition, the outer column of rivets on both the left and right hand side of the joint were drilled out and replaced with larger diameter rivets of the same type. The diameter was

only increased by 1/16". These larger rivets were also heavily expanded such that the driven head diameter was 1.8 times larger than the original rivet diameter ( $D/D_o = 1.8$ ). The stiffness of the type IV joint is lower than that of the type III joint; therefore, only the large, heavily expanded, outer column rivets were used to eliminate the finite width effect.

Once the test article was installed, 20 load cycles up to the maximum spectrum load were applied to seat the article in the load frame. A strain survey was conducted loading up to the maximum spectrum load while recording strain data every 0.5 seconds. The strain data was examined to determine if the article was being loaded symmetrically with respect to the loading axis. The article was then fatigue cycled at 1 – 2 Hz using the stress levels specified in section 3. A detailed test history is given in Appendix A.

## **4. Analytical Investigation**

### **4.1. FASTRAN**

Dr. James C. Newman, Jr. of the NASA Langley Research Center, Hampton, VA, developed FASTRAN III. For a complete theoretical discussion and user's manual of FASTRAN III, see reference [10] and the comment section at the beginning of the FASTRAN III FORTRAN source code. Although several FASTRAN III runs were completed at AFRL, the code in its current form isn't efficient in conducting EIFS calculations. Specifically, an EIFS calculation using FASTRAN would take the following form. The input file is prepared with an assumed initial flaw size. FASTRAN is executed. The results are then checked for correlation of the final crack length and cycles with the experimental result. If sufficient accuracy is not obtained in the prediction, the initial flaw size is adjusted and the process repeats. This procedure is not automated in any way, thus very time consuming. As a result, The Boeing Company-Long Beach conducted all EIFS calculations reported here.

### **4.2. AFGROW**

Mr. James A. Harter of the Air Force Research Laboratory, Wright-Patterson AFB, OH is the developer of AFGROW. For a complete theoretical discussion and user's manual of AFGROW, see reference [11]. The AFGROW analyses assumed a quarter-circular double corner crack at a straight shank hole that transitions to an oblique through crack once it grows through the sheet thickness. The applied loading is remote tension, secondary bending, and bearing with the tension and bending stresses being calculated from strain data and the bearing stress calculated using a strength of materials approach.

AFGROW for Windows95/98/NT4<sup>®</sup> operates in two different modes, as an interactive Windows program and as a Component Object Model (COM) Server. In the first mode, the AFGROW run procedure is similar to FASTRAN where one analysis is run at a time. However, using the COM Server capabilities, AFGROW can run successive analyses. Thus, in determining the EIFS, AFGROW automatically changes the initial flaw assumption until correlation between the experimental and analytical results reaches an analyst defined accuracy.

## 5. Results and Discussion

A total of 16 specimens were tested, four of each joint type, with fatigue crack growth data obtained from 12 specimens. Fatigue cracks were found at those locations listed in Table 2; however, crack growth data was not obtained for four of the 16 specimens; the reasons for which are discussed below. Bonding of the skin at the specimen edges was completely insufficient resulting in edge cracking of one type I joint. A second type I joint experienced edge cracking due to an improperly designed edge block which allowed contact between the edge block and skin outside the joint area. Visual examination of the fracture surface and nucleation site showed the specimen failed due to a crack in the skin initiated by fretting. The remaining type I joints were tested successfully with redesigned edge blocks with row C being the critical rivet row. The type II joints were tested with edge blocks and row A was the critical rivet row. Edge blocks did not preclude edge cracking in the type III joints although the secondary bending was lower at the specimen edge than center. The stiffness of the overlap area in the type III (and IV) joints is greater than in the types I and II where the edge blocks prohibited edge cracking. This suggests the restriction of the Poisson contraction at the outer rivet rows, and the subsequent higher rivet loads, is causing the edge cracking. The dog-bone shape of the skin outside the joint reduces the amount of load transferred by the rivets at the specimen edge. Care must be taken in designing the dog-bone notch since the stress concentration,  $K_T$ , may cause failure at the notch root,  $r$ . Indeed, when the  $r = 2.5$  in.,  $K_T = 1.75$  failure was at the notch root; whereas when  $r = 19.5$  in.,  $K_T = 1.3$  failure was in the critical rivet row. Using the larger notch root radius, edge cracking was prevented in the type III joints, and the outer rivet rows, A or F, were critical. The critical rivet row in the type IV joint was row D or E. The dog-boned skin does not reduce the rivet loading for rows D and E of the type IV joint. In order to prevent edge cracking, the outer column rivets were removed and replaced with an oversized rivet, and the driven head was expanded using a force controlled riveting machine until it was 1.8 times the original shank diameter. Three of the four type IV joints had dog-boned skins along with the larger rivets. The last type IV joint was tested with only the highly expanded outer column rivets demonstrating the effectiveness of using a high rivet squeeze force to keep cracks from nucleating.

### 5.1. Strain Survey

As mentioned earlier in section 3.3, the purpose of the strain survey is to determine if the test article is being loaded symmetrically and to investigate the global response of the joint to remote tensile loading. The tensile loading simulates the hoop stress in the fuselage skins as a result of cabin pressurization. The hoop stress then creates secondary bending in the joint, due to the eccentricity of the load path through the joint. The strain data recorded from gages close to the first rivet row are at best average strain values. The strain gradient is quite steep and although small strain gages were used (0.062 in. matrix length, see Table 3), the peak strains cannot be recorded. Furthermore, as seen in Figure 10 - Figure 13, the strain gages aren't near the rivet hole edge where the strains are anticipated to be highest. However, from an analysis verification point of view, the measured strains can be compared to finite element analysis (FEA) calculated strains to determine if the analysis correlates well to the experiments. If so, the FEA can be used to determine the most appropriate stresses to be used for the crack growth analyses.

The four load frames that comprise the Air Force Research Laboratory Wide Panel Test Facility, as shown in Figure 1, were designed specifically for this effort. As part of the verification of the loading fixture, the strain distribution through the width of a wide "dummy" panel was examined. Back to back strain gages were used at five locations. The back to back configuration allows for the bending strains, if any, to be measured. If the strain distribution was unsymmetric, either the specimen isn't being loaded properly or the strain gages are not mounted symmetrically about the specimen centerline with respect to the loading axis. Figure 18 shows the tensile strain variation through the width of the dummy panel. The strains are normalized by the maximum strain, which

is at the specimen centerline. The dummy panel was not loaded to the same maximum load for each of the load frames; thus, the strains are normalized by the strain at the specimen centerline, which is the maximum strain. Little variation is seen in the strains when comparing the right to left hand sides of the panel. The peak strain at the panel centerline is due to St. Venant's principle since the dummy panel isn't of sufficient length. The bending strain variation is shown in Figure 19. The bending strains should be zero since the dummy panel is loaded in pure tension. Interestingly, the calculated bending strains have a nonzero value, although they are quite small and within the data acquisition system accuracy of  $\pm 50 \mu\epsilon$ . Two strain surveys were completed for each load frame. After the first survey, the dummy panel was rotated  $180^\circ$  and the second strain survey was conducted. No systemic effect of off axis loading can be seen.

The first joint of each series received a full complement of strain gages, 24 in all, except for the type III joints, which only had 20 gages. These strain gage configurations were used not only to determine the global response, but also to try and capture the steep strain gradient, which exists close to the critical rivet row(s). The remaining panels in each series only had 8 gages. The reduced number of gages was used just to observe the global response of the panel. Each specimen was measured to determine the global dimensions and locations of the strain gages, see Appendix B. At a given location where the strain gages are mounted back-to-back, one gage on each side of the sheet, the mean strain is the tensile component and the strain amplitude is the bending component, which are calculated using the following equations.

$$\epsilon_{\text{mean}} = \epsilon_t = \frac{\epsilon_{\text{front}} + \epsilon_{\text{back}}}{2} \quad \epsilon_{\text{amplitude}} = \epsilon_b = \frac{\epsilon_{\text{front}} - \epsilon_{\text{back}}}{2} \quad (1)$$

where

$\epsilon_t$  = normal strain due to tension

$\epsilon_b$  = normal strain due to bending

$\epsilon_{\text{front}}, \epsilon_{\text{back}}$  = normal strain from gages that are "back-to-back"

It is common to describe the degree of secondary bending in terms of a bending factor,  $k$ .

$$k = \frac{\sigma_{\text{bending}}}{\sigma_{\text{tension}}} \quad (2)$$

Using a simple one-dimensional line model to calculate the in- and out-of-plane displacements, the tension and bending stresses are easily determined.<sup>12</sup> The bending factor is very sensitive to the rivet row pitch, defined in Figure 20, as can be seen in Figure 21. The  $k$  is weakly dependent on the sheet length outside the joint overlap region as shown in Figure 22. In Müller's lap joint experiments, he measured  $k$ 's as high as 1.0 for production like joints.<sup>5</sup> The measured  $k$  values in this effort never exceeded 0.5; however, the maximum bending strains cannot be measured with the relatively large strain gages used. For the strain gages close to the critical rivet row, the matrix length was 0.062". The  $k$  value range for each joint type is discussed below.

In Figure 23 - Figure 65 the strain behavior for each joint is presented. The strain response is as expected for all the joints although subtle variations in the strain values through the width of the specimens are observed, see Figure 66 - Figure 81. Observations and discussion of the strain behavior by joint type are in the paragraphs below. Although the joint configurations are distinct, there are some similarities in the global strain behavior.

1. As expected, the tensile strain is linearly related to the applied loading without exception. The nonlinear behavior seen in Figure 28 and Figure 61 was due to a data acquisition problem.

2. The bending strains are higher close to the joint due to the eccentricity of the load path and large out-of-plane displacement. For example, the joint type I bending strains are approximately 7% of the tensile strains outside the joint area, strain gages 1-12 in Figure 23 and Figure 24. However, near the joint, strain gages 13-20 in Figure 25, the bending strains are approximately 30% of the tensile strains.
3. The nonlinear contribution to the bending strains is dominant in the lower range of applied load. As the load is increased, kinematic stiffening of the joint occurs resulting in little if any increase in the bending strain with increasing applied load.
4. The strain varies through the width of the specimens due to two factors. One, some of the strain gages are not positioned exactly back to back as can be seen from the measurements listed in Appendix B. Two, fabrication variability such as top/bottom sheet being out of square, nonparallel rivet rows, uneven rivet spacing, etc; again, these measurements can be found in Appendix B.
5. The effect of St. Venant's principle should be small since the panel length to width ratio is 2.0; thus, the tensile strains through the width of the joint should only vary due to reasons listed above in item 3.

#### Joint Type I

The tension and bending strain behavior is shown in Figure 23 - Figure 32 with the strain variation through the width of the joint shown in Figure 66 - Figure 69. Away from the joint area, the bending response is linear with applied load once the applied load reaches 5 kips. Conversely, close to the joint, this linear relation is not observed until 10 kips. The range in  $k$  factors, calculated from strain gages 13-20 was  $0.29 \leq k \leq 0.4$ . The bending strains in the bottom sheet are of opposite sign compared to the top sheet indicating the bottom sheet is deflecting in the opposite direction compared to the top sheet.

#### Joint Type II

The tension and bending strain behavior is shown in Figure 33 - Figure 42 with the strain variation through the width of the joint shown in Figure 70 - Figure 73. Similar to the type I joint, the bending strain becomes linear with the applied load at approximately 8 kips for the gages away from the joint overlap. Near the joint, kinematic stiffening does not dominate and the bending strains continue to increase with increasing applied load. In comparing the type II joint to the other three joint types, the type II is most compliant in that it has the fewest structural elements and thin sheet material. The range in  $k$  factors, calculated from strain gages 13-20 was  $0.20 \leq k \leq 0.36$ . The bending strains in the bottom sheet are of opposite sign compared to the top sheet indicating the bottom sheet is deflecting in the opposite direction compared to the top sheet.

#### Joint Type III

The tension and bending strain behavior is shown in Figure 43 - Figure 55 with the strain variation through the width of the joint shown in Figure 74 - Figure 77. The type III joint is the stiffest of all joints tested having 0.09" thick skins and a massive I-beam stringer. The increased stiffness is manifested in lower bending strains in the critical row. Even though the bending strains are low, kinematic stiffening doesn't dominate the bending behavior just as in the type II joint where the bending strains increase with applied load throughout the loading range. The range in  $k$  factors, calculated from strain gages 9-12 was  $0.18 \leq k \leq 0.22$ . Gages 13-16 were not used to calculate  $k$ 's since the strains appear to be unrealistically low due to reasons stated in item 4 above. Furthermore, the strains outside the joint area, gages 1-8 and 17-20 show higher strain values than those recorded for gages 13-16 which is physically impossible if the effects of item 4 did not exist. The bending strains increase to a maximum at the first rivet row in the joint; thus, strain gages closer to the first rivet row will always have a larger strain than those away further away.

To combat the finite width effect, the type III joints were dogboned as shown in Figure 17. This technique was effective in eliminating the finite width effect. Strain surveys were conducted on the dogboned specimens to ensure the strain behavior was as expected. In Figure 49, the bending strains remain the same after dogboning. The slope of the tensile strains vs. load is higher than in the unmodified specimen since the dogboned specimen has a narrower width. This behavior was exhibited in all dogboned specimens.

#### Joint Type IV

The tension and bending strain behavior is shown in Figure 56 - Figure 65 with the strain variation through the width of the joint shown in Figure 78 - Figure 81. The type IV joint is a circumferential butt joint and the only stiffening element is a tapered doubler. The joint overlap region is relatively large, four rows of fasteners in each sheet. As stated earlier, large joint overlap regions restrict the large out-of-plane deflections resulting in low bending stresses. However, in this case, the doubler is close to twice the thickness of the sheet material and offers substantial bending stiffness; thus, the sheet deflects significantly creating the large bending strains in the critical rivet row. Note the large bending strains at the location of strain gages 13 and 14 in Figure 58. As seen in Appendix B, gage 13 is not exactly on the rivet row centerline but some 0.075" above it. A gage at this location should show smaller bending strains since it is further away from the joint; however, the opposite is observed. One possible explanation for this behavior is the rivet row pitch, also seen in Appendix B. The rivet rows are closer together on the left hand side of the panel where gages 13 and 14 are located; thus there are higher bending strains on the left hand side of the panel than on the right hand side. Great care was taken not to damage the strain gage instrumentation when the dogbone shape was being cut into the top and bottom sheet; however, as seen in Figure 61, gages 23 and 24 appear to be damaged.

### 5.1.1. Mechanical Property Testing

To calculate stresses from the measured strains, the one dimensional Hooke's Law is used which requires the modulus of elasticity as shown in Eqn (3). Tensile tests were conducted in accordance with ASTM E8-96A with the results given in Table 3 and graphically shown in Figure 82 and Figure 83. The numbers in parentheses are MIL-HNBK-5G A-basis values.<sup>13</sup>

$$\sigma = E\varepsilon \quad (3)$$

where

$\sigma$  = normal stress

$E$  = modulus of elasticity

$\varepsilon$  = normal strain, tension or bending

The mechanical properties determined here are consistent with those from reference [13]. One item of interest, the secondary modulus, is slightly higher than the reference values, which could indicate a small amount of extensometer slipping resulting in a measured increase in load (stress) with no corresponding increase in displacement (strain). However, the difference is small; thus, not warranting further investigation.

### 5.2. Fractographic Analysis

From reference [3], the purpose and use of a marker load spectrum, Figure 2 and Figure 3, can be described as follows.

The application of the marker loads presumes two requirements. First, the marker load cycles should leave striations or bands on the fracture surface that can be detected under the microscope. The markers then indicate where the crack front was at the moment that the marker load cycles were applied. Moreover, the crack front shape can also be determined, which for small and



large cracks in riveted lap joints is essential information. Secondly, crack growth during the marker load cycles should have a negligible effect on crack growth during the baseline cycles in order not to disturb the crack growth phenomenon to be studied.

The basic principle of the marker load method is that the crack growth history can be reconstructed from the markers after final failure of a specimen. It presumes that markers can be associated with known numbers of the CA baseline cycles.

The use of marker loads, typically an instantaneous or short duration variation in the CA maximum stress or stress ratio, can perturb the striation spacing created by the CA loading. If the perturbations can be reliably detected in the electron microscope, the crack growth history can then be determined if the number of cycles to failure, also known as the fatigue life, is known. If the entire crack history is not of interest for a particular test series, the number of cycles when the test is halted must be recorded since this serves as the starting point for reconstructing the crack history. Most likely, the number of cycles between the last marker load and specimen failure is not known; therefore, the accuracy of the number of cycles at each marker load is plus or minus the number of cycles between marker loads. For clarity in describing how the crack history is determined, assume the specimen fails at a (last) marker load. By viewing the fracture surface with the unaided eye, optical microscope, or scanning electron microscope, the previous marker band is found. The number of cycles to obtain the crack length corresponding to this marker band is simply the fatigue life less the number of cycles between marker loads. This procedure is repeated until the marker bands can no longer be detected. The success of marking the fracture surface with marker loads hinges on detection of the marker bands throughout the fatigue life. Furthermore, the marker load is generally not the load cycle of interest; thus, the marker loads should not significantly effect the fatigue crack growth.

Extensive testing of center cracked tension and lap splice joint specimens of aluminum 2024-T3 subject to CA with periodic marker block loading has been completed by The National Aerospace Laboratory of The Netherlands.<sup>14,15</sup> Two separate spectra were tried, one with periodic overloads and the other with periodic blocks of high stress ratio with a constant  $\sigma_{\max}$  but with an increase in  $\sigma_{\min}$ . Overall, neither spectrum effectively marked the fracture surface for small crack lengths, less than 0.5 mm, through failure. The peak load spectrum created traceable marker bands only when the peak load was 140% of the maximum CA load which results in unacceptable crack retardation after application of the peak load. The high stress ratio spectrum created marker bands, but only for crack lengths greater than 0.5 mm.

Thus, it is not surprising that the 130% overload spectrum used here did not adequately mark the fracture surface since the change in the effective stress intensity factor during the overload cycles was insufficient.

The second spectrum, Figure 3, created marker bands through final fracture and to crack lengths as small as 9  $\mu\text{m}$ . In Figure 84, the groups of 10 and 4 are clearly visible; a group of 6 marks could not be seen simply because it was outside the field of view of the SEM at the given magnification. To remove fretting debris and corrosion products, a cleaning protocol was developed using the commercially available MicroClean™, water, acetone, and an ultrasonic cleaner. The ultrasonic cleaner (also known as a sonicator) has a rectangular bath filled with two to three inches of tap water. The specimen is placed in a beaker filled with the desired solution, and then the beaker is placed in the water bath. The specimens were first ultrasonically cleaned in acetone for five minutes; in other words, the beaker was filled with acetone, specimen was put in the beaker, and the beaker was placed in the bath. The optimum soak time in the sonicator for the 2% solution of MicroClean™ and water was unknown; therefore, three different time intervals,

1, 5, and 25 minutes were used to study the effect of the cleaner on the fracture surface. Following the MicroClean™, the specimens were cleaned with isopropyl alcohol in the sonicator for five minutes. Lastly, the specimens were air dried with 100 psi compressed air. As can be seen in the series of fractures surfaces examined, see Appendix D starting with Figure 286 through Figure 300, the longer the specimen was in solution, the cleaner the fracture surface became. The difference between the MicroClean™ 5 and 25-minute soak time was very subtle; thus, all specimens were kept in solution for only 5 minutes.

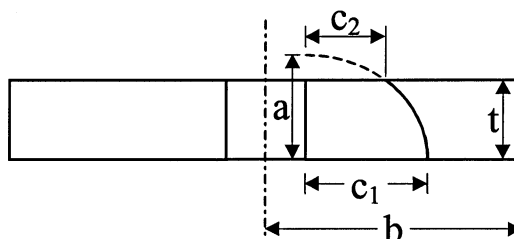
Preservation of marker bands during the fatigue life of a built up structure can be problematic since the interaction of the joined elements can damage or even “erase” the marks on the fracture surface. Furthermore, large-scale deformation of the rivet hole edge can not only erase the marker bands, but also remove or mask the crack nucleation site. The straight shank portion of a countersunk hole is initially perpendicular to the bottom surface of the sheet, which for lack of a better term will be called the faying surface corner. However, as can be seen in Figure 85, after fracture of the specimen, the faying surface corner is well rounded. In several of the fracture surfaces examined, up to 500  $\mu\text{m}$  of the faying surface corner experienced large plastic deformations giving the rounded appearance. In these instances the location of the crack nucleation site was estimated by using the intersection of two lines, one parallel to the bottom sheet (faying surface) and the other parallel to the straight shank portion of the countersunk hole.

The transport aircraft flight spectrum also effectively marked the fracture surface enabling post-test crack growth history reconstruction via the SEM. In Figure 86 and Figure 87, the large fatigue striations are clearly visible and easily detectable for a majority of the fatigue life. These striations are caused by the large  $\Delta K_{\text{eff}}$  due to the peak loads, see Figure 4, at the beginning of the flight spectrum.

Scanned Polaroid or digital images of all of the fracture surfaces examined in either the SEM or optical stereo microscope have been taken and are included in Appendix D.

### 5.2.1. Crack Growth Histories

For each of the cracks in all EIFS-1 through EIFS-12 and EIFS-15, crack history reconstruction in the SEM was attempted. However, not all attempts were successful due to fracture surface damage or in some cases, the cracks were so small the marker bands could not be detected. The crack shape is uniquely defined by the variables shown in the inset drawing where  $c_1$  is the



faying surface crack length,  $c_2$  the free surface crack length,  $a$  the crack depth,  $t$  the sheet thickness, and  $b$  the sheet half width. In Figure 88, 14 crack histories for EIFS-7 are presented. The distribution of crack histories appears to be quite uniform indicating the cracks are growing in a similar manner. The two outlying cracks, lower right portion of Figure 88, nucleated and grew late in the fatigue life of the panel. It is expected that the stress distribution at the crack tip for these two cracks is much different than the other cracks since substantial cracking has already occurred in the joint and the loads have been redistributed. In reference [3], the link between the local stress distribution and the crack shape development was established. Cracks growing in a tensile dominant stress field grow faster in the crack depth direction than crack length direction thus having a high aspect ratio (large  $a/c$ ). When the local stresses are combined tension and bending, the crack grows slower in the depth direction due to the lower stress at the crack depth resulting in low aspect ratio (small  $a/c$ ) cracks. In the simplest form, the bending stress is maximum at the faying surface,  $c_1$  dimension, and linearly decreasing through the thickness; thus, the stress is lowest in the crack depth direction. Indeed, the crack shapes of the two outlying cracks from EIFS-7 had high  $a/c$  ratios.

Crack histories for the remaining joints are in Figure 89 - Figure 95 with the raw data listed in Appendix C. Interestingly, many crack length measurements were obtained for crack lengths less than the inspection system threshold. In other words, using the marker band spectrum and the SEM is the only method for obtaining small crack data for hidden cracks in built-up structure. As can be determined from the test history in Appendix A, crack histories are *not* available for EIFS 1, 2, 5, and 6. Briefly, EIFS-1 experienced uncontrolled edge cracking. EIFS-2 experienced uncontrolled edge cracking but was then reduced in width to eliminate the edge cracks. Subsequent failure was in rivet row B that was not the typical failure row for this joint type. No fatigue data whatsoever is available from EIFS-1 and -2. EIFS-5 and -6 used the 130% marker load spectrum that did not adequately mark the fracture surface. However, NDI measured crack lengths (see section 5.2.3 for details) and TOM measured cracks lengths are available, shown in Figure 96 - Figure 97 and listed in Table 4 and Table 5. These measurements are difficult to interpret since the NDI measured crack lengths should be the crack length at the faying surface,  $c_1$ ; whereas, the TOM measured crack lengths are at the free surface,  $c_2$ . Since the cracks grow with a part-elliptical shape for nearly all their lives, a decrease in the crack length is expected when transitioning from crack measurement by NDI to TOM. Indeed this is evident in several of the crack histories, A10R, A16R, and A7R, in EIFS-5, Figure 96.

## 5.2.2. Crack Growth Rates

From the reconstructed crack histories, shown in Figure 88 - Figure 95, the crack growth rates were calculated using the secant method, Eqn (5), as prescribed in ASTM E647-95A. Since a good estimate of the  $K$  solution is not known, the crack growth rates are plotted versus the average faying surface crack length, Eqn. (4).

$$\bar{c}_1 = \frac{1}{2}(c_{i+1} + c_i) \quad (4)$$

$$\frac{dc_1}{dN} = \frac{(c_{i+1} - c_i)}{(N_{i+1} - N_i)} \quad (5)$$

The crack growth rate vs. average faying surface crack length for EIFS-3, -4, -7, -8, -9, -10, -11, and -15 are shown in Figure 98 - Figure 105. In view of making crack growth predictions of the fatigue performance of these lap joints, the behavior of the cracks in a given joint ideally should be similar. Of course this is not the case due to scatter in crack nucleation times; therefore the fatigue lives of each crack will be different. Furthermore, variation in crack propagation is also possible which is counter-intuitive. The scatter in crack propagation is due to the changing stress state near the crack tip. Specifically, the fatigue critical rivet row, generally the first row in the joint, is subject to tension stress due to the remote tensile loading, secondary bending due to the eccentricity of the joint, bearing due to the load transfer through the rivets, shear stress due to load transmission by friction, and residual stress around the rivet hole due to rivet installation. In the uncracked state, all five stress contributions are active. Although the magnitude has yet to be determined, except for the remote tensile stress, stresses change with increasing crack length. When a large portion of the joint is cracked, the bending stiffness decreases causing a reduction in the bending stress. In addition, the bending stress is varying through the width of the joint depending on which edge "treatments" are used to prevent edge cracking. The bearing stress also decreases with increasing crack length since the rivet load is redistributed to other less or uncracked rivets. The load transmission by friction decreases with crack length as well due to the reduction of clamping force the rivet exerts on the two adjoining sheets. Lastly, the residual stress around the rivet hole due to rivet installation is maximum in compression at the hole edge and decreases with increasing distance from the hole edge. In addition, cracking in the residual stress zone causes redistribution of the stresses again adding to the changing nature of the stress field around the rivet hole.

With the aid of the reconstructed crack histories, evaluations of the observed crack growth rates are possible. For EIFS-3, see Figure 89 and Figure 98, four rather distinct crack growth curves exist which makes predictions problematic. The limited number of reconstructed crack histories is a result of the short time available for crack nucleation and growth since the test was stopped at 170,000 cycles to prohibit edge cracking from interfering with the fatigue behavior of the cracks growing at the rivet holes away from the specimen edge. Cracking is occurring in two different rivet rows, C and D, where the secondary bending stresses are unequal due to the asymmetry of the joint. Cracking first started in row D, crack 3D15L, and then progressed to row C, 3C17R. The bending stress in row C is less than that in row D; therefore, a lower growth rate in the former is expected and evident when comparing 3D15L and 3C17R. The behavior of 3C14R is odd in that it is a relatively small crack, but grows at a faster rate than another crack in EIFS-3. Possibly, load is being shed from adjacent rivets causing a larger bearing stress contribution than experienced by the other crack locations. An interesting observation of the small crack behavior, cracks less than 1.0 mm, is a nearly constant growth rate as exhibited by all cracks in EIFS-3 except for 3C14R.

For EIFS-4, see Figure 90 and Figure 99, the cracking behavior of the four cracks is similar. The failure mode is slightly different than EIFS-3 in that no cracks in row D were detected. Cracks were first detected in 4C14 and 4C24; however, due to extensive fracture surface damage, the crack history could not be reconstructed. Similarly to EIFS-3, the growth rates are fairly constant for cracks lengths less than 1.0 mm.

By far, the fractographic examination of EIFS-7 was the most successful of all joints under consideration. Fourteen crack histories were reconstructed as shown in Figure 88 with the corresponding crack growth rates shown in Figure 100. The crack nucleation times range from under 25,000 cycles to over 100,000 cycles indicating a significant variation in the surface quality at each of the fastener holes. Crack nucleation is a surface phenomenon, not a bulk material property as is the crack growth behavior; thus, variation in the time to crack nucleation can only be attributed to surface quality. The surface quality can be affected by specimen fabrication; in other words, how were the rivet holes drilled and countersunk, are the fasteners close-fit or interference fit, is the faying surface sealant evenly distributed around the fastener hole. For cracks that may have nucleated at the faying surface, the condition of the sheet surface is of prime importance.

All of the cracks in EIFS-7 nucleated in the upper rivet row, row A. The general trend of the crack histories, Figure 88, are similar; however, 7A17L initiates later in the fatigue life of the joint and when the crack is about 0.8 mm, it grows at a faster rate than the other cracks indicating a difference in the crack driving force. Where the crack growth rate of 7A17L diverges from the general trend of the other 13 cracks, 7A17R is approximately twice as large as 7A17L; thus the ligament between rivets 17 and 18 is becoming more compliant and the load is shed to the ligament between rivets 16 and 17. Furthermore, the joint is substantially cracked with the five rivet holes to the left of A17 being cracked. Two cracks, 7A16R and 7A17R, nucleated very late in the fatigue life of the joint; however, they appear to be growing at the same rate as the other cracks. The crack growth rate data, Figure 100, is bi-modal in that cracks less than 1.0 mm grow at a nearly constant rate; whereas, cracks greater than 1.0 mm grow at an increasing rate with crack length. As the corner cracks grow, they get closer to the high stress concentration at the knuckle of the countersunk hole which is possibly the cause for dramatic shift in crack growth rate behavior.

The data for EIFS-8, crack growth histories shown in Figure 91 and crack growth rates Figure 101, is limited since the test was halted at 130,000 cycles in an attempt to avoid damaging the rivet hole edges and fracture surfaces. Crack 8A19L grew very late in the fatigue life and interestingly, this crack nucleated and grew under the edge block which is intended to stop crack growth at the outer columns of rivets, rivets 1 and 19. It is difficult to determine the stress system that 8A19L experienced since the edge blocks reduce the secondary bending and increase load transmission by friction due to high clamping forces. It is sufficient to conclude the stresses at the outer column rivets are different than those at the other rivets in the same row. The crack growth rates

again appear to be constant with increasing crack length for cracks less than 1.0 mm with increasing growth rates with increasing crack length for cracks greater than 1.0 mm.

The EIFS-9 data, crack growth histories shown in Figure 92 and crack growth rates Figure 102, is presented for completeness only since this joint failed in row B which is not the fatigue critical rivet row. A good estimate of the stress system and thus crack driving force is questionable for the cracks in row A with substantial cracking in row B.

Edge cracking was also prevalent in EIFS-10; however, the crack data, crack histories in Figure 93 and crack growth rates Figure 103, is of value since the edge cracking was controlled. The first edge crack was found at 10B1L and was small; thus, in all likelihood, this small edge crack did not affect the crack driving force in the anticipated failure rows A or F. The panel was reduced in width thereby removing the outer most rivet columns and thus the edge crack at 10B1L. Six crack growth histories were reconstructed and are quite similar. The crack growth rates, in general, increase with increasing crack length, which is different from what was observed for joint types I and II. A possible explanation of this behavior is offered. Joint types I and II (EIFS-1 through -8) are longitudinal lap-splices; whereas, Joint type III (EIFS-9 through -12) are longitudinal butt splices. The upper and lower sheets in the former joints are thinner than the latter, 0.063" compared to 0.09". Also, since the joint type III has six rivet rows, the secondary bending is less than that in joint type I with four rivet rows and joint type II with three rivet rows. The higher bending in joint types I and II causes a reduced crack growth rate through the thickness of the sheet since the bending stress is less at the "a" crack tip than at the  $c_1$  crack tip. As a result, the crack maintains a low aspect ratio ( $a/c_1$ ) and grows at a slow rate. Conversely, in the type III joint with low bending stress and thicker sheets, the crack tip at "a" is not pinned down and the crack quickly grows through the thickness. This behavior is characteristic of the growth of corner cracks in tensile dominant stress fields.

The reconstructed crack histories and crack growth rates for EIFS-11 are shown in Figure 94 and Figure 104, respectively. Except for 11F6R, all the cracks nucleated late and grew quickly. The scatter in the crack growth rates is larger than that of the cracks discussed above. From the data presented in Appendix C, the y-location, which is the distance from the faying surface to the location the marker band was found in the sheet thickness direction, is quite large. Recall, all the cracks propagate as part-elliptical cracks; thus, a change in crack length,  $\Delta c_1$ , for example, might be too small if the first  $c_1$  measurement is at the faying surface and the subsequent  $c_1$  measurement is far away from the faying surface. Every attempt was made to measure the marker bands at the faying surface; however, as shown in Appendix C, this was not always possible.

The reconstructed crack histories and crack growth rates for EIFS-15 are shown in Figure 95 and Figure 105, respectively. Two distributions of cracks are evident, cracks 15E2R, 15E16L, and 15E29R nucleated later than the other cracks. However, all the cracks appear to be growing at a similar rate indicating a similar crack driving force amongst all cracks examined. The marker bands created by the flight spectrum, shown in Figure 4, were rather distinct as shown in Figure 86 and Figure 87.

To further evaluate the data produced by the NDI system and TOM, the crack growth rate vs. average crack length is shown in Figure 106 and Figure 107 for EIFS-5 and EIFS-6, respectively. The scatter in data is tremendous primarily due to errors in crack length measurement. In general, the crack growth rate is nearly constant with increasing crack length. This behavior has no physical basis and this data has no technical use.

The magnitude and range of crack growth rate data derived from the reconstructed crack histories is similar to that of the Newman and Edwards<sup>16</sup> AGARD study of 1988 and Piascik<sup>17</sup> transport aircraft teardown investigation in 1997. All three data sets are shown in Figure 108. Comparisons of this sort are problematic since the test conditions of each data set are not similar. The AGARD study used single edge notch tension (SENT) specimens which nucleated surface cracks along the bore of the hole. The Piascik data are for corner cracks nucleating from Briles™ rivet holes. Typically, crack growth rates are plotted against the change in the stress intensity

factor ( $da/dN$  vs.  $\Delta K$ ); however, of the three data sets, a good estimate of the  $K$  solution is only known for the SENT specimen. As a result, the crack growth rates are plotted against the average crack length in Figure 108.

The scatter in all three data sets is largest at the lower crack lengths which can be a result of measuring error or the small crack effect. Recall, the small crack effect is evident when cracks in nominally similar test specimens with a given  $\Delta K$  grow at an accelerated rate when compared to the long crack data. The smallest crack lengths measured were 4.7, 50, and 36  $\mu\text{m}$  for the AGARD, Piascik, EIFS data sets, respectively. The latter two data sets used a marker spectrum and the SEM to reconstruct the crack history post test; however, the AGARD investigation used the replica technique since the crack nucleation site was accessible. Thus, the large difference in smallest detected crack is expected. Although the lower limits of the EIFS and Piascik data is 7-10 times as large as the AGARD data, they are still in the small crack regime. Furthermore, the AGARD and Piascik data appear to be of the same distribution; however, due to the differences in applied stress levels and the geometric correction factor, additional conclusions can only be conjecture. The EIFS data is bi-modal exhibiting a rather flat slope for cracks less than 1.0 mm and an increasing slope for cracks greater than 1.0 mm. This bi-modality is not seen in the other two data sets.

For 2024-T3 aluminum, a typical crack growth rate plot is shown in Figure 109<sup>11</sup>. A  $K$  estimate was made for joint type II using bypass, bending, and bearing stress ratios of 0.654, 0.395, and 1.978, respectively. The stresses were normalized by the 15 ksi (103.4 MPa) remote tension stress to obtain the stress ratios. The joint was idealized as a finite width plate with a single, centrally located hole with two diametrically opposed corner cracks growing in the plane of the net section of the plate. The geometry of the idealized plate had a width = 28.96 mm, thickness = 1.6 mm, rivet hole diameter = 4.76 mm. For the given remote tensile stress and a quarter-circular crack shape, the stress intensity factor is  $7.23 \text{ MPa}\sqrt{\text{m}}$ . Plotting this  $K$  value with the handbook material data, see Figure 109, indicates this  $K$  value is in the crack growth region between the two “knees” in the curve. Thus, the bi-modal behavior seen in the EIFS crack growth rate data can simply be due to the basic material properties of 2024-T3 aluminum. For the given stress levels and SENT geometry used in the AGARD study, the  $\Delta K$  values were not large enough to clearly show the bi-modal behavior in the crack growth rate data. The Piascik data is limited in that a maximum of six crack length measurements are possible since only six marker band loading blocks were in the entire spectrum. Although six measurements were possible, the most recorded for any single crack was four. As a result, the change in crack length between measurements,  $\Delta a$ , can be as large as 1 – 2 mm; thus, the data resolution is much lower than obtained in the AGARD and EIFS efforts. For the data shown in Figure 109, the  $\Delta a$  was approximately 0.25 mm. Had the Piascik data more resolution, the bi-modal crack growth behavior may have been evident.

### **5.2.3. Evaluation of Rotating Self-Nulling Eddy Current Probe System**

The NASA Langley Research Center (NASA-LaRC) developed the Rotating Self-Nulling Eddy Current Probe System (RPS) to detect small fatigue cracks around mechanical fasteners which remain hidden by the countersunk head of the fastener. The RPS initially showed great promise obtaining a probability of detection (POD) of 90/95% for 0.032” fatigue cracks during a POD study conducted at the FAA NDI Validation Center in Albuquerque, New Mexico. This represents a 20% decrease in detection size as compared to the POD study reported in reference [2]. The RPS was to be used in this effort for detection and measurement of cracks ranging in length from 0.032” – 0.10”. Once the crack was greater than 0.10”, a traveling optical microscope would be used to measure the crack length. The output of the RPS is a measured voltage. This voltage is compared to output voltage from a reference standard with a known crack size. The reference standards provided by LaRC are shown in Figure 110 for joint types I, II, and IV which had 0.063”

sheets and NAS1097-AD6 rivets and Figure 111 for joint type III which had 0.09" sheets and proprietary Boeing flush head fasteners.

The RPS was used for EIFS-1 through EIFS-12, but could not be used for EIFS-13 through EIFS-16 since the cracks in these latter joints occurred in the doubler which had the driven head of the rivet. Recall that the test order was EIFS-5 through EIFS-8, then EIFS-1 through EIFS-4, and finally EIFS-9 through EIFS-16. For EIFS-5 and -6, the RPS and TOM were the only techniques used to measure the crack length in time. The accuracy of the RPS was to be evaluated by comparing the RPS measured crack lengths of EIFS-5 or EIFS-6 to those determined from fractographic analysis using the SEM. Unfortunately, since the 130% overload spectrum did not mark the fracture surface adequately, no crack lengths could be measured in the SEM. After switching to the 10-4-6 marker spectrum, EIFS-7 was tested and fractographic analysis completed. Of the 38 possible crack nucleation sites, 15 crack histories were reconstructed. A comparison between the RPS and SEM results is shown in Figure 112. Similar RPS performance was observed for the 14 other cracks in EIFS-7. The RPS consistently underestimated the crack length and did not detect several cracks, which were well above the 0.032" detection threshold. Due to inaccuracies in crack detection and measurement by the RPS, the primary technique for obtaining the crack growth history was post-test fractographic analysis of the fracture surface. Even though the RPS measurements were in question, it was still used on EIFS-1 through EIFS-12 in hopes that the data, listed in Appendix E might be useful in developing future enhancements to the system.

### 5.3. Fatigue Crack Growth Predictions

Fatigue life predictions for each of the four joint types were made using AFGROW which makes use of the Component Object Model (COM) technology. The COM implementation in AFGROW allows the EIFS to be determined without the analyst performing thousands of predictions requiring user interaction.<sup>18</sup> Specifically, using Microsoft Excel and AFGROW, an initial guess at the EIFS is made. The fatigue life is calculated in AFGROW with output going back to Excel. A comparison is made between the predicted and test data. The EIFS is adjusted to reduce the error and the process repeats until the user specified error tolerance is obtained. No analyst interaction is required. In FASTRAN, the analyst is required to manually adjust the EIFS with each iteration. For this reason, predictions for only one type II joint have been completed using FASTRAN.<sup>21</sup> As mentioned previously, not all crack histories could be reconstructed; thus, EIFS calculations using AFGROW were made for all the cracks whose histories were available.

In its most basic formulation, the stress intensity factor range,  $\Delta K$  is calculated by

$$\Delta K = \Delta \sigma \sqrt{\pi a} \beta \quad (6)$$

where

- $\Delta \sigma$      $\equiv$     Applied stress range
- $a$          $\equiv$     Crack length or depth
- $\beta$          $\equiv$     Geometry correction factor

Both FASTRAN and AFGROW convert the  $\Delta K$  to the effective stress intensity factor range,  $\Delta K_{\text{eff}}$  via their respective crack closure models which account for load interaction effects. Using the  $\Delta K_{\text{eff}}$  and crack growth rate data for the given material, the crack growth increment per load cycle is obtained by means of a table look-up procedure. For additional information and a comparison of these crack growth codes, see reference [19].

Based on the fractographic evidence gained in this investigation and others<sup>20</sup>, the initial flaw shape is assumed to be quarter circular for all EIFS predictions. The crack shape is permitted to develop naturally during its life; in other words, the crack shape is not controlled or prescribed. Once the crack grows through the thickness, it continues to propagate with a part-elliptical shape.

For the part-through stage of crack growth, the well-known Raju/Newman equations are used. For the through crack portion of the fatigue life, K solutions from reference [20] are used.

Currently, the fatigue crack growth prediction codes in the public domain cannot account for multiple part-through cracks growing in one structural detail. Therefore, the cracks in the four complex joint types are modeled as two diametrically opposed part-through cracks growing from a centrally located straight shank hole in a finite width plate subject to remote tension, secondary bending, and bearing, see Figure 113. For each of the joint types, the idealized model dimensions and stress levels are listed in Table 5. The bypass, bending, and bearing stresses are normalized by the remote applied tensile stress to give the corresponding stress ratios shown in Table 1.

The bending stress ratio is calculated from the strain data using Eqn. (1) for the gages closest to the critical rivet row. The bending stresses are higher in all likelihood since the strain gradient is very steep and the strain gages are measuring an average value over the grid area of the gage. Furthermore, the bending stress doesn't scale linearly with the applied remote tensile stress; thus for joint type II with a remote tensile stress of 103.4 MPa, the bending stress ratio is 0.36.

The percent load transfer, listed in Table 6, is the portion of the total load transferred through each individual fastener and is calculated using

$$\gamma = \frac{p_s}{P_a} \quad (7)$$

$$p_s = \frac{P_s}{s} \quad (8)$$

$$P_a = t * \sigma_o \quad (9)$$

where

- $\sigma_o$      $\equiv$     Applied stress
- $\gamma$         $\equiv$     Percent load transfer
- $P_a$       $\equiv$     Applied load per inch
- $P_s$       $\equiv$     Fastener shear at critical rivet row<sup>21</sup>
- $p_s$       $\equiv$     Average fastener load per inch
- $t$         $\equiv$     Sheet thickness
- $s$         $\equiv$     Rivet row pitch

The bearing stress is estimated using a basic mechanics of materials approach and is calculated as follows.

$$\sigma_{brg} = \frac{\gamma P}{ntD} \quad (10)$$

where

- $\sigma_{brg}$     $\equiv$     Average bearing stress
- $P$         $\equiv$     Applied load
- $n$         $\equiv$     Number of rivets per rivet row
- $D$         $\equiv$     Hole diameter

The bypass stress,  $\sigma_{bypass}$ , is similarly calculated using



$$\sigma_{\text{bypass}} = \frac{(1-\gamma)P}{tW} \quad (11)$$

The FASTRAN analysis conducted by The Boeing Company used similar input data as described above; however, the crack was modeled differently in that the through crack portion of the fatigue life was modeled as a straight through crack. The predictions did not correlate well with the experimental data; therefore, Boeing developed an additional geometry correction factor to account for effects of rivet interference, friction between contact surfaces, and load shedding in order to increase the correlation between predicted and actual lives. This correction factor,  $\beta_u$ , is shown in Figure 114. To aid in comparing the AFGROW and FASTRAN results,  $\beta_u$  was also used for the AFGROW predictions. Since the AFGROW predictions are completed in an entirely automated procedure, calculating an EIFS for each crack length-cycle count pair for a given crack is possible. Thus, the EIFS determined by AFGROW is the average value from all EIFS' calculated for the given crack. Automated EIFS calculation using FASTRAN is currently not possible; therefore, the FASTRAN EIFS is one value that appears to match most of the crack growth curve for a given crack. The difference in the two approaches can be seen in Figure 115 and Figure 116. Comparing the FASTRAN and AFGROW predictions of 7A6R, using the former code, one prediction is made; whereas using the latter, 50 predictions are made to determine the EIFS.

Enforcing a high accuracy on the EIFS calculations results in long computation times for each crack length-cycle count pair. To reduce the computation time, the EIFS calculation was stopped when the predicted crack length and cycle count was within 2% of the SEM data. An initial guess was made for the first crack length-cycle count pair and AFGROW iterates on the initial crack length and depth until the desired correlation with the experimental data is obtained. Recall, the initial flaw shape is assumed to be quarter circular based on fractographic results here, Appendix D, and in reference [20]. The source code for the EIFS iteration algorithm is written in Visual Basic for Applications (VBA) and is listed in Appendix F. AFGROW version 3.9844.11.8 was used for all calculations and can be obtained at <http://fibec.flight.wpafb.af.mil/fibec/afgrow.html>. The mean and standard deviation in EIFS is listed in Table 7. The statistical parameters were calculated using only the information from those cracks for which crack history reconstruction data exists, see Figure 88 - Figure 95. The mean EIFS for joint types I, II, and III was 12.572  $\mu\text{m}$  and standard deviation of 4.122  $\mu\text{m}$ . The mean EIFS for the one joint type IV analyzed was 301.560  $\mu\text{m}$ , which is much larger than the other three joint types. The standard deviation was 217.512  $\mu\text{m}$ . The large standard deviation illustrates the sensitivity of the EIFS calculation on small perturbations in the EIFS. This sensitivity was not observed for joint types I-III where load sequence effects were negligible. It is interesting to note that the K solutions for the joint type IV are more accurate than those for joint types I-III since the cracks in the former are growing from straight shank holes. An initial flaw size of 301.560  $\mu\text{m}$  would have been easily visible during the fractographic examination; however, it was not. Thus, the K solution is too low indicating the use of  $\beta_u$  for joint type IV might be inappropriate.

Several observations can be made regarding the AFGROW predictions in Figure 116. The crack growth curves for the smaller crack lengths, less than 0.02 in for 7A6R, show a smaller standard deviation in EIFS than the larger crack lengths. The correlation with the SEM data is worst when the crack length is less than the sheet thickness, which was the case for all EIFS calculations. Once the "a" crack tip intersects the countersunk edge, the K solutions used here don't adequately represent the crack driving force which can be seen by the large difference between the measured and predicted crack history.

In examining the mean EIFS vs. final crack length data in Figure 117, no systematic trend is apparent except that the largest mean EIFS occurs at the larger crack lengths, but not at the largest crack length. Moreover, the longest crack lengths don't exhibit the largest standard deviation in EIFS, see Figure 118. The largest mean EIFS and standard deviation in EIFS is when the final crack lengths vary from 1.0 – 3.0 mm. All that is known is that the crack is in transition from a part-elliptical corner crack to a through crack with a straight front. It is expected that the crack growth calculations for the larger crack lengths are more susceptible to variability in

the final EIFS. For the larger cracks, multiple K solutions are used; double corner crack at a hole, part-elliptical through crack, and finally a through crack with a straight front. In addition, the local stress field changes through the ligament between adjacent rivets. Specifically, pin loading and residual stresses due to rivet installation exist near the rivet hole but not usually more than one rivet diameter away from the hole. The bending stress is maximum near the rivet hole as well since the rivet is offering bending restraint. The change in local stress field between adjacent rivets is not accounted for in the EIFS calculations. Much of the fatigue life is spent while the cracks are in the long crack threshold regime where the crack growth rate data is most unreliable.

As mentioned previously, most of the fatigue life is consumed while the cracks are part-elliptical corner cracks at a (countersunk) hole. Recall, the Newman/Raju solutions are used for predicting this portion of the fatigue life; thus, errors in these solutions will have a large effect on the EIFS calculations. As was shown in reference [22], the errors in the Newman/Raju solutions can be as large as 30% for some crack geometries and load conditions. Thus, the large standard deviations in EIFS calculations could also be due to this error.

A comparison, shown in Figure 119, is made of a part-elliptical corner crack with  $a/c = 0.6$  at a straight shank hole and a countersunk hole. The global geometry used for this comparison was the same as that used in the joint type II EIFS calculations. The straight shank hole solution is much higher than the countersunk hole for remote tension and bending. In other words, the EIFS calculations made here are using an over-conservative K solution in the small crack regime,  $c_1 < 1.0$  mm. The end result is an EIFS value that is smaller than it should be. Care must be taken in using this EIFS value for fatigue life predictions of structure other than the structure from which it was derived. Furthermore, since the EIFS is dependent on the crack growth model and all inputs to the model, the EIFS should only be used for geometrically similar and likely loaded structure.

To mitigate the affect of the compounding error associated with the EIFS determined from the larger cracks, the EIFS mean and standard deviation values are recalculated only for crack lengths less than 1.27 mm, see Table 8. Selecting 1.27 mm is arbitrary, but ensures only one K solution is used in the EIFS calculation and that the cracks are most likely still small part-through cracks hidden by the countersunk rivet head. The mean EIFS for joint types I, II, and III was  $10.947 \mu\text{m}$  and standard deviation of  $1.599 \mu\text{m}$ . The reduction in the mean EIFS was small; however, the standard deviation in mean EIFS values is for the most part greatly reduced. The mean EIFS for the one joint type IV analyzed was  $86.853 \mu\text{m}$ , which is much larger than the other three joint types. The standard deviation was  $70.575 \mu\text{m}$ . Further evaluation of the calculated EIFS will be problematic until a more accurate K solution is obtained.

## 5.4. Comparison between AFGROW and FASTRAN

Eight cracks from EIFS-7, listed in Table 9, were used to compare the crack growth algorithms implemented in AFGROW and FASTRAN. The differences between the two EIFS calculations have a wide range from  $0.1 \mu\text{m}$  for 7A7R to  $22.1 \mu\text{m}$  for 7A14L. The spectrum used for EIFS-7 was the 10-4-6 marker spectrum and was shown in reference [20] not to affect the crack growth rate. In other words, this spectrum does not result in any load sequence effects; thus, plasticity induced crack closure should be minimal. As a result, the only parameters contributing to the differences in the predictions by the two codes are the stress intensity range,  $\Delta K$  (since crack closure is minimal,  $\Delta K \approx \Delta K_{\text{eff}}$ ), and stop criteria for determining the EIFS.

Both codes use the Newman/Raju double corner crack at a straight shank hole K solution. However, AFGROW does not use the stress ratio based fitting factor,  $\beta_R$ , developed by Newman and Raju in [23]. The  $\beta_R$  parameter is used to account for the plane strain/plane stress transition that occurs at the free surface of the material. To account for this behavior, AFGROW does not use the parametric angle of the ellipse at the  $a$  and  $c_1$  crack tips,  $0^\circ$  and  $90^\circ$ ; but instead uses  $2^\circ$  and  $88^\circ$ . The affect of both techniques is the same;  $\Delta K$  is slightly reduced. In addition, FASTRAN assumes the crack shape,  $a/c_1$ , is constant; whereas, AFGROW allows the crack shape to develop naturally. Furthermore, when the part-through crack grows through the

thickness and transitions to a through crack, FASTRAN assumes a through crack with a straight front while AFGROW uses the actual crack shape which is a through crack with an oblique or part-elliptical crack front.

Using FASTRAN, the EIFS calculation is halted when by visual examination the predicted and measured crack growth histories show good correlation. Although this method is acceptable and rational, it is not repeatable. In other words, for a given set of data various analysts will determine a different EIFS distribution. On the other hand, AFGROW determines the EIFS for each data point in the crack growth history within an analyst defined error tolerance; thus, different analyst will calculate the same EIFS distribution if both are using the same error tolerance.

No attempt is made to determine which code yields the most accurate predictions; however, the AFGROW analyses use a more complete K solution than FASTRAN as outlined above. Furthermore, the AFGROW analyses are repeatable which is a distinct advantage.

## 6. Conclusion

Four different transport aircraft fuselage flat panel skin joints were successfully fatigue tested. The four joint types represent joint designs used in many commercial aircraft that are in-service today. The joint configurations are two longitudinal lap-splice (type I and II), one longitudinal butt splice (type III), and one circumferential butt splice (type IV) joints. For joint types I-III a blocked programmed spectrum was used which adequately marked the fracture surface to aid in post test crack history reconstruction. The type four joint used an operational loading spectrum representative of a transport aircraft fuselage spectrum. The type IV spectrum also adequately marked the fracture surface. Due to the dependence of the EIFS calculation on the crack growth model and all inputs to the crack growth model, the EIFS should only be used for geometrically similar structure subject to the same or similar load conditions as those used in this study. The conclusions are separated into two categories, testing and analysis, as listed below.

### 6.1. Testing

**Critical Rivet Row:** The fatigue critical rivet row(s) for joint type I was row C, joint types II and III were the outer rows, and joint type IV were the inner most rows. The critical row of the type I and IV joints was not expected. For the former, the calculated stresses in Row C were the same or lower than those in row D; thus initial hole quality dictated which row was critical.

**Finite Width Effect:** The finite width effect which results in edge cracking in the critical row of the outer most column of rivets was eliminated by one of three methods; cutting a dog-bone shape in the skins, over-sizing and -expanding the rivets at the specimen edges, first and last column of rivets, or a combination of these two techniques.

**Strain Surveys:** The strain surveys showed average bending factors,  $k (= \sigma_{\text{bending}} / \sigma_{\text{tension}})$ , of 0.34, 0.27, 0.20, 0.28 for joint types I-IV, respectively. The methods used to eliminate edge cracking did not affect the strains away from the outer column of rivets; thus MSD developed in the joints.

**Fractography:** The 10-4-6 marker spectrum adequately marked the fracture surface allowing crack history reconstruction to crack sizes as small as 20  $\mu\text{m}$ . The transport aircraft spectrum performed similarly. On average, the smallest size measured for a given crack ranged from 100 – 500  $\mu\text{m}$  due to hole and fracture surface damage during fatigue loading or final fracture.

### 6.2. Analysis

**Analysis Codes:** The equivalent initial flaw size using the FASTRAN and AFGROW was  $3.6 \mu\text{m} \leq c_i \leq 29.2 \mu\text{m}$  and  $3.31 \mu\text{m} \leq c_i \leq 56.43 \mu\text{m}$ , respectively. EIFS calculations using AFGROW was automated using the Component Object Model technology and required no user input once the analysis was started.

**Stress Intensity Factor Solutions:** Fractographic investigations showed the cracks nucleated as corner cracks for the most part; however, a few surface cracks nucleated on the hole bore and on the faying surface. The corner cracks were part-elliptical, grew through the thickness, then transitioned to a through crack with a part-elliptical front. In both AFGROW and FASTRAN, the Newman/Raju solutions were used for the corner crack phase. For the part-elliptical through crack phase, AFGROW used the K solution developed in reference 20; whereas, FASTRAN used the (straight) through crack at a hole solution of Newman. An additional geometric correction factor,  $\beta_u$  had to be developed in order to increase the correlation between predicted and experimental crack growth behavior.

**Closure Models:** The closure models of FASTRAN and AFGROW were only used on the type IV joints since plasticity induced crack closure in the 10-4-6 spectrum is negligible.<sup>20</sup> Both models performed equally well as expected.

## 7. Recommendation

Future work is required in several areas to increase the correlation between predicted and actual crack growth histories from the four joint types. The most glaring need is to use the most appropriate K solution, that being double corner cracks growing from a countersunk hole subject to general loading. This work is underway in a separate AFRL/VASM effort. Furthermore, a limited number of cracks nucleated and grew as surface cracks along the rivet hole bore or along the faying surface of the sheet. K solutions for these two cases in a countersunk hole are also needed. The residual stresses due to rivet installation have not adequately been considered here. The  $\beta_u$  correction factor attempts to account for "all" unknown variables in the EIFS predictions; however, this parameter is only a fitting factor with no physical basis.

Reconstructing the crack growth history for small cracks, less than 1.0 mm, was challenging due to the severe damage to the area near the crack nucleation site. Plastic deformation of the hole and crack face contact are the suspected root cause. If the panel were prohibited from failing by fatigue or by static overload, the hole would not have significant plastic deformation. In hindsight, the method used by Piascik in reference [17] should have been used to expose the fracture surfaces. In addition, the 10-4-6 marker spectrum worked best for crack lengths ranging from 0.5 - 4.0 mm. For the shorter crack lengths, the marker bands are not very distinct indicating the  $\Delta K_{eff}$  needs to be increased but care must be taken not to cause retardation. For the longer crack lengths, the marker bands look very similar to the baseline cycles, modifying the marker sequence or relation between cycles at  $S_{max}$  and 75%  $S_{max}$  is a promising approach. An optimized marker spectrum that adequately marks the fracture surface for both short and long crack lengths is currently under development in AFRL/VASM.

A more thorough comparison of the closure models in FASTRAN and AFGROW is needed. Incorporating the Newman closure model into AFGROW is the most efficient way to conduct this comparison since the Component Object Model capability in AFGROW can be exploited. This effort is currently underway in AFRL/VASM.

## 8. References

- 
- <sup>1</sup> Rudd, J. and Gray, T., "Equivalent Initial Quality Method," AFFDL-TM-76-83-FBE, 1976.
  - <sup>2</sup> Hagemaijer, D., "Eddy Current Detection of Short Cracks Under Installed Fasteners." Materials Evaluation, 55, No. 1, 1997.
  - <sup>3</sup> Fawaz, S., Schijve, J., and de Koning, A., "Fatigue Crack Growth in Riveted Lap-Splice Joints," Proc. of the 19<sup>th</sup> ICAF Symposium, EMAS, Scotland, UK, 1997.
  - <sup>4</sup> Yu, J., "Equivalent Initial Flaw Size Study Test Plan," The Boeing Company, USA, 1997.
  - <sup>5</sup> Müller, Richard Paul Gerhard. An Experimental and Analytical Investigation on the Fatigue Behaviour of Fuselage Riveted Lap Joints, The Significance of the Rivet Squeeze Force, and a Comparison of 2024-T3 and Glare 3. Diss. Delft University of Technology, 1995. Delft, NL.
  - <sup>6</sup> Wit, G., MSD in Fuselage Lap Joints - Requirements for Inspection Intervals for Typical Fuselage Lap Joint Panels with Multiple Site Damage, LR-697, Delft Univ. of Tech., 1992.
  - <sup>7</sup> Vlieger, H. Results of Uniaxial and Biaxial Tests on Riveted Fuselage Lap Joint Specimens, Hampton, VA, NASA-CP-3274, 1994.
  - <sup>8</sup> Mayville, R. and Warren, T. "A Laboratory Study of Fracture in the Presence of Lap Splice Multiple Site Damage," Eds. S. N. Atluri, S. G. Sampath, and P. Tong. Structural Integrity of Aging Airplanes, Springer Series in Computational Mechanics. Berlin: Springer Verlag, 1991.
  - <sup>9</sup> Eastaugh, G., Simpson, D., Straznicki, P., and Wakeman, R. "A Special Uniaxial Coupon Test Specimen for the Simulation of Multiple Site Fatigue Crack Growth and Link-Up in Fuselage Skin Splices," AGARD-CP-568. Neuilly-Sur-Seine, Fr. 1995.
  - <sup>10</sup> Newman Jr., J. C., "FASTRAN-II – A Fatigue Crack Growth Structural Analysis Program, NASA TM-104159, February 1992.
  - <sup>11</sup> Harter, James A., "AFGROW Users Guide and Technical Manual," AFRL-VA-WP-TR-1999-3016, February 1999.
  - <sup>12</sup> Schijve, J., Some Elementary Calculations on Secondary Bending in Simple Lap Joints, NLR-TR-72036. Amsterdam, NL: National Aerospace Laboratory, 1972.
  - <sup>13</sup> United States. Dept. of Defense. Metallic Materials and Elements for Aerospace Vehicle Structures, MIL-HDBK-5G. 1 Nov 1994.
  - <sup>14</sup> Wanhill, R. J. H. Damage Tolerance Engineering Property Evaluations of Aerospace Aluminum Alloys with Emphasis on Fatigue Crack Growth, NLR-TR-94177L. Amsterdam: National Laboratory of The Netherlands, 1994.
  - <sup>15</sup> Mussert, K. M. Fracture Surface Marking of Alclad 2024-T3 Sheet, NLR-CR-94456C, Amsterdam: National Laboratory of The Netherlands, 1994.
  - <sup>16</sup> Newman Jr., J. C. and P. R. Edwards, "Short-Crack Growth Behaviour in an Aluminum Alloy-An AGARD Cooperative Test Programme," AGARD-R-732, Specialised Printing Services Limited, Essex, 1988.
  - <sup>17</sup> Piascik, Robert S. and Scott A. Willard. The Growth of Multi-Site Damage in Fuselage Lap Joints. Proc. of The 2ND Joint NASA/FAA/DoD Conference on Aging Aircraft, Aug 31- Sep 3, 1998, Williamsburg, VA. NASA/CP-1999-208982.

---

<sup>18</sup> Harter, James, A. and Alexander Litvinov. "Development of Structural Integrity Analysis Methods for Aircraft Structures: AFGROW COM Server Interface Manual, Release 7." AFRL-VA-WP-TR-1999-xxxx, 1999.

<sup>19</sup> Harter, James, A. "Comparison of Contemporary FCG Life Prediction Tools." International Journal of Fatigue, 21 (1999):S181-S185.

<sup>20</sup> Fawaz, Scott Anthony. Fatigue Crack Growth in Riveted Joints. Diss. Delft University of Technology, 1997. Delft, NL.

<sup>21</sup> Hsu, Ching and Jin Yu, "Initial Quality of Typical Aircraft Fuselage Splice Joints Investigated in WFD Program," International Conference on Computational Engineering Science, October 6-9, 1998, Atlanta, GA.

<sup>22</sup> Fawaz, S. A. and B. Andersson. "Accurate Stress Intensity Factor Solutions for Unsymmetric Corner Cracks at Hole." Proceedings of the Fourth Joint DoD/FAA/NASA Conference on Aging Aircraft, 15-18 May 2000, St. Louis, MO.

<sup>23</sup> Newman, Jr., J. C. and I. S. Raju. "Prediction of Fatigue Crack-Growth Patterns and Lives in Three-Dimensional Crack Bodies." Advances in Fracture Research (Fracture 84), Sixth International Conference on Fracture, Vol 3, 1984, pp.1597-1608.



Table 1 Crack Growth Analysis Model Parameters

Joint Type	Joint Number	Sheet Thickness, T mm(in)	Number of Rivets in Critical Row, n (Critical Row)	Hole Diameter, D mm(in)	Hole Pitch, s mm(in)	Baseline Remote Stress, $\sigma_o$ MPa(ksi)	Bypass Stress Ratio	Bending Stress Ratio	Bearing Stress Ratio	Baseline Cycles
I	1	1.6(0.063)	15( C )	4.0(5/32)	38.1(1.50)	103.4(15.0)	0.76	0.38	2.23	2000
I	2	1.6(0.063)	15( C )	4.0(5/32)	38.1(1.50)	103.4(15.0)	0.76	0.38	2.23	2000
I	3	1.6(0.063)	15( C )	4.8(3/16)	20.8(0.81)	103.4(15.0)	0.43	0.40	1.92	3000
I	3	1.6(0.063)	15( D )	4.0(5/32)	38.1(1.50)	103.4(15.0)	0.76	0.38	2.23	3000
I	4	1.6(0.063)	15( C )	4.0(5/32)	38.1(1.50)	103.4(15.0)	0.76	0.38	2.23	3000
II	5	1.6(0.063)	19(A)	4.8(3/16)	29.0(1.14)	117.2(17.0)	0.66	0.36	2.09	N/A <sup>†</sup>
II	6	1.6(0.063)	19(A)	4.8(3/16)	29.0(1.14)	105.5(15.3)	0.66	0.36	2.09	N/A <sup>†</sup>
II	7	1.6(0.063)	19(A)	4.8(3/16)	29.0(1.14)	103.4(15.0)	0.66	0.36	2.09	1000
II	8	1.6(0.063)	19(A)	4.8(3/16)	29.0(1.14)	103.4(15.0)	0.66	0.36	2.09	1000
III	9	2.3(0.090)	13(F)	4.8(3/16)	40.6(1.60)	103.4(15.0)	0.87	0.23	1.16	3000
III	10	2.3(0.090)	13(F)	4.8(3/16)	40.6(1.60)	117.2(17.0) <sup>‡</sup>	0.87	0.23	1.16	3000
III	11	2.3(0.090)	13(F)	4.8(3/16)	40.6(1.60)	117.2(17.0)	0.87	0.23	1.16	3000
III	12	2.3(0.090)	13(F)	4.8(3/16)	40.6(1.60)	117.2(17.0)	0.87	0.23	1.16	3000
IV	13	2.0(0.080)	29(D or E)	4.8(3/16)	19.0(0.75)	168.2(24.4)	0.82	0.18 <sup>##</sup>	0.74	N/A <sup>††</sup>
IV	14	2.0(0.080)	29(D or E)	4.8(3/16)	19.0(0.75)	168.2(24.4)	0.82	0.18 <sup>##</sup>	0.74	N/A <sup>††</sup>
IV	15	2.0(0.080)	29(D or E)	4.8(3/16)	19.0(0.75)	168.2(24.4)	0.82	0.18 <sup>##</sup>	0.74	N/A <sup>††</sup>
IV	16	2.0(0.080)	29(D or E)	4.8(3/16)	19.0(0.75)	168.2(24.4)	0.82	0.18 <sup>##</sup>	0.74	N/A <sup>††</sup>

Number of cycles at  $S_{max}$  separating marker cycles for 10-4-6 Marker Spectrum

<sup>†</sup> 130% Overload spectrum was used.

<sup>††</sup> Transport Aircraft Spectrum Loading

<sup>‡</sup> First 32,000 cycles at a remote stress of 103.4 MPa (15 ksi)

<sup>##</sup> Based on unpublished Delft University/AFRL neutral line model calculations

Table 2 Crack Locations

Crack Locations					
3C7R	4C19R	8A2R	10F9R	14E20R	15E17L
3C8R	4C20L	8A3L	10F10R	14E21L	15E17R
3C9R	4C20R	8A4L	10F11L	14E21R	15E18L
3C11R	4C21L	8A4R	10F11R	14E22L	15E18R
3C12L	4C21R	8A5L	10F12R	14E22R	15E19L
3C12R	4C22L	8A5R	11F5R	14E23L	15E19R
3C13L	4C22R	8A6L	11F6L	14E23R	15E20L
3C14L	4C23L	8A6R	11F6R	14E24L	15E20R
3C14R	4C23R	8A7L	11F7L	14E25L	15E21L
3C16L	4C24L	8A7R	11F7R	14E25R	15E21R
3C16R	4C24R	8A8L	11F8L	14E26L	15E22L
3C17L	4C25L	8A8R	11F8R	14E26R	15E22R
3C17R	4C25R	8A9L	11F9L	14E27L	15E23L
4A11R	4C26L	8A9R	11F9R	14E27R	15E23R
4A12L	7A1L	8A10L	11F10R	14E29L	15E24L
4A15L	7A2L	8A10R	11F11L	14E29R	15E24R
4A15R	7A2R	8A11L	11F11R	15E1L	15E25L
4C4R	7A4R	8A11R	12A5L	15E1R	15E25R
4C5R	7A6R	8A12L	12A6L	15E2L	15E26L
4C6L	7A7L	8A12R	12A7L	15E2R	15E27L
4C6R	7A7R	8A13L	12A7R	15E3L	15E27R
4C7L	7A8L	8A13R	12A8L	15E3R	15E28L
4C7R	7A8R	8A14L	12A8R	15E4L	15E28R
4C8R	7A9L	8A14R	12A9L	15E4R	15E29L
4C9L	7A9R	8A15L	13E1L	15E5L	15E29R
4C9R	7A10L	8A15R	13E1R	15E5R	16E1L
4C10R	7A10R	8A16L	13E2L	15E6L	16E1R
4C11L	7A11L	8A16R	13E3L	15E7L	16E2L
4C11R	7A11R	8A17L	13E4L	15E7R	16E2R
4C12L	7A12L	8A17R	13E4R	15E8R	16E3R
4C12R	7A12R	8A19L	13E5L	15E9L	16E4R
4C13L	7A13R	8A19R	13E5R	15E10L	16E6L
4C13R	7A14L	9A5L	13E26L	15E10R	16E7L
4C14L	7A14R	9A5R	13E27L	15E11R	16E10L
4C14R	7A15L	10F5L	14D1L	15E12R	16E10R
4C15L	7A15R	10F5R	14D9L	15E13L	16E12L
4C15R	7A16L	10F6L	14D9R	15E13R	16E19R
4C16L	7A17L	10F6R	14D10R	15E14L	16E21R
4C16R	7A17R	10F7L	14D15R	15E14R	16E22L
4C17L	7A18L	10F7R	14D17L	15E15L	16E27L
4C17R	7A18R	10F8L	14E19L	15E15R	16E27R
4C18R	7A19R	10F8R	14E19R	15E16L	16E29L
4C19L	8A1L	10F9L	14E20L	15E16R	16E29R

Table 3 MicroMeasurements® Strain Gage Type

Type	Option	Lot Number	Resistance in Ohms at 20°C	Gage Factor (20°C)	Transverse Sensitivity (20°C)	Code
EA-13-062AQ-350	W	R-A55BF00	350.0±0.3%	2.145±0.5%	0.7±0.2%	062116-956
EA-13-250AQ-350	W	R-A55AF00	350.0±0.3%	2.140±0.5%	0.2±0.2%	073315-2463

Table 4 2024-T3 Clad Mechanical Properties

	Tensile Yield Stress, F <sub>y</sub> (ksi)	Tensile Ultimate Stress, F <sub>u</sub> (ksi)	Secondary Modulus of Elasticity, E (x 10 <sup>3</sup> ksi)	% Elongation
TL Direction	44.82 (40)	62.78 (61)	10.3 (10)	13.1
LT Direction	45.83 (44)	63.97 (62)	10.1 (10)	12.9

Table 5 EIFS-5 Eddy Current and Travel Optical Microscope Crack Growth Data

	Crack Length, $c_2$ (mm)															
Cycles	A7	A8	A11	A15	A12	A9	A10	A13	A16	A14	A17	A5	A6	A18	A19	A3
0																
8000																
16000																
24000	0.351	0.386	0.404													
28000	0.691	0.589	0.580	0.447												
30000	0.782	0.655	0.711	0.553												
32000	0.797	0.819	0.727	0.257												
34000	0.846	0.868	0.849	0.732												
36000	0.679	0.602	0.797	0.566	0.406											
38000	0.824	0.891	0.808	0.520	0.598											
40000	0.886	0.976	0.859	0.688	0.547	0.406	0.473	0.441								
42000	0.923	1.060	0.911	0.705	0.642	0.448	0.692	0.458	0.424							
44000	0.916	1.028	0.904	0.841	0.807	0.660	0.783	0.765	0.553	0.469						
46000	0.995	1.153	0.989	0.826	0.842	0.721	0.765	0.760	0.608	0.389						
48000	1.102	1.151	1.063	0.876	0.877	0.711	0.821	0.740	0.654	0.344	0.391					
50000	1.009	1.102	0.973	0.809	0.830	0.713	0.753	0.711	0.790	0.468	0.465					
52000	1.076	1.176	1.025	0.851	0.932	0.778	0.843	0.828	0.861	0.491	0.537					
54000	1.159	1.300	1.103	0.893	0.862	0.797	0.843	0.859	0.841	0.721	0.539	0.450	0.705			
56000	1.163	1.264	1.105	0.921	1.039	0.812	0.958	0.890	0.924	0.762	0.540	0.504	0.782			
58000	1.202	1.293	1.169	0.900	0.986	0.860	0.954	0.896	0.908	0.782	0.747	0.683	0.801			
60000	1.205	1.353	1.175	0.899	1.011	0.863	0.935	0.952	0.923	0.797	0.698	0.629	0.796			
62000	1.271	1.330	1.152	1.002	1.035	0.872	0.977	0.971	1.020	0.815	0.776	0.741	0.861	0.599		
64000	1.294	1.450	1.247	1.018	1.067	0.964	1.047	0.955	1.041	0.791	0.754	0.643	0.894	0.508		
66000	1.339	1.427	1.268	1.050	1.050	0.969	1.010	1.022	1.008	0.822	0.773	0.736	0.881	0.583		
68000	1.320	1.473	1.293	1.013	1.193	0.959	1.063	1.050	1.079	0.843	0.769	0.772	0.905	0.691		
70000	1.378	1.498	1.367	1.066	1.155	1.027	1.084	1.087	1.069	0.845	0.783	0.785	0.928	0.644		
72000	1.395	1.553	1.324	1.106	1.163	1.074	1.128	1.160	1.147	0.846	0.824	0.762	0.967	0.727		
74000	1.432	1.688	1.333	1.110	1.122	1.015	1.120	1.108	1.142	0.880	0.825	0.813	0.946	0.801		
76000	1.457	1.706	1.383	1.177	1.260	1.065	1.197	1.145	1.172	0.877	0.852	0.803	0.968	0.831	0.656	
78000	1.528	1.815	1.407	1.206	1.271	1.108	1.210	1.198	1.252	1.023	0.843	0.787	0.979	0.795	0.442	
80000	1.600	1.840	1.425	1.251	1.334	1.171	1.256	1.185	1.283	1.036	0.906	0.837	1.060	0.828	0.726	
82000	1.630	1.898	1.455	1.230	1.263	1.162	1.279	1.212	1.282	1.035	0.864	0.858	1.069	0.799	0.508	
84000	1.754	1.865	1.509	1.453	1.394	1.261	1.363	1.323	1.367	1.049	0.877	0.864	1.102	0.862	0.559	
86000	1.826	1.971	1.541	1.501	1.369	1.236	1.373	1.289	1.369	1.053	0.886	0.851	1.165	0.874	0.608	
88000	1.905	1.925	1.628	1.507	1.378	1.258	1.349	1.308	1.379	1.052	0.922	0.902	1.154	0.926	0.728	
90000	1.962	1.925	1.787	1.543	1.415	1.293	1.399	1.285	1.414	1.071	0.950	0.922	1.193	0.985	0.763	
92000	1.933	1.791	1.815	1.525	1.546	1.250	1.379	1.334	1.387	1.063	0.879	0.936	1.177	0.976	0.791	
94000	1.869	1.766	1.925	1.611	1.588	1.436	1.552	1.410	1.555	1.285	0.933	0.935	1.305	1.010	0.806	
96000	1.942	1.755	1.948	1.630	1.671	1.443	1.571	1.430	1.586	1.288	0.933	0.931	1.312	1.006	0.867	
98000	2.129	2.031	2.211	1.886	1.901	1.667	1.810	1.533	1.791	1.311	1.031	0.988	1.398	1.075	0.919	
100000	2.101	1.908	2.182	1.977	2.103	1.856	2.002	1.635	1.977	1.350	0.980	0.899	1.513	1.117	0.957	
102000	1.736	1.716	1.894	1.870	2.007	1.731	1.872	1.669	1.881	1.342	1.037	1.017	1.510	1.159	0.891	
104000	1.661	1.708	1.842	1.898	2.044	1.892	1.930	1.900	1.900	1.398	1.060	1.010	1.618	1.193	0.920	
106000	1.627	1.848	1.770	1.879	2.253	1.960	1.873	2.154	2.041	1.457	1.092	1.116	1.797	1.217	1.042	
108000	1.791	1.847	1.844	1.906	2.299	1.865	1.881	2.281	2.060	1.530	1.200	1.141	1.936	1.319	1.160	
110000	1.829	1.741	1.783	1.863	2.436	1.815	1.962	2.138	2.083	1.520	1.182	1.174	1.925	1.356	1.181	
112000	1.866	1.634	1.700	1.847	2.338	1.766	1.946	1.999	1.927	1.472	1.249	1.207	1.914	1.386	1.067	
114000	1.832	1.729	1.840	1.861	2.232	1.849	1.796	1.870	1.900	1.449	1.224	1.240	1.921	1.352	1.239	0.408
116000	1.920	1.732	1.821	1.818	2.402	2.022	1.880	1.975	1.985	1.415	1.283	1.260	1.932	1.383	1.209	0.469
118000	1.794	1.340	1.857	1.812	2.052	1.452	1.705	1.874	1.786	1.417	1.230	1.267	1.721	1.624	1.145	0.492

119926 PanelFracture

Table 6 EIFS-6 Eddy Current and Travel Optical Microscope Crack Growth Data

	Crack Length, c <sub>2</sub> (mm)																									
Cycles 0	A15L	A15R	A13L	A13R	A11L	A11R	A10L	A10R	A5L	A5R	A8L	A8R	A14L	A14R	A7R	A6L	A6R	A17L	A17R	A4L	A4R	A12L	A9L	A9R	A16L	A16R
90000	0.816																									
96000	0.856																									
102000	0.915		0.392																							
108000	1.065		0.814			0.628																				
114000	1.153		0.685			0.578																				
120000	1.164		0.757			0.775		0.613	0.497																	
126000	1.277	0.799	0.822			0.752	0.575	0.599	0.566			0.494	0.623													
132000	1.344	0.824	0.823		0.511	0.774	0.639	0.707	0.570			0.541	0.681													
138000	1.436	0.969	0.890	0.665	0.532	0.887	0.753	0.775	0.682			0.744	0.798		0.465											
144000	1.448	0.936	0.898	0.639	0.639	0.892	0.783	0.799	0.519			0.764	0.785													
150000	1.535	1.065	1.000	0.737	0.859	0.936	0.848	0.860	0.803			0.813	0.664	0.590												
156000	1.935	1.124	1.081	0.826	0.826	1.033	0.838	0.926	0.697			0.834	0.929	0.814	0.580		0.413	0.413								
162000	1.883	1.137	1.057	0.813	0.824	1.067	0.834	0.927	0.800			0.892	0.962	0.824	0.503		0.435	0.523		0.463		0.618				
168000	1.903	1.261	1.056	0.868	0.835	0.959	0.884	0.962	0.836			0.924	0.951	0.884	0.792		0.642	0.767		0.566		0.796	0.546			
174000	1.994	1.375	1.077	0.865	0.865	1.156	0.785	1.016	0.803			0.965	1.065	0.934	0.689		0.754	0.607		0.491		0.758	0.348			
180000	1.861	1.442	1.230	1.059	1.059	1.202	0.960	1.079	0.873		0.595	1.057	1.082	1.085	0.647		0.798	0.750		0.528	0.476	0.767	0.480			
186000	1.837	1.741	1.184	0.940	1.094	1.290	1.042	1.223	0.928		0.776	1.065	1.077	1.094	0.776		0.791	0.725		0.725	0.367	0.954	0.721		0.668	
192000	1.988	1.806	1.373	1.208	1.183	1.376	1.067	1.266	0.931		0.813	1.138	1.167	1.202	0.828		0.828	0.794		0.763	0.391	0.977	0.516		0.680	
198000	3.861	2.163	1.509	1.312	1.368	1.431	1.211	1.421	0.997		0.845	1.276	1.443	1.463	0.846		0.873	0.852	0.845	0.823	0.361	1.112	0.762		0.822	
204000	4.801	2.261	1.502	1.326	1.218	1.426	1.181	1.550	1.060		0.863	1.224	1.365	1.512	0.877		0.844	0.896	0.874	0.883	0.468	1.014	0.681		0.937	
210000	5.359	2.489	1.957	1.941	1.595	2.148	1.248	1.955	1.024		0.880	1.429	1.621	1.760	0.928		0.957	0.848	0.973	0.880	0.489	1.189	0.770		1.020	
216000	5.512	3.302	1.942	1.941	1.837	2.261	1.339	2.054	1.077		1.026	1.401	1.546	1.843	0.950		0.990	0.890	1.050	0.976	0.577	1.279	0.839		1.140	0.577
222000	6.350	3.581	1.679	2.413	1.981	2.515	1.355	2.028	1.052		1.040	1.577	1.636	1.783	0.950		0.933	0.851	1.038	0.956	0.529	1.357	0.786		1.140	0.529
228000	7.087	3.988	3.404	2.667	2.007	2.743	1.789	2.337	1.078		1.153	1.840	3.886	3.226	0.959		0.982	0.960	1.077	0.995	0.581	1.739	0.847	0.435	1.304	0.472
234000	8.299	4.794	4.261	3.499	2.965	3.423	2.483	2.534	1.138	0.474	1.314	1.937	4.743	4.134	1.105		0.988	0.984	1.264	1.028	0.752	2.216	0.877	0.547	1.581	0.868
240000	10.179	5.683	5.912	4.248	3.435	3.854	2.686	2.407	1.138	0.767	1.209	1.886	5.455	5.696	1.090	0.653	1.065	1.055	1.107	1.072	0.824	2.584	0.942	0.804	1.828	1.021
244547	Final Fracture																									

Table 7 Load Transfer Parameters

Joint Type	Baseline Remote Stress, $\sigma_o$	Applied Load per inch, $P_a$	Critical Rivet Row	Fastener Shear, $P_s$	Average Fastener Load per inch, $p_s$	Percent Load Transfer, $\gamma$
	ksi	lb/in		lb	lb/in	
I	10	630	C	225	150	23.8
I	10	630	D	121	149	23.7
II	10	630	A	243	213.2	33.8
III	10	900	A or F	184	115.0	12.8
IV	10	630	D or E	106	116.0	18.4

Table 8 EIFS Summary

Joint Type	Crack	By Crack Location		By Joint Type	
		EIFS Mean $\mu\text{m}$	EIFS Standard Deviation $\mu\text{m}$	EIFS Mean $\mu\text{m}$	EIFS Standard Deviation $\mu\text{m}$
I	3C14R	8.319	0.599	7.729	0.487
	3C17R	11.444	0.703		
	3D13R	3.310	0.052		
	3D15L	5.326	0.275		
	4C9R	8.623	1.186		
	4C10R	8.403	0.340		
	4C11R	7.892	0.125		
	4C12R	8.514	0.613		
II	7A6L	24.297	7.430	22.410	11.114
	7A6R	30.105	8.073		
	7A7L	18.352	1.290		
	7A7R	10.763	0.561		
	7A8L	6.704	0.171		
	7A12R	21.492	13.139		
	7A13R	11.856	0.308		
	7A14L	56.426	5.109		
	7A14R	22.517	6.246		
	7A15R	15.279	1.923		
	7A16L	22.380	1.916		
	7A16R	6.321	0.200		
	7A17L	7.254	0.962		
	7A17R	33.931	5.955		
	8A10L	45.316	68.341		
	8A10R	37.294	63.612		
	8A19L	10.688	3.693		
III	10F5R	6.655	0.235	7.577	0.765
	10F6L	7.299	0.629		
	10F6R	7.975	1.016		
	10F7L	7.190	0.896		
	10F7R	7.404	0.970		
	10F8L	7.719	0.475		
	10F8R	7.076	0.716		
	10F10R	8.895	0.919		
	11F6L	7.462	1.002		
	11F6R	8.280	0.304		
	11F7L	7.506	0.849		
	11F7R	7.693	1.135		
	11F8L	6.482	0.380		
	11F8R	6.815	0.753		
	11F9R	8.561	1.189		
	11F10R	8.216	0.770		
IV	15E2R	151.218	141.618	301.560	217.512
	15E11R	625.560	302.542		
	15E16L	167.476	199.048		
	15E16R	426.098	361.638		
	15E20L	54.238	40.583		
	15E26R	580.870	359.352		
	15E28R	105.458	117.803		

Table 9 EIFS Summary Using Crack Lengths to 1.27 mm

Joint Type	Crack	By Crack Location		By Joint Type	
		EIFS Mean $\mu\text{m}$	EIFS Standard Deviation $\mu\text{m}$	EIFS Mean $\mu\text{m}$	EIFS Standard Deviation $\mu\text{m}$
I	3C14R	8.319	0.599	7.729	0.487
	3C17R	11.444	0.703		
	3D13R	3.310	0.052		
	3D15L	5.326	0.275		
	4C9R	8.623	1.186		
	4C10R	8.403	0.340		
	4C11R	7.892	0.125		
	4C12R	8.514	0.613		
II	7A6L	16.672	1.236	18.033	3.784
	7A6R	26.854	9.677		
	7A7L	19.896	0.099		
	7A7R	10.806	0.645		
	7A8L	6.704	0.171		
	7A12R	15.989	1.984		
	7A13R	11.873	0.326		
	7A14L	49.960	2.410		
	7A14R	17.812	4.343		
	7A15R	15.221	2.007		
	7A16L	23.043	1.353		
	7A16R	6.317	0.205		
	7A17L	7.935	0.705		
	7A17R	29.117	10.420		
	8A10L	15.271	4.161		
	8A10R	22.396	20.901		
	8A19L	10.688	3.693		
III	10F5R	6.655	0.235	7.080	0.526
	10F6L	6.966	0.226		
	10F6R	7.347	0.518		
	10F7L	6.647	0.263		
	10F7R	7.101	0.801		
	10F8L	7.723	0.503		
	10F8R	6.691	0.429		
	10F10R	7.871	1.003		
	11F6L	6.681	0.581		
	11F6R	8.188	0.250		
	11F7L	6.949	0.672		
	11F7R	6.775	0.565		
	11F8L	6.482	0.380		
	11F8R	6.364	0.552		
	11F9R	7.499	0.757		
	11F10R	7.343	0.687		
IV	15E2R	74.545	60.319	86.853	70.575
	15E11R	161.290	131.112		
	15E16L	66.501	57.705		
	15E16R	133.874	139.338		
	15E20L	20.742	5.554		
	15E26R	103.542	74.588		
	15E28R	47.477	25.408		

Table 10 EIFS Comparison: AFGROW vs. FASTRAN

Crack ID	AFGROW EIFS Mean, $\mu\text{m}$	FASTRAN EIFS Mean, $\mu\text{m}$
7A6L	20.258	25.146
7A6R	32.953	31.242
7A7L	25.189	20.320
7A7R	12.059	11.938
7A8L	7.287	6.350
7A12R	18.789	20.320
7A13R	13.246	13.970
7A14L	61.953	39.878

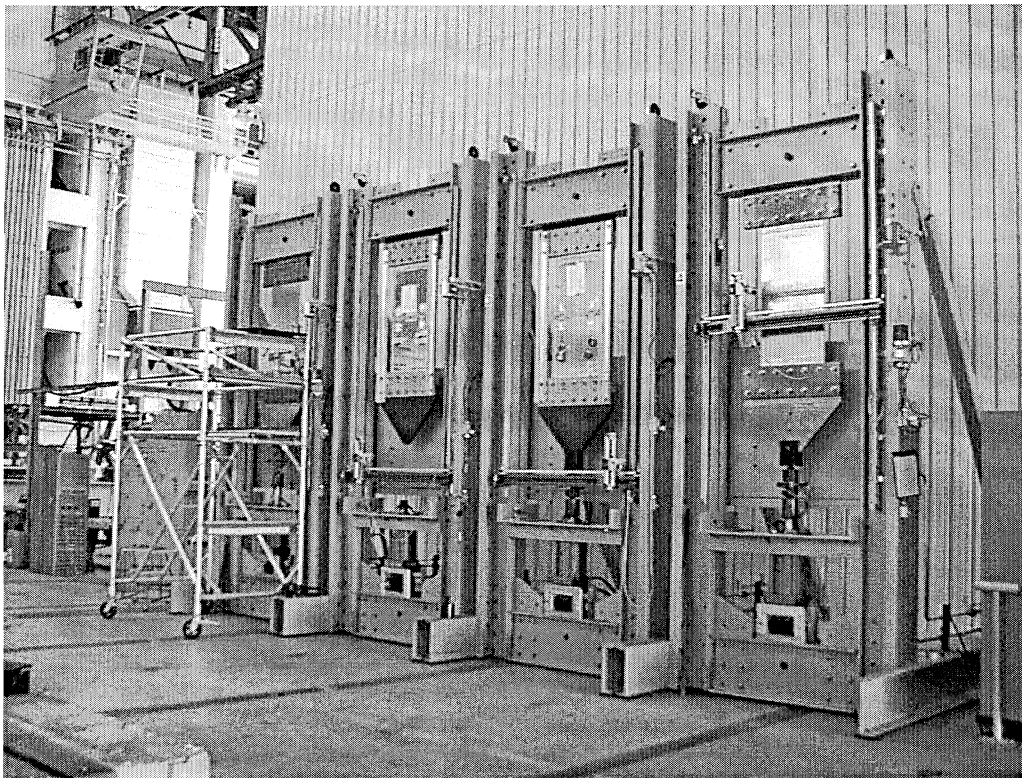


Figure 1 Air Force Research Laboratory Wide Panel Test Facility

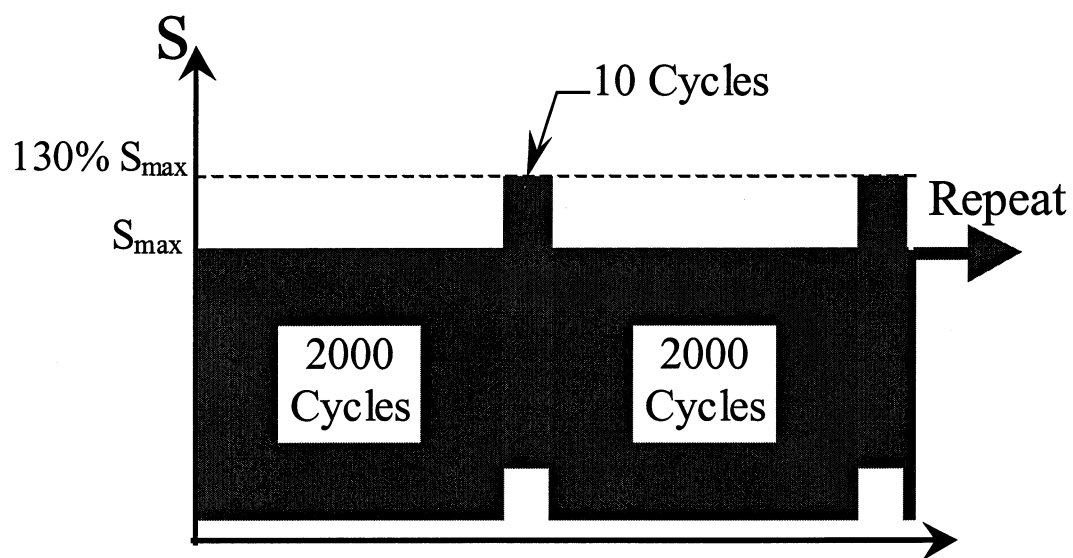
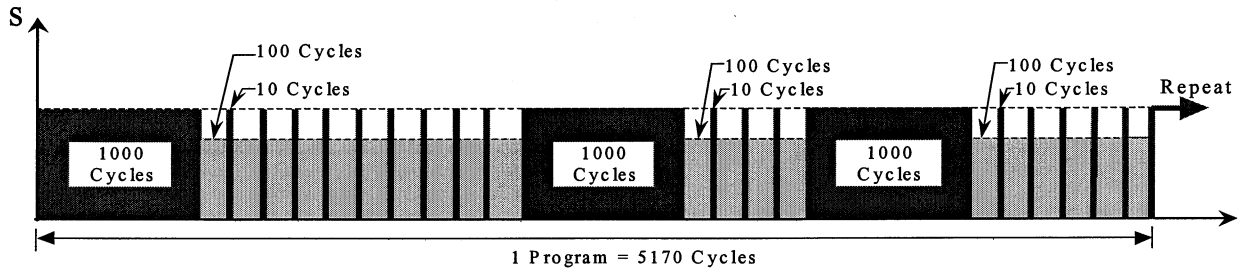


Figure 2 Overload Spectrum





Baseline cycles varied between EIFS joints, see Table 5.

**Figure 3 10-4-6 Marker Spectrum**

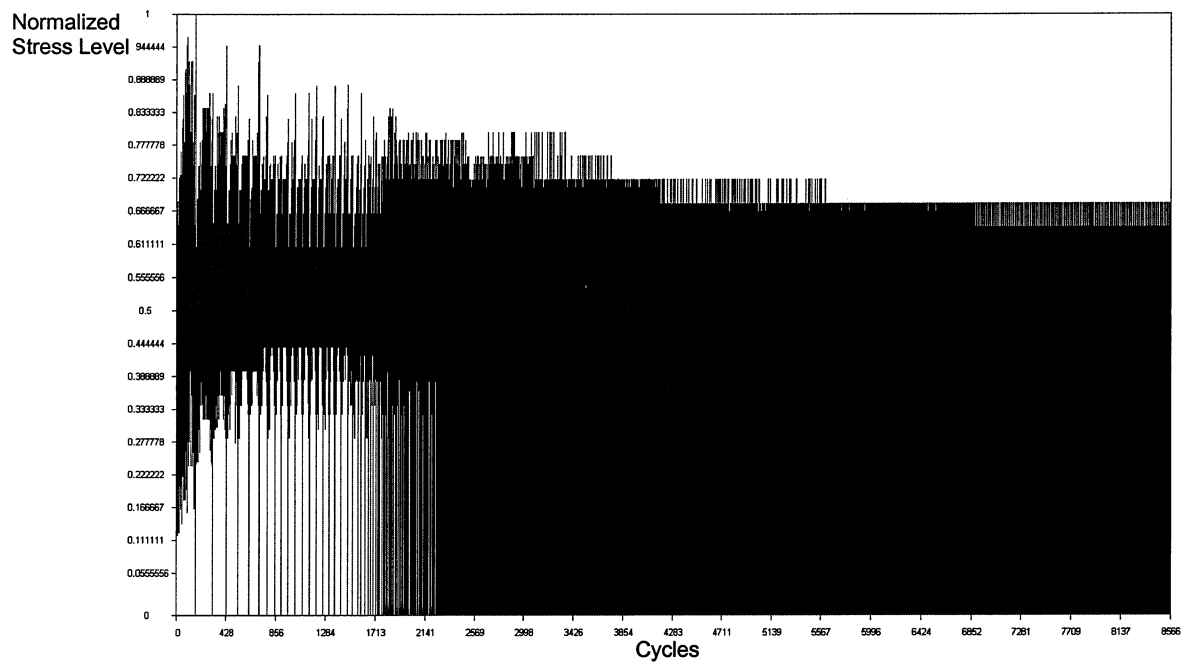


**Figure 4 Joint Type IV Spectrum**

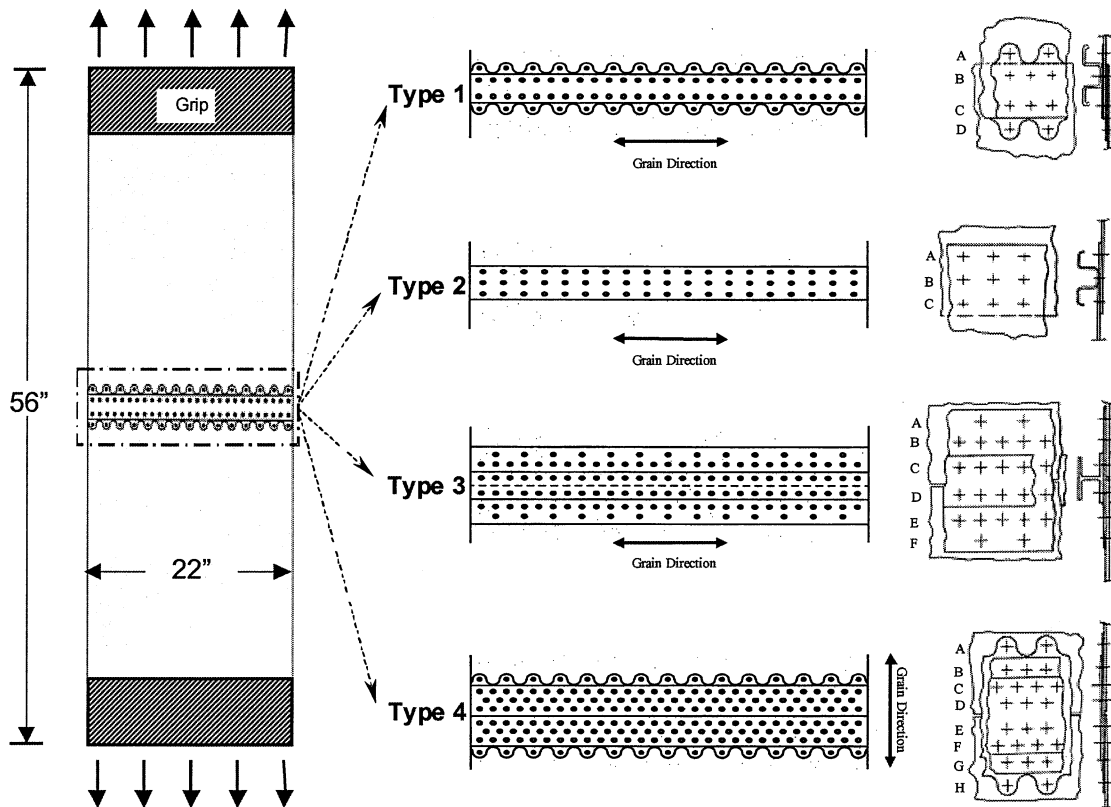


**Figure 5 EIFS Joint Types**

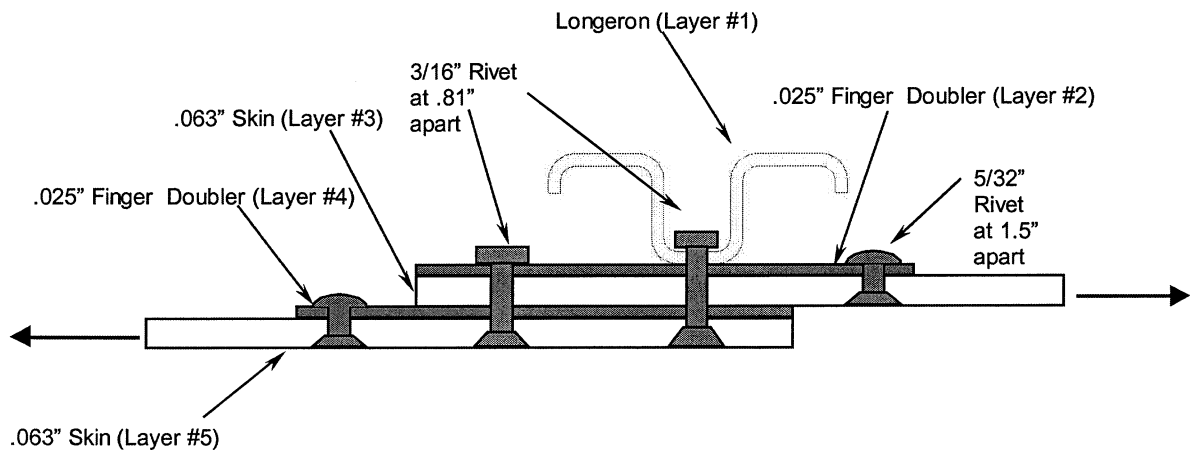


**Figure 6 Joint Type I Configuration**

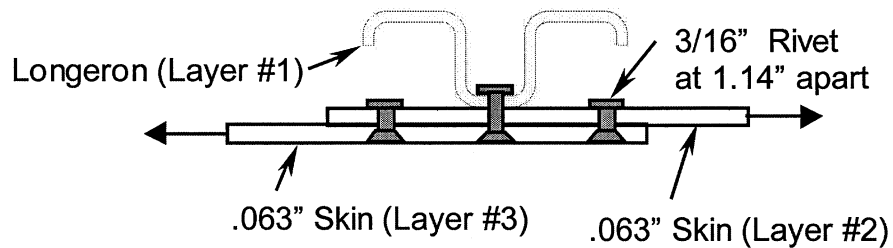


**Figure 7 Joint Type II Configuration**

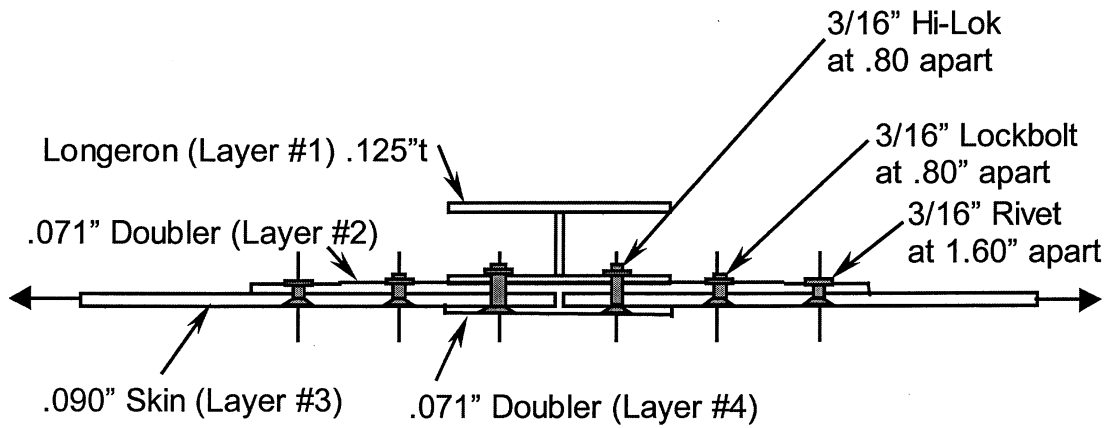


Figure 8 Joint Type III Configuration

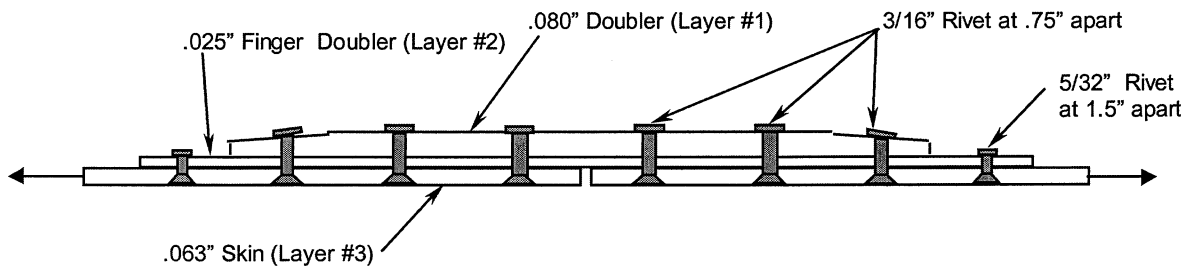


Figure 9 Joint Type IV Configuration

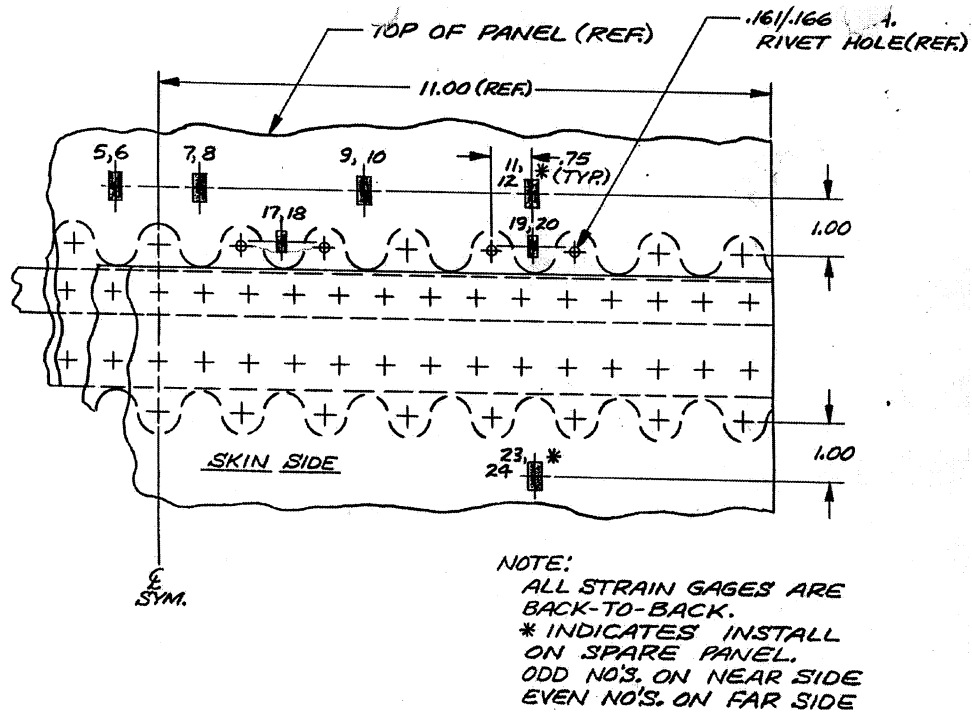


Figure 10 Strain Gage Locations for EIFS Type I

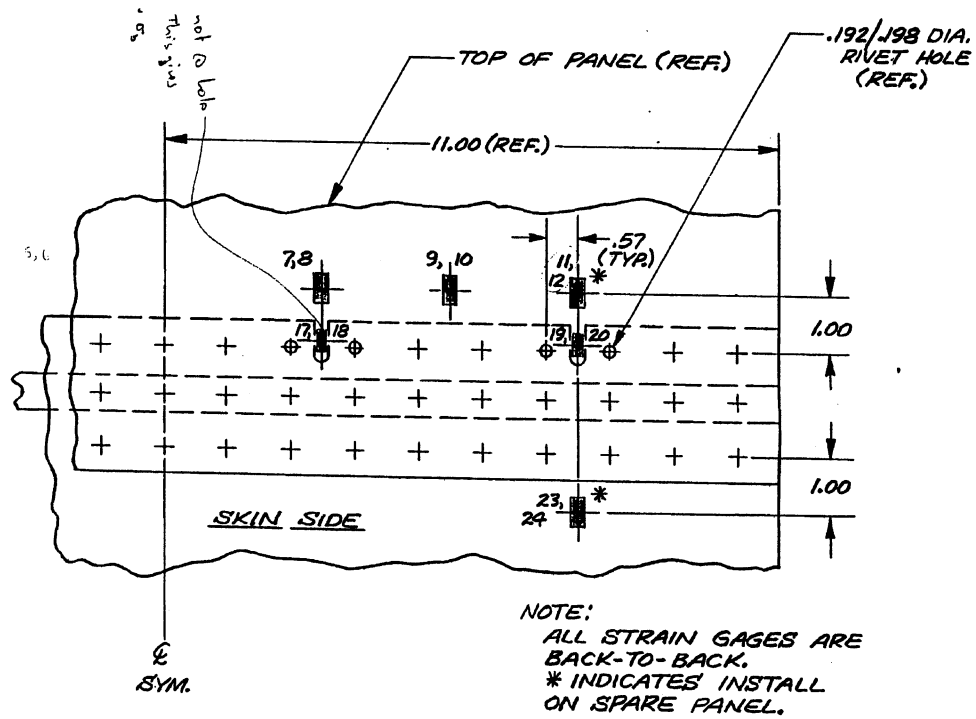


Figure 11 Strain Gage Locations for EIFS Type II

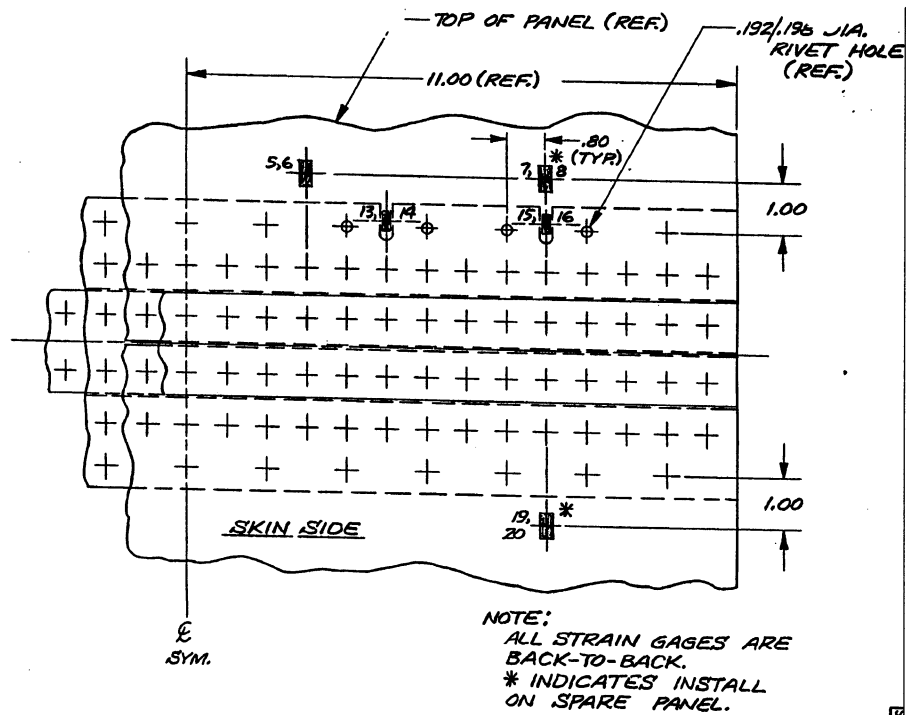
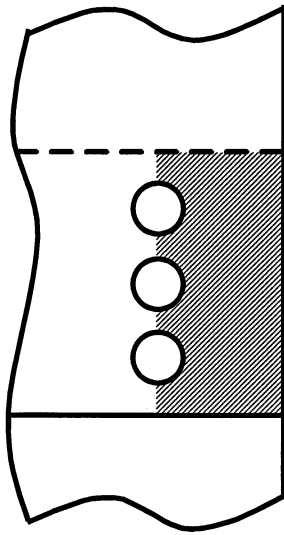
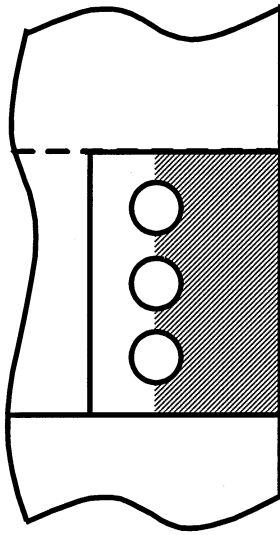


Figure 12 Strain Gage Locations for EIFS Type III

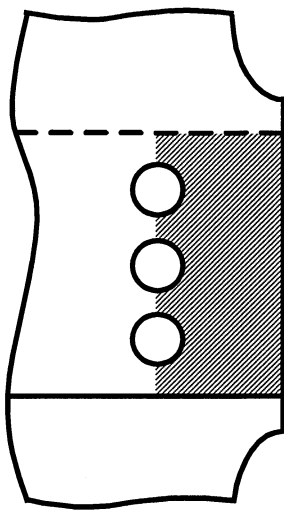
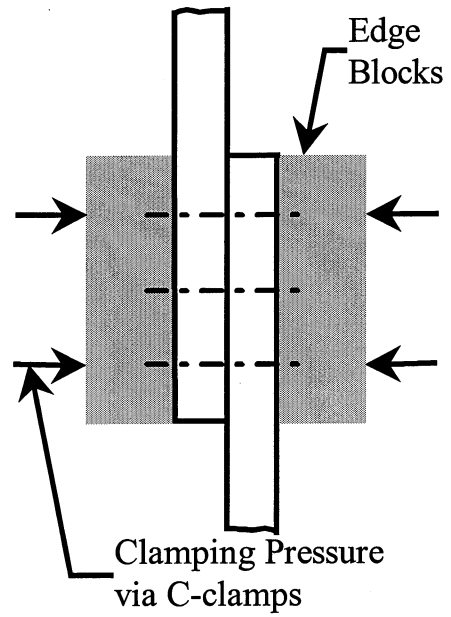




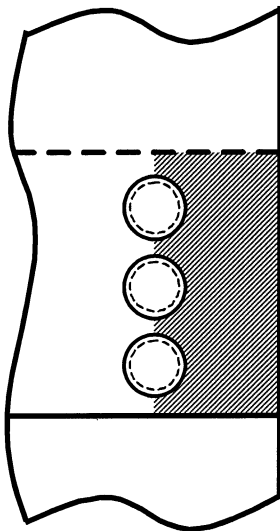
Bonded Skin



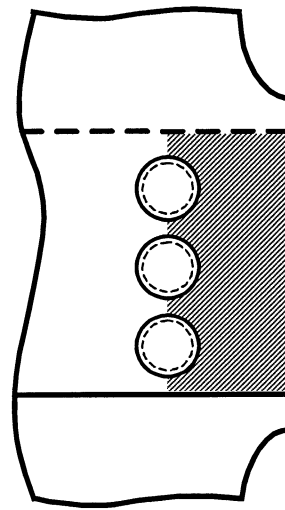
Bonded Skin and  
Edge Blocks



Bonded, Dog-boned  
Skin



Bonded Skin,  
Oversized, Heavily  
Expanded Edge Rivets



Bonded, Dog-boned Skin  
Oversized, Heavily  
Expanded Edge Rivets

**Figure 15 Methods of Reducing the *Edge Effect***



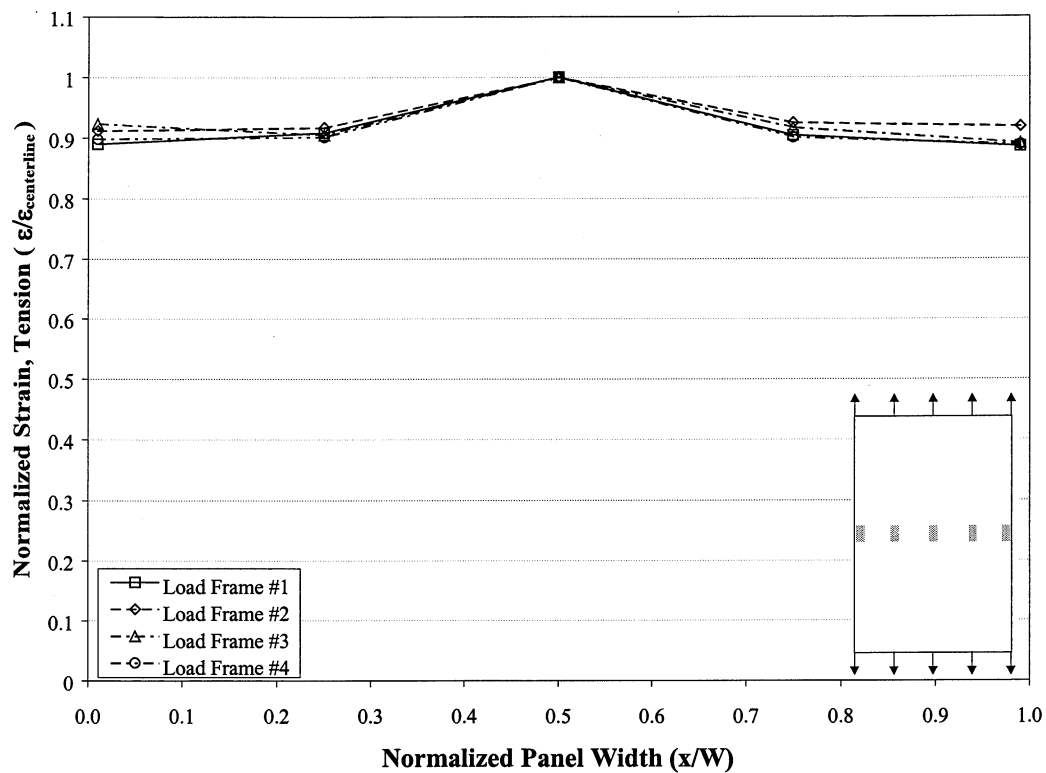


Figure 18 Tensile Strain Variation Through the Panel Width

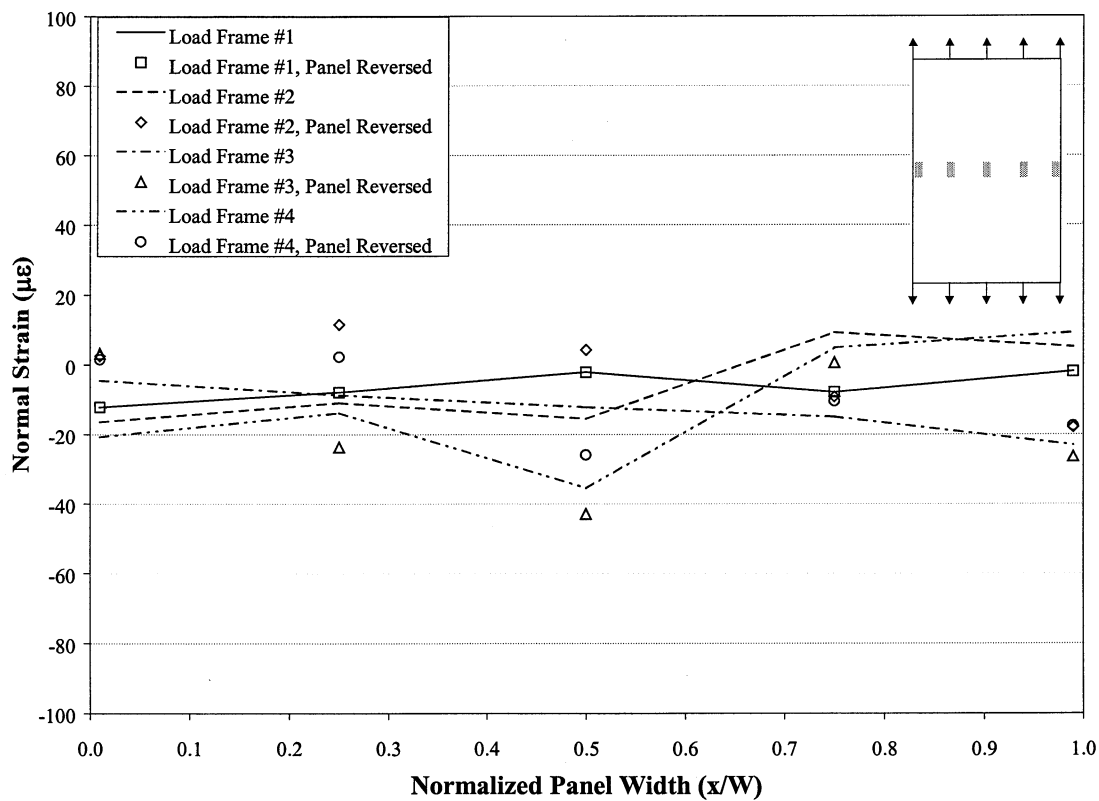
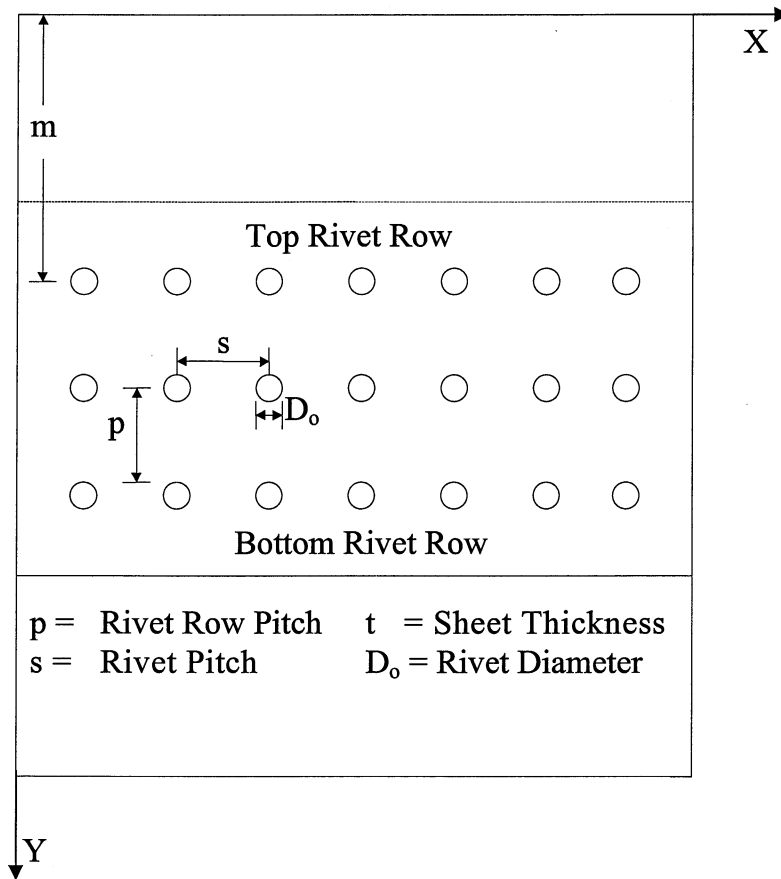
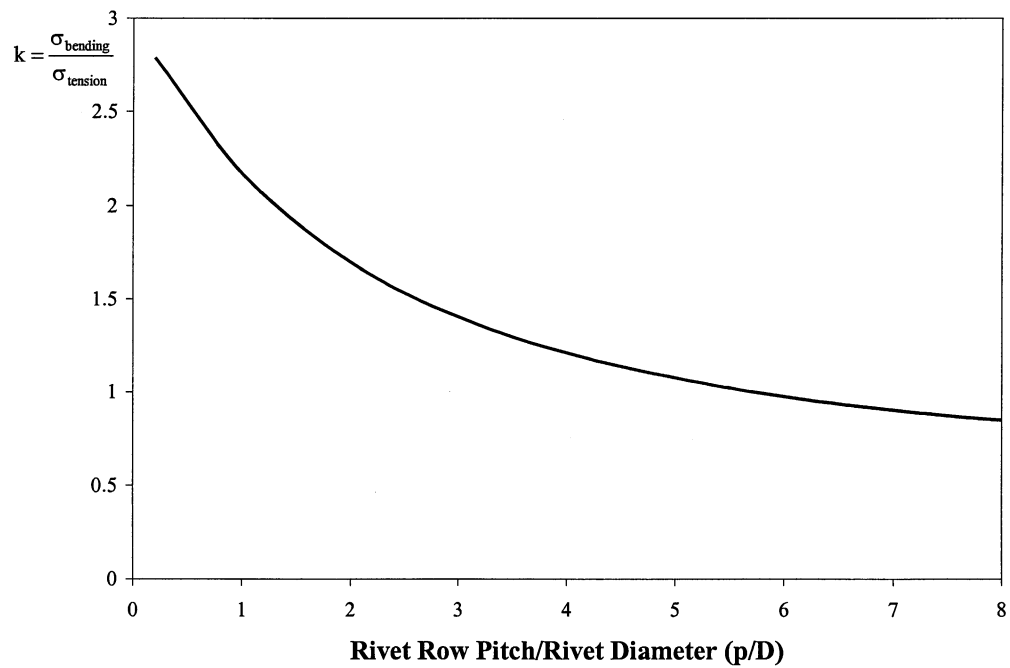


Figure 19 Bending Strain Variation Through the Panel Width





**Figure 20 Parameter Definition for Generic Riveted Joint**



**Figure 21 Effect of Rivet Row Pitch on Bending Factor,  $k$**

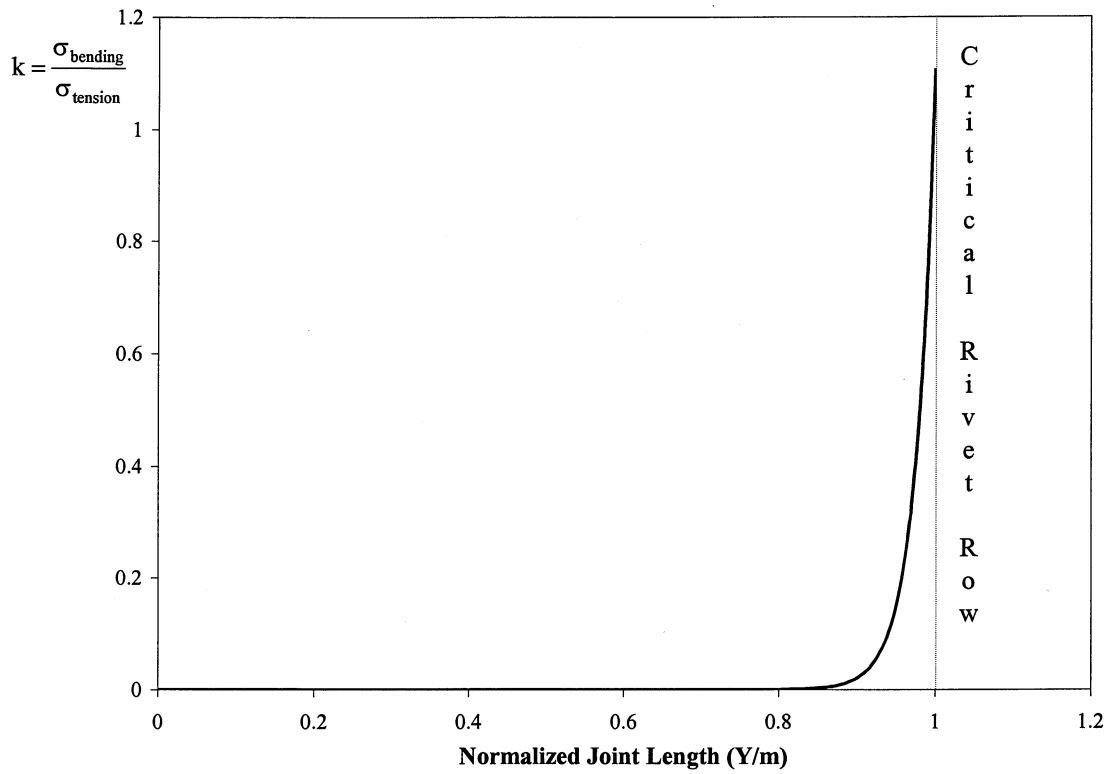


Figure 22 Effect of Sheet Length on Bending Factor,  $k$

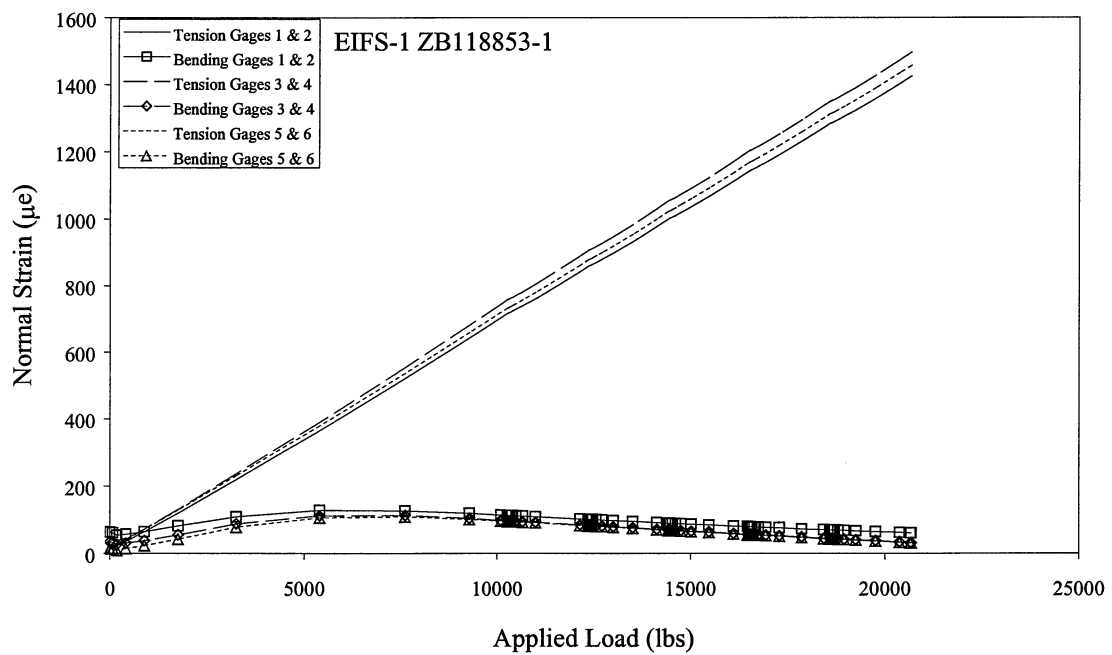
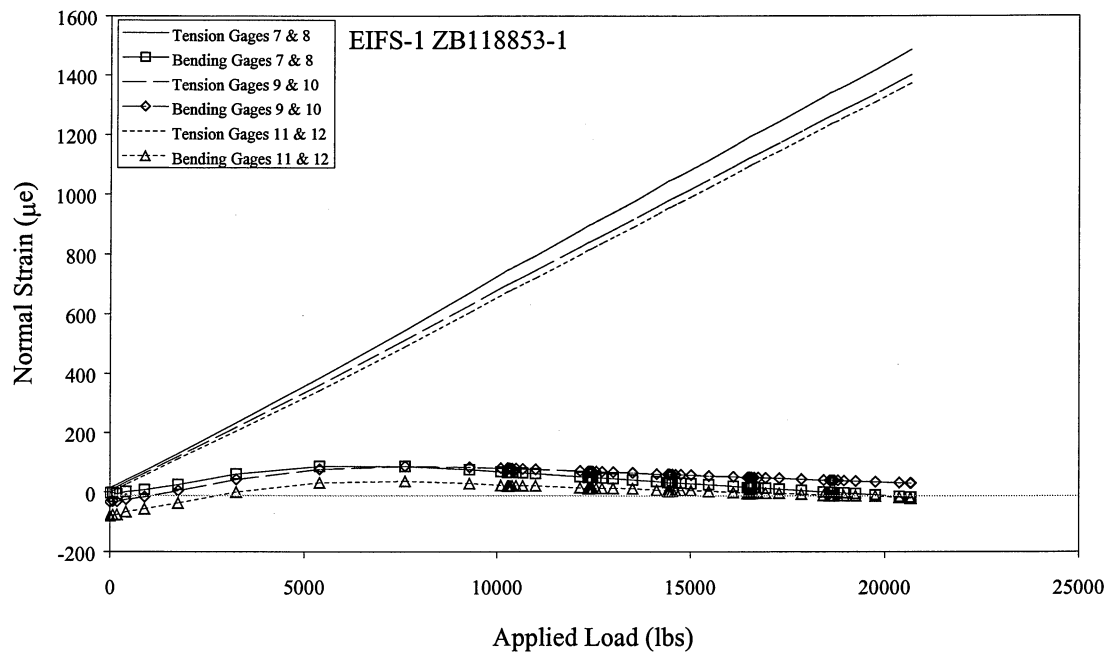
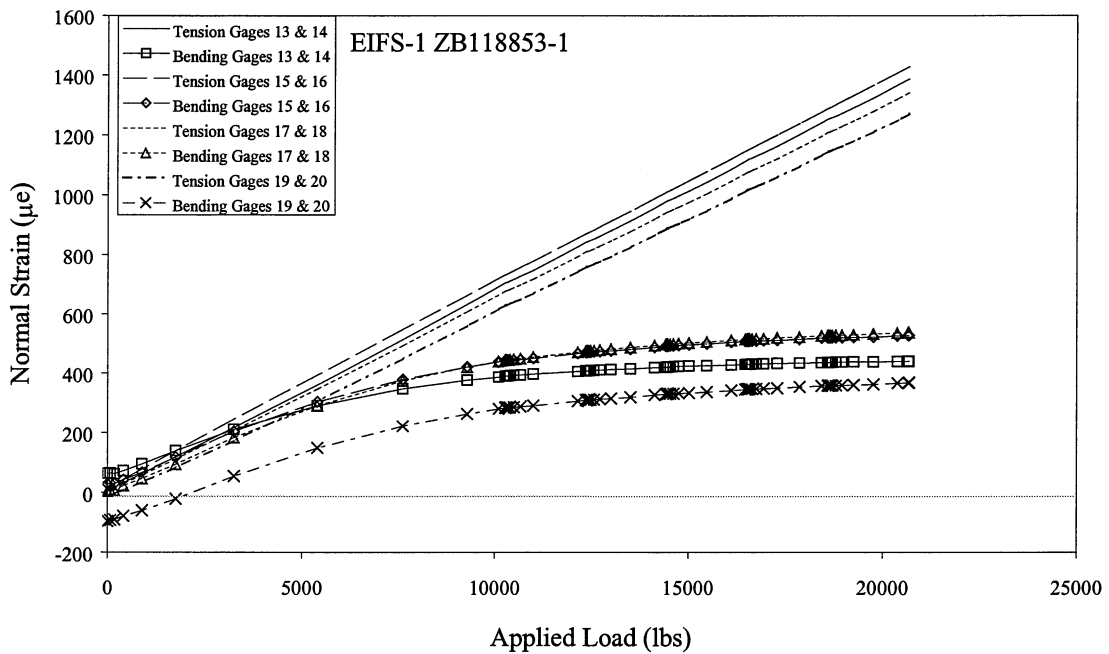


Figure 23 EIFS-1 Top Sheet, Left Side Normal Strains



**Figure 24 EIFS-1 Top Sheet, Right Side Normal Strains**



**Figure 25 EIFS-1 Top Sheet, Critical Rivet Row Normal Strains**

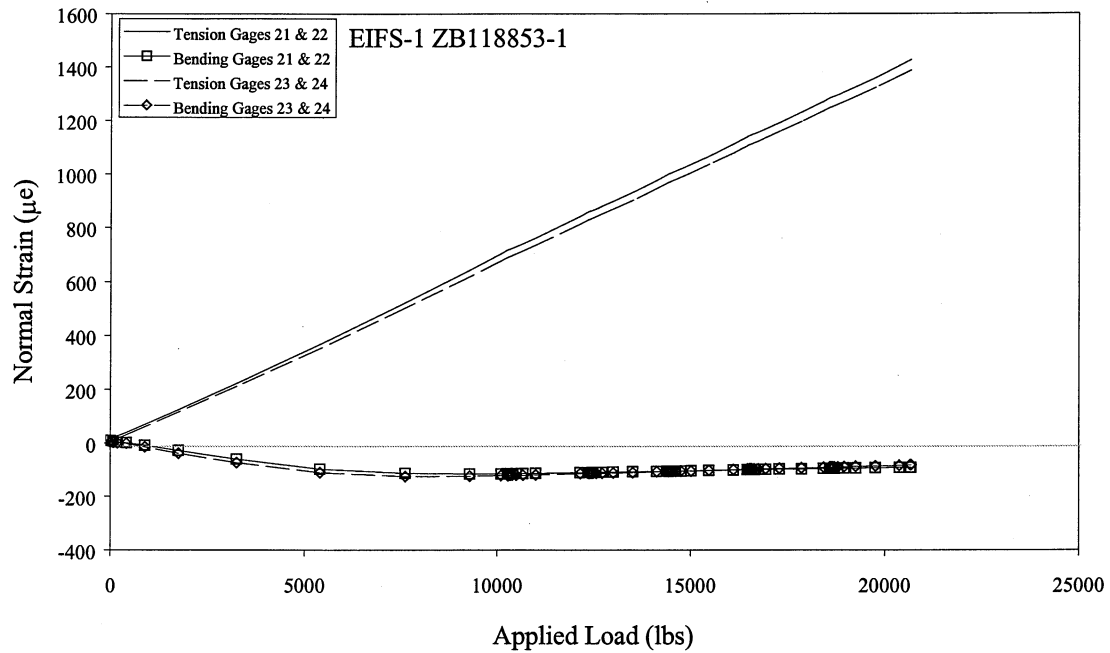


Figure 26 EIFS-1 Bottom Sheet Normal Strains

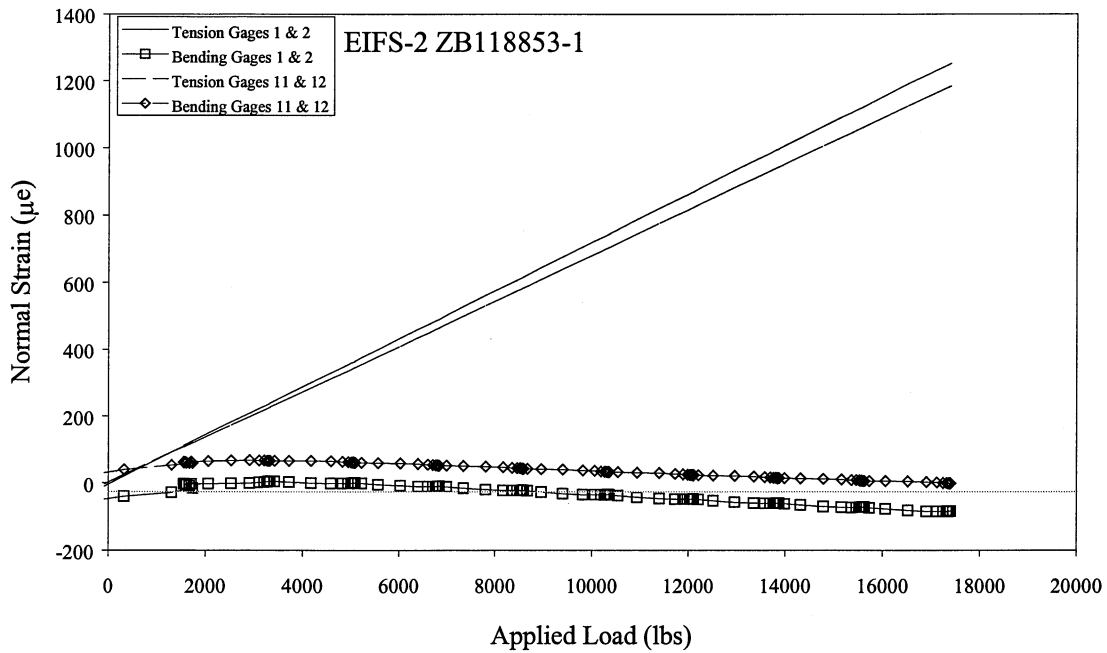
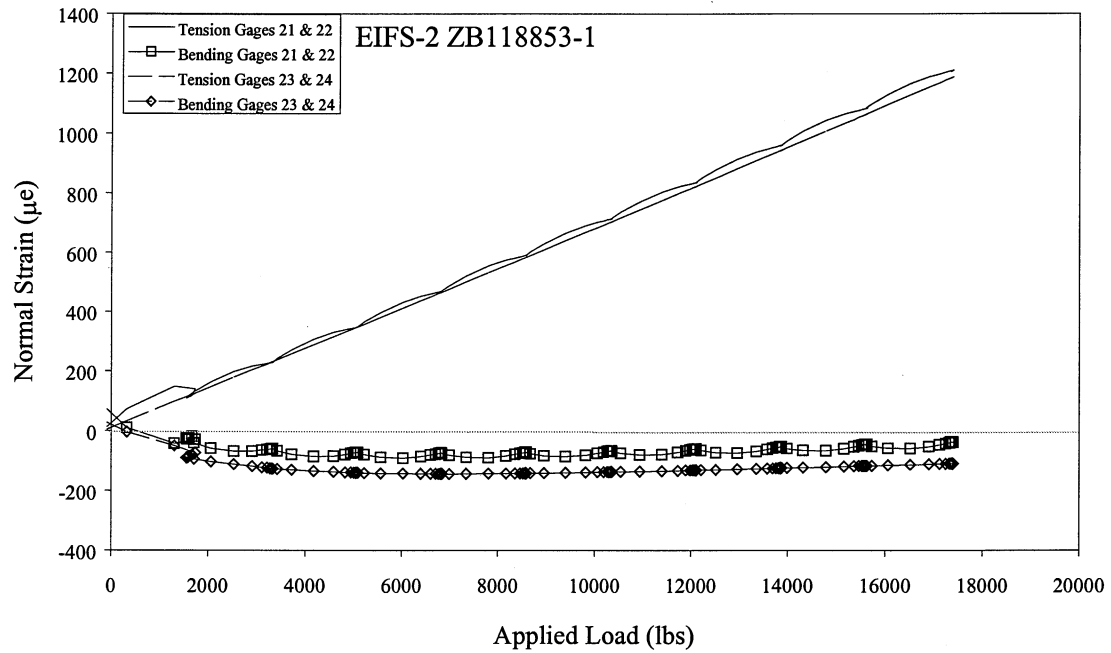
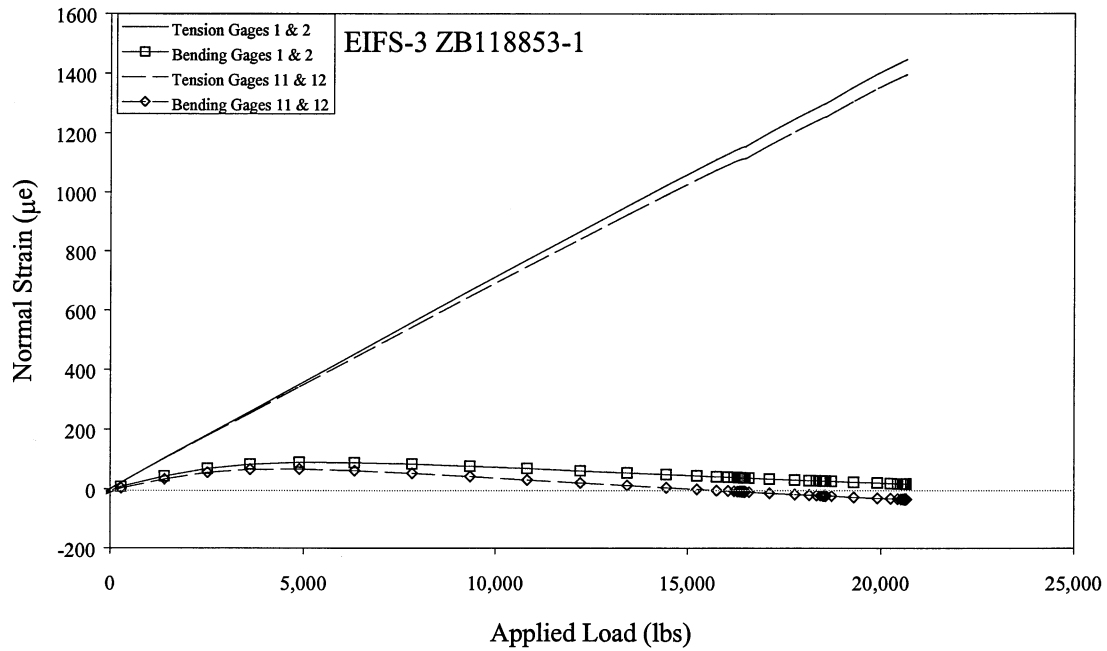


Figure 27 EIFS-2 Top Sheet Normal Strains



**Figure 28 EIFS-2 Bottom Sheet Normal Strains**



**Figure 29 EIFS-3 Tope Sheet Normal Strains**

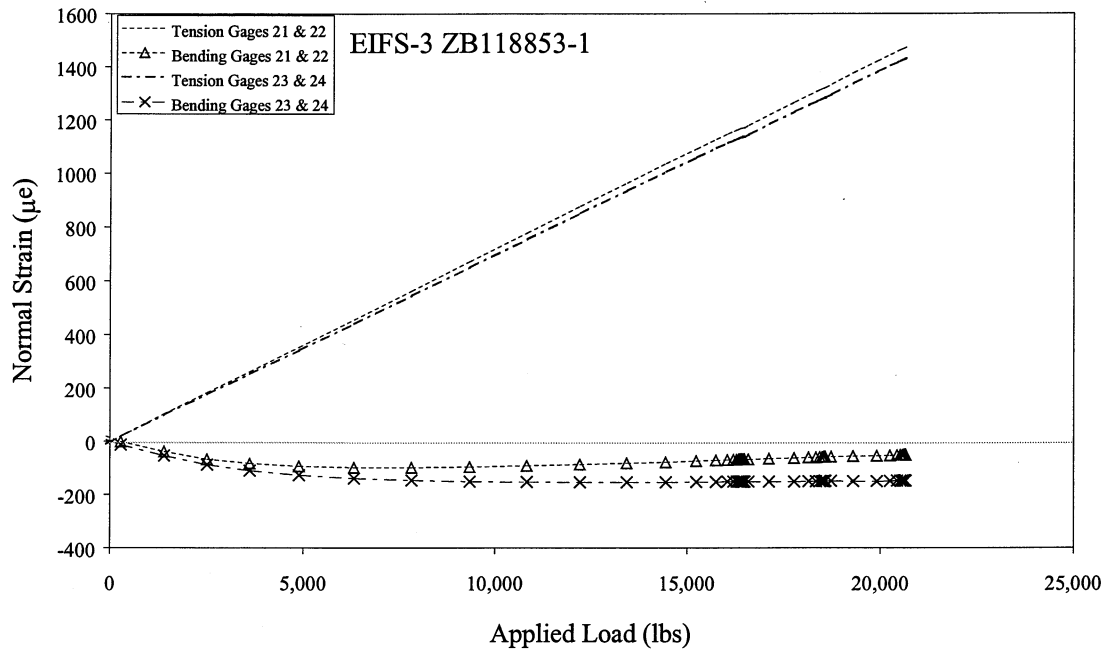


**Figure 30 EIFS-3 Bottom Sheet Normal Strains**

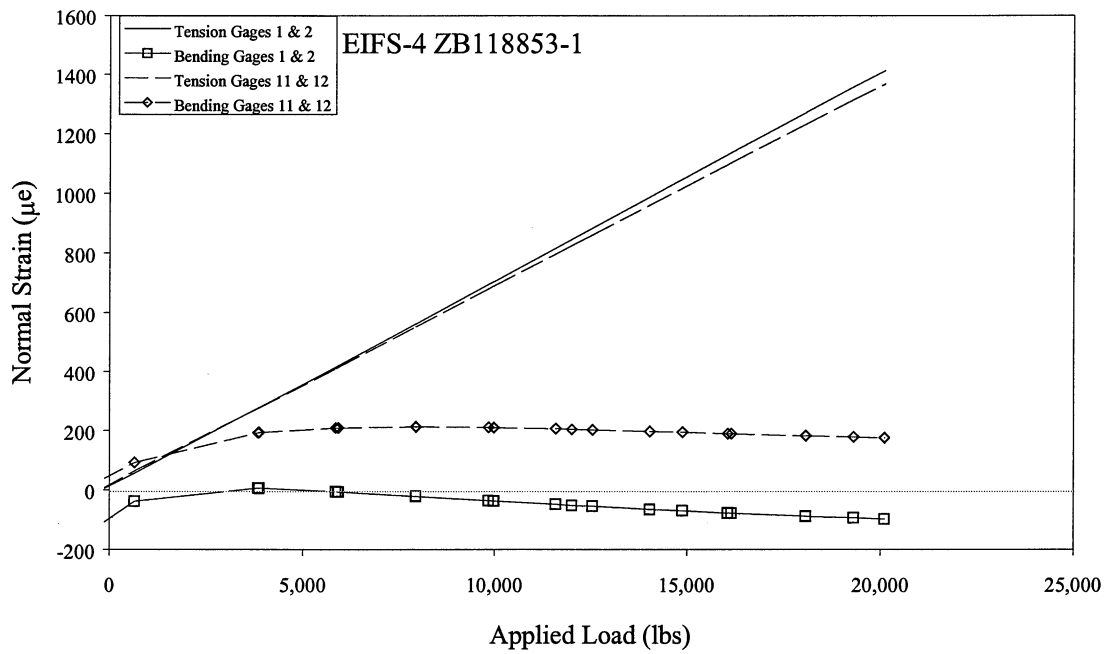


**Figure 31 EIFS-4 Top Sheet Normal Strains**

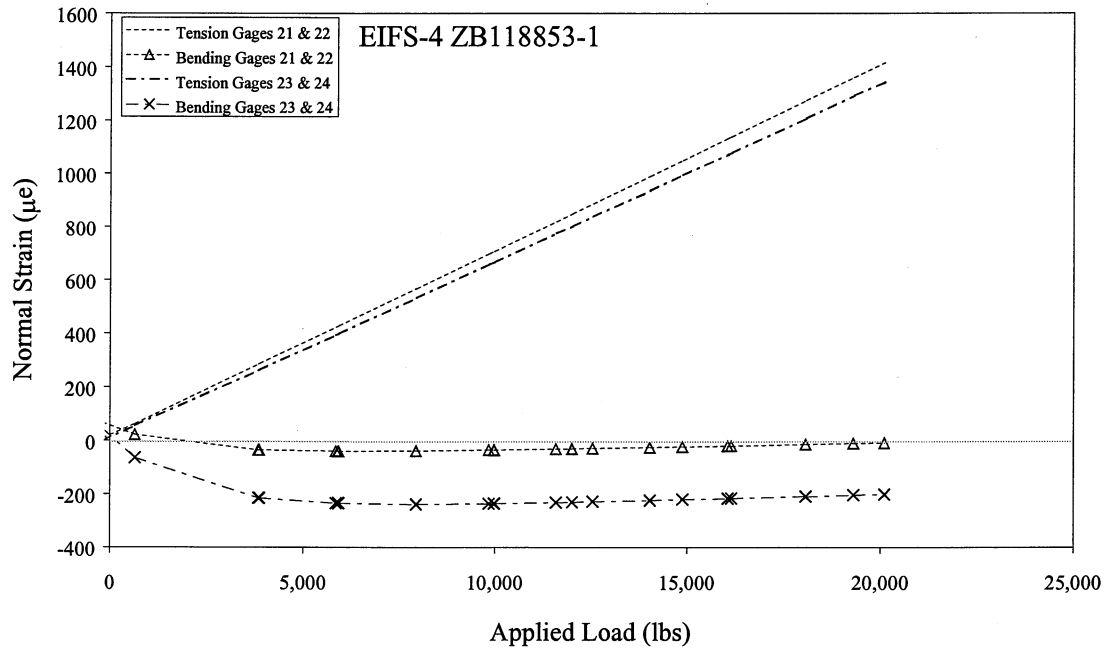


Figure 32 EIFS-4 Bottom Sheet Normal Strains

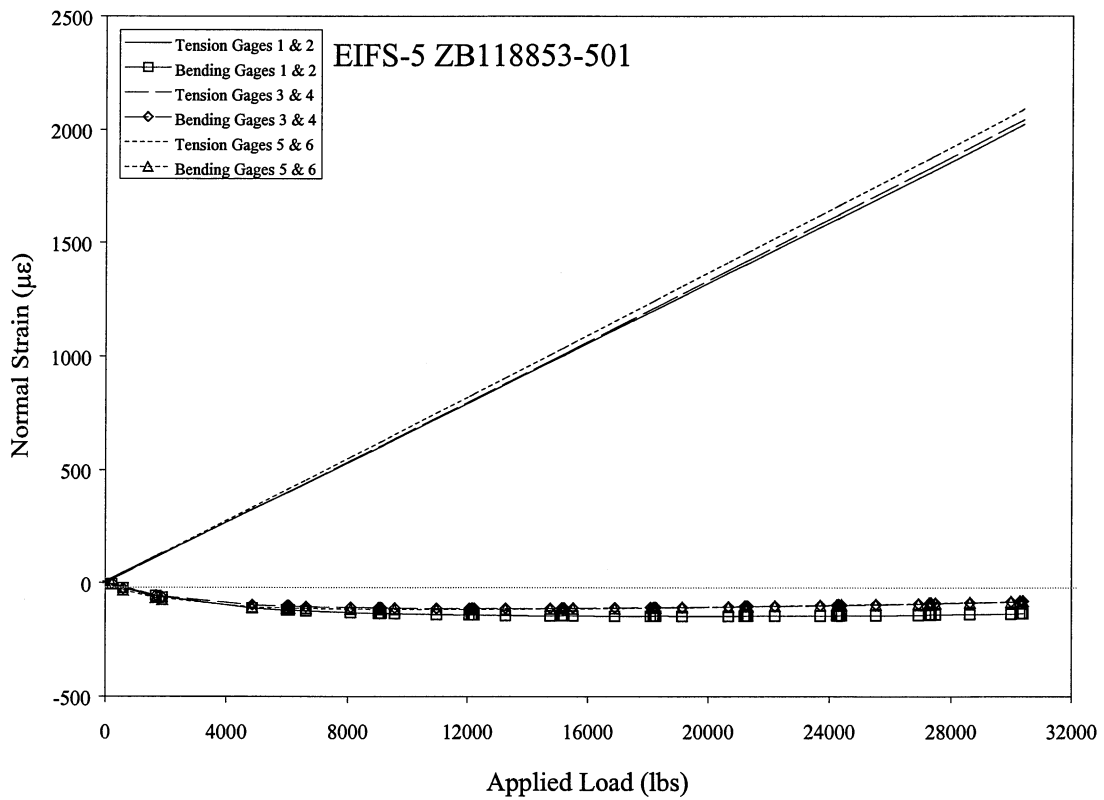


Figure 33 EIFS-5 Top Sheet, Left Side Normal Strains

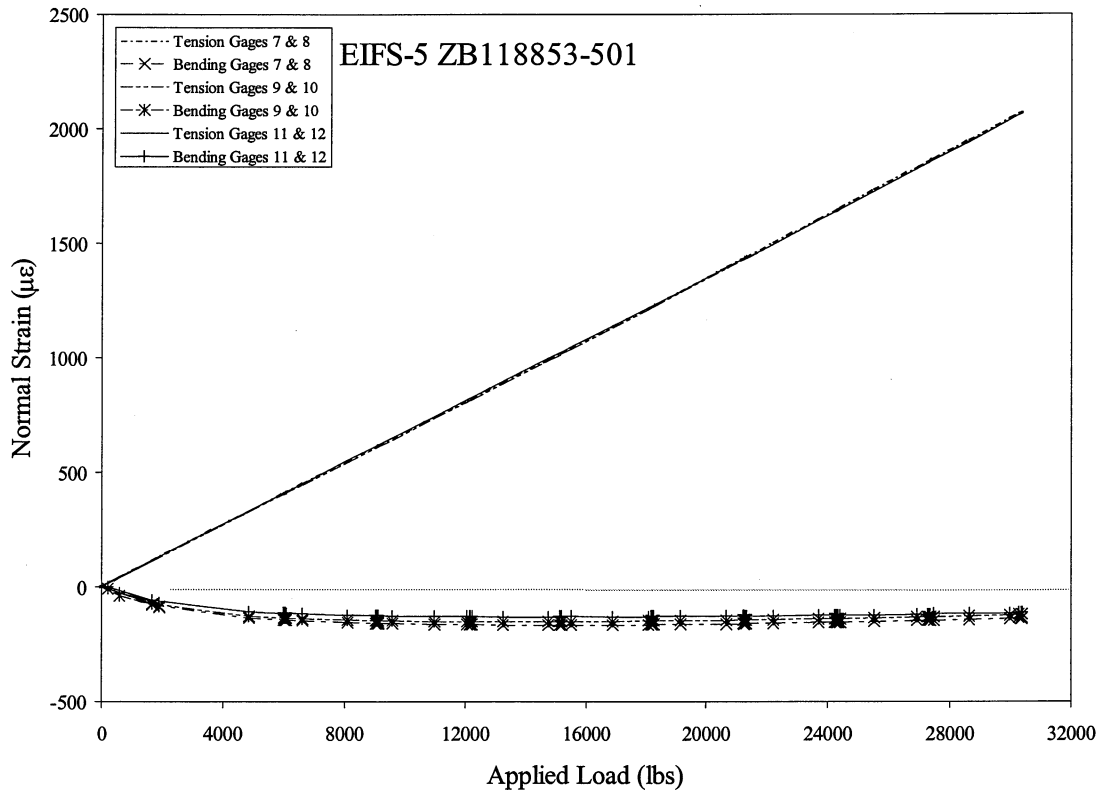


Figure 34 EIFS-5 Top Sheet, Right Side Normal Strains

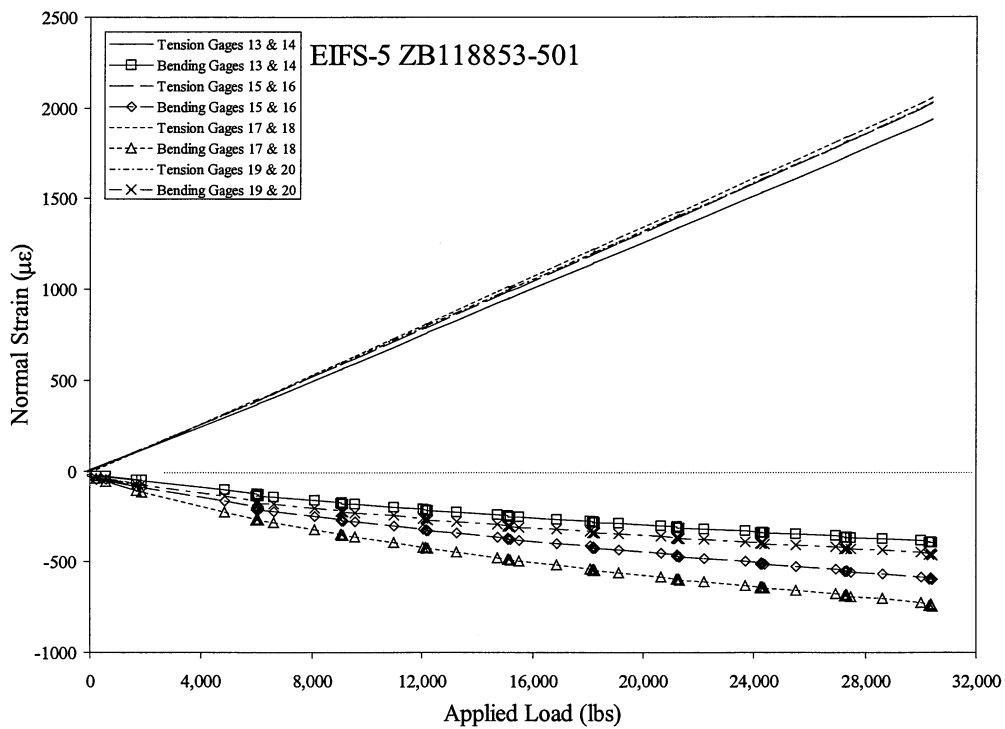


Figure 35 EIFS-5 Top Sheet Critical Rivet Row Normal Strains



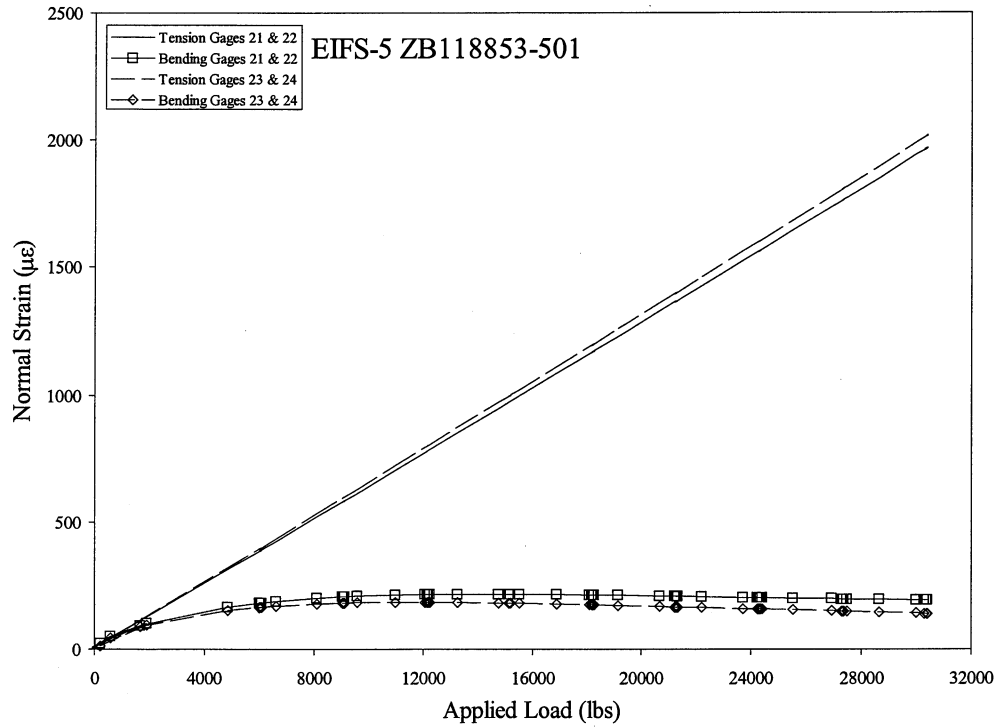


Figure 36 EIFS-5 Bottom Sheet Normal Strains

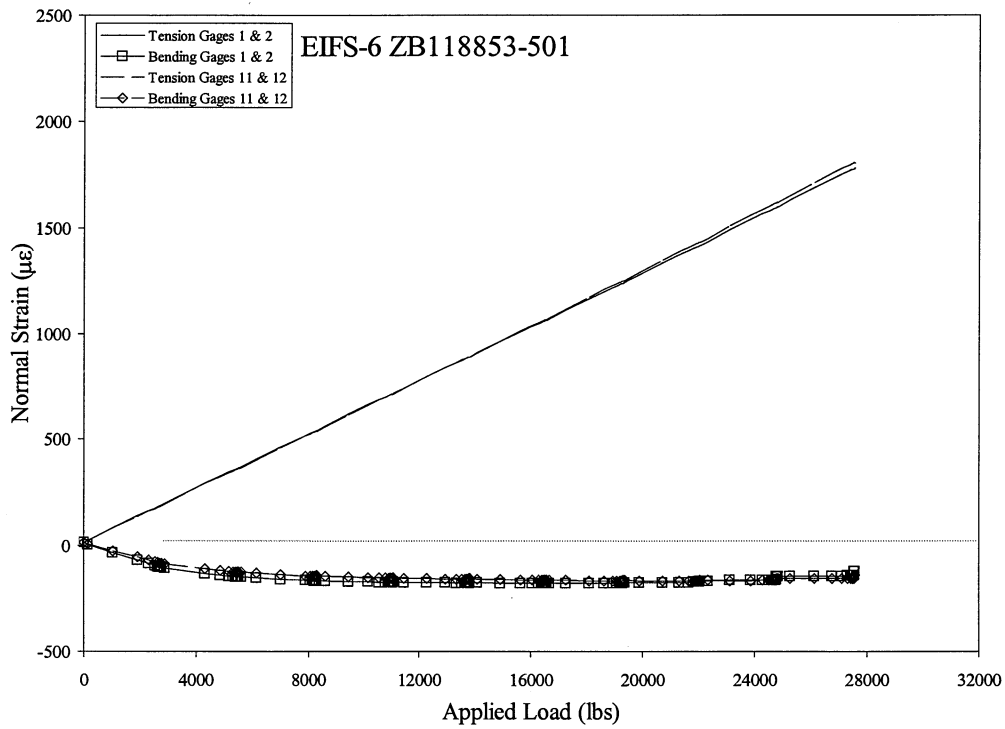


Figure 37 EIFS-6 Top Sheet Normal Strains

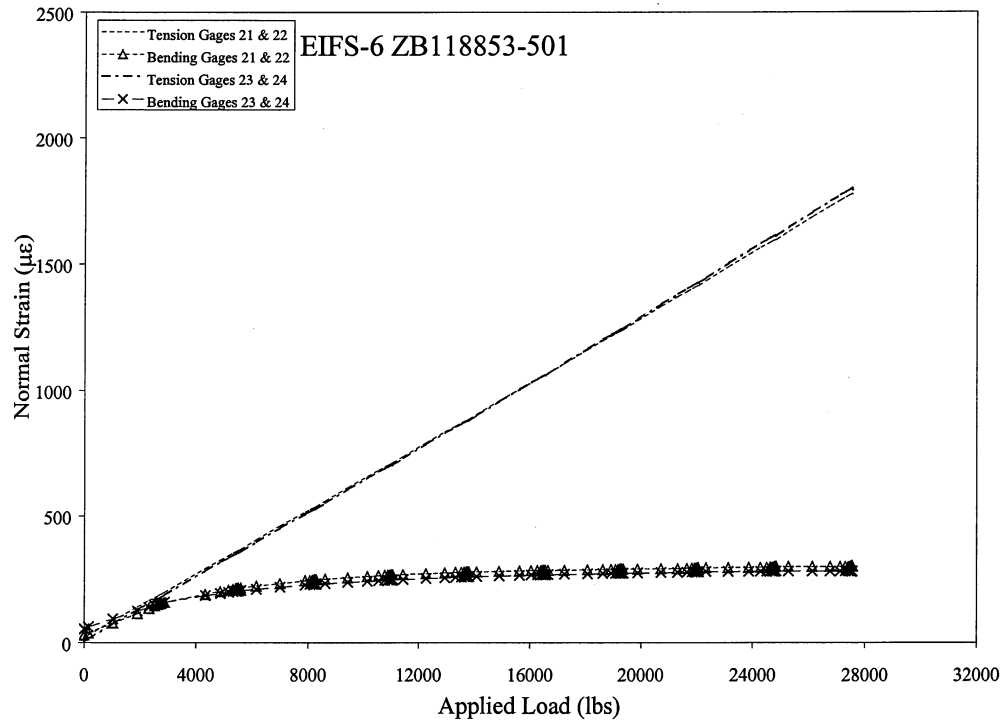


Figure 38 EIFS-6 Bottom Sheet Normal Strains

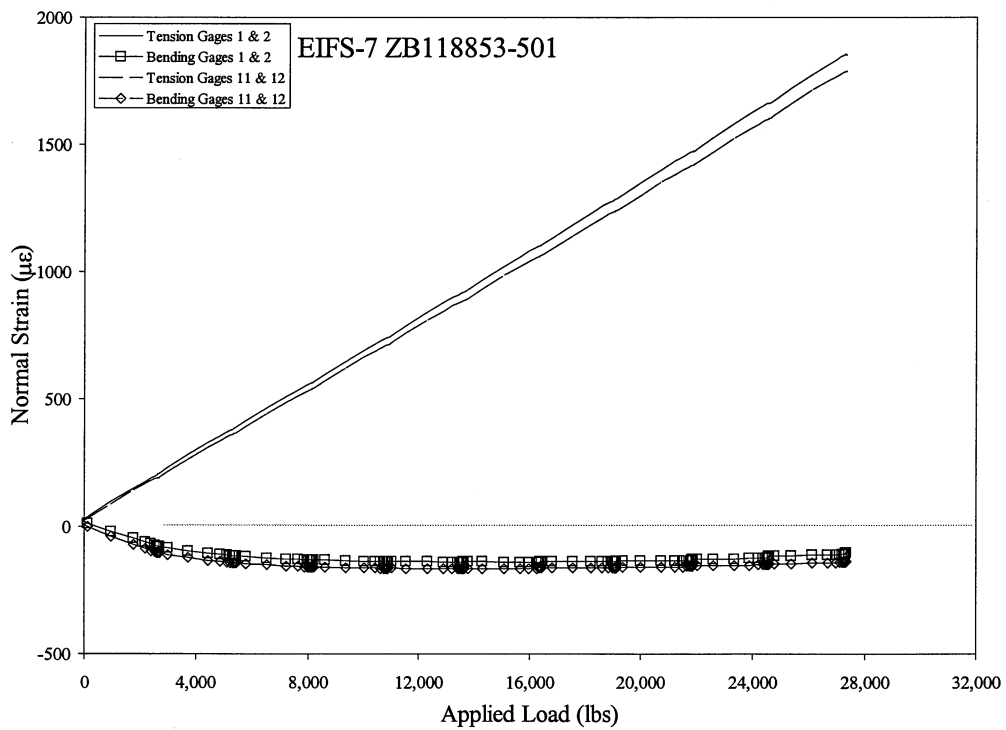


Figure 39 EIFS-7 Top Sheet Normal Strains

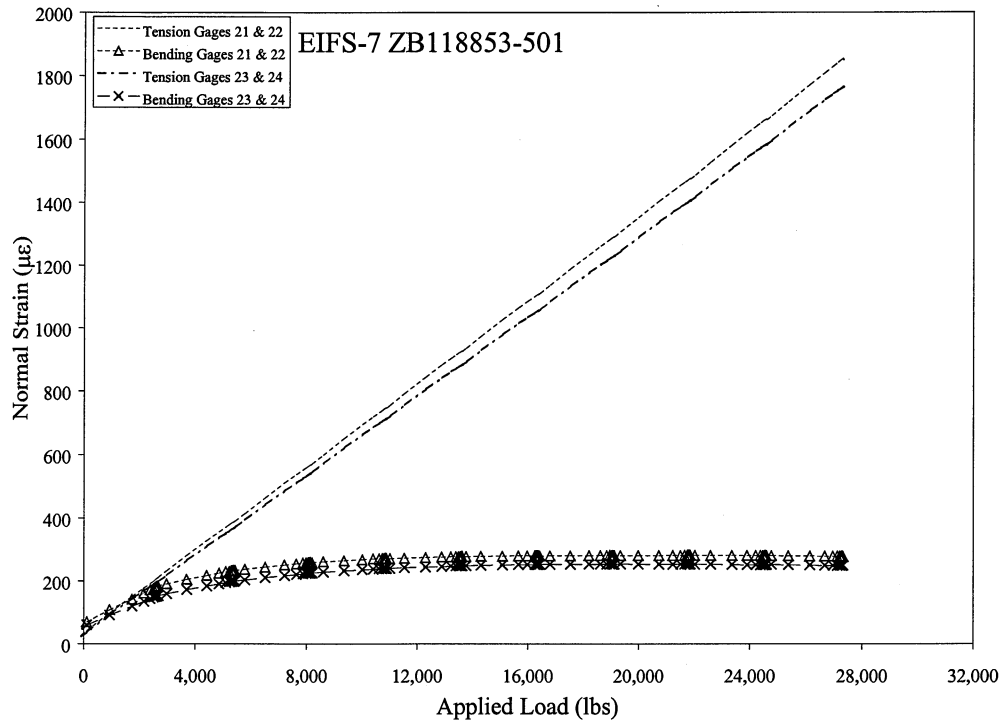


Figure 40 EIFS-7 Bottom Sheet Normal Strains

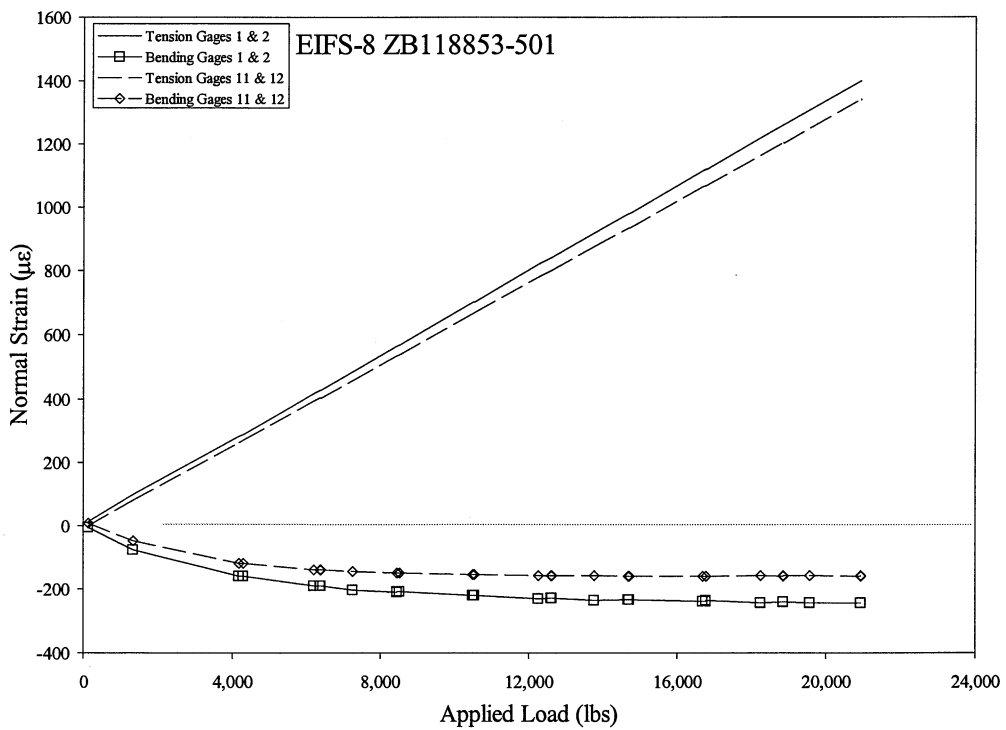


Figure 41 EIFS-8 Top Sheet Normal Strains

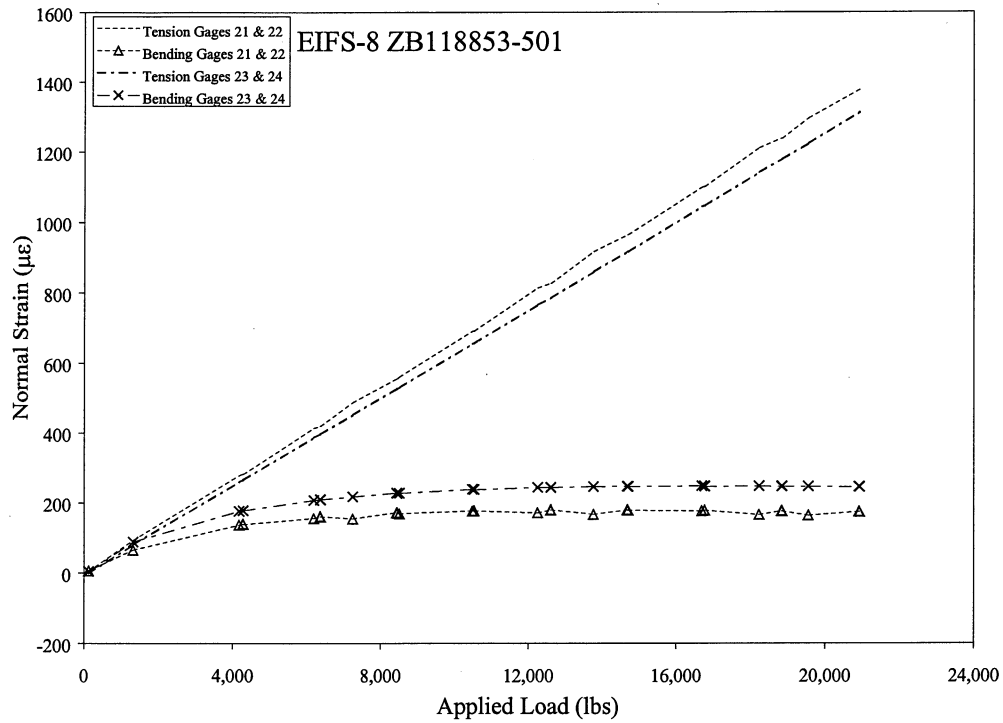


Figure 42 EIFS-8 Bottom Sheet Normal Strains

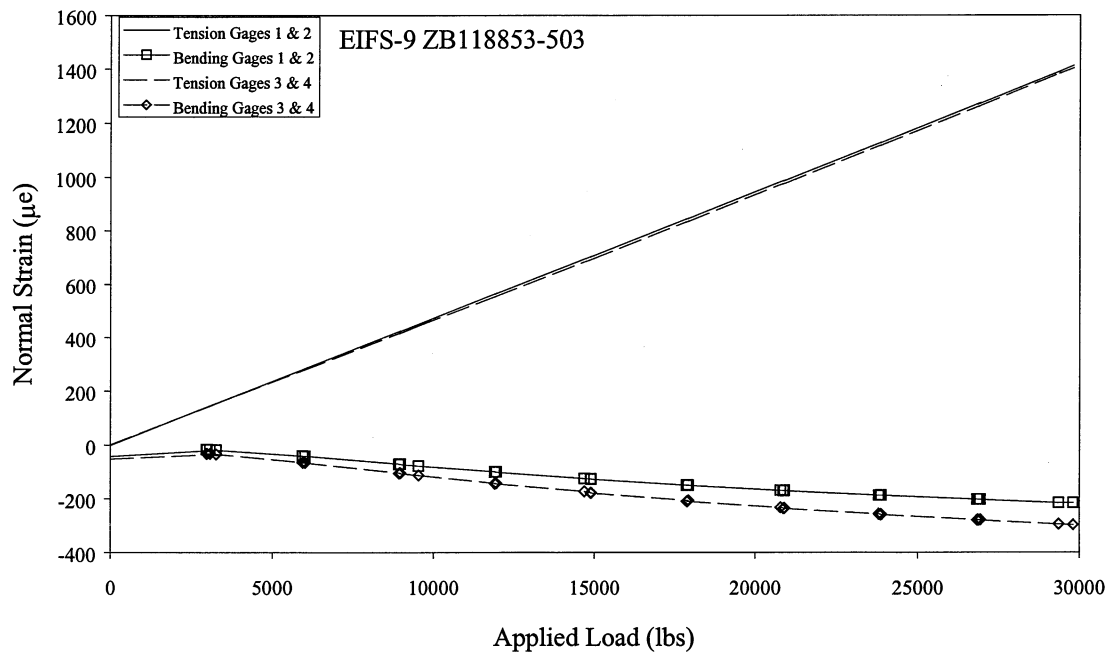


Figure 43 EIFS-9 Top Sheet, Left Side Normal Strains

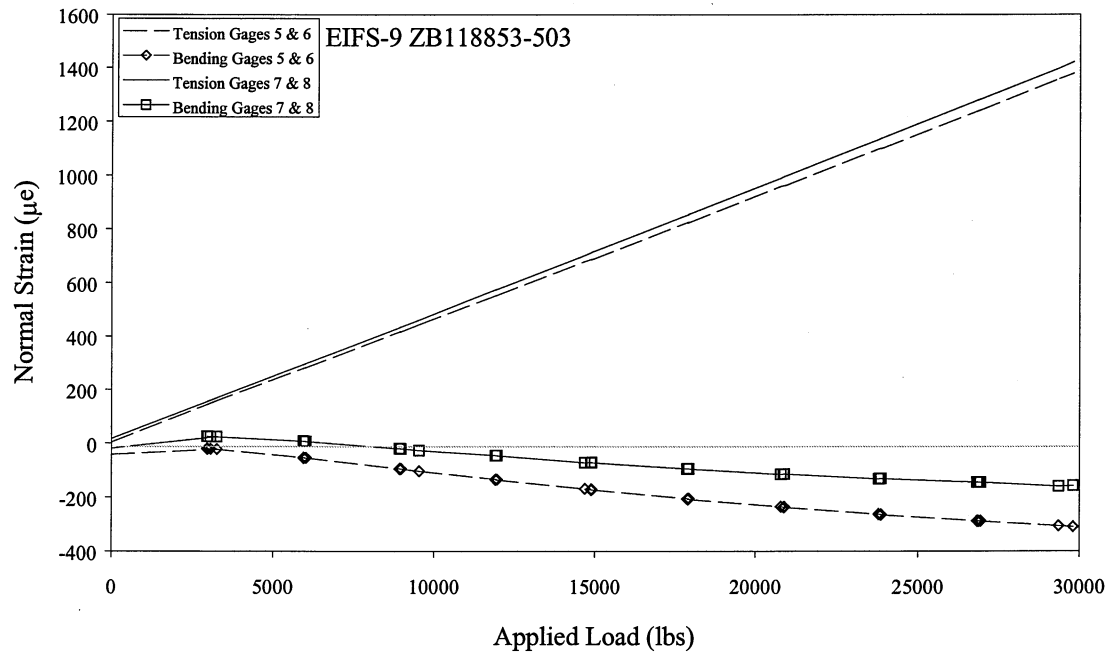


Figure 44 EIFS-9 Top Sheet, Right Side Normal Strains

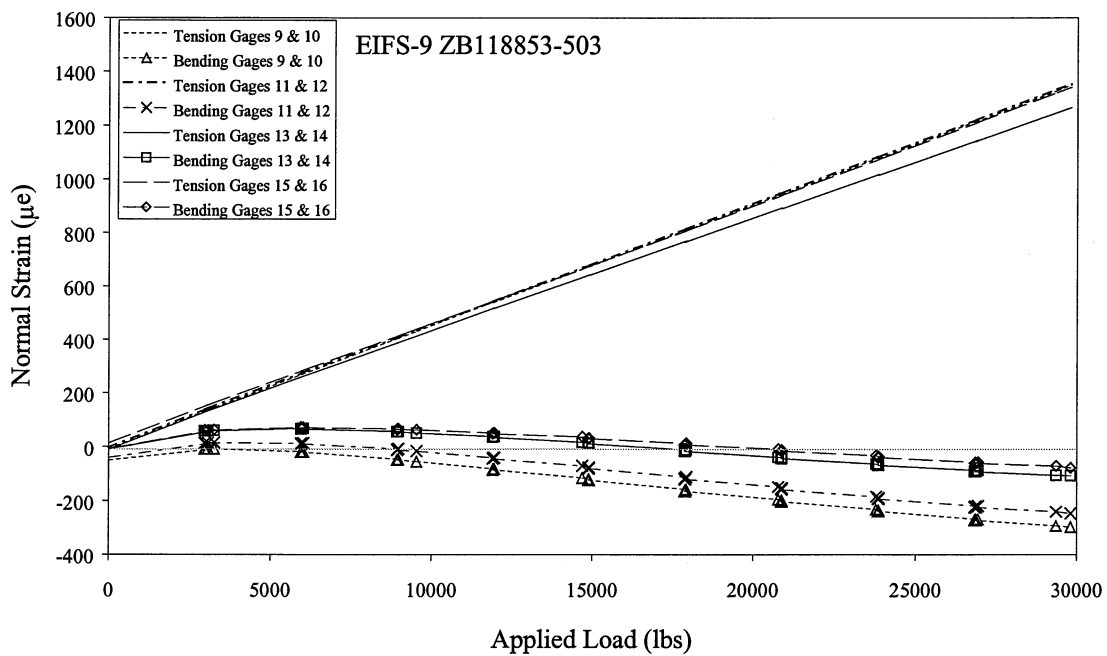


Figure 45 EIFS-9 Top Sheet, Critical Rivet Row Normal Strains

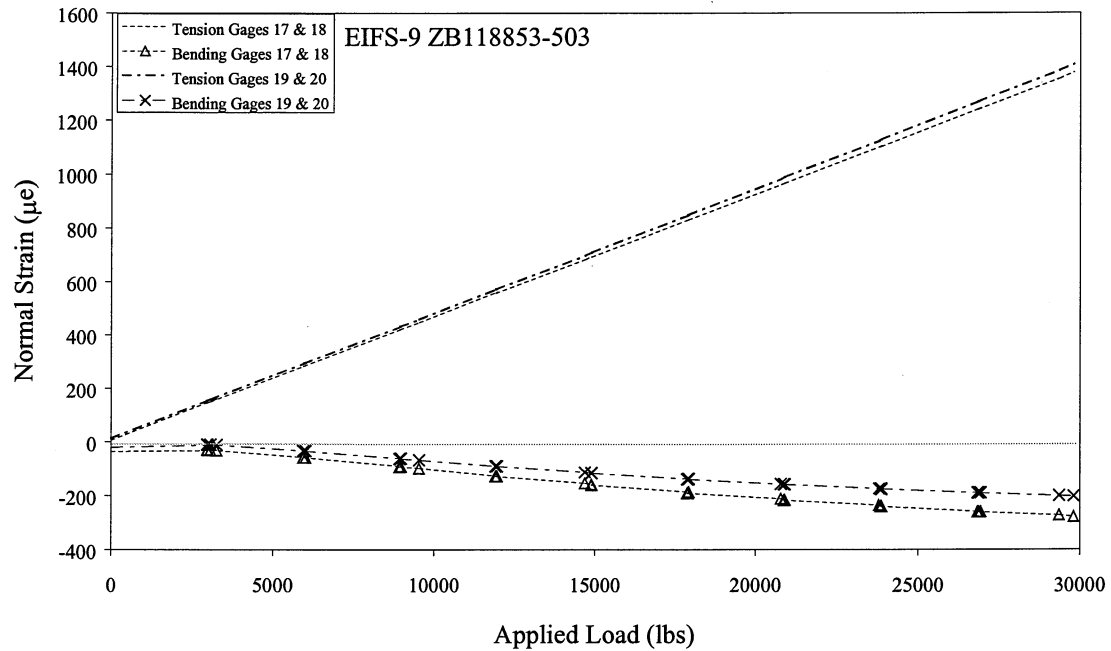


Figure 46 EIFS-9 Bottom Sheet Normal Strains

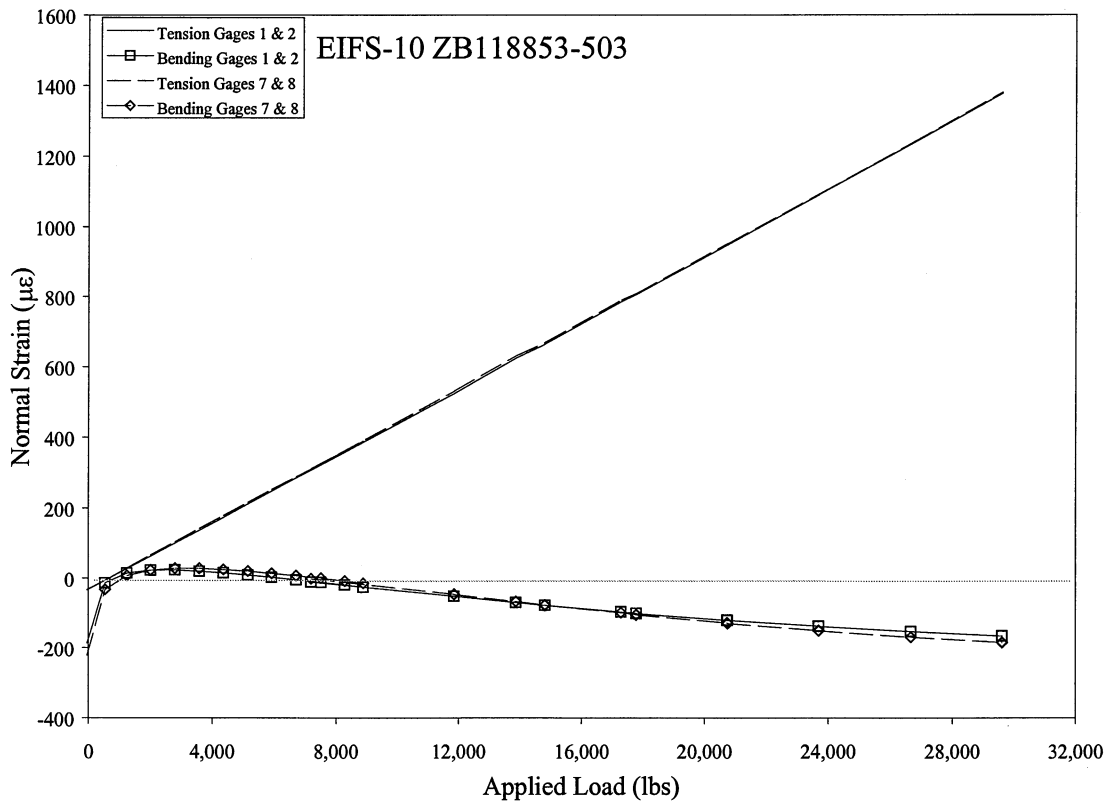
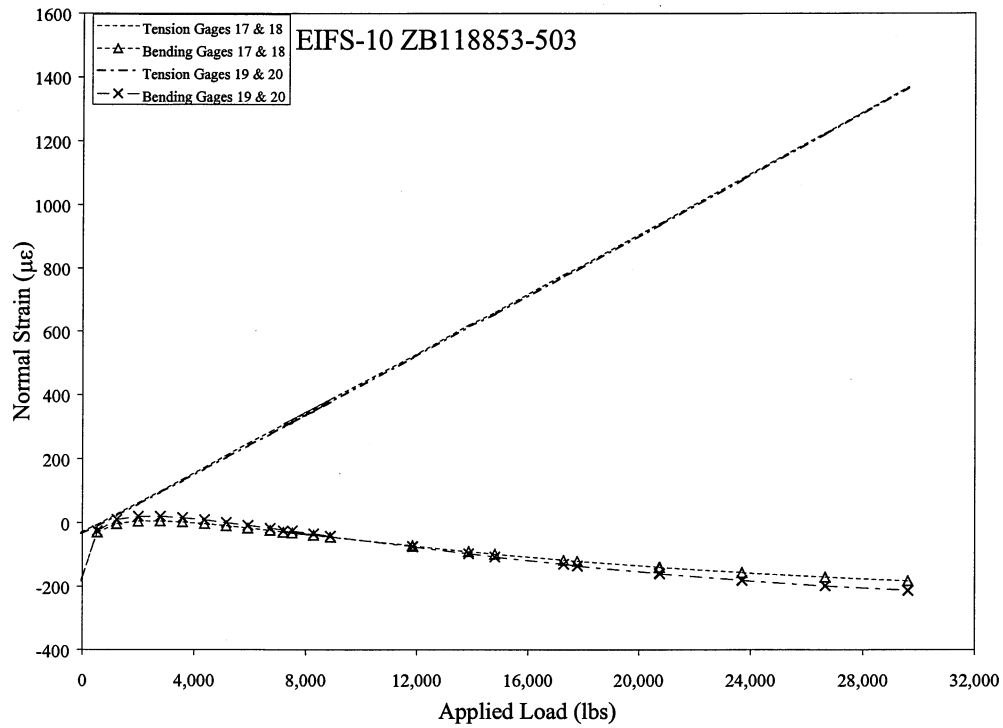
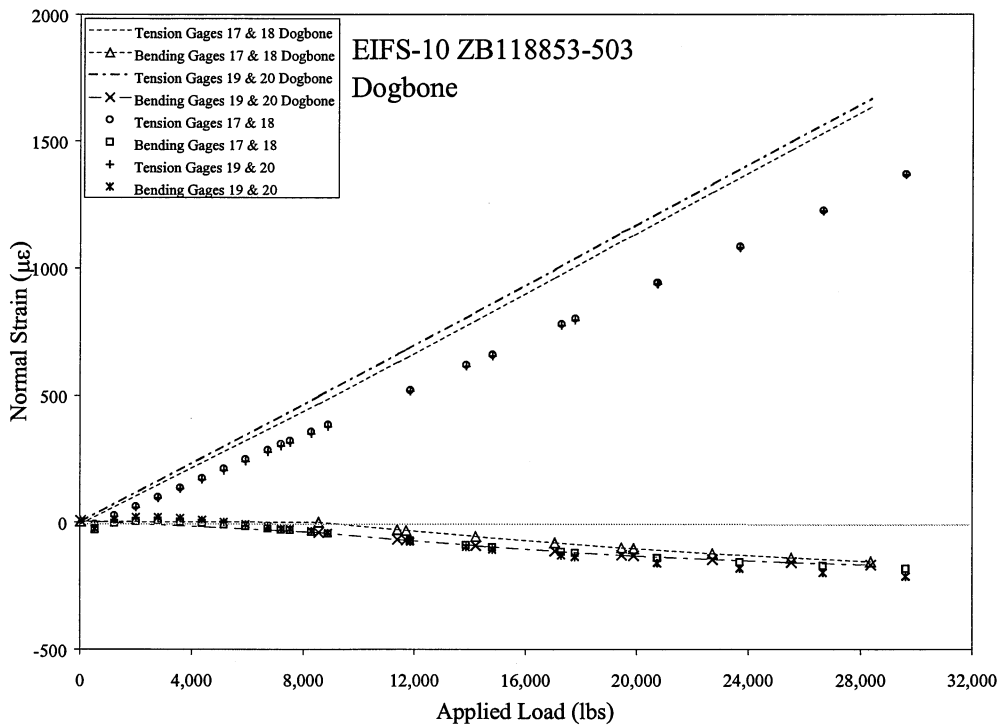


Figure 47 EIFS-10 Top Sheet Normal Strains



**Figure 48 EIFS-10 Bottom Sheet Normal Strains**



**Figure 49 EIFS-10 Bottom Sheet Normal Strains after Dogbone Shape Cut into Top and Bottom Sheets and Applied Load Adjusted to Maintain Constant Remote Tensile Stress**

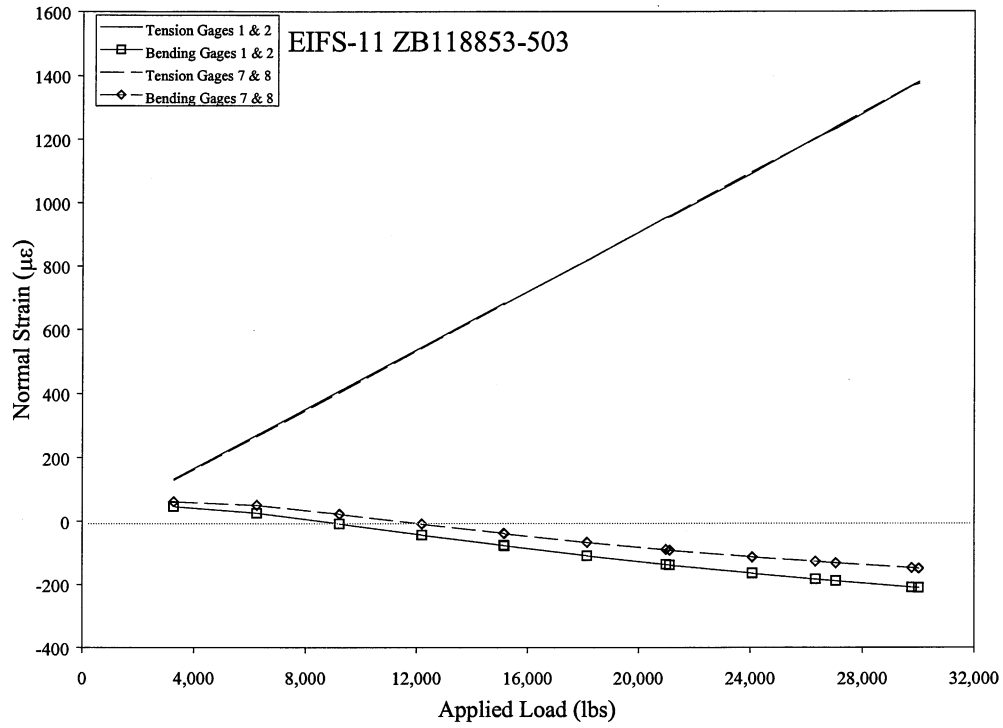


Figure 50 EIFS-11 Top Sheet Normal Strains

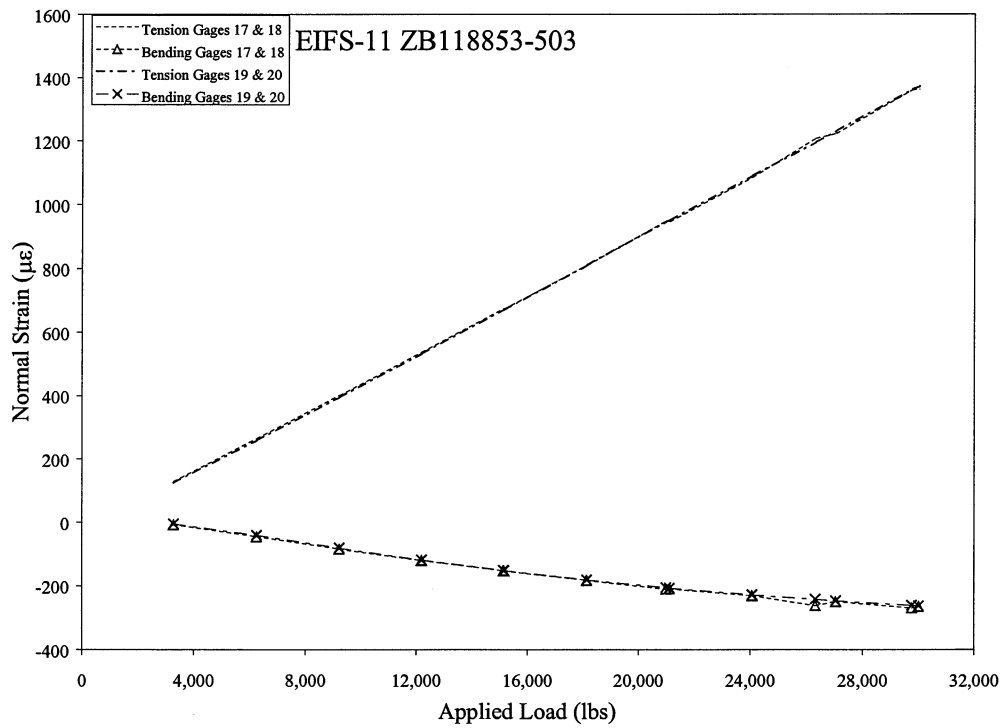
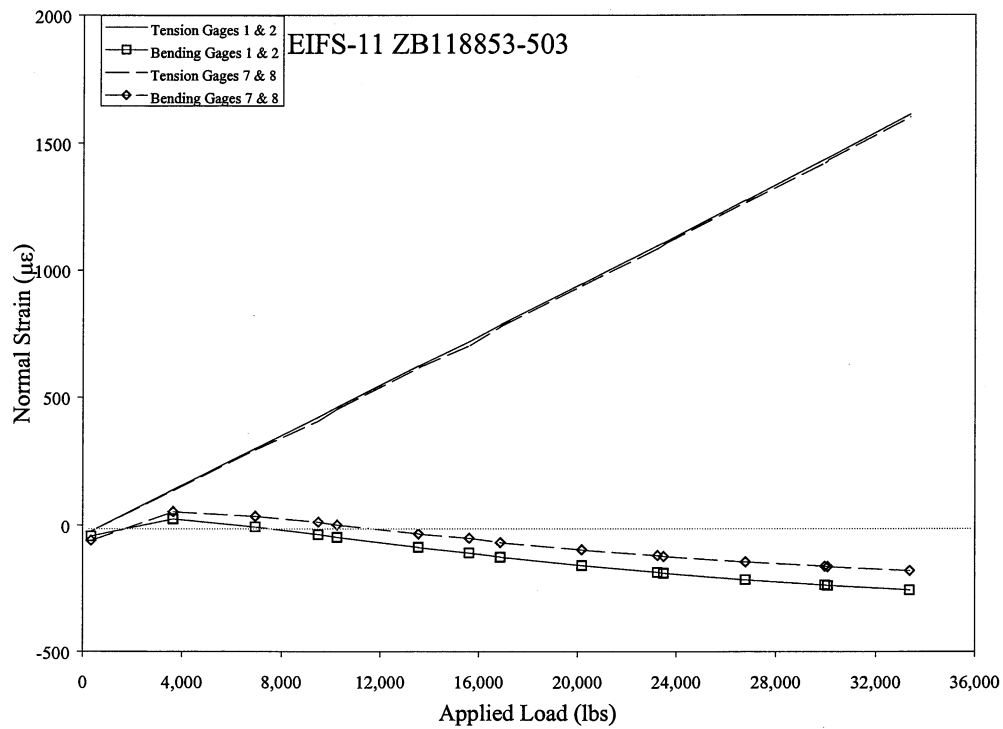
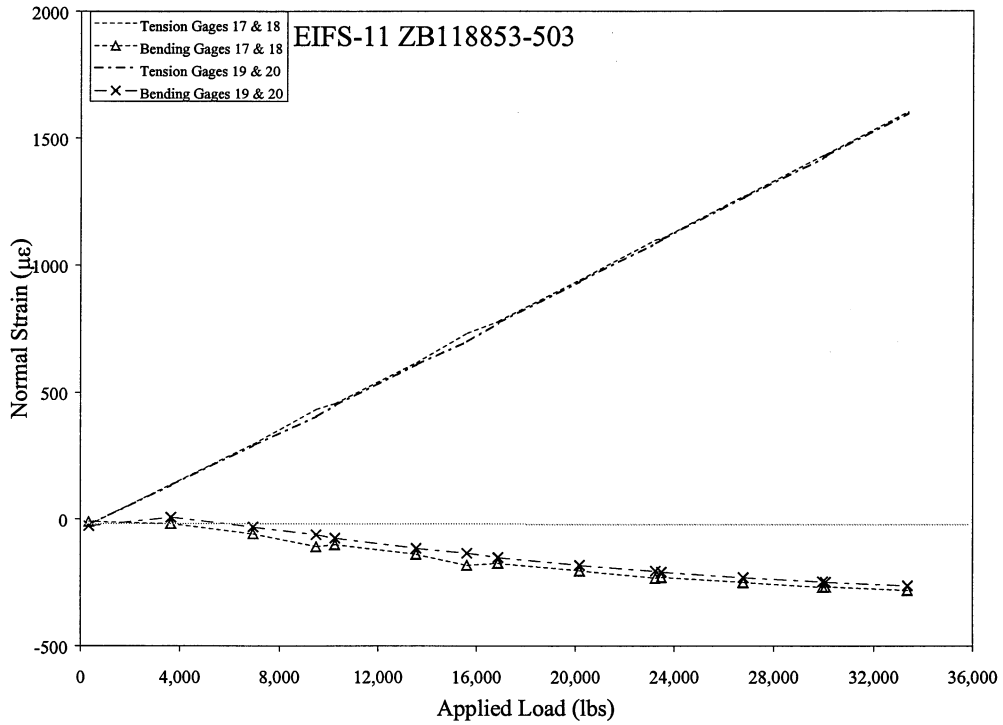


Figure 51 EIFS-11 Bottom Sheet Normal Strains





**Figure 52 EIFS-11 Top Sheet Normal Strains after Dogbone and Load Adjustment**



**Figure 53 EIFS-11 Bottom Sheet Normal Strains after Dogbone and Load Adjustment**

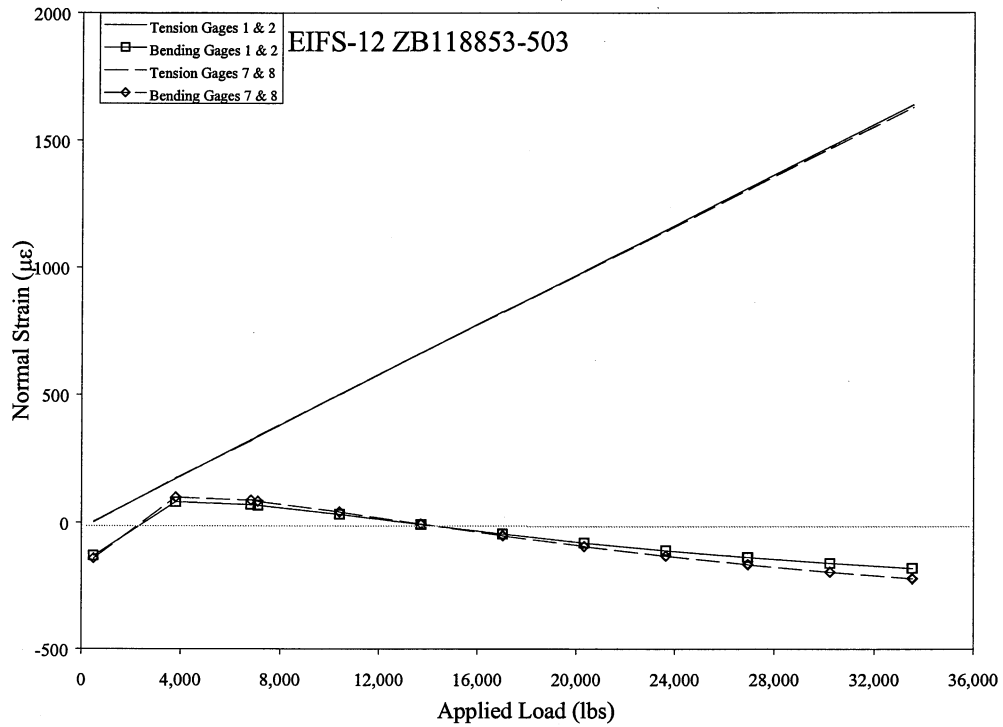


Figure 54 EIFS-12 Top Sheet Normal Strains after Dogbone and Load Adjustment

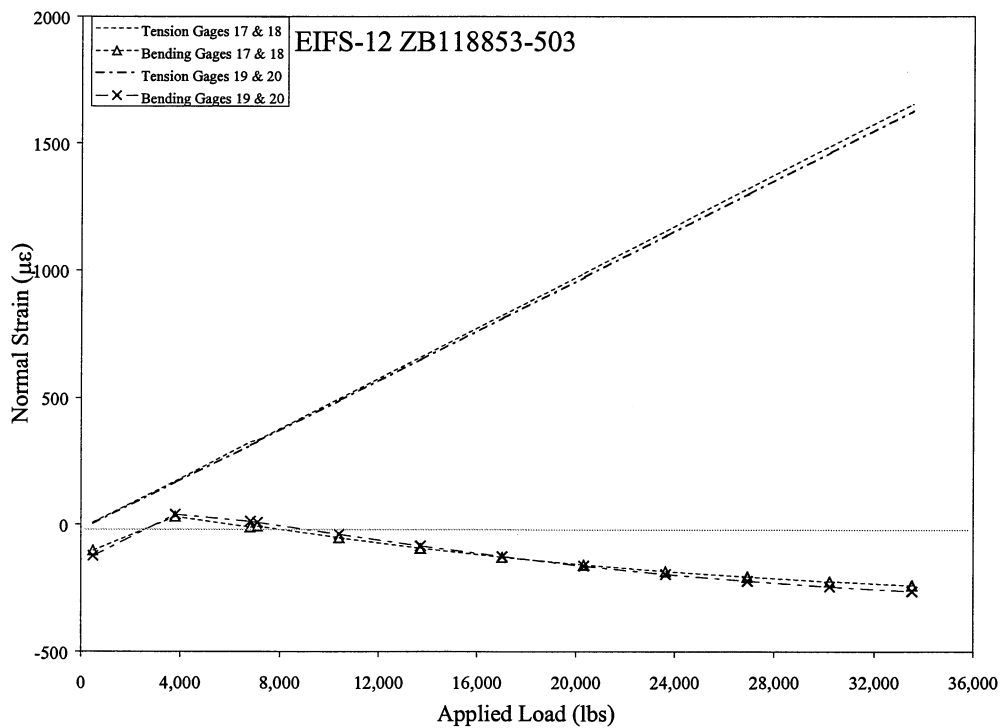


Figure 55 EIFS-12 Bottom Sheet Normal Strains after Dogbone and Load Adjustment

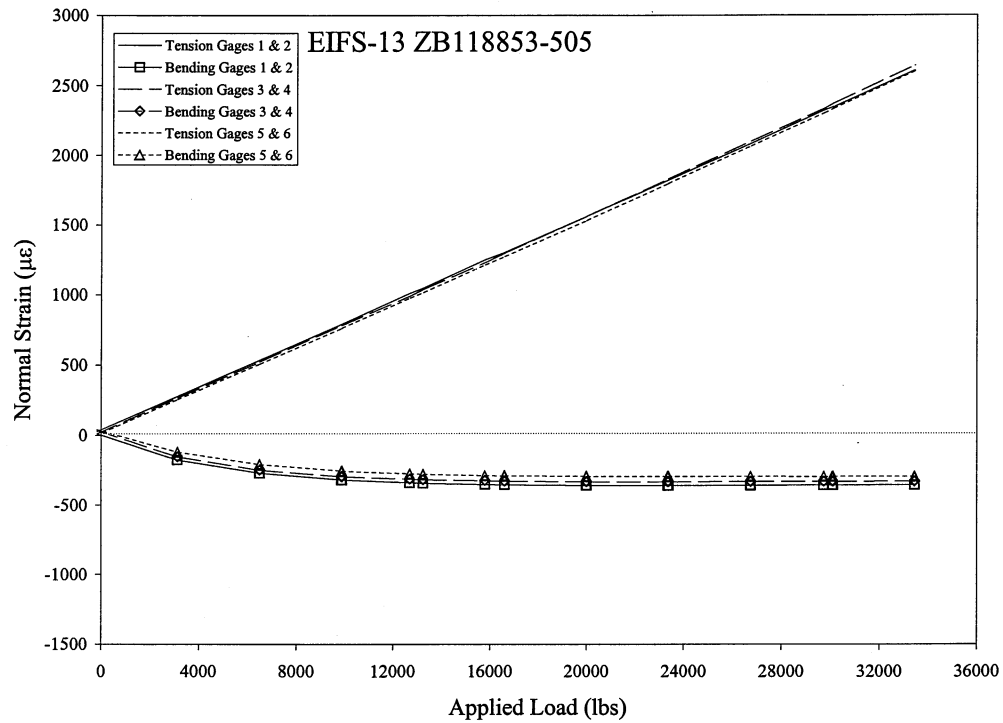


Figure 56 EIFS-13 Top Sheet, Left Side Normal Strains

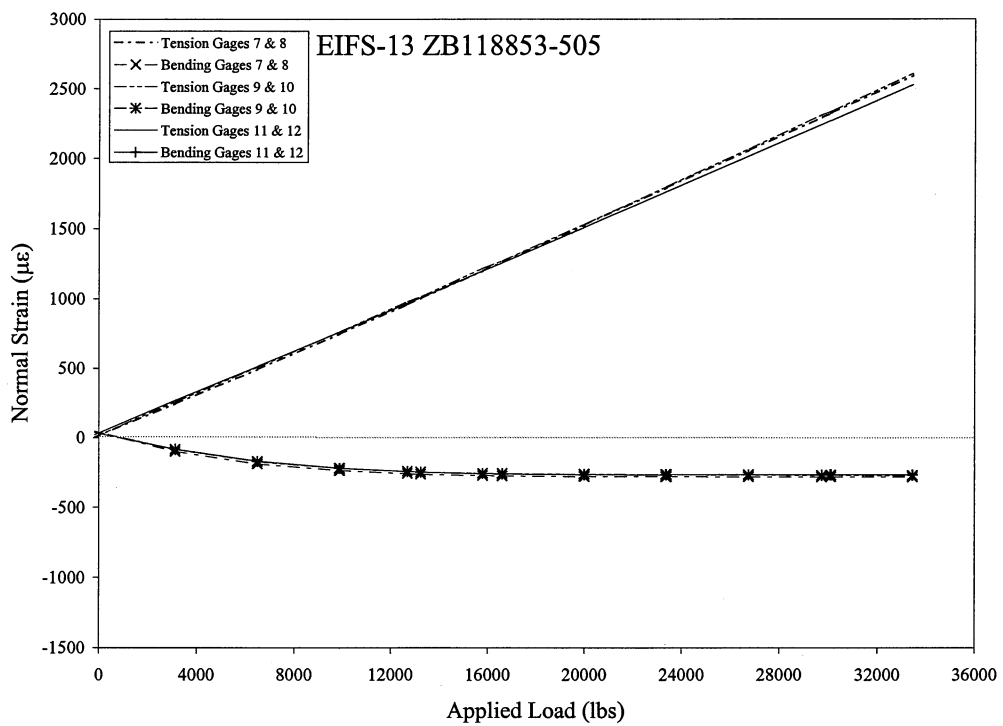


Figure 57 EIFS-13 Top Sheet, Right Side Normal Strains

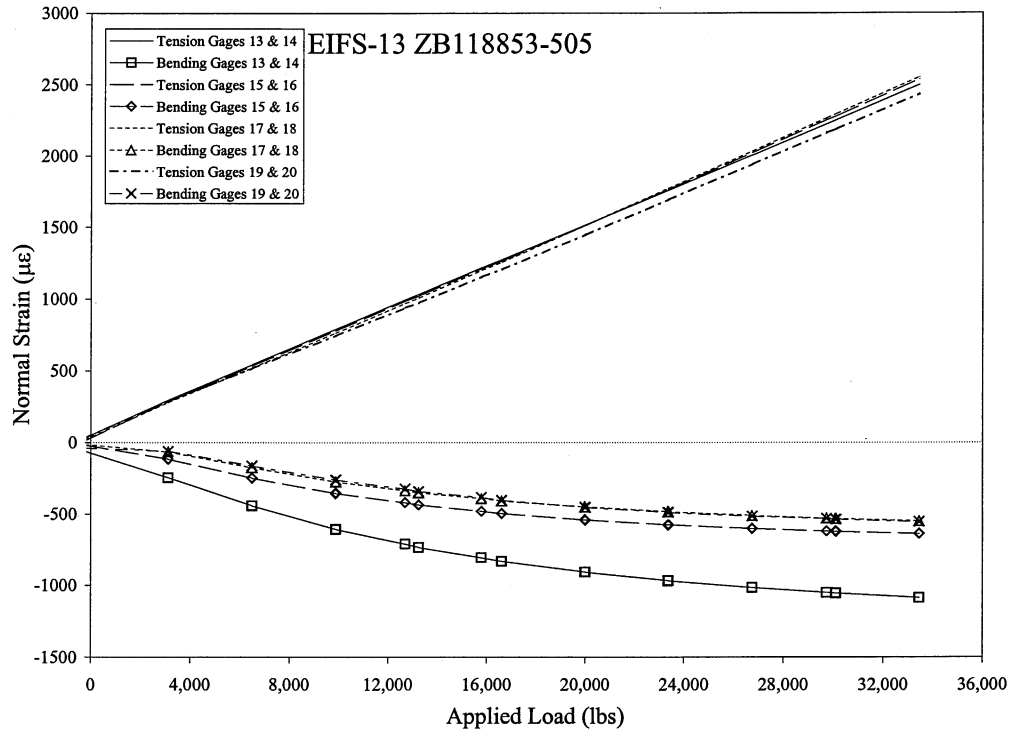


Figure 58 EIFS-13 Top Sheet, Critical Rivet Row Normal Strains

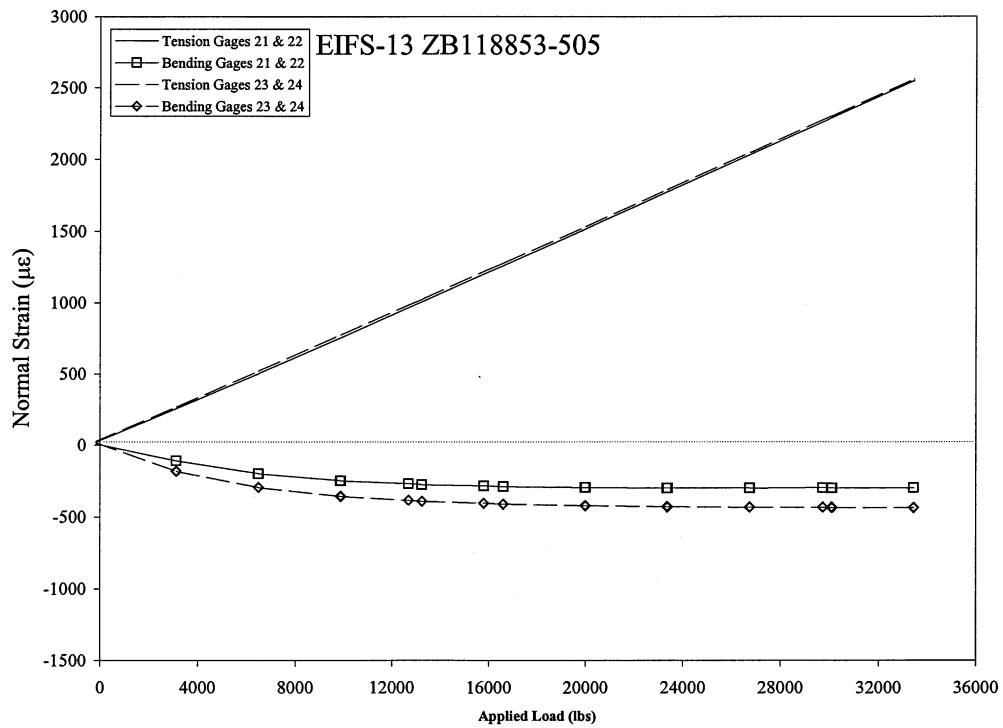


Figure 59 EIFS-13 Bottom Sheet Normal Strains

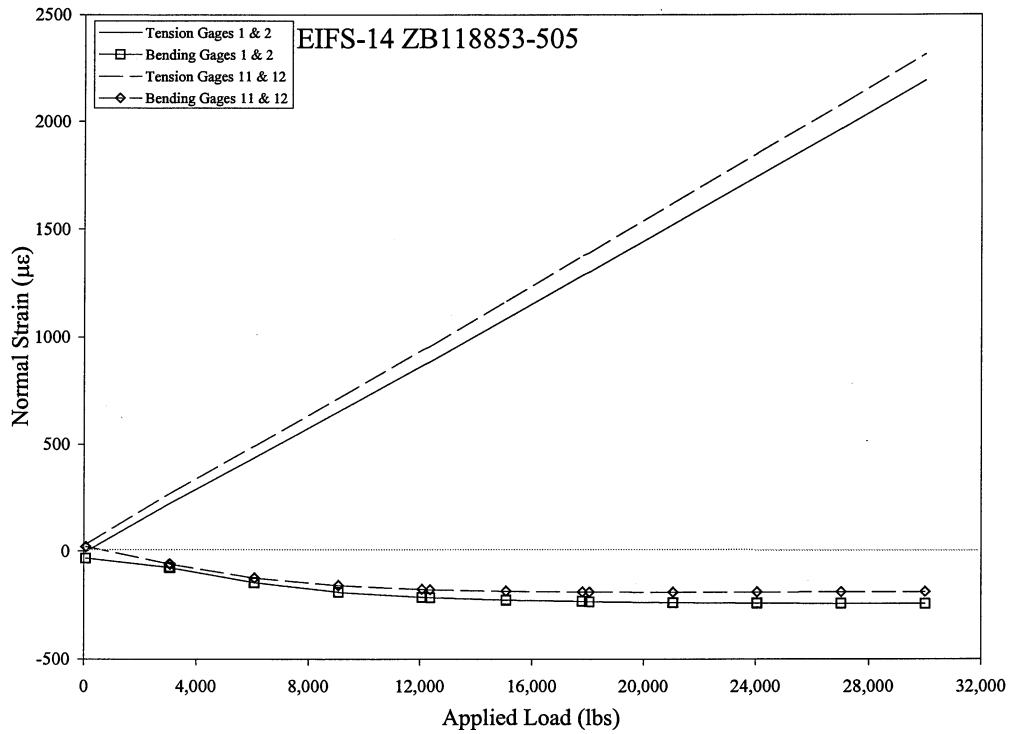


Figure 60 EIFS-14 Top Sheet Normal Strains

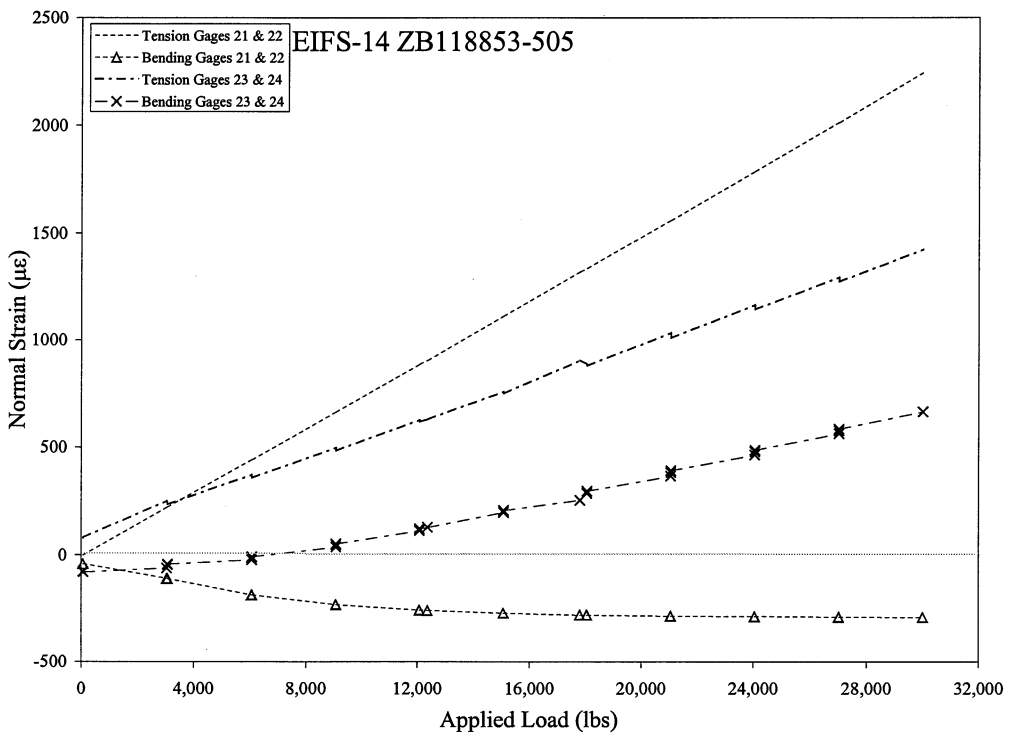
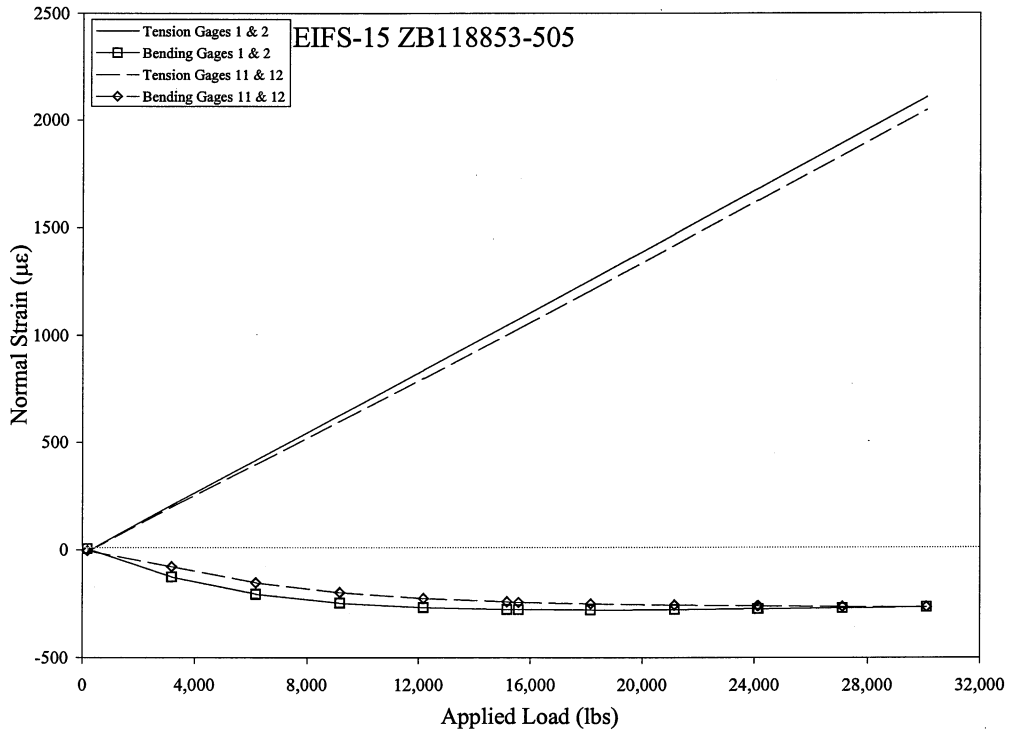
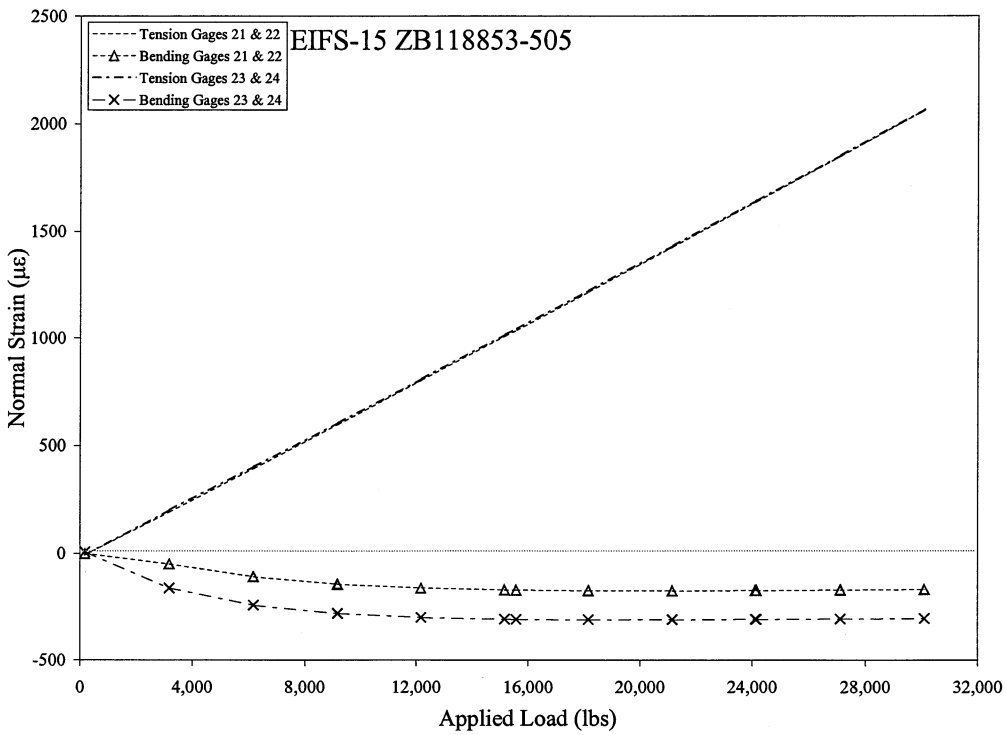


Figure 61 EIFS-14 Bottom Sheet Normal Strains



**Figure 62 EIFS-15 Top Sheet Normal Strains**



**Figure 63 EIFS-15 Bottom Sheet Normal Strains**

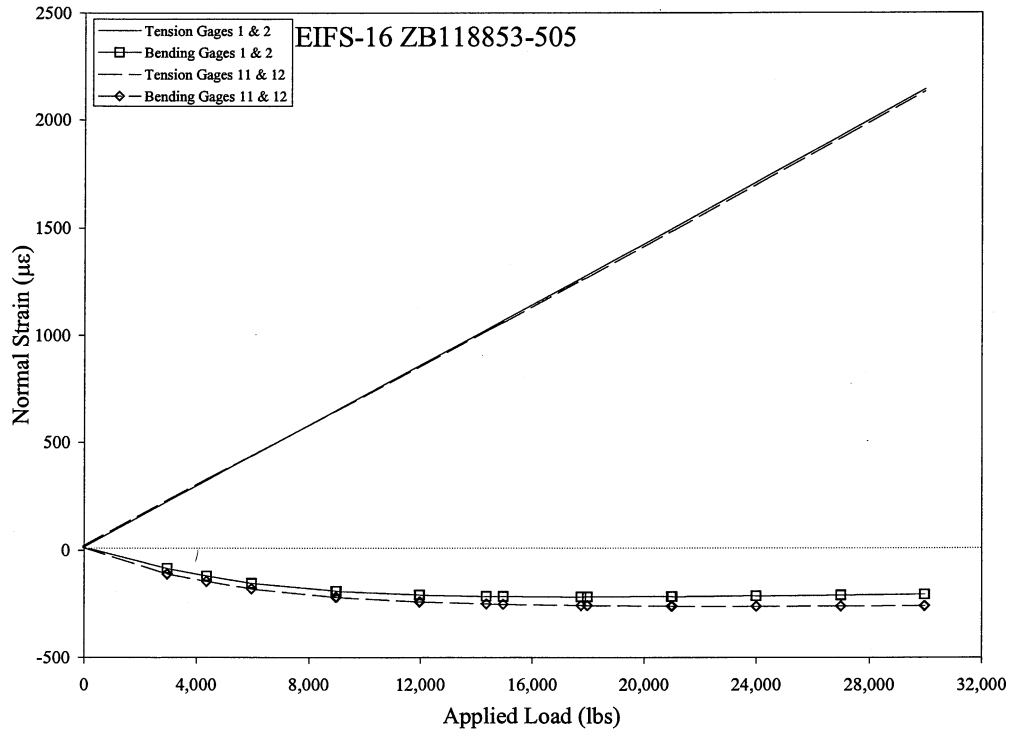


**Figure 64 EIFS-16 Top Sheet Normal Strains**

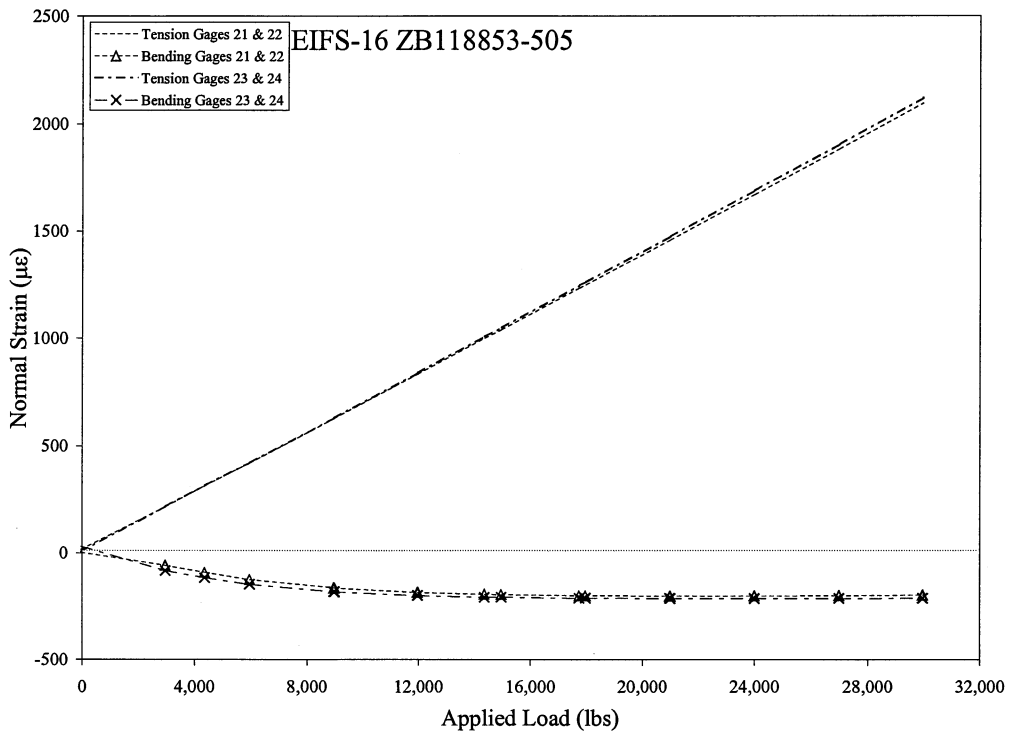


**Figure 65 EIFS-16 Bottom Sheet Normal Strains**

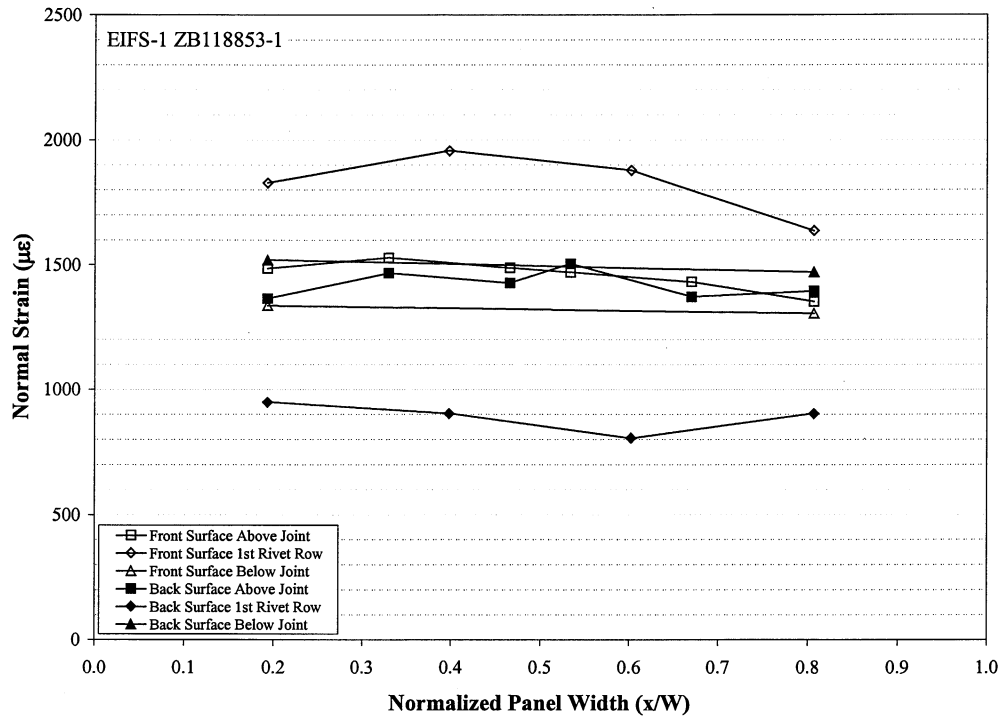


Figure 66 Strain Variation Through the Width of the Joint, EIFS-1

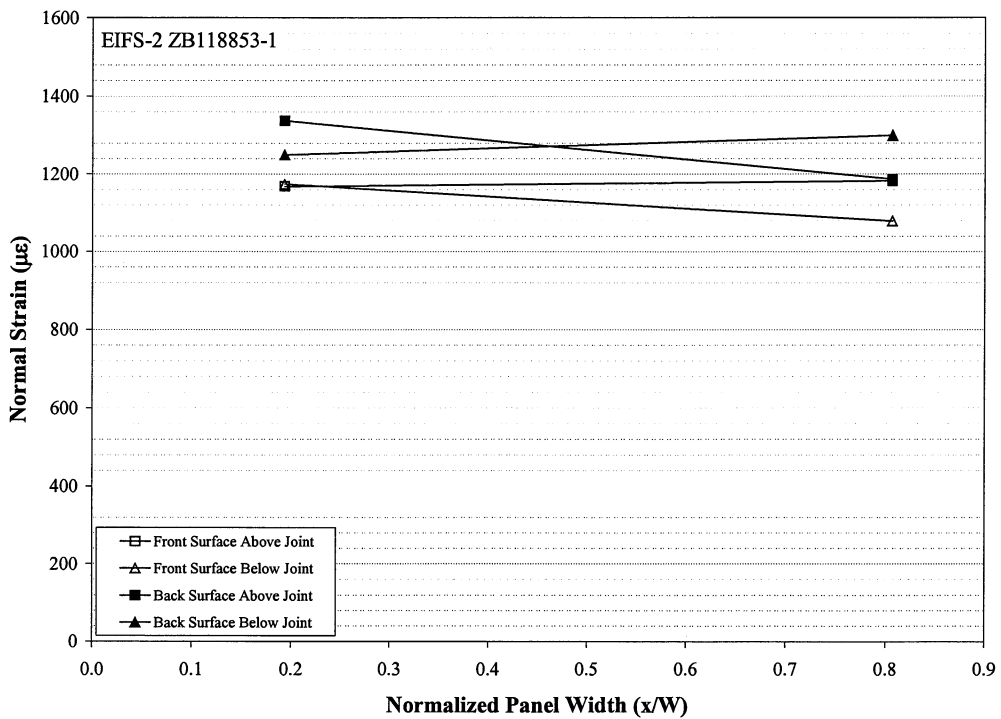
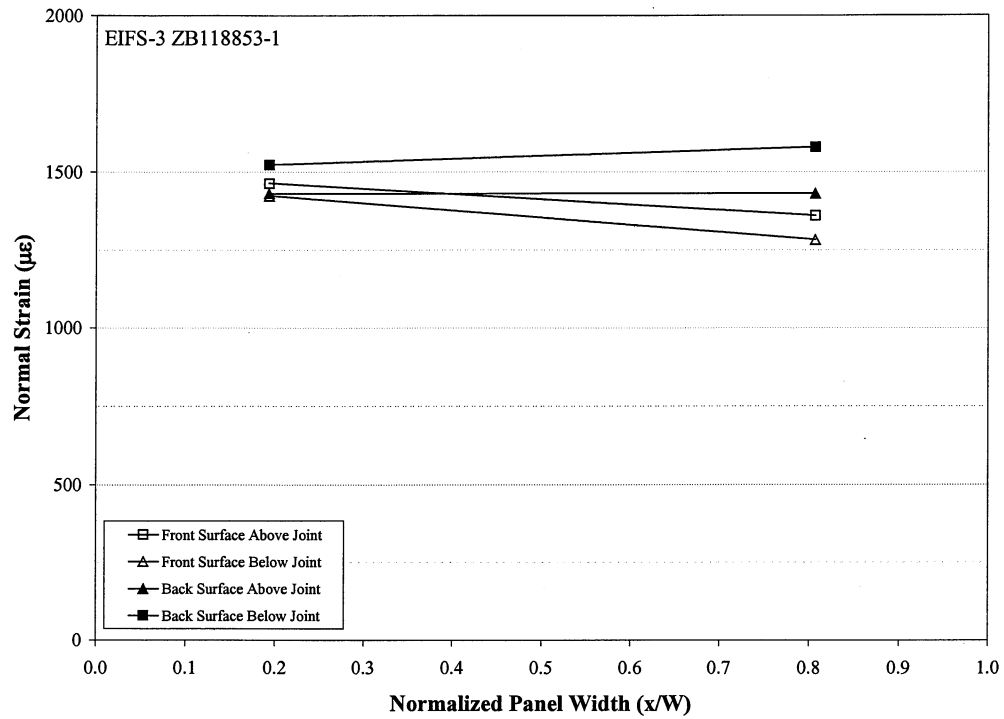
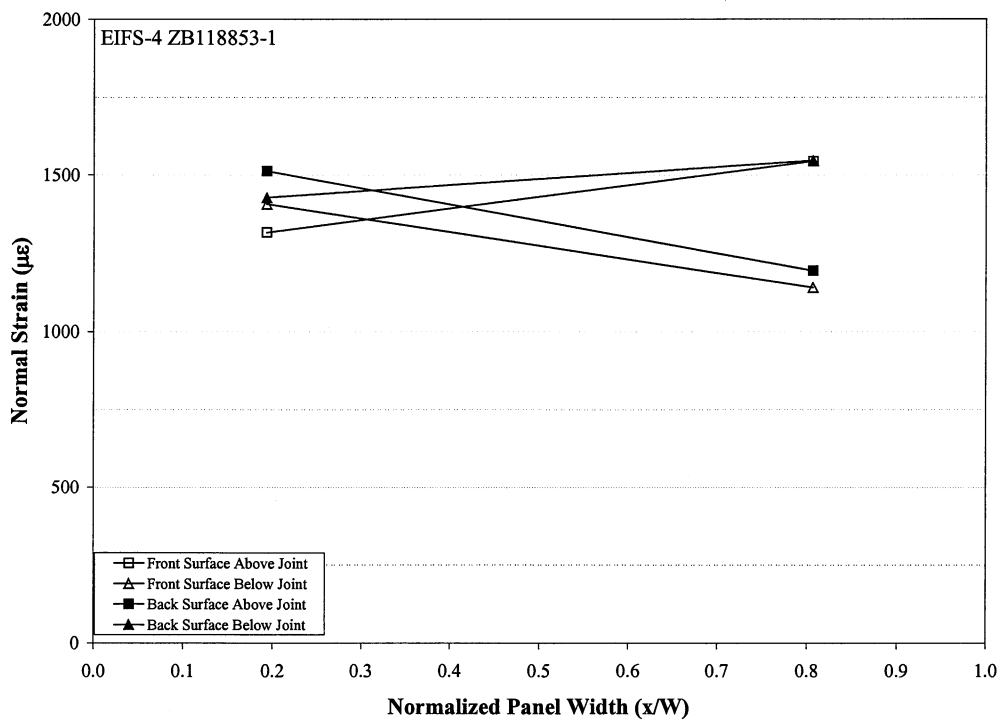


Figure 67 Strain Variation Through the Width of the Joint, EIFS-2





**Figure 68 Strain Variation Through the Width of the Joint, EIFS-3**



**Figure 69 Strain Variation Through the Width of the Joint, EIFS-4**

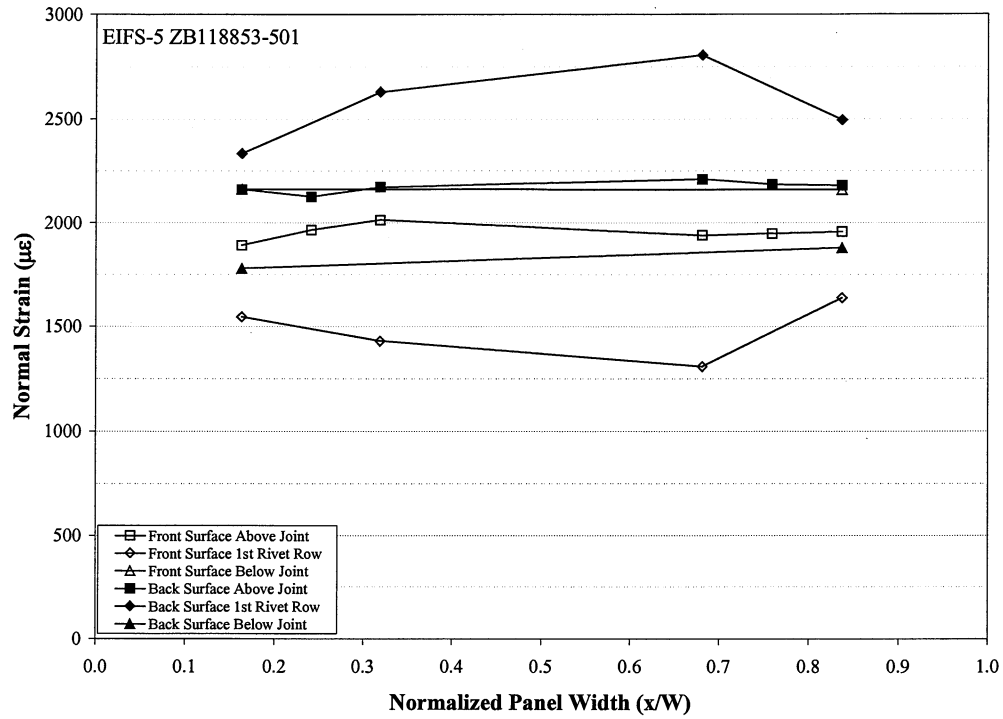


Figure 70 Strain Variation Through the Width of the Joint, EIFS-5

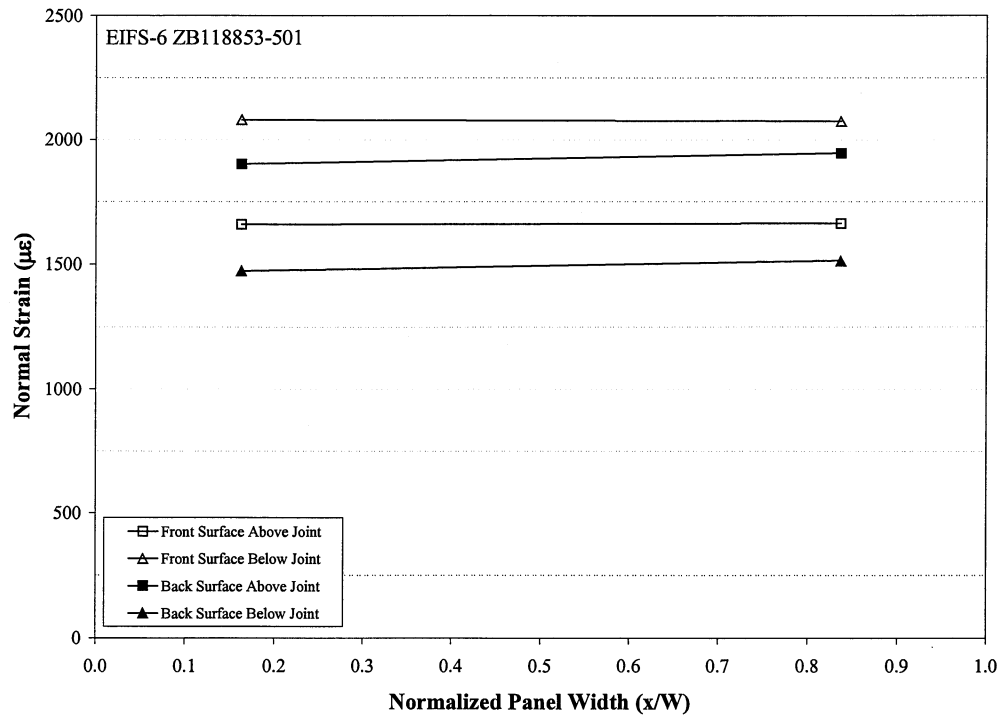


Figure 71 Strain Variation Through the Width of the Joint, EIFS-6

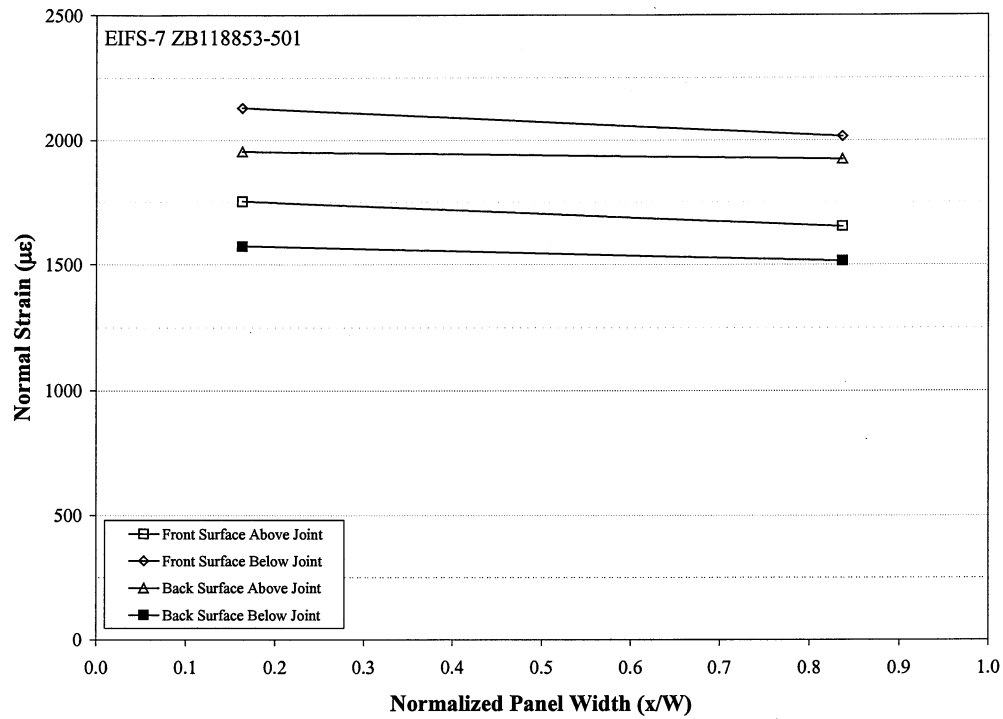


Figure 72 Strain Variation Through the Width of the Joint, EIFS-7

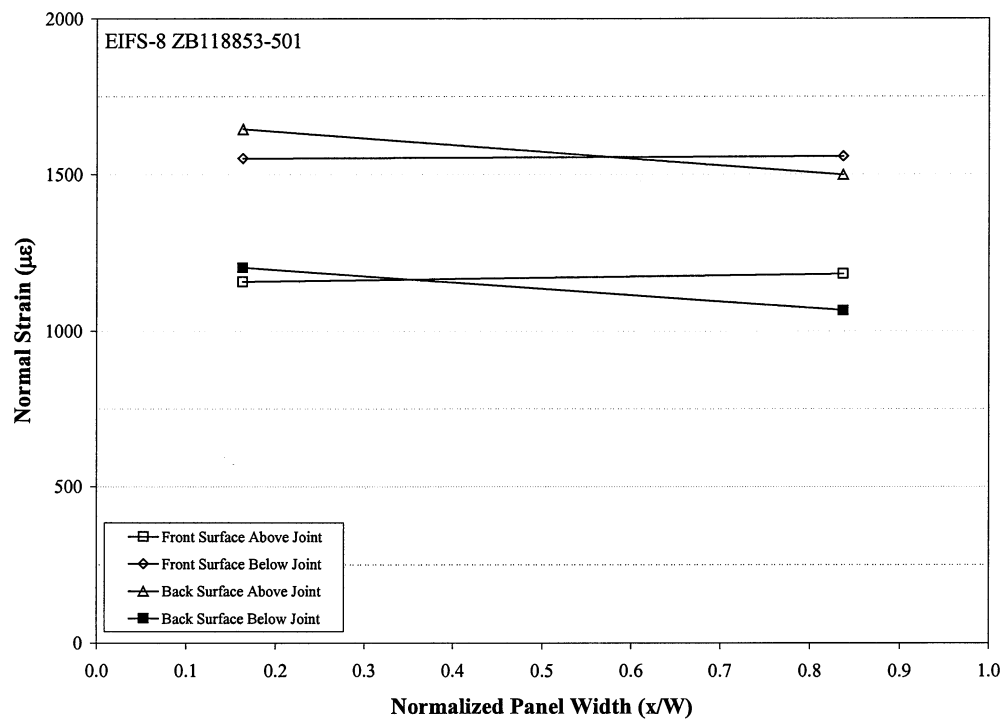


Figure 73 Strain Variation Through the Width of the Joint, EIFS-8

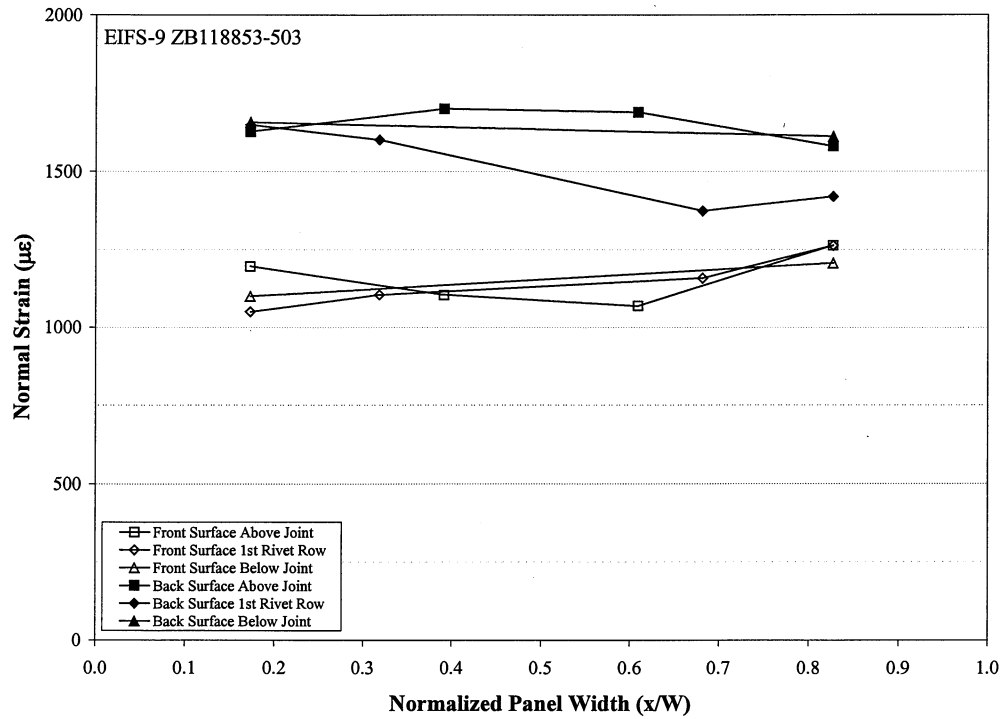


Figure 74 Strain Variation Through the Width of the Joint, EIFS-9

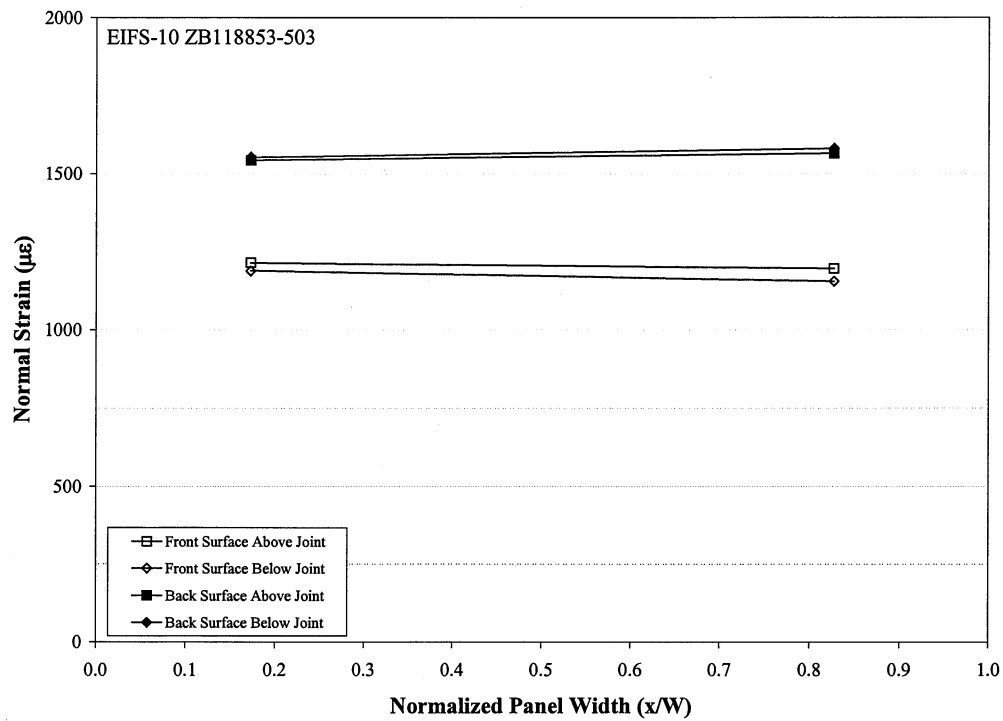
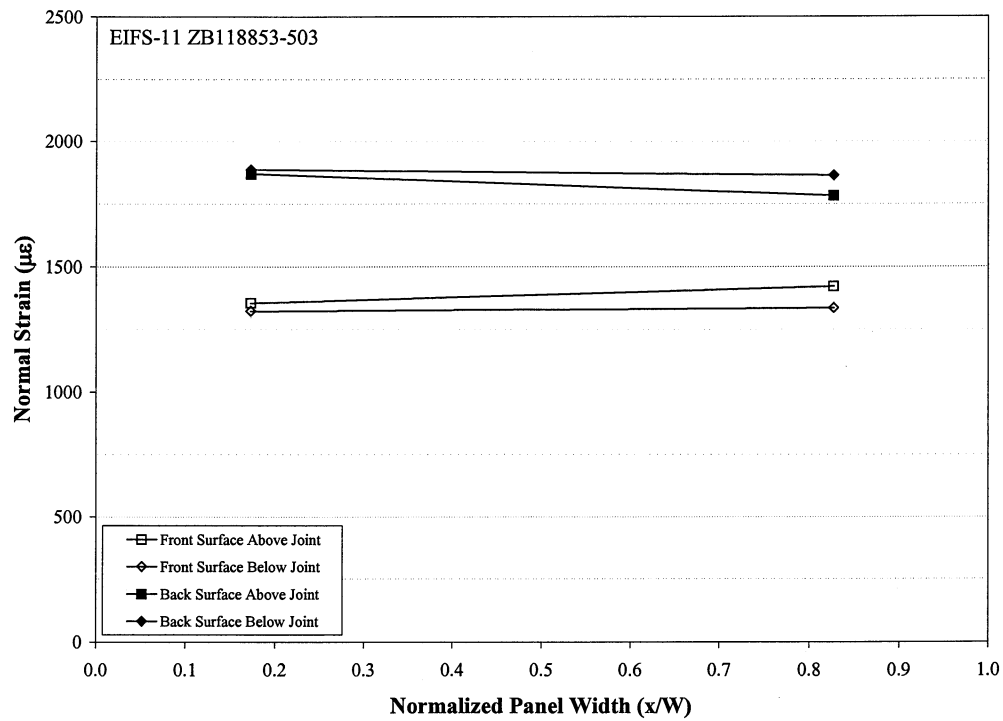
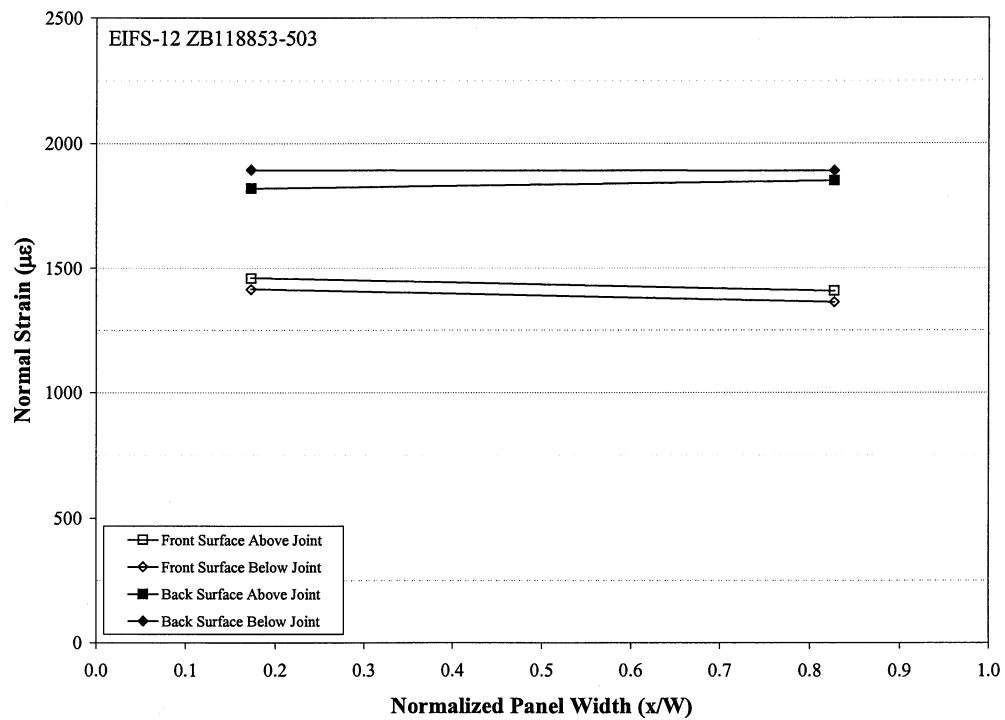


Figure 75 Strain Variation Through the Width of the Joint, EIFS-10



**Figure 76 Strain Variation Through the Width of the Joint, EIFS-11**



**Figure 77 Strain Variation Through the Width of the Joint, EIFS-12**

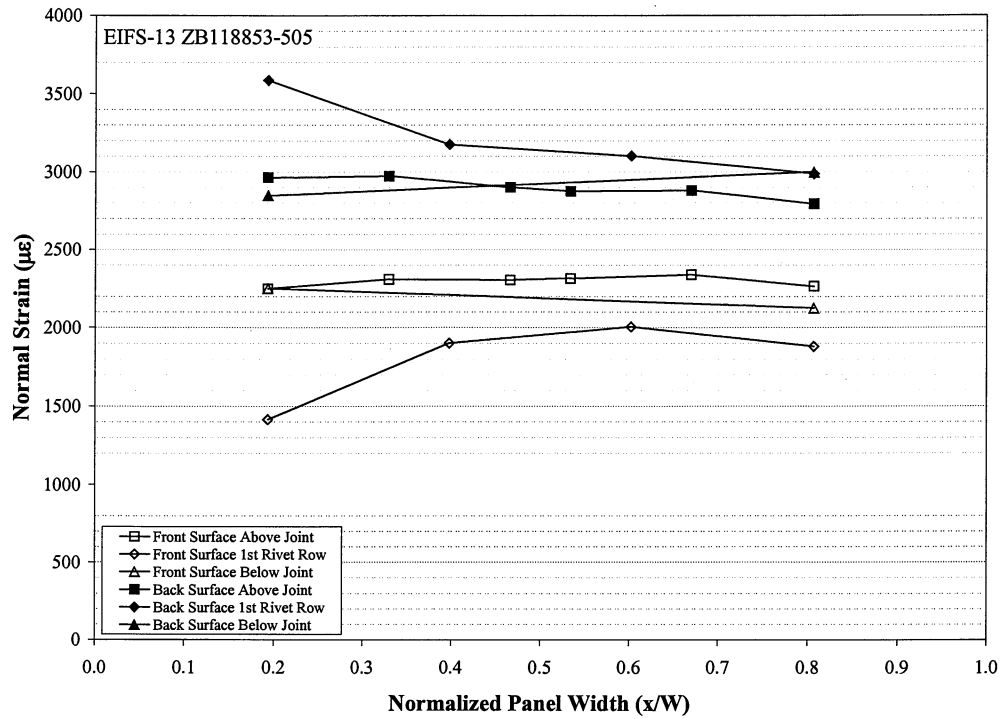


**Figure 78 Strain Variation Through the Width of the Joint, EIFS-13**

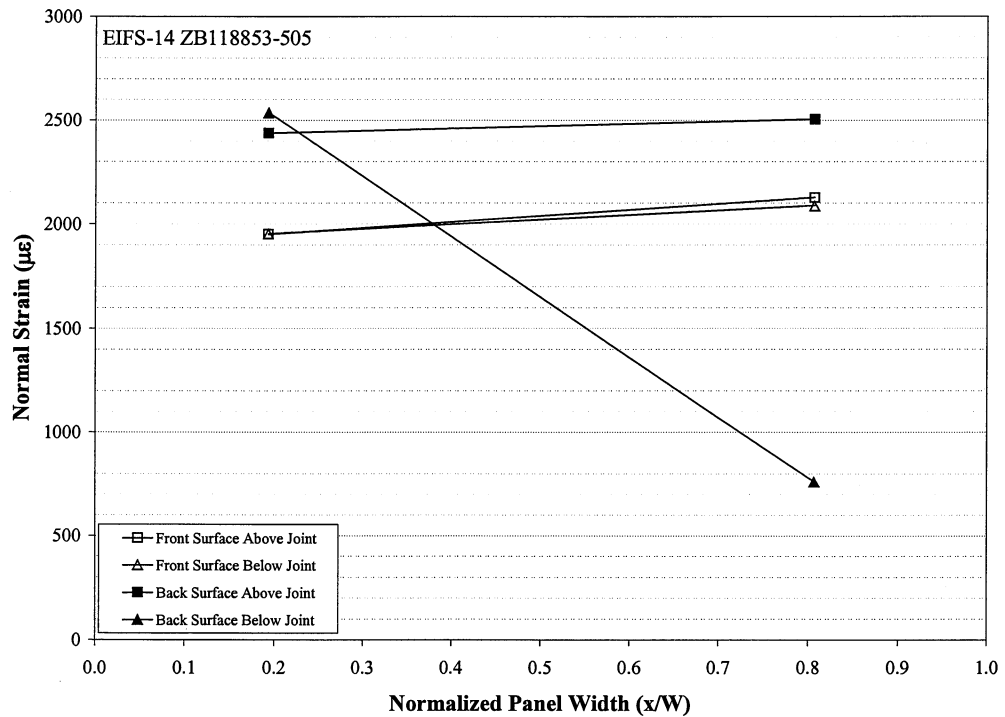


**Figure 79 Strain Variation Through the Width of the Joint, EIFS-14**

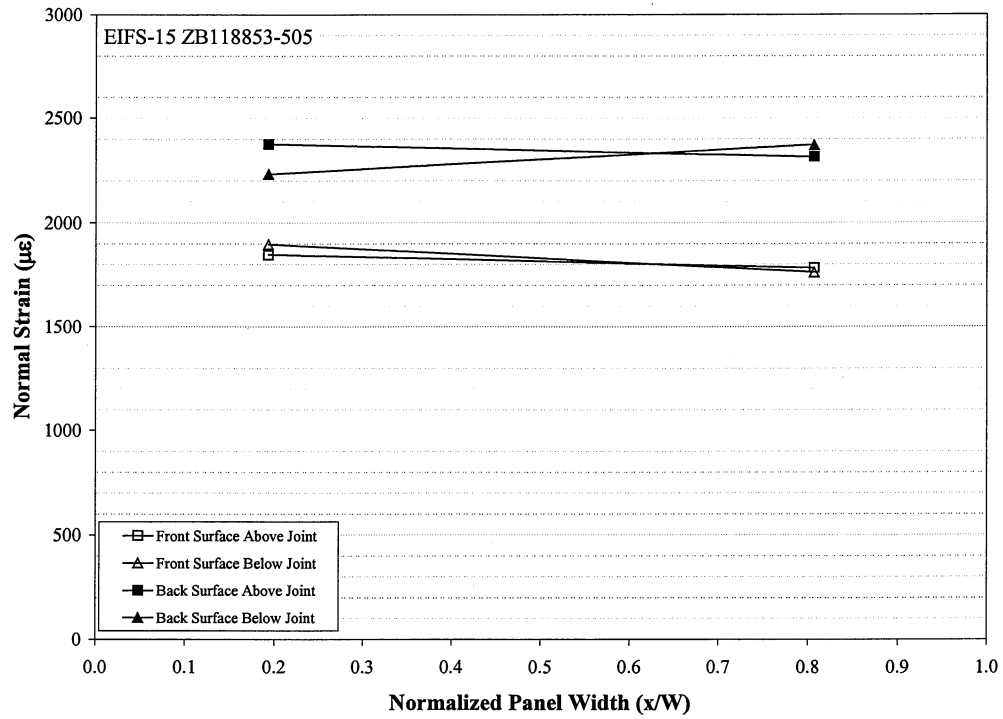


**Figure 80 Strain Variation Through the Width of the Joint, EIFS-15**

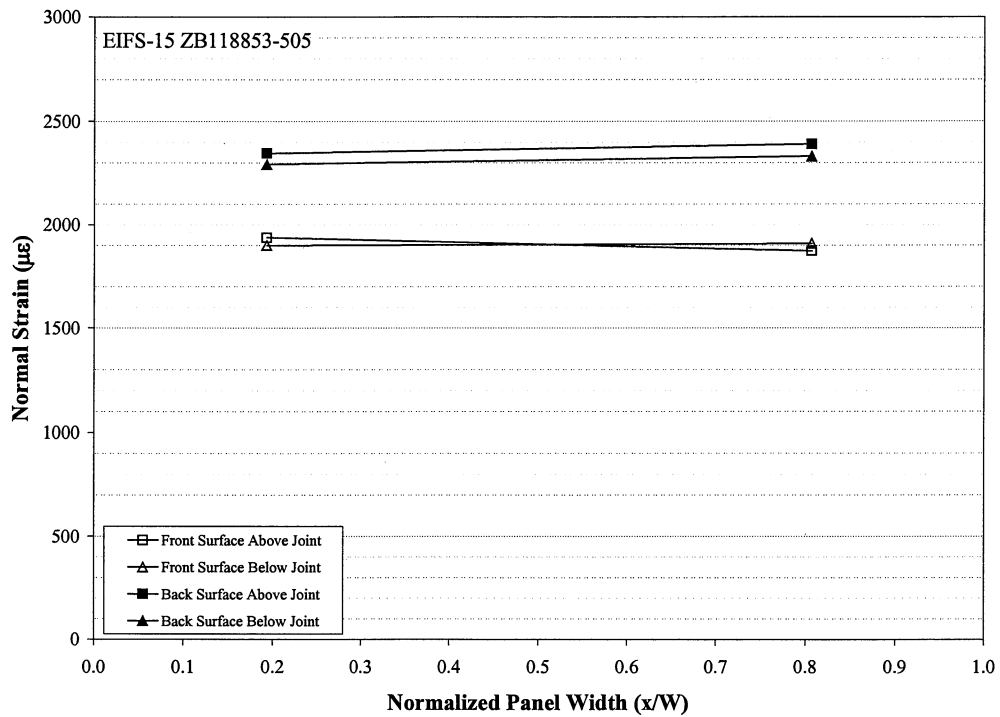


**Figure 81 Strain Variation Through the Width of the Joint, EIFS-16**

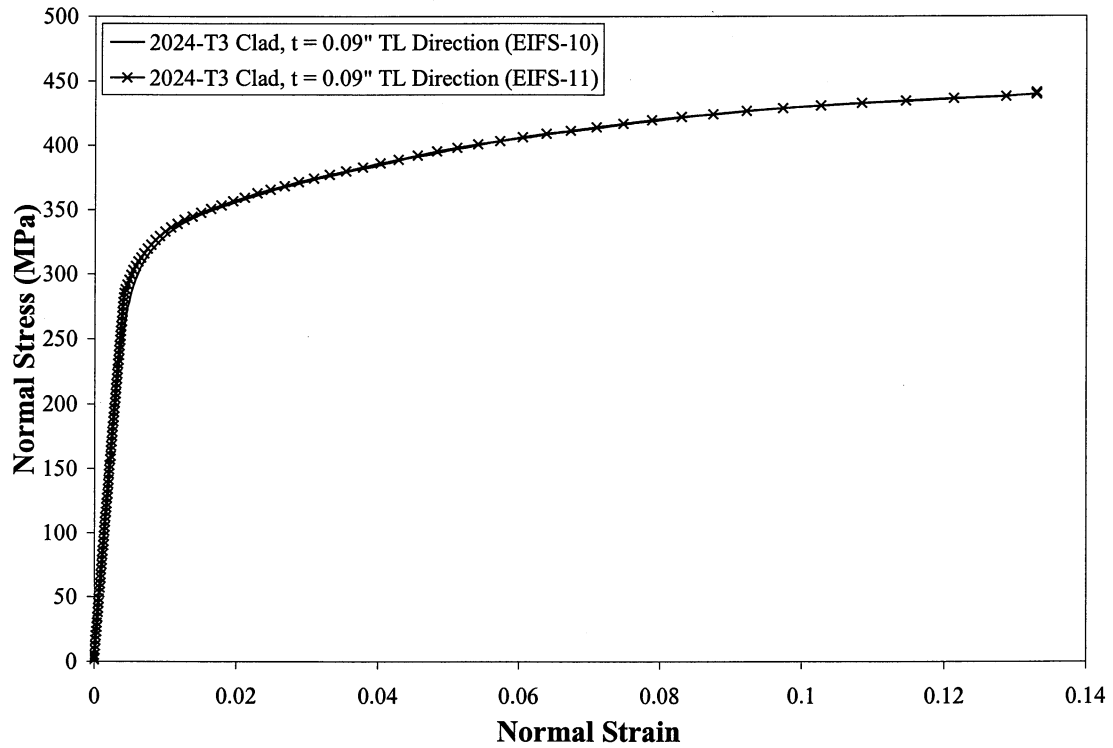


**Figure 82 2024-T3 Stress-Strain Curve, LT-Direction**

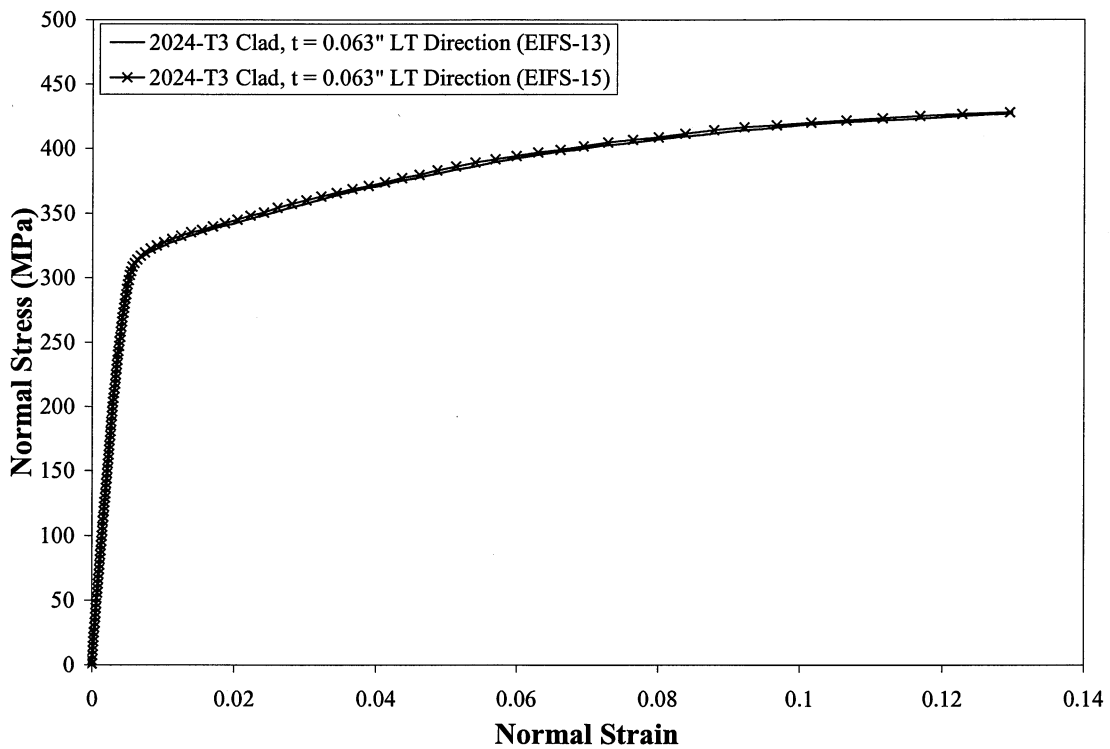


**Figure 83 2024-T3 Stress-Strain Curve, TL-Direction**



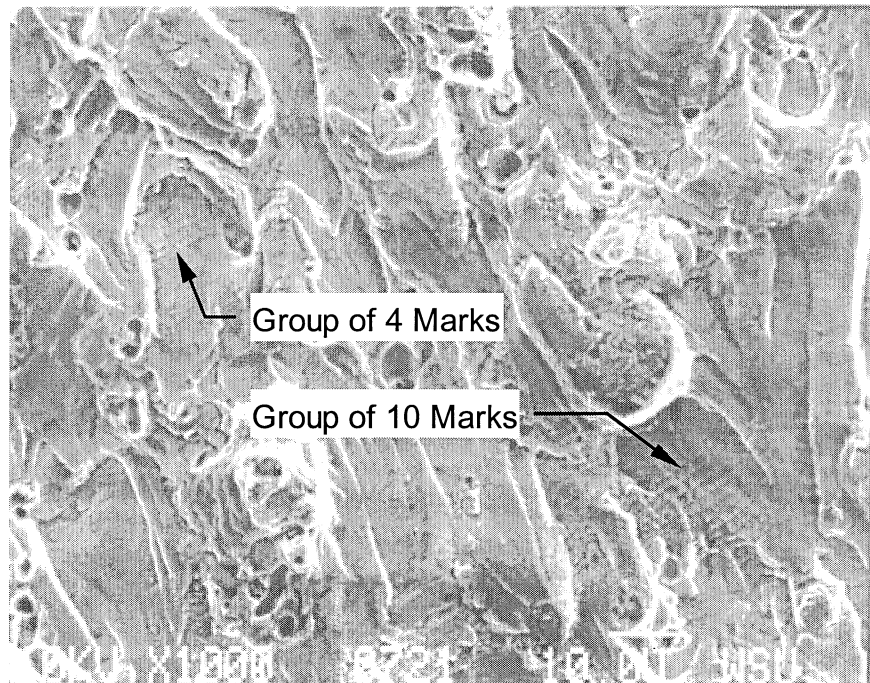


**Figure 84 Marker Bands on Fracture Surface**

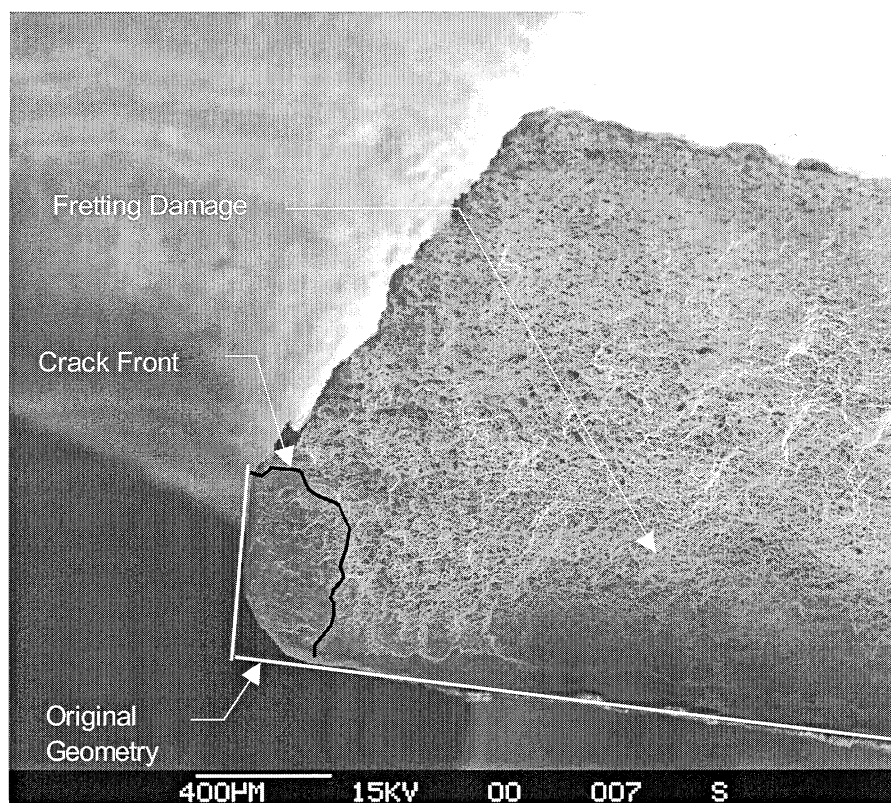


**Figure 85 Fracture Surface Showing Hole Edge and Fretting Damage**

Peak Loads at  
Beginning of  
Spectrum

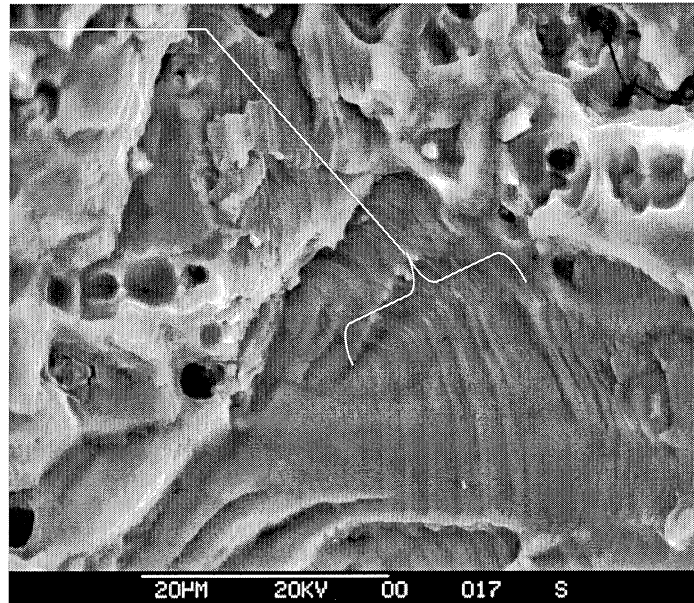


**Figure 86 Fatigue Striations from 15E20L, Low Magnification**

Peak Loads at  
Beginning of  
Spectrum



**Figure 87 Fatigue Striations from 15E20L, High Magnification**

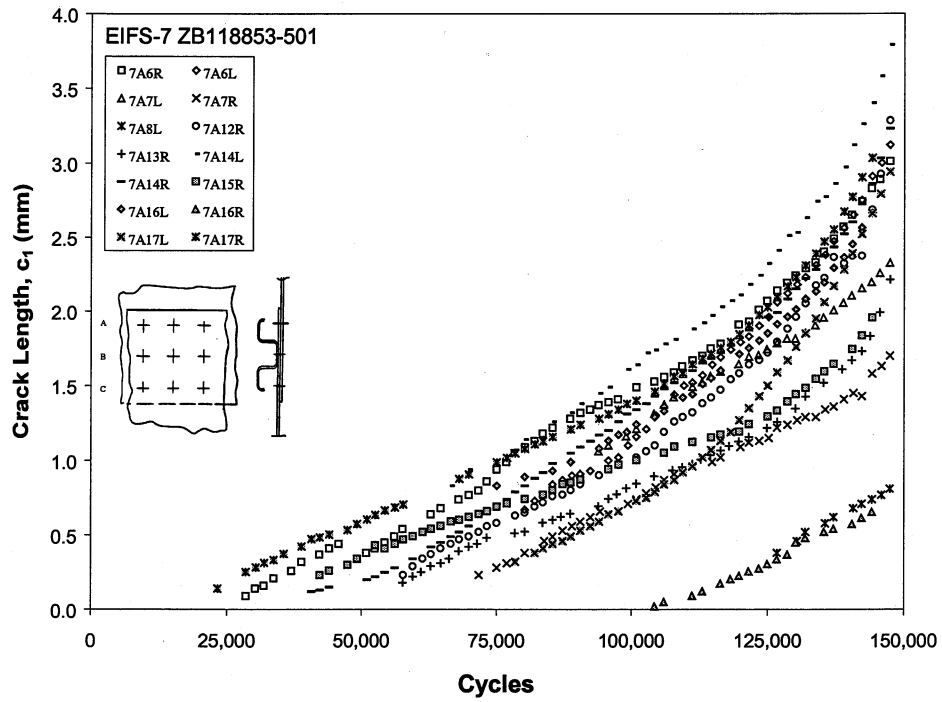


**Figure 88 EIFS-7 Reconstructed Crack Histories**

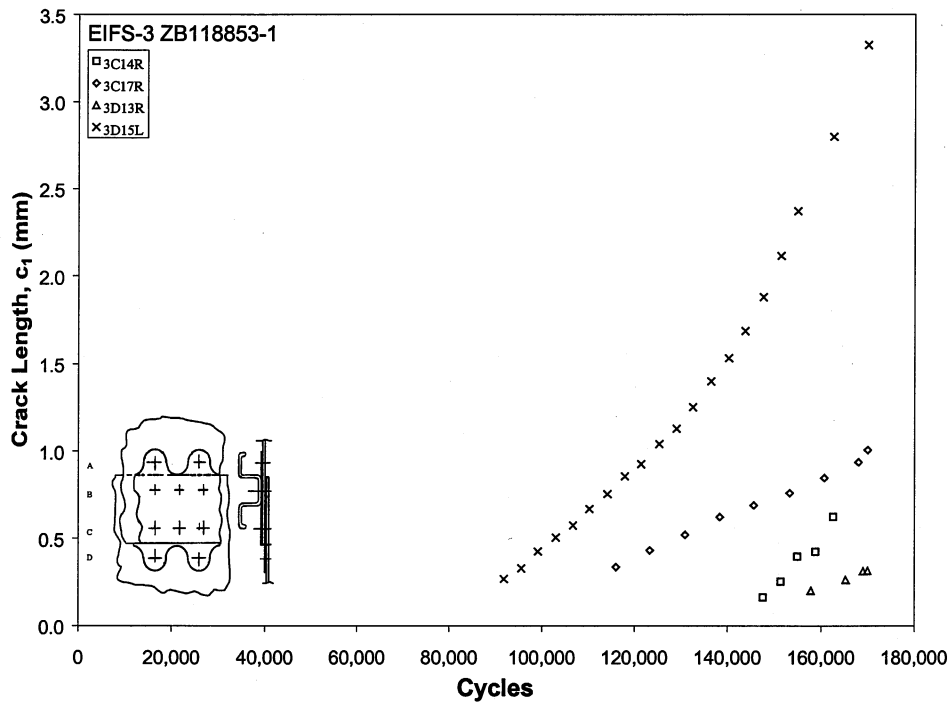


**Figure 89 EIFS-3 Reconstructed Crack Histories**

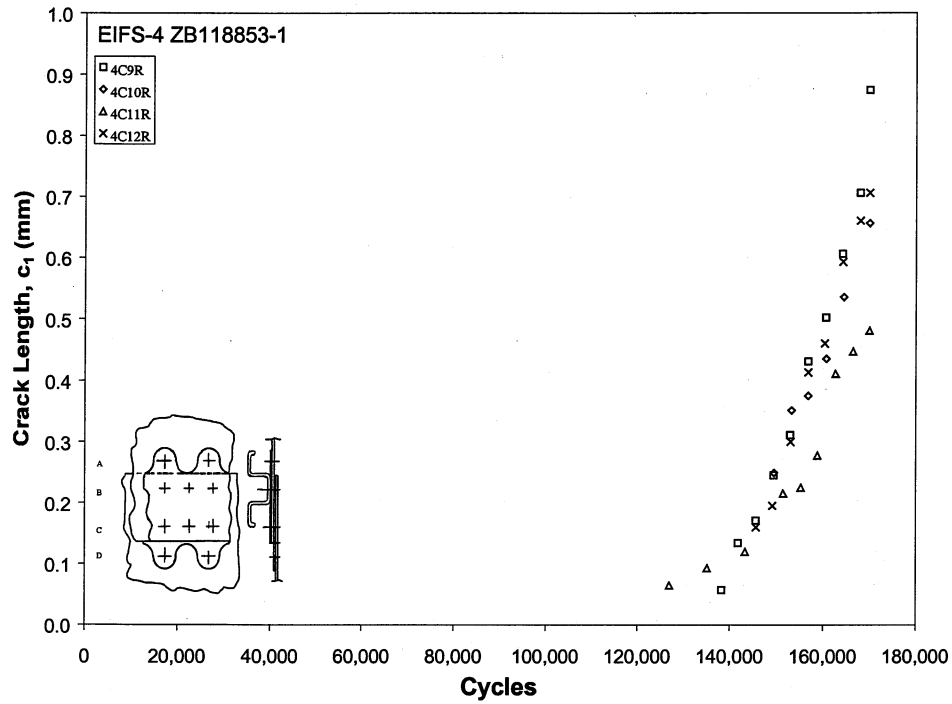


Figure 90 EIFS-4 Reconstructed Crack Histories

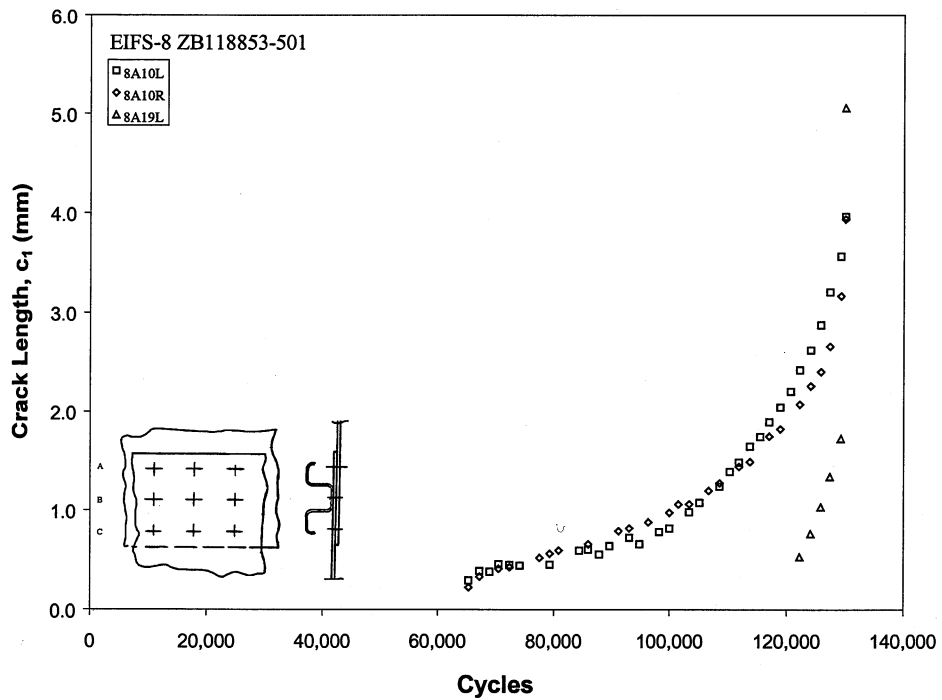
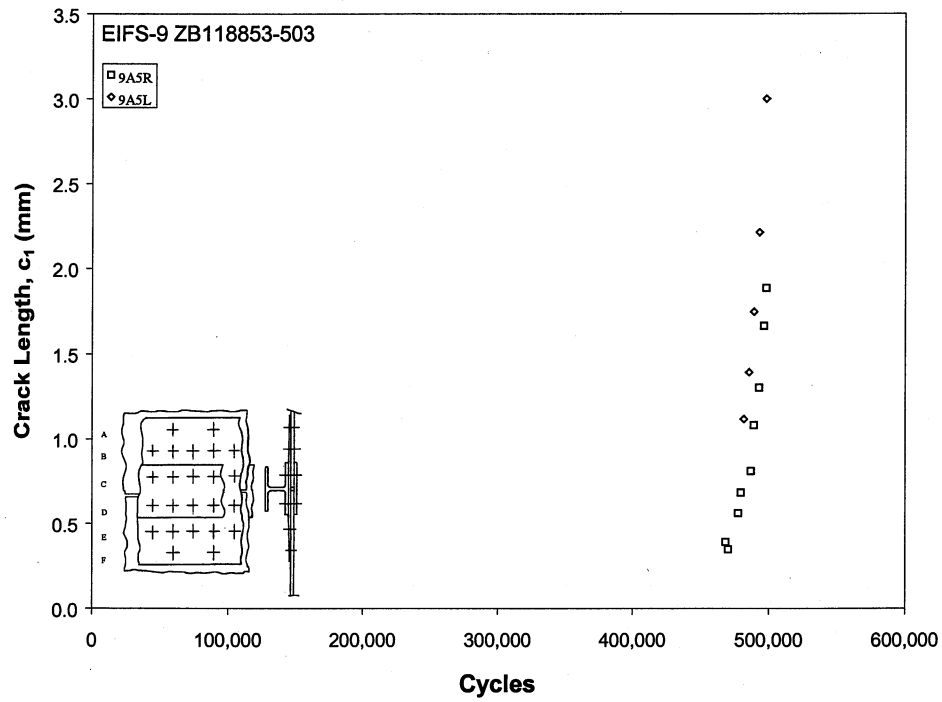
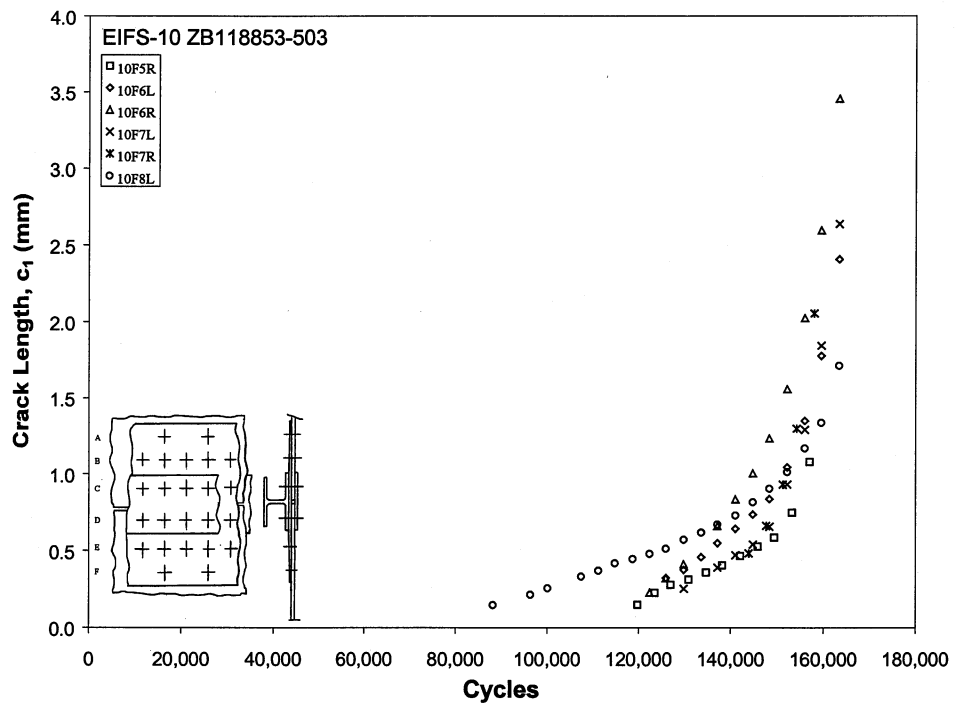


Figure 91 EIFS-8 Reconstructed Crack Histories



**Figure 92 EIFS-9 Reconstructed Crack Histories**



**Figure 93 EIFS-10 Reconstructed Crack Histories**

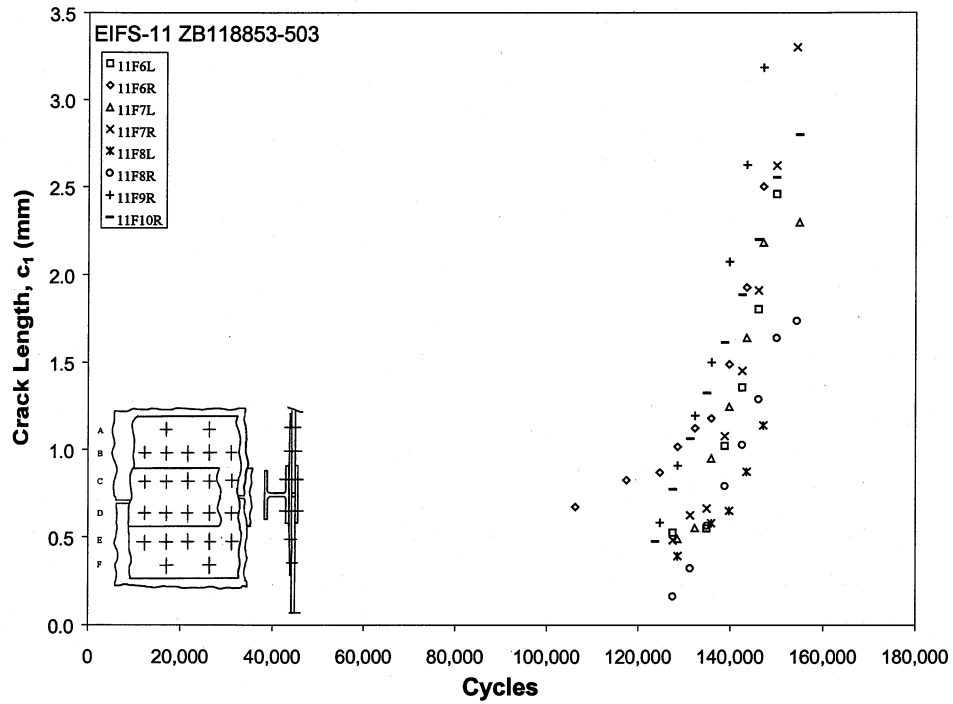


**Figure 94 EIFS-11 Reconstructed Crack Histories**

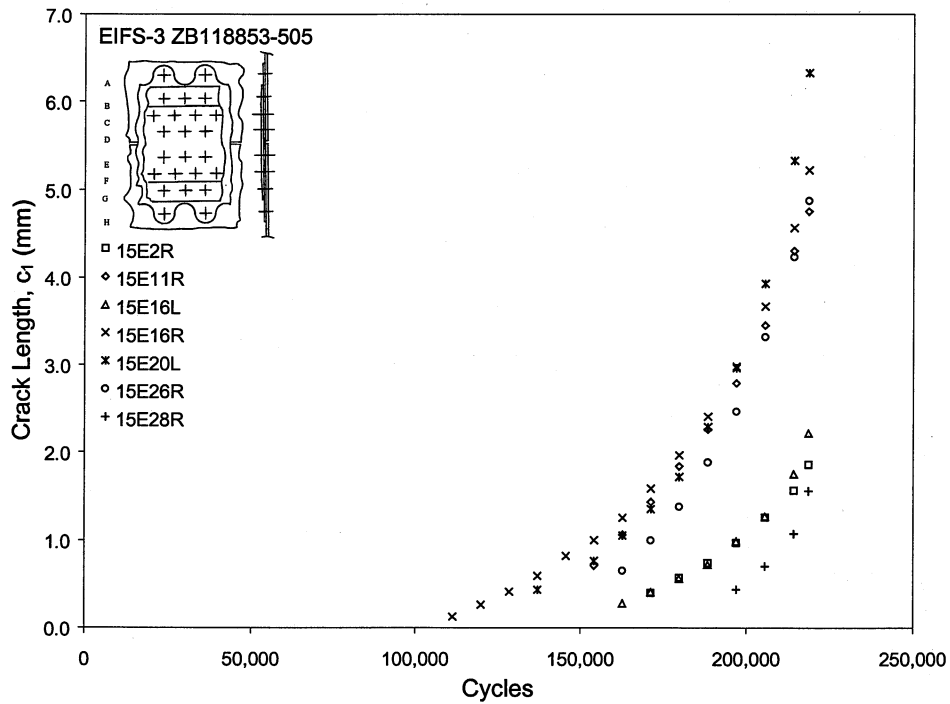


**Figure 95 EIFS-15 Reconstructed Crack Histories**

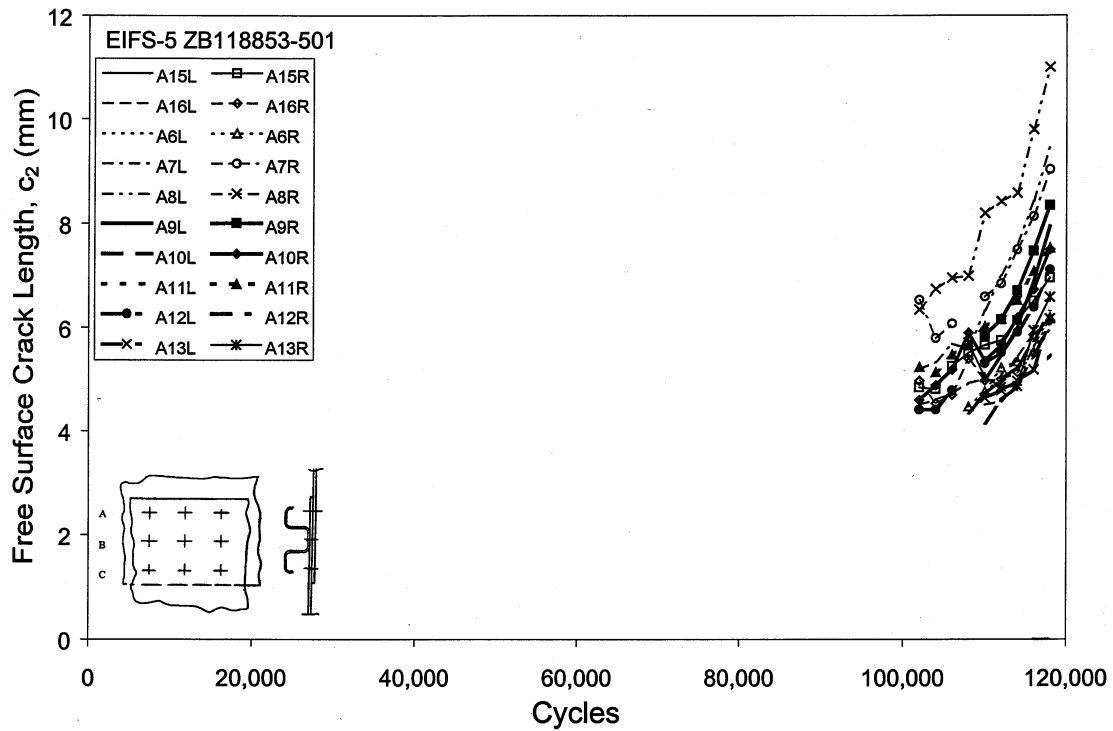


Figure 96 EIFS-5 Crack Histories Measured using the RPS and TOM

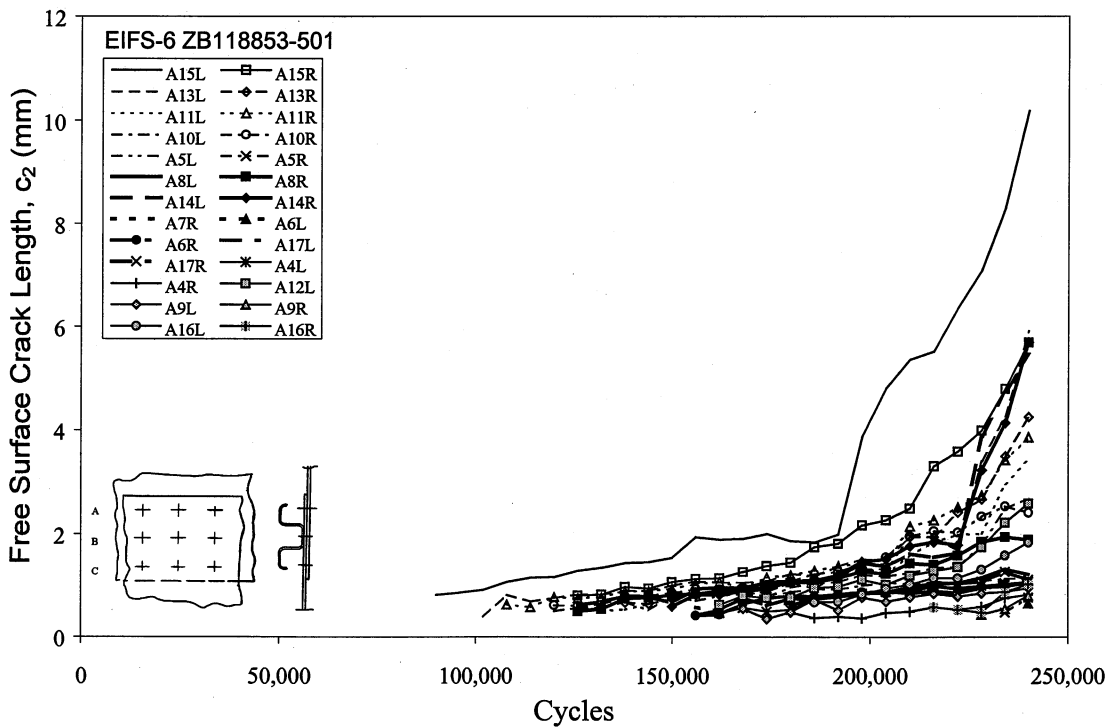


Figure 97 EIFS-6 Crack Histories Measured using the RPS and TOM

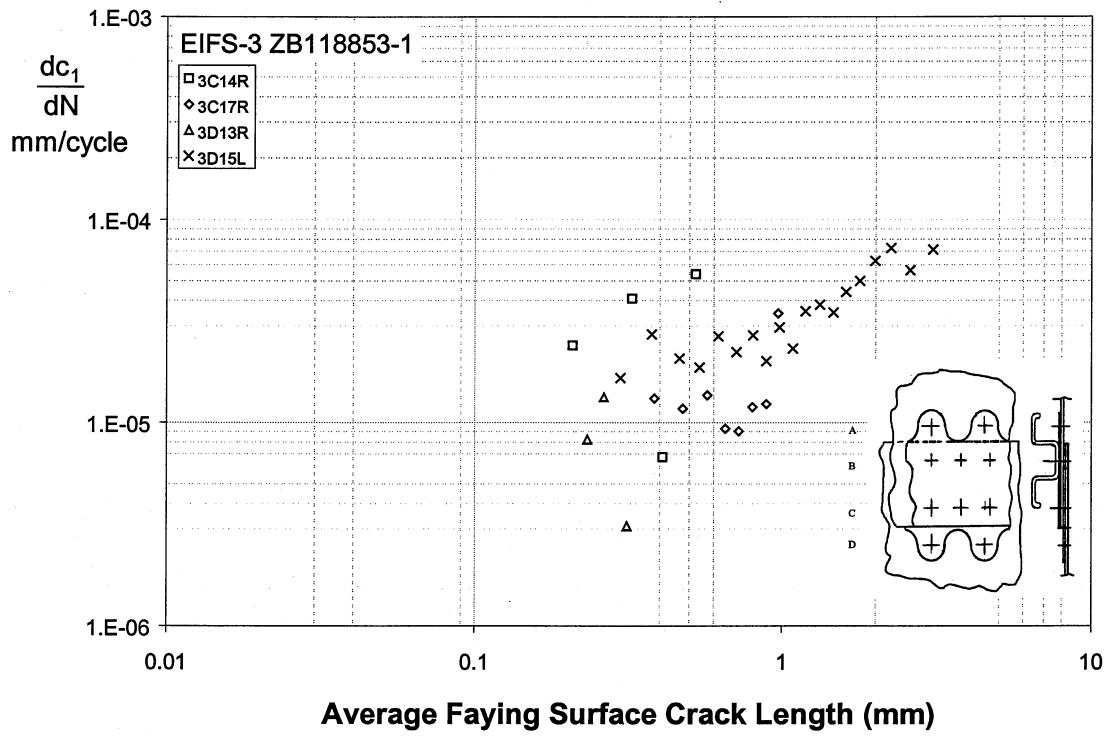


Figure 98 EIFS-3 Crack Growth Rates

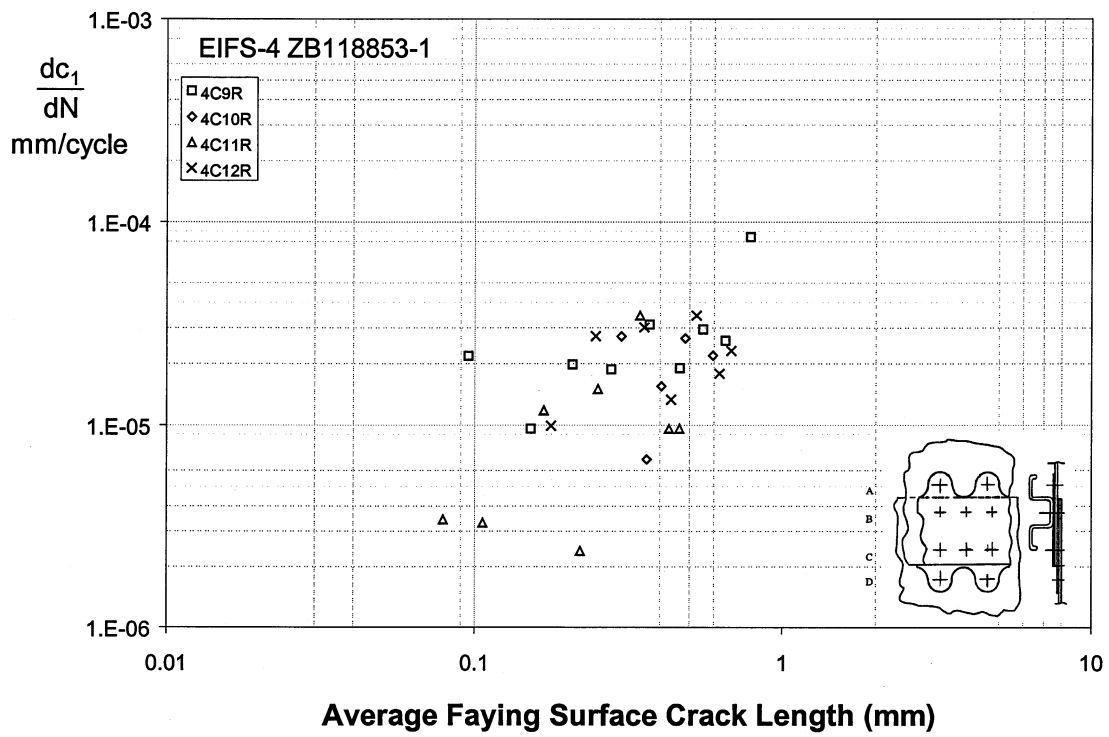


Figure 99 EIFS-4 Crack Growth Rates



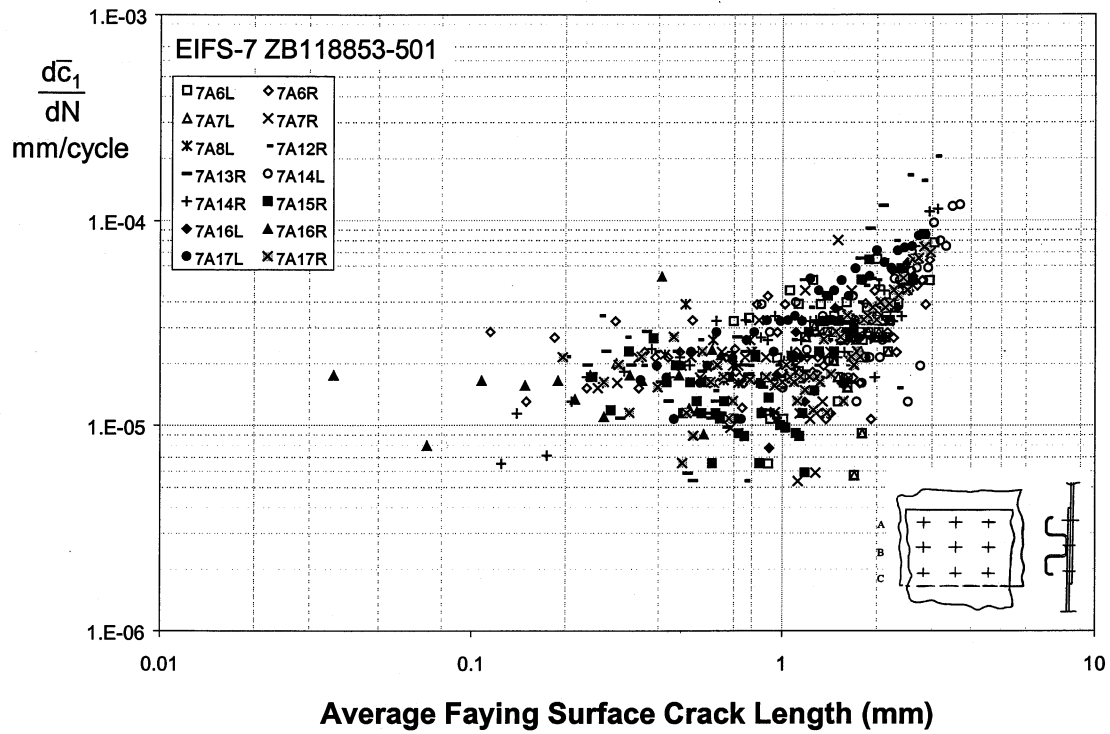


Figure 100 EIFS-7 Crack Growth Rates

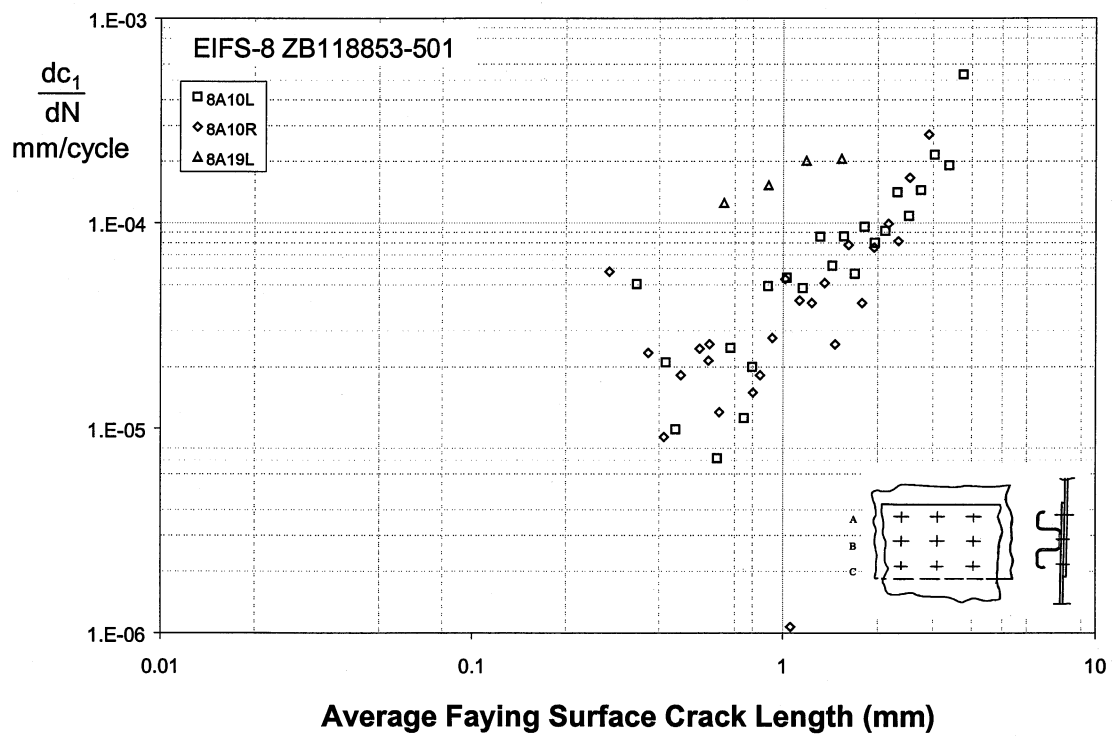
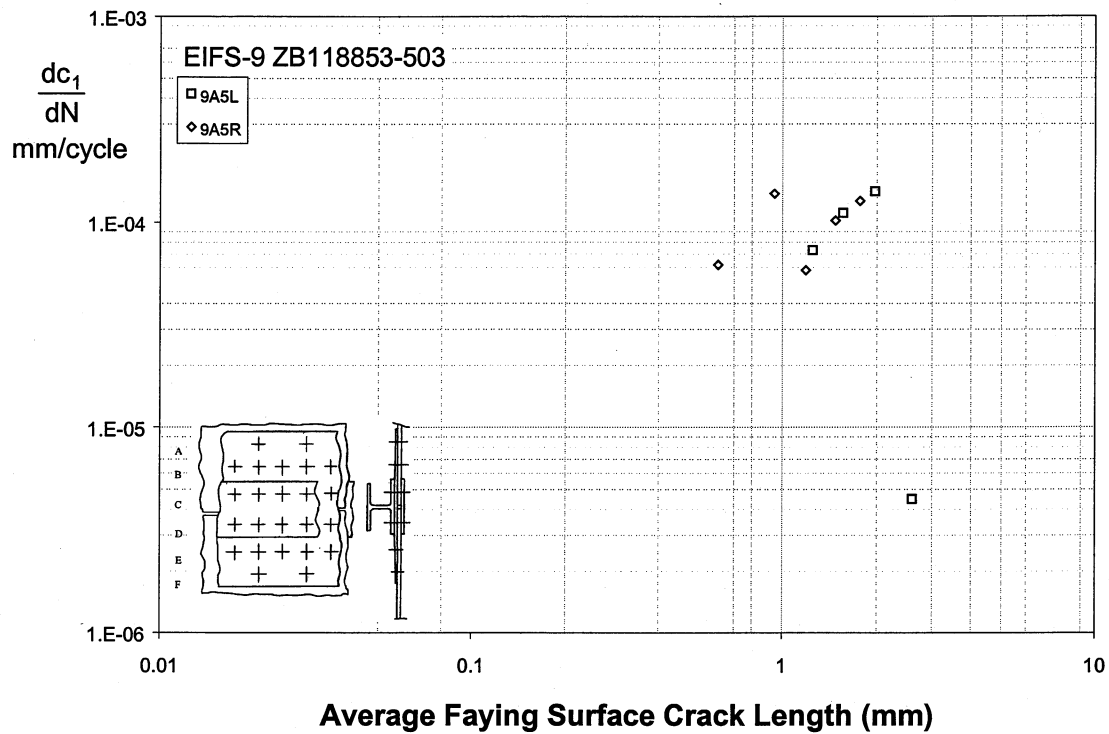


Figure 101 EIFS-8 Crack Growth Rates



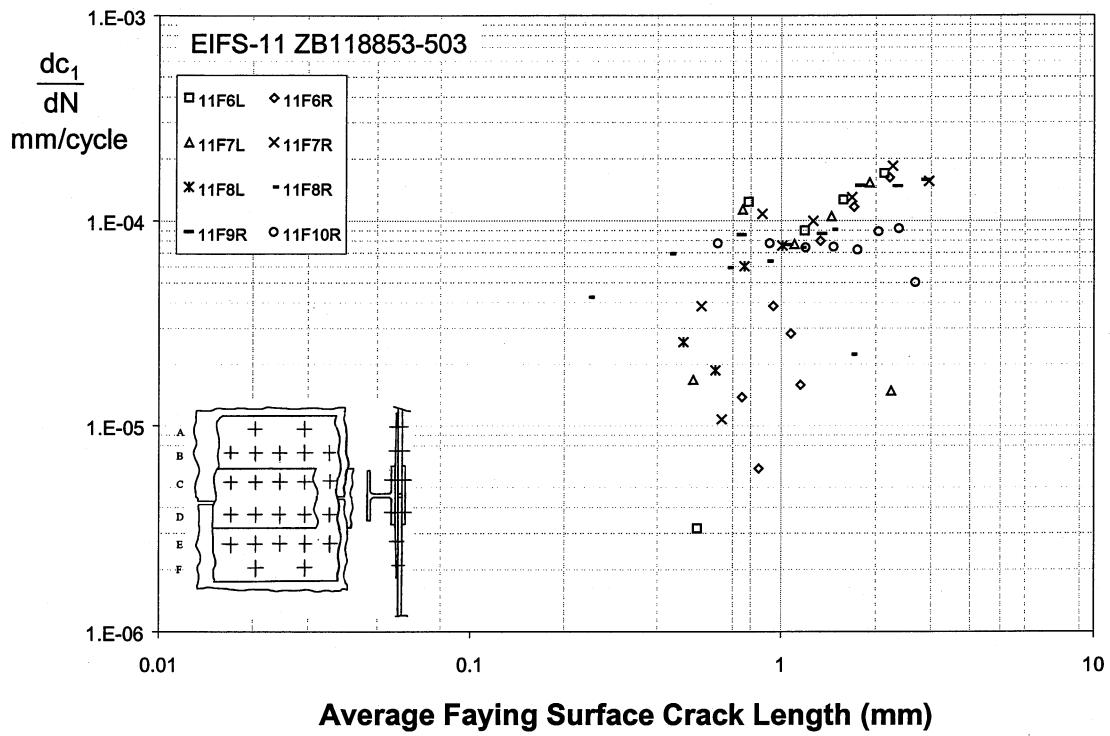


Figure 104 EIFS-11 Crack Growth Rates

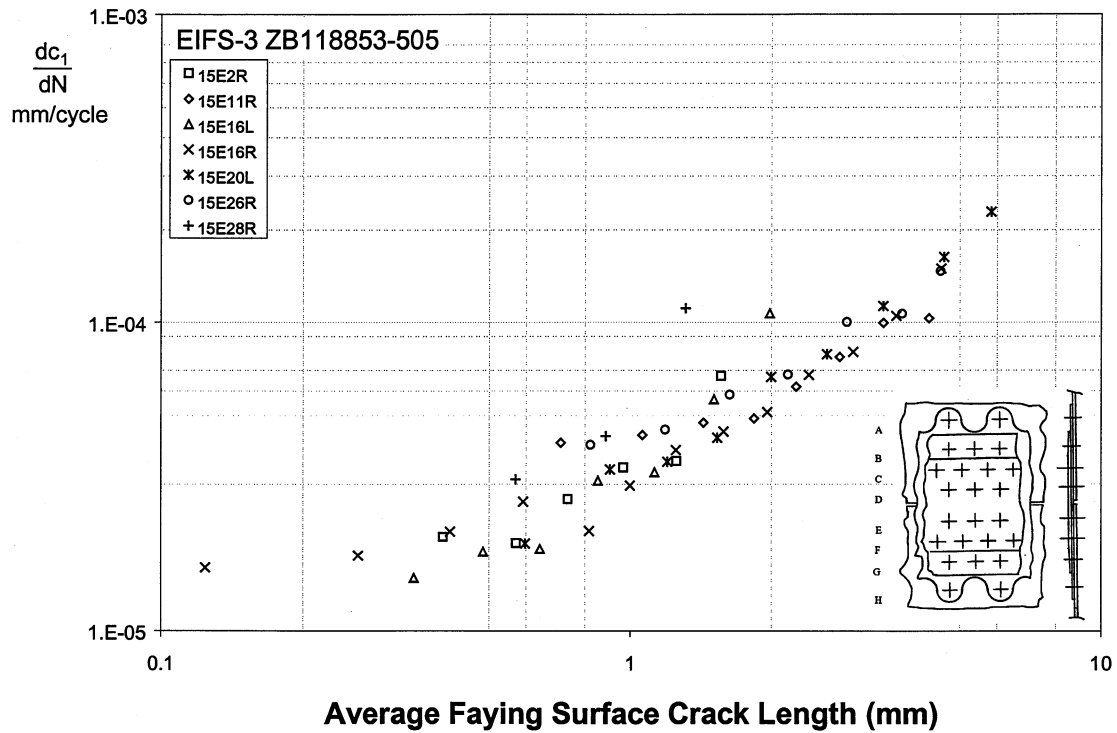


Figure 105 EIFS-15 Crack Growth Rates

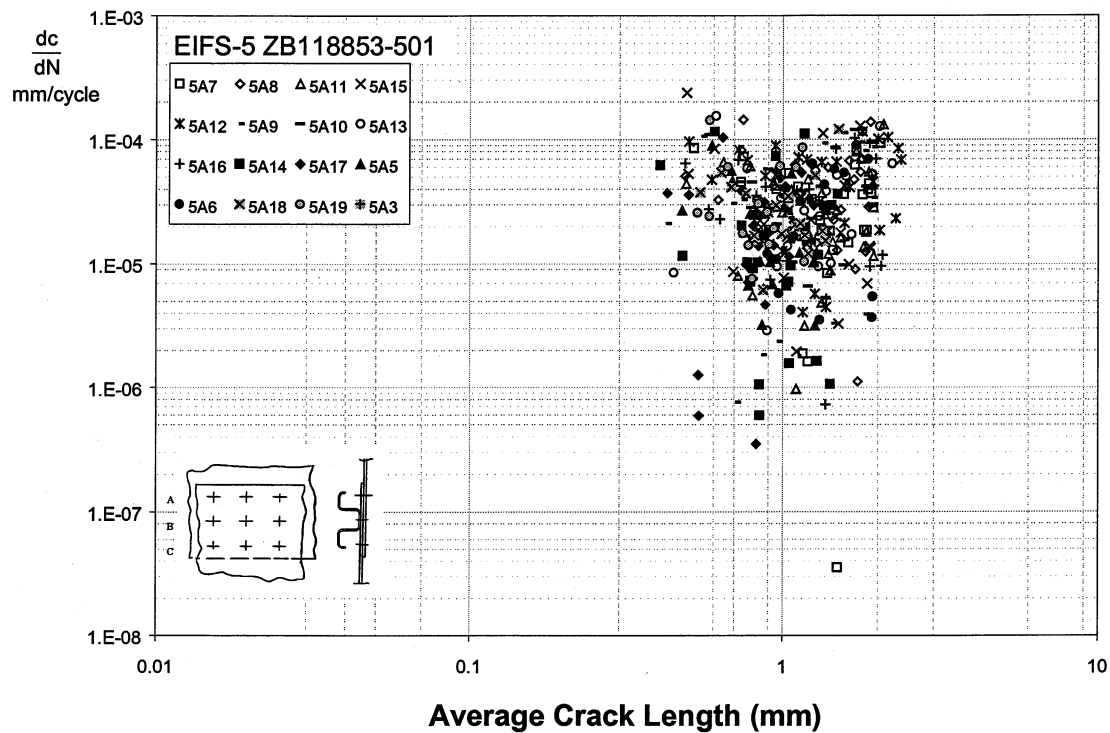


Figure 106 EIFS-5 Crack Growth Rates

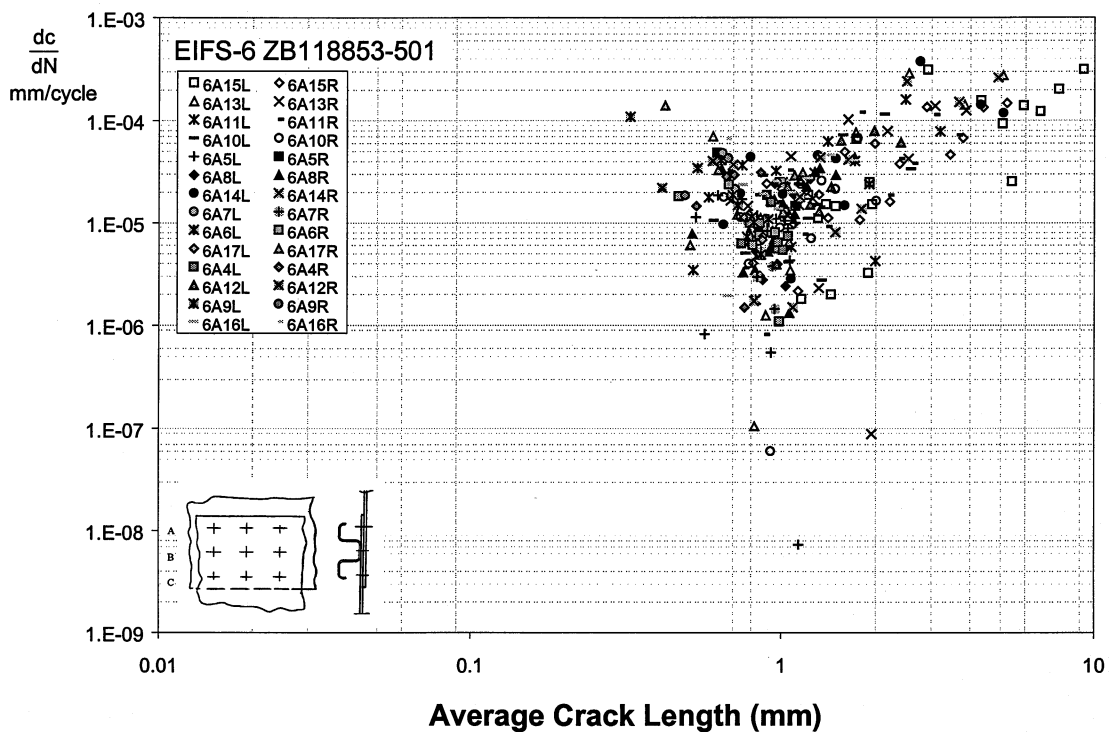


Figure 107 EIFS-6 Crack Growth Rates

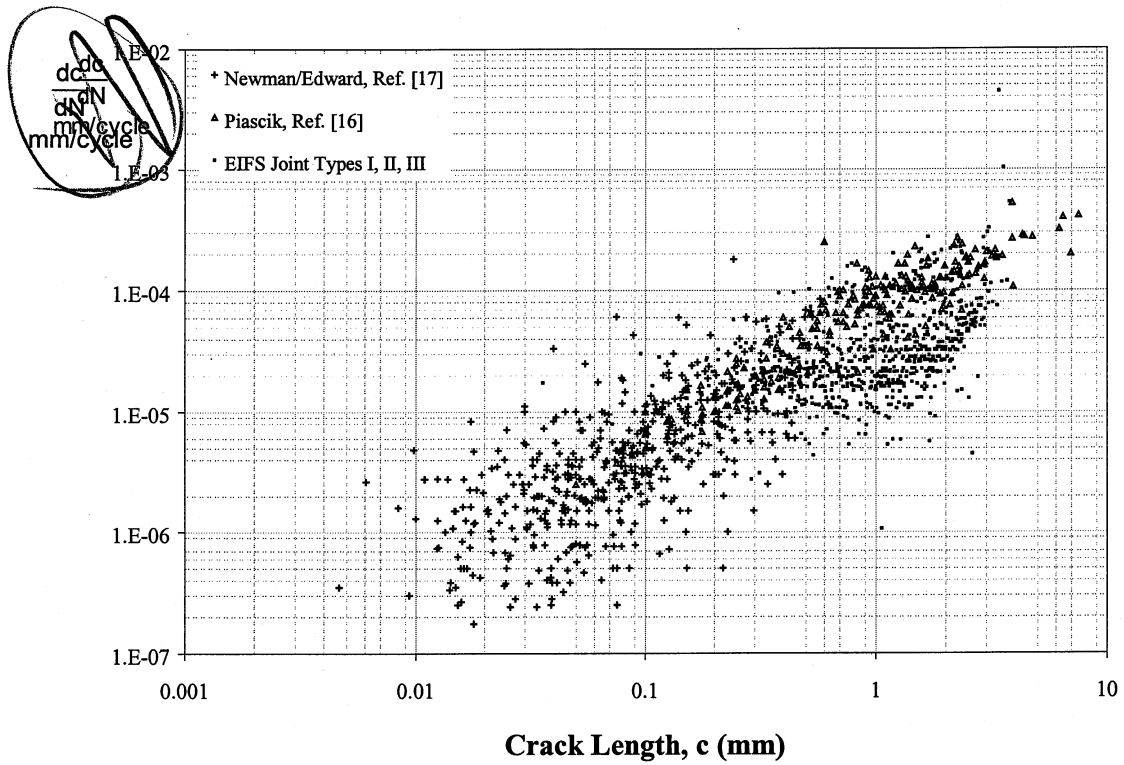


Figure 108 Comparison of Small Crack Data

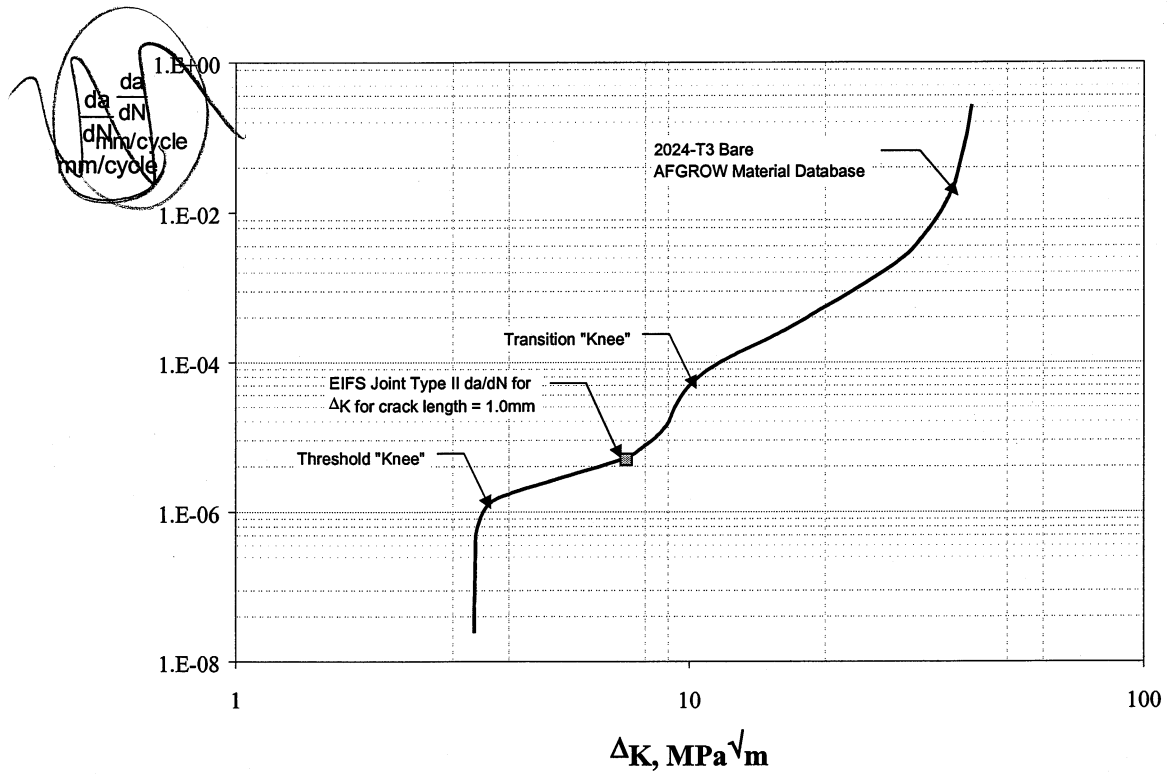


Figure 109 2024-T3 Bare Crack Growth Rate Curve from AFGROW Material Database

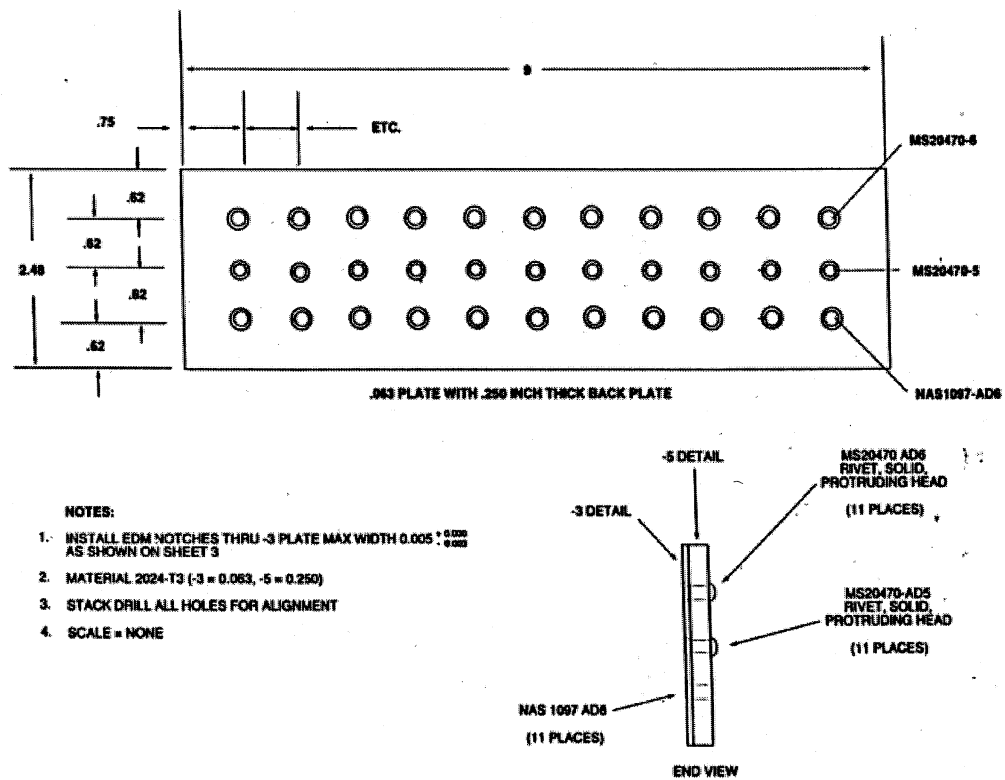


Figure 110 RPS Reference Standard for Joint Type I and II

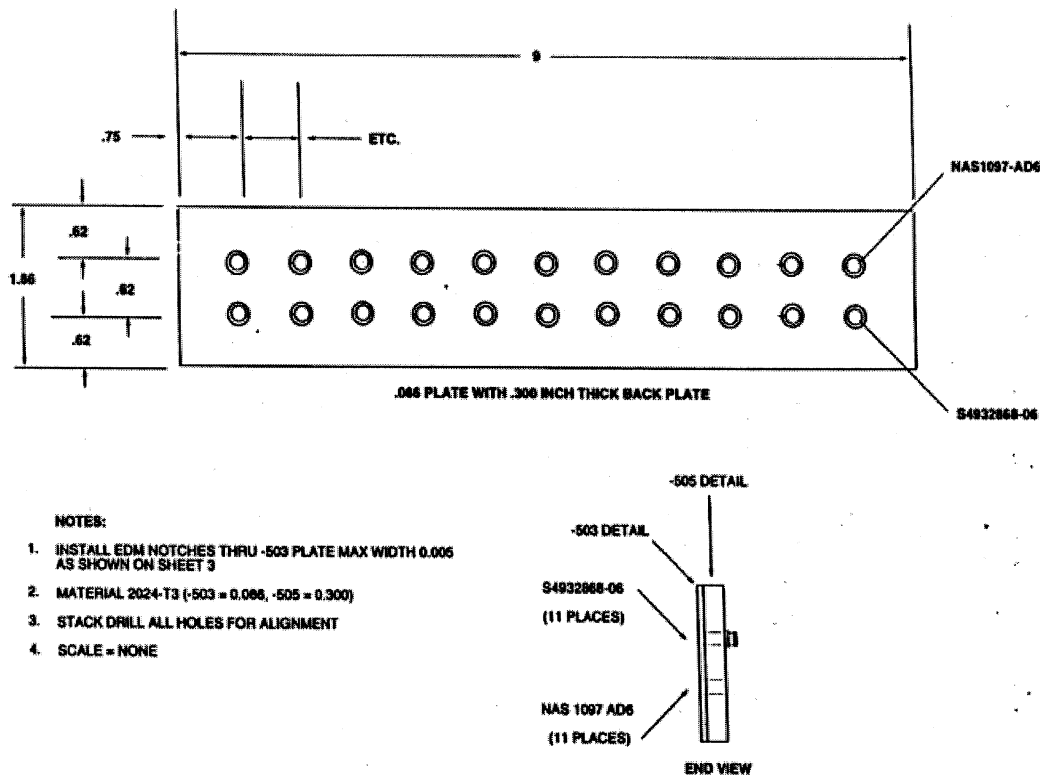


Figure 111 RPS Reference Standard for Joint Type III and IV

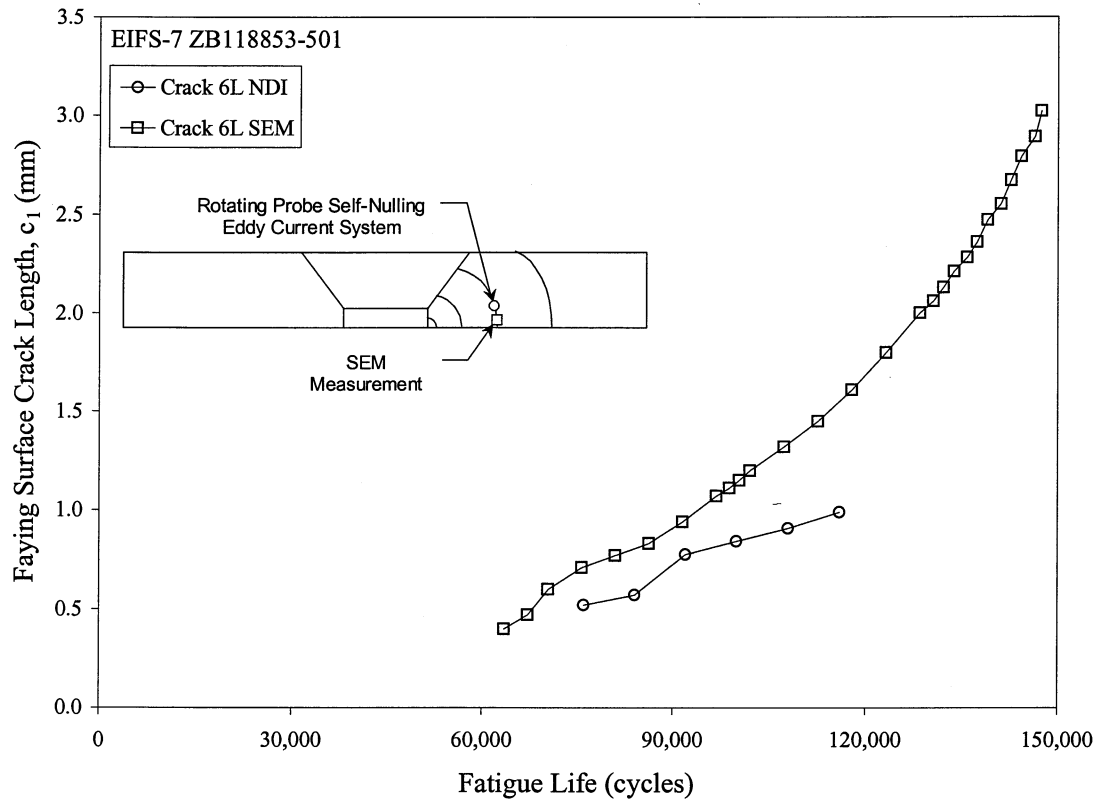


Figure 112 Comparison of Crack Growth History Obtained using the RPS and SEM

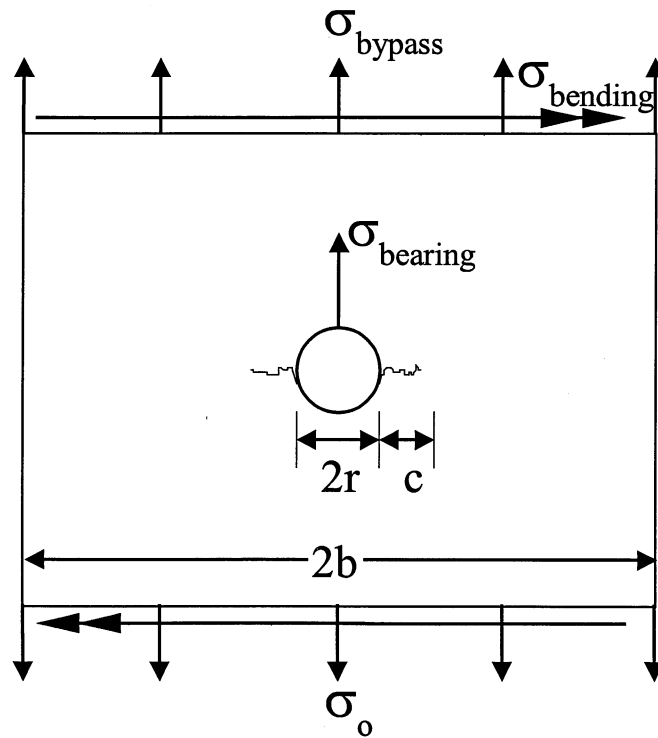


Figure 113 Crack Model for EIFS Predictions

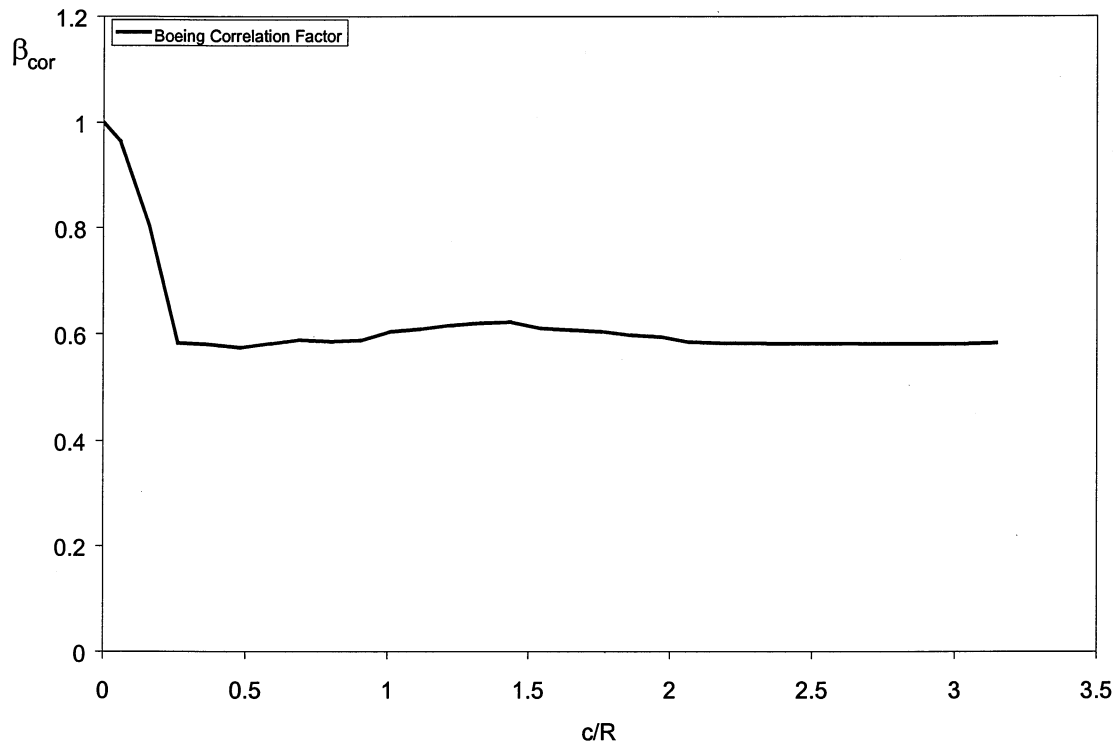


Figure 114 Boeing Correlation Factor

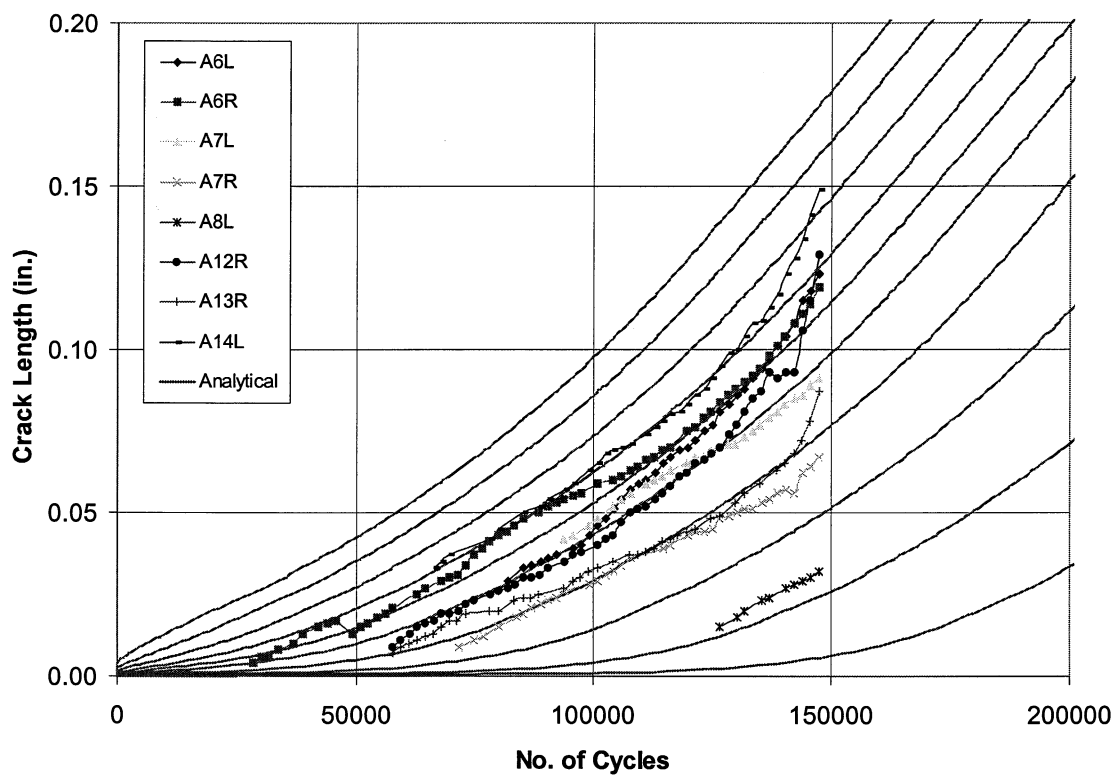


Figure 115 FASTRAN Fatigue Life Predictions for EIFS-7<sup>20</sup>



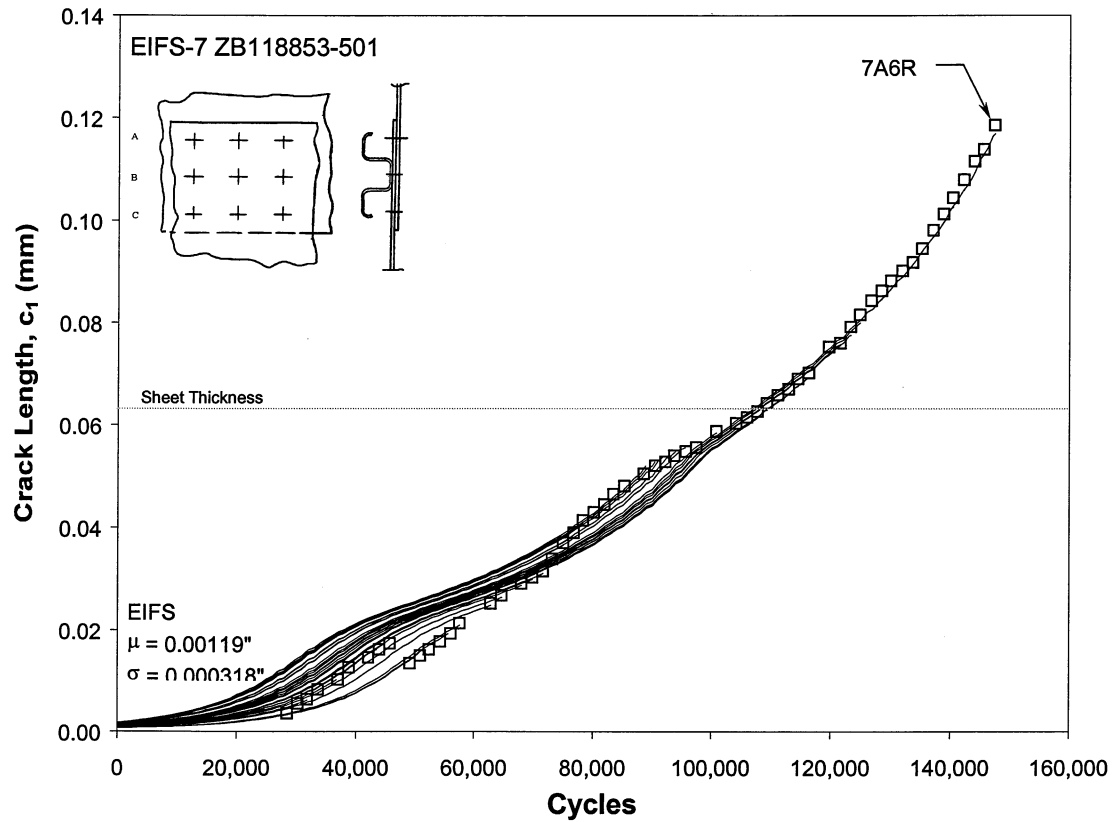


Figure 116 AFGROW Fatigue Life Predictions for EIFS-7, Crack 7A6R

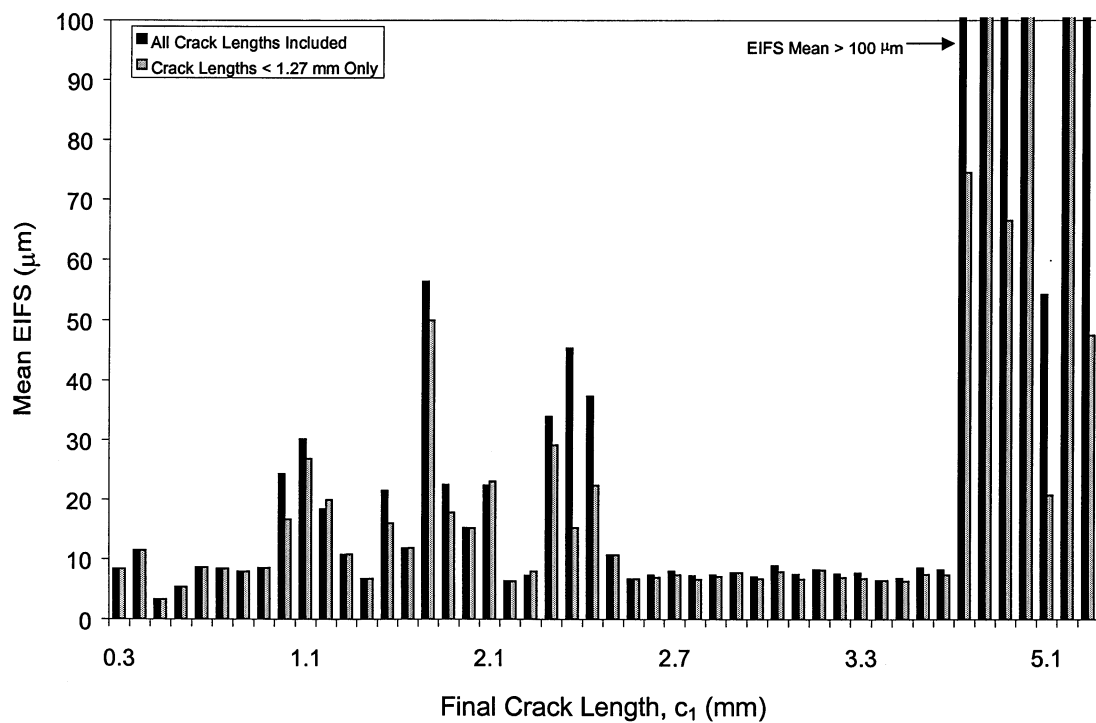


Figure 117 Variation in Mean EIFS with Final Crack Length for All Cracks

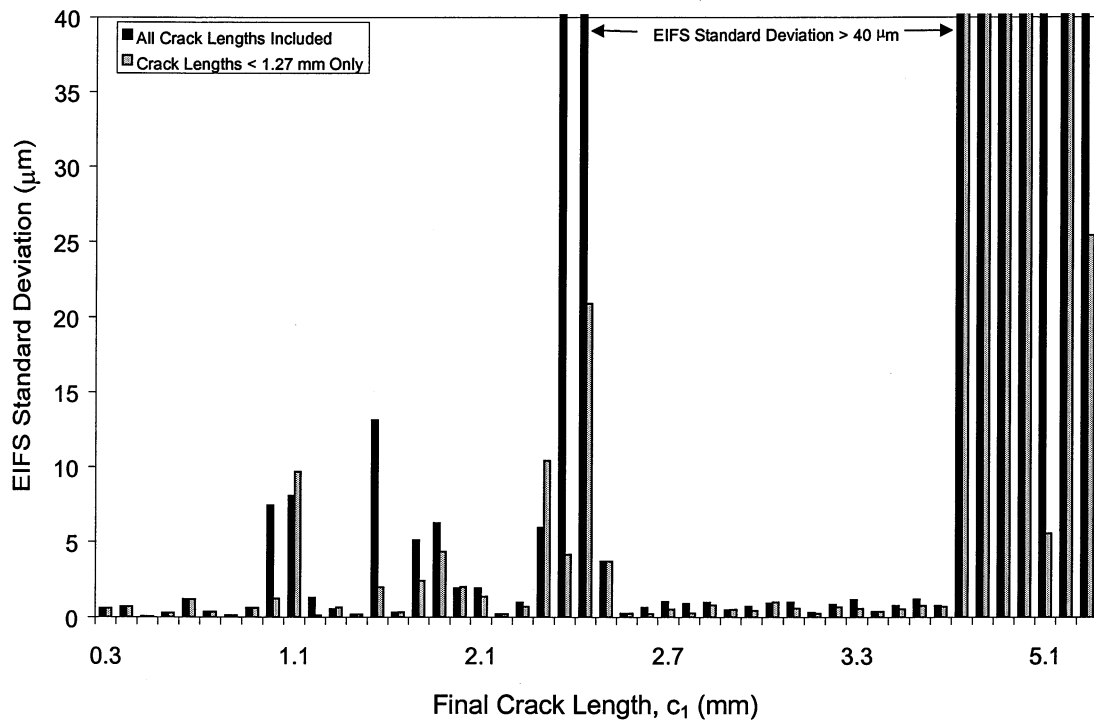


Figure 118 Variation in EIFS Standard Deviation with Final Crack Length for All Cracks

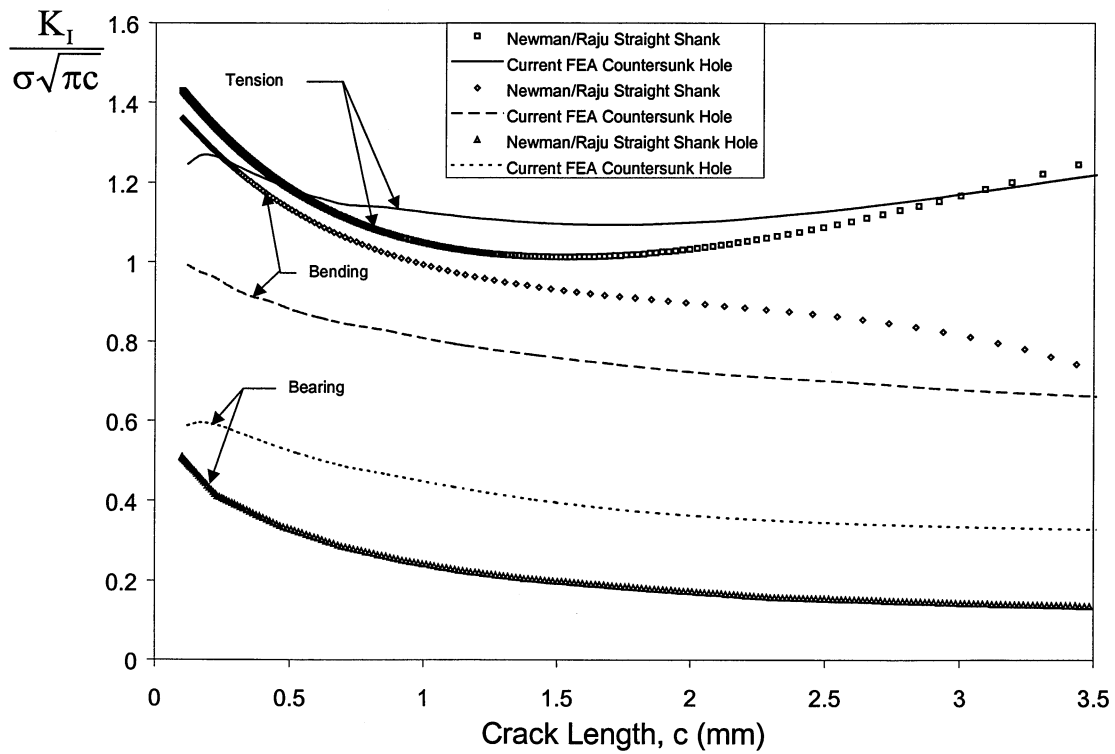


Figure 119 Comparison of Straight Shank and Countersunk Hole K Solutions

## **Appendix A Test History**

### **EIFS-1 (TYPE I)**

Install panel in load frame #1.

10-4-6 marker band spectrum has 2,000 cycle spacing.

Panel failed at 101,670 cycles due to fretting nucleated crack from edge blocks.

### **EIFS-2 (TYPE I)**

Install panel in load frame #3.

Edge crack found in row C at C25

Panel width reduced to 34.3125" and peak load adjusted to maintain 15ksi at 136,000 cycles.

Panel failed in row B, was not an edge crack, at 209,324 cycles.

### **EIFS-3 (TYPE I)**

Install panel in load frame #1.

10-4-6 marker band spectrum has 3,000 cycle spacing.

Maximum load: 20,790lbs.

Crack detected in C4 at 80,000 cycles.

Panel failed in row C with approximate residual strength of 50,400lbs.

### **EIFS-4 (TYPE I)**

Install panel in load frame #2.

Maximum load is 20,790lbs.

First Marker Band is run at 4033 cycles, at intervals of 3000 afterward.

Cracks detected in C14, C24 at 80,000 cycles.

Pulled panel to failure at 170,000 cycles. Rivet row C was critical

Approximate residual strength: 43,000lbs.

### **EIFS-5 (TYPE II)**

Install panel in load frame #1.

Maximum load is 30,631lbs.

Cracks in A7, A8, A11 detected at 30,000 cycles.

Cracks at A5-A18 at 72,000 cycles.

Panel failed in row A at 119,926 cycles.

### **EIFS-6 (TYPE II)**

Install panel in load frame #1.

Reduce maximum load 10% from test plan.

Crack detected in A15 at 90,000 cycles.

Panel failed in row A at 244,547 cycles.

### **EIFS-7 (TYPE II)**

Install panel upside-down in load frame #1 to check for grip alignment. Strain survey conducted.

Grip is aligned, panels are being loaded symmetrically.

Program 75% marker bands in a sequence of 6, 10, 4 every 1,000 cycles.

Maximum load is 20,790lbs.

Crack detected in A11 at 60,000 cycles.

Panel failed in row A at 147,410 cycles.

### **EIFS-8 (TYPE II)**

Install panel in load frame #3.

Stress is 15ksi.

10-4-6 marker spectrum used.

Pulled panel to failure at 130,000 cycles. Rivet row A was critical

Approximate residual strength: 43,000lbs.

#### EIFS-9 (TYPE III)

Installed test specimen in Load Frame #4.  
Crack in A2 found at 130,000 cycles.  
Crack in F1 found at 200,000 cycles.  
Broke a load fitting at 259,601 cycles.  
Removed specimen from frame and sliced ~4" from both sides of test panel to remove the edge cracks. New panel width is 13.969"  
Install panel back into load frame #4.  
New maximum load is 18,858lbs.  
Edge crack detected in A1 at 350,000 cycles, specimen removed to machine into dogbone configuration.  
Reinstall dogbone geometry panel, and set new maximum load to 14,580lbs.  
Maximum load increased to 16,038 at 430,000 cycles.  
Maximum load increased to 19,800lbs. at 464,310 cycles for 20 ksi remote stress.  
Panel failed at 498,063 cycles.

#### EIFS-10 (TYPE III)

Install panel in load frame #1.  
Edge crack found in B1 at 32,000 cycles.  
Trimmed edges off panel, B1-E1, and B27-E27.  
Modify to dog-bone geometry with 2" radius into joint section.  
Drilled out and replaced A1, A2, A12, A13, F1, F2, F12, F13 with AD6 rivets squeezed to 1.8D<sub>o</sub> on the backside.  
Maximum load changed to 24,214lbs. for remote stress of 17 ksi.  
Maximum load changed to 28,380lbs. for correct joint stress.  
Panel failed in row F at 165,390 cycles.

#### EIFS-11 (TYPE III)

Panel modified to hourglass geometry and installed in Load Frame #3.  
Polished edges and oversize rivets installed in A1, A2, A12, A13, F1, F2, F12, and F13.  
Maximum load set at 28,380lbs. for strain survey.  
Maximum load changed to 33,000lbs. to achieve joint stress of 17 ksi.  
Broke a load fitting at 123,987 cycles.  
Replace hydraulic accumulator at 129,937 cycles.  
NDI at 135,000 cycles indicated 0.050" cracks in F6, F7.  
Multi-site cracking in row F at 145,000 cycles as indicated by NDI.  
Test stopped at 154,827 cycles and pulled to failure. Rivet row F was critical  
Residual strength: 24.4 ksi.

#### EIFS-12 (TYPE III)

Panel modified to hourglass geometry and installed in Load Frame #3.  
Panel reinstalled in load frame #1.  
Crack detected in A8 at 175,000 cycles.  
Panel failed in row A at approximately 205,001 cycles.

#### EIFS-13 (TYPE IV)

Panel modified to hourglass geometry and installed in Load Frame #3.  
Fasteners A1, A2, A14, A15, H1, H2, H14, H15 were removed, oversized, and cold-worked.  
Maximum load 33,818lbs. Conducted strain survey.  
Install MTS slope washers in the load frame.  
Change maximum load to 30,000lbs. to obtain 24.3 ksi in joint.  
After multiple 'dumps', all zero minimum spectrum loads are changed to a 2% offset to allow greater control at 8568 cycles.  
Test now runs smoothly at a rate of 35,000lbs.s<sup>-1</sup>.

Panel failed in the doubler at the skin splice at 308,682 cycles. Rivet row F was critical.  
Panel pulled apart with a residual strength of 6,000lbs.

#### EIFS-14 (TYPE IV)

Panel modified to hourglass geometry with oversize edge rivets and installed in Load Frame #1.  
Fasteners A1, A2, A14, A15, B1, B29, D1, D29, E1, E29, G1, G29, H1, H2, H14, H15 were removed, oversized, and cold-worked.

Maximum load defined as 30,000lbs., with random spectrum.

Remove panel at 217,000 cycles to remove an edge crack.

Large oversize bolt installed in source hole of the edge crack.

Panel failed in the doubler at the skin splice at 270,681 cycles. Rivet row F was critical.

#### EIFS-15 (TYPE IV)

Panel modified with oversize edge rivets and installed in Load Frame #1.

Fasteners A1, A2, A14, A15, B1, B29, D1, D29, E1, E29, G1, G29, H1, H2, H14, H15 were removed, oversized, and cold-worked.

Ran 20 seat cycles and 2 strain survey cycles at 30,000lbs.

Increased load to 33,047lbs. to achieve 24.4 ksi in joint.

Start random spectrum at 22 cycles.

Panel failed in the doubler at the skin splice with 218,484 cycles. Rivet row F was critical.

#### EIFS-16 (TYPE IV)

Panel modified with oversize edge rivets and installed in Load Frame #4.

Fasteners A1, A2, A14, A15, B1, B29, D1, D29, E1, E29, G1, G29, H1, H2, H14, H15 were removed, oversized, and cold-worked.

Maximum load defined as 30,000lbs. for random spectrum.

Panel failed in the doubler at the skin splice at 217,735 cycles. Rivet row F was critical.

## Appendix B Test Article Dimensions and Strain Gage Locations

After the strain survey for EIFS-7 was completed the strain data was examined. The tension and bending strains varied through the width of the specimen. The cause was not readily apparent; thus, the specimen geometry and strain gage locations were measured to evaluate the overall symmetry of the specimen and strain gage locations. As seen by the following data, specimen and gage symmetry was lacking in all the specimens. In the tables below, the top skin is the skin with countersunk fasteners. The alpha-numeric measurement descriptor, "A1-B1 Measurement" for example is the distance from the center of rivet one in row A to the center of rivet one in row B. "S.G." is the Strain Gage location being measured, The "splice overlap" is the distance from the bottom of the top sheet to the top of the bottom sheet. Items left blank were not measured. All other information is self-explanatory.

Article ID: ZB5118853-1 #1 (EIFS-1)

Date: 17-Nov-97

Measurements Taken By: McCann / Grommon

Top Skin Width @ Grips:	22.063	inches	
Top Skin Width @ Splice:	22.000	inches	
Top Skin Length (Left):	23.219	inches	
Top Skin Length (Right):	23.438	inches	
Bottom Skin Width @ Grips:	22.063	inches	
Bottom Skin Width @ Splice:	22.031	inches	
Bottom Skin Length (Left):	23.250	inches	
Bottom Skin Length (Right):	23.281	inches	
Splice Overlap (Left):	2.072	inches	
Splice Overlap (Right):	2.065	inches	
A1 - B1 Measurement:	0.811	inches	
A15 - B27 Measurement:	0.740	inches	
A1 - C1 Measurement:	2.006	inches	
A15 - C27 Measurement:	1.950	inches	
A1 - D1 Measurement:	2.827	inches	
A15 - D15 Measurement:	2.835	inches	
B1 - C1 Measurement:	1.207	inches	
B27 - C27 Measurement:	1.205	inches	
S.G. #1 Above A1 - A15 Line:	0.998	inches	from Panel Center: 6.715 inches
S.G. #2 Above A1 - A15 Line:	0.977	inches	from Panel Center: * inches
S.G. #3 Above A1 - A15 Line:	0.993	inches	from Panel Center: 3.723 inches
S.G. #4 Above A1 - A15 Line:	0.977	inches	from Panel Center: * inches
S.G. #5 Above A1 - A15 Line:	0.977	inches	from Panel Center: 0.693 inches
S.G. #6 Above A1 - A15 Line:	0.977	inches	from Panel Center: * inches
S.G. #7 Above A1 - A15 Line:	0.977	inches	from Panel Center: 0.793 inches
S.G. #8 Above A1 - A15 Line:	0.983	inches	from Panel Center: * inches
S.G. #9 Above A1 - A15 Line:	0.980	inches	from Panel Center: 3.803 inches
S.G. #10 Above A1 - A15 Line:	0.993	inches	from Panel Center: * inches
S.G. #11 Above A1 - A15 Line:	0.979	inches	from Panel Center: 6.768 inches
S.G. #12 Above A1 - A15 Line:	0.999	inches	from Panel Center: * inches
S.G. #13 Above A1 - A15 Line:	0.064	inches	from Panel Center: 6.717 inches
S.G. #14 Above A1 - A15 Line:	0.120	inches	from Panel Center: * inches
S.G. #15 Above A1 - A15 Line:	0.059	inches	from Panel Center: 2.182 inches
S.G. #16 Above A1 - A15 Line:	0.111	inches	from Panel Center: * inches
S.G. #17 Above A1 - A15 Line:	0.070	inches	from Panel Center: 2.261 inches
S.G. #18 Above A1 - A15 Line:	0.095	inches	from Panel Center: * inches
S.G. #19 Above A1 - A15 Line:	0.072	inches	from Panel Center: 6.774 inches
S.G. #20 Above A1 - A15 Line:	0.105	inches	from Panel Center: * inches
S.G. #21 Below D1 - D15 Line:	0.975	inches	from Panel Center: 5.299 inches
S.G. #22 Below D1 - D15 Line:	1.000	inches	from Panel Center: * inches
S.G. #23 Below D1 - D15 Line:	0.973	inches	from Panel Center: 5.208 inches
S.G. #24 Below D1 - D15 Line:	0.993	inches	from Panel Center: * inches

\* Inaccessible on back of panel in test fixture.

Measurements Taken By: McCann / Grommon

Top Skin Width @ Grips:	<u>22.063</u>	inches	
Top Skin Width @ Splice:	<u>22.063</u>	inches	
Top Skin Length (Left):	<u>23.375</u>	inches	
Top Skin Length (Right):	<u>23.375</u>	inches	
Bottom Skin Width @ Grips:	<u>22.031</u>	inches	
Bottom Skin Width @ Splice:	<u>22.000</u>	inches	
Bottom Skin Length (Left):	<u>23.281</u>	inches	
Bottom Skin Length (Right):	<u>23.344</u>	inches	
Splice Overlap (Left):	<u>2.078</u>	inches	
Splice Overlap (Right):	<u>2.068</u>	inches	
A1 - B1 Measurement:	<u>0.812</u>	inches	
A15 - B27 Measurement:	<u>0.800</u>	inches	
A1 - C1 Measurement:	<u>1.995</u>	inches	
A15 - C27 Measurement:	<u>1.991</u>	inches	
A1 - D1 Measurement:	<u>2.834</u>	inches	
A15 - D15 Measurement:	<u>2.820</u>	inches	
B1 - C1 Measurement:	<u>1.205</u>	inches	
B27 - C27 Measurement:	<u>1.205</u>	inches	
S.G. #1 Above A1 - A15 Line:	<u>0.995</u>	inches	from Panel Center: <u>6.769</u> inches
S.G. #2 Above A1 - A15 Line:	<u>0.998</u>	inches	from Panel Center: <u>6.773</u> inches
S.G. #3 Above A1 - A15 Line:		inches	from Panel Center: _____ inches
S.G. #4 Above A1 - A15 Line:		inches	from Panel Center: _____ inches
S.G. #5 Above A1 - A15 Line:		inches	from Panel Center: _____ inches
S.G. #6 Above A1 - A15 Line:		inches	from Panel Center: _____ inches
S.G. #7 Above A1 - A15 Line:		inches	from Panel Center: _____ inches
S.G. #8 Above A1 - A15 Line:		inches	from Panel Center: _____ inches
S.G. #9 Above A1 - A15 Line:		inches	from Panel Center: _____ inches
S.G. #10 Above A1 - A15 Line:		inches	from Panel Center: _____ inches
S.G. #11 Above A1 - A15 Line:	<u>1.028</u>	inches	from Panel Center: <u>6.691</u> inches
S.G. #12 Above A1 - A15 Line:	<u>0.977</u>	inches	from Panel Center: <u>6.719</u> inches
S.G. #13 Above A1 - A15 Line:		inches	from Panel Center: _____ inches
S.G. #14 Above A1 - A15 Line:		inches	from Panel Center: _____ inches
S.G. #15 Above A1 - A15 Line:		inches	from Panel Center: _____ inches
S.G. #16 Above A1 - A15 Line:		inches	from Panel Center: _____ inches
S.G. #17 Above A1 - A15 Line:		inches	from Panel Center: _____ inches
S.G. #18 Above A1 - A15 Line:		inches	from Panel Center: _____ inches
S.G. #19 Above A1 - A15 Line:		inches	from Panel Center: _____ inches
S.G. #20 Above A1 - A15 Line:		inches	from Panel Center: _____ inches
S.G. #21 Below D1 - D15 Line:	<u>1.020</u>	inches	from Panel Center: <u>6.783</u> inches
S.G. #22 Below D1 - D15 Line:	<u>1.046</u>	inches	from Panel Center: <u>6.786</u> inches
S.G. #23 Below D1 - D15 Line:	<u>1.008</u>	inches	from Panel Center: <u>6.671</u> inches
S.G. #24 Below D1 - D15 Line:	<u>1.016</u>	inches	from Panel Center: <u>6.695</u> inches

Measurements Taken By: MCCann / Grommon

Top Skin Width @ Grips:	<u>22.063</u>	inches	
Top Skin Width @ Splice:	<u>22.063</u>	inches	
Top Skin Length (Left):	<u>23.281</u>	inches	
Top Skin Length (Right):	<u>23.313</u>	inches	
Bottom Skin Width @ Grips:	<u>22.094</u>	inches	
Bottom Skin Width @ Splice:	<u>22.063</u>	inches	
Bottom Skin Length (Left):	<u>23.250</u>	inches	
Bottom Skin Length (Right):	<u>23.344</u>	inches	
Splice Overlap (Left):	<u>2.060</u>	inches	
Splice Overlap (Right):	<u>2.071</u>	inches	
A1 - B1 Measurement:	<u>0.801</u>	inches	
A15 - B27 Measurement:	<u>0.844</u>	inches	
A1 - C1 Measurement:	<u>1.979</u>	inches	
A15 - C27 Measurement:	<u>2.026</u>	inches	
A1 - D1 Measurement:	<u>1.817</u>	inches	
A15 - D15 Measurement:	<u>2.864</u>	inches	
B1 - C1 Measurement:	<u>1.209</u>	inches	
B27 - C27 Measurement:	<u>1.211</u>	inches	
S.G. #1 Above A1 - A15 Line:	<u>1.047</u>	inches	from Panel Center: <u>6.801</u> inches
S.G. #2 Above A1 - A15 Line:	<u>1.020</u>	inches	from Panel Center: <u>6.788</u> inches
S.G. #3 Above A1 - A15 Line:		inches	from Panel Center: inches
S.G. #4 Above A1 - A15 Line:		inches	from Panel Center: inches
S.G. #5 Above A1 - A15 Line:		inches	from Panel Center: inches
S.G. #6 Above A1 - A15 Line:		inches	from Panel Center: inches
S.G. #7 Above A1 - A15 Line:		inches	from Panel Center: inches
S.G. #8 Above A1 - A15 Line:		inches	from Panel Center: inches
S.G. #9 Above A1 - A15 Line:		inches	from Panel Center: inches
S.G. #10 Above A1 - A15 Line:		inches	from Panel Center: inches
S.G. #11 Above A1 - A15 Line:	<u>1.024</u>	inches	from Panel Center: <u>6.750</u> inches
S.G. #12 Above A1 - A15 Line:	<u>1.018</u>	inches	from Panel Center: <u>6.734</u> inches
S.G. #13 Above A1 - A15 Line:		inches	from Panel Center: inches
S.G. #14 Above A1 - A15 Line:		inches	from Panel Center: inches
S.G. #15 Above A1 - A15 Line:		inches	from Panel Center: inches
S.G. #16 Above A1 - A15 Line:		inches	from Panel Center: inches
S.G. #17 Above A1 - A15 Line:		inches	from Panel Center: inches
S.G. #18 Above A1 - A15 Line:		inches	from Panel Center: inches
S.G. #19 Above A1 - A15 Line:		inches	from Panel Center: inches
S.G. #20 Above A1 - A15 Line:		inches	from Panel Center: inches
S.G. #21 Below D1 - D15 Line:	<u>1.024</u>	inches	from Panel Center: <u>6.787</u> inches
S.G. #22 Below D1 - D15 Line:	<u>0.993</u>	inches	from Panel Center: <u>6.768</u> inches
S.G. #23 Below D1 - D15 Line:	<u>0.984</u>	inches	from Panel Center: <u>6.764</u> inches
S.G. #24 Below D1 - D15 Line:	<u>1.009</u>	inches	from Panel Center: <u>6.748</u> inches



Measurements Taken By: McCann & Grommon

Top Skin Width @ Grips:	<u>22.125</u>	inches		
Top Skin Width @ Splice:	<u>22.031</u>	inches		
Top Skin Length (Left):	<u>23.313</u>	inches		
Top Skin Length (Right):	<u>23.313</u>	inches		
Bottom Skin Width @ Grips:	<u>22.125</u>	inches		
Bottom Skin Width @ Splice:	<u>22.063</u>	inches		
Bottom Skin Length (Left):	<u>23.188</u>	inches		
Bottom Skin Length (Right):	<u>23.188</u>	inches		
Splice Overlap (Left):	<u>2.680</u>	inches		
Splice Overlap (Right):	<u>2.530</u>	inches		
A1 - B1 Measurement:	<u>0.800</u>	inches		
A15 - B27 Measurement:	<u>0.807</u>	inches		
A1 - C1 Measurement:	<u>1.963</u>	inches		
A15 - C27 Measurement:	<u>2.005</u>	inches		
A1 - D1 Measurement:	<u>2.804</u>	inches		
A15 - D15 Measurement:	<u>1.869</u>	inches		
B1 - C1 Measurement:	<u>1.170</u>	inches		
B27 - C27 Measurement:	<u>1.185</u>	inches		
S.G. #1 Above A1 - A15 Line:	<u>1.004</u>	inches	from Panel Center:	<u>6.807</u> inches
S.G. #2 Above A1 - A15 Line:	<u>0.983</u>	inches	from Panel Center:	<u>6.734</u> inches
S.G. #3 Above A1 - A15 Line:		inches	from Panel Center:	inches
S.G. #4 Above A1 - A15 Line:		inches	from Panel Center:	inches
S.G. #5 Above A1 - A15 Line:		inches	from Panel Center:	inches
S.G. #6 Above A1 - A15 Line:		inches	from Panel Center:	inches
S.G. #7 Above A1 - A15 Line:		inches	from Panel Center:	inches
S.G. #8 Above A1 - A15 Line:		inches	from Panel Center:	inches
S.G. #9 Above A1 - A15 Line:		inches	from Panel Center:	inches
S.G. #10 Above A1 - A15 Line:		inches	from Panel Center:	inches
S.G. #11 Above A1 - A15 Line:	<u>0.977</u>	inches	from Panel Center:	<u>6.767</u> inches
S.G. #12 Above A1 - A15 Line:	<u>0.989</u>	inches	from Panel Center:	<u>6.821</u> inches
S.G. #13 Above A1 - A15 Line:		inches	from Panel Center:	inches
S.G. #14 Above A1 - A15 Line:		inches	from Panel Center:	inches
S.G. #15 Above A1 - A15 Line:		inches	from Panel Center:	inches
S.G. #16 Above A1 - A15 Line:		inches	from Panel Center:	inches
S.G. #17 Above A1 - A15 Line:		inches	from Panel Center:	inches
S.G. #18 Above A1 - A15 Line:		inches	from Panel Center:	inches
S.G. #19 Above A1 - A15 Line:		inches	from Panel Center:	inches
S.G. #20 Above A1 - A15 Line:		inches	from Panel Center:	inches
S.G. #21 Below D1 - D15 Line:	<u>0.983</u>	inches	from Panel Center:	<u>6.813</u> inches
S.G. #22 Below D1 - D15 Line:	<u>0.983</u>	inches	from Panel Center:	<u>6.756</u> inches
S.G. #23 Below D1 - D15 Line:	<u>0.981</u>	inches	from Panel Center:	<u>6.761</u> inches
S.G. #24 Below D1 - D15 Line:	<u>1.001</u>	inches	from Panel Center:	<u>6.788</u> inches

Measurements Taken By: Sean Coghlan

Top Panel Width @ Grips: \_\_\_\_\_ inches  
Top Skin Width @ Splice: \_\_\_\_\_ inches  
Top Skin Length (Left): \_\_\_\_\_ inches  
Top Skin Length (Right): \_\_\_\_\_ inches

Bottom Skin Width @ Grips: \_\_\_\_\_ inches  
Bottom Skin Width @ Splice: \_\_\_\_\_ inches  
Bottom Skin Length (Left): \_\_\_\_\_ inches  
Bottom Skin Length (Right): \_\_\_\_\_ inches

A2 - C2 Measurement: 1.669 inchesA1 - C1 Measurement: 1.672 inchesA18 - C18 Measurement: 1.637 inchesA19-C19 Measurement: 1.650 inches

S.G. #1 Above A1 - A19 Line: \_\_\_\_\_ inches

S.G. #2 Above A1 - A19 Line: \_\_\_\_\_ inches

S.G. #3 Above A1 - A19 Line: \_\_\_\_\_ inches

S.G. #4 Above A1 - A19 Line: \_\_\_\_\_ inches

S.G. #5 Above A1 - A19 Line: \_\_\_\_\_ inches

S.G. #6 Above A1 - A19 Line: \_\_\_\_\_ inches

S.G. #7 Above A1 - A19 Line: \_\_\_\_\_ inches

S.G. #8 Above A1 - A19 Line: \_\_\_\_\_ inches

S.G. #9 Above A1 - A19 Line: \_\_\_\_\_ inches

S.G. #10 Above A1 - A19 Line: \_\_\_\_\_ inches

S.G. #11 Above A1 - A19 Line: \_\_\_\_\_ inches

S.G. #12 Above A1 - A19 Line: \_\_\_\_\_ inches

S.G. #13 Above A1 - A19 Line: \_\_\_\_\_ inches

S.G. #14 Above A1 - A19 Line: \_\_\_\_\_ inches

S.G. #15 Above A1 - A19 Line: \_\_\_\_\_ inches

S.G. #16 Above A1 - A19 Line: \_\_\_\_\_ inches

S.G. #17 Above A1 - A19 Line: \_\_\_\_\_ inches

S.G. #18 Above A1 - A19 Line: \_\_\_\_\_ inches

S.G. #19 Above A1 - A19 Line: \_\_\_\_\_ inches

S.G. #20 Above A1 - A19 Line: \_\_\_\_\_ inches

S.G. #21 Below C1 - C19 Line: \_\_\_\_\_ inches

S.G. #22 Below C1 - C19 Line: \_\_\_\_\_ inches

S.G. #23 Below C1 - C19 Line: \_\_\_\_\_ inches

S.G. #24 Below C1 - C19 Line: \_\_\_\_\_ inches

Measurements Taken By: Sean Coghlan

Top Panel Width @ Grips:	_____	inches
Top Skin Width @ Splice:	_____	inches
Top Skin Length (Left):	_____	inches
Top Skin Length (Right):	_____	inches
Bottom Skin Width @ Grips:	_____	inches
Bottom Skin Width @ Splice:	_____	inches
Bottom Skin Length (Left):	_____	inches
Bottom Skin Length (Right):	_____	inches
A1 - C1 Measurement:	<u>1.676</u>	inches
A2 - C2 Measurement:	<u>1.687</u>	inches
A18 - C18 Measurement:	<u>1.617</u>	inches
A19 - C19 Measurement:	<u>1.644</u>	inches
S.G. #1 Above A1 - A19 Line:	_____	inches
S.G. #2 Above A1 - A19 Line:	_____	inches
S.G. #3 Above A1 - A19 Line:	_____	inches
S.G. #4 Above A1 - A19 Line:	_____	inches
S.G. #5 Above A1 - A19 Line:	_____	inches
S.G. #6 Above A1 - A19 Line:	_____	inches
S.G. #7 Above A1 - A19 Line:	_____	inches
S.G. #8 Above A1 - A19 Line:	_____	inches
S.G. #9 Above A1 - A19 Line:	_____	inches
S.G. #10 Above A1 - A19 Line:	_____	inches
S.G. #11 Above A1 - A19 Line:	_____	inches
S.G. #12 Above A1 - A19 Line:	_____	inches
S.G. #13 Above A1 - A19 Line:	_____	inches
S.G. #14 Above A1 - A19 Line:	_____	inches
S.G. #15 Above A1 - A19 Line:	_____	inches
S.G. #16 Above A1 - A19 Line:	_____	inches
S.G. #17 Above A1 - A19 Line:	_____	inches
S.G. #18 Above A1 - A19 Line:	_____	inches
S.G. #19 Above A1 - A19 Line:	_____	inches
S.G. #20 Above A1 - A19 Line:	_____	inches
S.G. #21 Below C1 - C19 Line:	_____	inches
S.G. #22 Below C1 - C19 Line:	<u>1.008</u>	inches
S.G. #23 Below C1 - C19 Line:	_____	inches
S.G. #24 Below C1 - C19 Line:	<u>0.970</u>	inches

Measurements Taken By: Anselmo, McCann, Smith

Top Panel Width @ Grips:	_____	inches
Top Skin Width @ Splice:	_____	inches
Top Skin Length (Left):	_____	inches
Top Skin Length (Right):	_____	inches
Bottom Skin Width @ Grips:	_____	inches
Bottom Skin Width @ Splice:	_____	inches
Bottom Skin Length (Left):	_____	inches
Bottom Skin Length (Right):	_____	inches
A2 - C2 Measurement:	<u>1.675</u>	inches
A18 - C18 Measurement:	<u>1.637</u>	inches
S.G. #1 Above A1 - A19 Line:	<u>1.010</u>	inches
S.G. #2 Above A1 - A19 Line:	<u>1.025</u>	inches
S.G. #3 Above A1 - A19 Line:	_____	inches
S.G. #4 Above A1 - A19 Line:	_____	inches
S.G. #5 Above A1 - A19 Line:	_____	inches
S.G. #6 Above A1 - A19 Line:	_____	inches
S.G. #7 Above A1 - A19 Line:	_____	inches
S.G. #8 Above A1 - A19 Line:	_____	inches
S.G. #9 Above A1 - A19 Line:	_____	inches
S.G. #10 Above A1 - A19 Line:	_____	inches
S.G. #11 Above A1 - A19 Line:	<u>0.973</u>	inches
S.G. #12 Above A1 - A19 Line:	<u>1.011</u>	inches
S.G. #13 Above A1 - A19 Line:	_____	inches
S.G. #14 Above A1 - A19 Line:	_____	inches
S.G. #15 Above A1 - A19 Line:	_____	inches
S.G. #16 Above A1 - A19 Line:	_____	inches
S.G. #17 Above A1 - A19 Line:	_____	inches
S.G. #18 Above A1 - A19 Line:	_____	inches
S.G. #19 Above A1 - A19 Line:	_____	inches
S.G. #20 Above A1 - A19 Line:	_____	inches
S.G. #21 Below C1 - C19 Line:	<u>0.977</u>	inches
S.G. #22 Below C1 - C19 Line:	<u>1.016</u>	inches
S.G. #23 Below C1 - C19 Line:	_____	inches
S.G. #24 Below C1 - C19 Line:	_____	inches

Measurements Taken By: Larry Mack, Jeff Vannorsdall

Top Panel Width @ Grips:	<u>21.934</u>	inches	
Top Skin Width @ Splice:	<u>21.973</u>	inches	
Top Skin Length (Left):	<u>24.125</u>	inches	
Top Skin Length (Right):	<u>24.187</u>	inches	
Bottom Skin Width @ Grips:	<u>21.930</u>	inches	
Bottom Skin Width @ Splice:	<u>21.971</u>	inches	
Bottom Skin Length (Left):	<u>24.062</u>	inches	
Bottom Skin Length (Right):	<u>24.125</u>	inches	
A2 - C2 Measurement:	<u>1.655</u>	inches	
A18 - C18 Measurement:	<u>1.653</u>	inches	
S.G. #1 Above A1 - A19 Line:	<u>0.987</u>	inches	
S.G. #2 Above A1 - A19 Line:	<u>1.014</u>	inches	
S.G. #3 Above A1 - A19 Line:		inches	
S.G. #4 Above A1 - A19 Line:		inches	
S.G. #5 Above A1 - A19 Line:		inches	
S.G. #6 Above A1 - A19 Line:		inches	
S.G. #7 Above A1 - A19 Line:		inches	
S.G. #8 Above A1 - A19 Line:		inches	
S.G. #9 Above A1 - A19 Line:		inches	
S.G. #10 Above A1 - A19 Line:		inches	
S.G. #11 Above A1 - A19 Line:	<u>0.983</u>	inches	
S.G. #12 Above A1 - A19 Line:	<u>1.032</u>	inches	
S.G. #13 Above A1 - A19 Line:		inches	
S.G. #14 Above A1 - A19 Line:		inches	
S.G. #15 Above A1 - A19 Line:		inches	
S.G. #16 Above A1 - A19 Line:		inches	
S.G. #17 Above A1 - A19 Line:		inches	
S.G. #18 Above A1 - A19 Line:		inches	
S.G. #19 Above A1 - A19 Line:		inches	
S.G. #20 Above A1 - A19 Line:		inches	
S.G. #21 Below C1 - C19 Line:	<u>0.987</u>	inches	26.073
S.G. #22 Below C1 - C19 Line:	<u>1.000</u>	inches	26.060
S.G. #23 Below C1 - C19 Line:	<u>0.973</u>	inches	26.087
S.G. #24 Below C1 - C19 Line:	<u>0.986</u>	inches	26.074

Measurements Taken By: McCann / Grommon

Top Skin Width @ Grips:	<u>22.063</u>	inches	
Top Skin Width @ Splice:	<u>21.875</u>	inches	
Top Skin Length (Left):	<u>22.100</u>	inches	
Top Skin Length (Right):	<u>22.150</u>	inches	
Bottom Skin Width @ Grips:	<u>22.063</u>	inches	
Bottom Skin Width @ Splice:	<u>22.031</u>	inches	
Bottom Skin Length (Left):	<u>22.150</u>	inches	
Bottom Skin Length (Right):	<u>22.080</u>	inches	
Splice Overlap (Left):		inches	
Splice Overlap (Right):		inches	
A1 - B2 Measurement:	<u>0.803</u>	inches	A1 - F1 Measurement: <u>4.732</u> inches
A13 - B26 Measurement:	<u>0.779</u>	inches	A13 - F13 Measurement: <u>4.681</u> inches
A1 - C2 Measurement:	<u>1.744</u>	inches	
A13 - C26 Measurement:	<u>1.726</u>	inches	
A1 - D2 Measurement:	<u>2.914</u>	inches	
A13 - D26 Measurement:	<u>2.880</u>	inches	
A1 - E2 Measurement:	<u>3.885</u>	inches	
A13 - E26 Measurement:	<u>3.859</u>	inches	
S.G. #1 Above A1 - A13 Line:	<u>0.968</u>	inches	from Panel Center: <u>7.275</u> inches
S.G. #2 Above A1 - A13 Line:	<u>1.007</u>	inches	from Panel Center: <u>7.250</u> inches
S.G. #3 Above A1 - A13 Line:	<u>1.007</u>	inches	from Panel Center: <u>4.096</u> inches
S.G. #4 Above A1 - A13 Line:	<u>1.003</u>	inches	from Panel Center: <u>2.472</u> inches
S.G. #5 Above A1 - A13 Line:	<u>0.994</u>	inches	from Panel Center: <u>2.430</u> inches
S.G. #6 Above A1 - A13 Line:	<u>1.003</u>	inches	from Panel Center: <u>2.472</u> inches
S.G. #7 Above A1 - A13 Line:	<u>1.009</u>	inches	from Panel Center: <u>7.181</u> inches
S.G. #8 Above A1 - A13 Line:	<u>1.003</u>	inches	from Panel Center: <u>7.218</u> inches
S.G. #9 Above A1 - A13 Line:	<u>0.127</u>	inches	from Panel Center: <u>2.275</u> inches
S.G. #10 Above A1 - A13 Line:	<u>0.150</u>	inches	from Panel Center: <u>2.250</u> inches
S.G. #11 Above A1 - A13 Line:	<u>0.121</u>	inches	from Panel Center: <u>4.093</u> inches
S.G. #12 Above A1 - A13 Line:	<u>0.152</u>	inches	from Panel Center: <u>4.045</u> inches
S.G. #13 Above A1 - A13 Line:	<u>0.125</u>	inches	from Panel Center: <u>3.977</u> inches
S.G. #14 Above A1 - A13 Line:	<u>0.165</u>	inches	from Panel Center: <u>3.986</u> inches
S.G. #15 Above A1 - A13 Line:	<u>0.125</u>	inches	from Panel Center: <u>7.181</u> inches
S.G. #16 Above A1 - A13 Line:	<u>0.971</u>	inches	from Panel Center: <u>7.218</u> inches
S.G. #17 Above A1 - A13 Line:	<u>1.003</u>	inches	from Panel Center: <u>7.308</u> inches
S.G. #18 Above F1 - F13 Line:	<u>1.003</u>	inches	from Panel Center: <u>7.224</u> inches
S.G. #19 Above F1 - F13 Line:	<u>1.020</u>	inches	from Panel Center: <u>7.235</u> inches
S.G. #20 Above F1 - F13 Line:		inches	from Panel Center: <u>7.164</u> inches

Measurements Taken By: Jeff Vannorsdall / Larry Mack

Top Skin Width @ Grips:	<u>22.090</u>	inches		
Top Skin Width @ Splice:	<u>22.065</u>	inches		
Top Skin Length (Left):	<u>22.140</u>	inches		
Top Skin Length (Right):	<u>22.150</u>	inches		
Bottom Skin Width @ Grips:	<u>22.025</u>	inches		
Bottom Skin Width @ Splice:	<u>22.045</u>	inches		
Bottom Skin Length (Left):	<u>22.070</u>	inches		
Bottom Skin Length (Right):	<u>22.060</u>	inches		
Splice Overlap (Left):	<u>          </u>	inches		
Splice Overlap (Right):	<u>          </u>	inches		
A1 - B2 Measurement:	<u>0.815</u>	inches	A1 - F1 Measurement:	<u>4.730</u> inches
A13 - B26 Measurement:	<u>0.825</u>	inches	A13 - F13 Measurement:	<u>4.792</u> inches
A1 - C2 Measurement:	<u>1.777</u>	inches		
A13 - C26 Measurement:	<u>1.820</u>	inches		
A1 - D2 Measurement:	<u>2.884</u>	inches		
A13 - D26 Measurement:	<u>2.923</u>	inches		
A1 - E2 Measurement:	<u>3.895</u>	inches		
A13 - E26 Measurement:	<u>3.938</u>	inches		
S.G. #1 Above A1 - A13 Line:	<u>1.000</u>	inches	from Panel Center:	<u>7.210</u> inches
S.G. #2 Above A1 - A13 Line:	<u>1.011</u>	inches	from Panel Center:	<u>7.265</u> inches
S.G. #3 Above A1 - A13 Line:	<u>          </u>	inches	from Panel Center:	<u>          </u> inches
S.G. #4 Above A1 - A13 Line:	<u>          </u>	inches	from Panel Center:	<u>          </u> inches
S.G. #5 Above A1 - A13 Line:	<u>          </u>	inches	from Panel Center:	<u>          </u> inches
S.G. #6 Above A1 - A13 Line:	<u>          </u>	inches	from Panel Center:	<u>          </u> inches
S.G. #7 Above A1 - A13 Line:	<u>1.000</u>	inches	from Panel Center:	<u>7.110</u> inches
S.G. #8 Above A1 - A13 Line:	<u>1.011</u>	inches	from Panel Center:	<u>7.155</u> inches
S.G. #9 Above A1 - A13 Line:	<u>          </u>	inches	from Panel Center:	<u>          </u> inches
S.G. #10 Above A1 - A13 Line:	<u>          </u>	inches	from Panel Center:	<u>          </u> inches
S.G. #11 Above A1 - A13 Line:	<u>          </u>	inches	from Panel Center:	<u>          </u> inches
S.G. #12 Above A1 - A13 Line:	<u>          </u>	inches	from Panel Center:	<u>          </u> inches
S.G. #13 Above A1 - A13 Line:	<u>          </u>	inches	from Panel Center:	<u>          </u> inches
S.G. #14 Above A1 - A13 Line:	<u>          </u>	inches	from Panel Center:	<u>          </u> inches
S.G. #15 Above A1 - A13 Line:	<u>          </u>	inches	from Panel Center:	<u>          </u> inches
S.G. #16 Above A1 - A13 Line:	<u>          </u>	inches	from Panel Center:	<u>          </u> inches
S.G. #17 Above A1 - A13 Line:	<u>0.982</u>	inches	from Panel Center:	<u>7.210</u> inches
S.G. #18 Above F1 - F13 Line:	<u>1.000</u>	inches	from Panel Center:	<u>7.233</u> inches
S.G. #19 Above F1 - F13 Line:	<u>0.984</u>	inches	from Panel Center:	<u>7.130</u> inches
S.G. #20 Above F1 - F13 Line:	<u>1.000</u>	inches	from Panel Center:	<u>7.135</u> inches

Measurements Taken By: J. Vannorsdall / L. Mack

Top Skin Width @ Grips:	<u>22.059</u>	inches		
Top Skin Width @ Splice:	<u>22.018</u>	inches		
Top Skin Length (Left):	<u>22.100</u>	inches		
Top Skin Length (Right):	<u>22.130</u>	inches		
Bottom Skin Width @ Grips:	<u>22.043</u>	inches		
Bottom Skin Width @ Splice:	<u>22.028</u>	inches		
Bottom Skin Length (Left):	<u>22.000</u>	inches		
Bottom Skin Length (Right):	<u>22.020</u>	inches		
Splice Overlap (Left):	<u>          </u>	inches		
Splice Overlap (Right):	<u>          </u>	inches		
A1 - B2 Measurement:	<u>0.800</u>	inches	A1 - F1 Measurement:	<u>4.723</u> inches
A13 - B26 Measurement:	<u>0.775</u>	inches	A13 - F13 Measurement:	<u>4.684</u> inches
A1 - C2 Measurement:	<u>1.789</u>	inches		
A13 - C26 Measurement:	<u>1.815</u>	inches		
A1 - D2 Measurement:	<u>2.944</u>	inches		
A13 - D26 Measurement:	<u>2.954</u>	inches		
A1 - E2 Measurement:	<u>3.915</u>	inches		
A13 - E26 Measurement:	<u>3.873</u>	inches		
S.G. #1 Above A1 - A13 Line:	<u>0.995</u>	inches	from Panel Center:	<u>7.210</u> inches
S.G. #2 Above A1 - A13 Line:	<u>1.006</u>	inches	from Panel Center:	<u>7.255</u> inches
S.G. #3 Above A1 - A13 Line:	<u>          </u>	inches	from Panel Center:	<u>          </u> inches
S.G. #4 Above A1 - A13 Line:	<u>          </u>	inches	from Panel Center:	<u>          </u> inches
S.G. #5 Above A1 - A13 Line:	<u>          </u>	inches	from Panel Center:	<u>          </u> inches
S.G. #6 Above A1 - A13 Line:	<u>          </u>	inches	from Panel Center:	<u>          </u> inches
S.G. #7 Above A1 - A13 Line:	<u>0.995</u>	inches	from Panel Center:	<u>7.130</u> inches
S.G. #8 Above A1 - A13 Line:	<u>1.021</u>	inches	from Panel Center:	<u>7.140</u> inches
S.G. #9 Above A1 - A13 Line:	<u>          </u>	inches	from Panel Center:	<u>          </u> inches
S.G. #10 Above A1 - A13 Line:	<u>          </u>	inches	from Panel Center:	<u>          </u> inches
S.G. #11 Above A1 - A13 Line:	<u>          </u>	inches	from Panel Center:	<u>          </u> inches
S.G. #12 Above A1 - A13 Line:	<u>          </u>	inches	from Panel Center:	<u>          </u> inches
S.G. #13 Above A1 - A13 Line:	<u>          </u>	inches	from Panel Center:	<u>          </u> inches
S.G. #14 Above A1 - A13 Line:	<u>          </u>	inches	from Panel Center:	<u>          </u> inches
S.G. #15 Above A1 - A13 Line:	<u>          </u>	inches	from Panel Center:	<u>          </u> inches
S.G. #16 Above A1 - A13 Line:	<u>          </u>	inches	from Panel Center:	<u>          </u> inches
S.G. #17 Above A1 - A13 Line:	<u>0.991</u>	inches	from Panel Center:	<u>7.220</u> inches
S.G. #18 Above F1 - F13 Line:	<u>0.988</u>	inches	from Panel Center:	<u>7.185</u> inches
S.G. #19 Above F1 - F13 Line:	<u>1.003</u>	inches	from Panel Center:	<u>7.040</u> inches
S.G. #20 Above F1 - F13 Line:	<u>0.971</u>	inches	from Panel Center:	<u>7.220</u> inches



Measurements Taken By: J. Vannorsdall/L. Mack

Top Skin Width @ Grips:	<u>22.067</u>	inches	
Top Skin Width @ Splice:	<u>22.126</u>	inches	
Top Skin Length (Left):	<u>22.060</u>	inches	
Top Skin Length (Right):	<u>22.130</u>	inches	
Bottom Skin Width @ Grips:	<u>22.083</u>	inches	
Bottom Skin Width @ Splice:	<u>22.045</u>	inches	
Bottom Skin Length (Left):	<u>22.240</u>	inches	
Bottom Skin Length (Right):	<u>22.160</u>	inches	
Splice Overlap (Left):		inches	
Splice Overlap (Right):		inches	
A1 - B2 Measurement:	<u>0.782</u>	inches	A1 - F1 Measurement: <u>4.696</u> inches
A13 - B26 Measurement:	<u>0.775</u>	inches	A13 - F13 Measurement: <u>4.696</u> inches
A1 - C2 Measurement:	<u>1.725</u>	inches	
A13 - C26 Measurement:	<u>1.800</u>	inches	
A1 - D2 Measurement:	<u>2.863</u>	inches	
A13 - D26 Measurement:	<u>2.951</u>	inches	
A1 - E2 Measurement:	<u>3.869</u>	inches	
A13 - E26 Measurement:	<u>3.902</u>	inches	
S.G. #1 Above A1 - A13 Line:	<u>1.023</u>	inches	from Panel Center: <u>7.185</u> inches
S.G. #2 Above A1 - A13 Line:	<u>1.018</u>	inches	from Panel Center: <u>7.210</u> inches
S.G. #3 Above A1 - A13 Line:		inches	from Panel Center: <u>        </u> inches
S.G. #4 Above A1 - A13 Line:		inches	from Panel Center: <u>        </u> inches
S.G. #5 Above A1 - A13 Line:		inches	from Panel Center: <u>        </u> inches
S.G. #6 Above A1 - A13 Line:		inches	from Panel Center: <u>        </u> inches
S.G. #7 Above A1 - A13 Line:	<u>0.997</u>	inches	from Panel Center: <u>7.210</u> inches
S.G. #8 Above A1 - A13 Line:	<u>1.024</u>	inches	from Panel Center: <u>7.220</u> inches
S.G. #9 Above A1 - A13 Line:		inches	from Panel Center: <u>        </u> inches
S.G. #10 Above A1 - A13 Line:		inches	from Panel Center: <u>        </u> inches
S.G. #11 Above A1 - A13 Line:		inches	from Panel Center: <u>        </u> inches
S.G. #12 Above A1 - A13 Line:		inches	from Panel Center: <u>        </u> inches
S.G. #13 Above A1 - A13 Line:		inches	from Panel Center: <u>        </u> inches
S.G. #14 Above A1 - A13 Line:		inches	from Panel Center: <u>        </u> inches
S.G. #15 Above A1 - A13 Line:		inches	from Panel Center: <u>        </u> inches
S.G. #16 Above A1 - A13 Line:		inches	from Panel Center: <u>        </u> inches
S.G. #17 Above A1 - A13 Line:	<u>1.004</u>	inches	from Panel Center: <u>7.240</u> inches
S.G. #18 Above F1 - F13 Line:	<u>1.015</u>	inches	from Panel Center: <u>7.130</u> inches
S.G. #19 Above F1 - F13 Line:	<u>0.996</u>	inches	from Panel Center: <u>7.270</u> inches
S.G. #20 Above F1 - F13 Line:	<u>1.024</u>	inches	from Panel Center: <u>7.140</u> inches

Measurements Taken By: Jeff Vannorsdall

Top Skin Width @ Grips:	<u>22.027</u>	inches		
Top Skin Width @ Splice:	<u>22.057</u>	inches		
Top Skin Length (Left):	<u>22.200</u>	inches		
Top Skin Length (Right):	<u>22.140</u>	inches		
Bottom Skin Width @ Grips:	<u>22.025</u>	inches		
Bottom Skin Width @ Splice:	<u>22.047</u>	inches		
Bottom Skin Length (Left):	<u>22.160</u>	inches		
Bottom Skin Length (Right):	<u>22.200</u>	inches		
A1 - B1 Measurement:	<u>0.855</u>	inches	A1 - F1 Measurement:	<u>3.714</u> inches
A15 - B29 Measurement:	<u>0.907</u>	inches	A15 - F28 Measurement:	<u>3.772</u> inches
A1 - C1 Measurement:	<u>1.490</u>	inches	A1 - G1 Measurement:	<u>4.365</u> inches
A15 - C28 Measurement:	<u>1.542</u>	inches	A15 - G29 Measurement:	<u>4.425</u> inches
A1 - D1 Measurement:	<u>2.102</u>	inches	A1 - H1 Measurement:	<u>5.248</u> inches
A15 - D29 Measurement:	<u>2.144</u>	inches	A15 - H15 Measurement:	<u>5.310</u> inches
A1 - E1 Measurement:	<u>3.092</u>	inches		
A15 - E29 Measurement:	<u>3.169</u>	inches		
S.G. #1 Above A1 - A15 Line:	<u>1.000</u>	inches	from Panel Center:	<u>6.800</u> inches
S.G. #2 Above A1 - A15 Line:	<u>0.982</u>	inches	from Panel Center:	<u>6.800</u> inches
S.G. #3 Above A1 - A15 Line:	<u>1.000</u>	inches	from Panel Center:	<u>3.820</u> inches
S.G. #4 Above A1 - A15 Line:	<u>0.965</u>	inches	from Panel Center:	<u>3.840</u> inches
S.G. #5 Above A1 - A15 Line:	<u>1.000</u>	inches	from Panel Center:	<u>0.820</u> inches
S.G. #6 Above A1 - A15 Line:	<u>0.975</u>	inches	from Panel Center:	<u>0.800</u> inches
S.G. #7 Above A1 - A15 Line:	<u>1.000</u>	inches	from Panel Center:	<u>0.700</u> inches
S.G. #8 Above A1 - A15 Line:	<u>0.990</u>	inches	from Panel Center:	<u>0.700</u> inches
S.G. #9 Above A1 - A15 Line:	<u>1.000</u>	inches	from Panel Center:	<u>3.640</u> inches
S.G. #10 Above A1 - A15 Line:	<u>0.964</u>	inches	from Panel Center:	<u>3.680</u> inches
S.G. #11 Above A1 - A15 Line:	<u>1.000</u>	inches	from Panel Center:	<u>6.640</u> inches
S.G. #12 Above A1 - A15 Line:	<u>0.971</u>	inches	from Panel Center:	<u>6.680</u> inches
S.G. #13 Above A1 - A15 Line:	<u>0.075</u>	inches	from Panel Center:	<u>6.840</u> inches
S.G. #14 Above A1 - A15 Line:	<u>c/l</u>	inches	from Panel Center:	<u>6.800</u> inches
S.G. #15 Above A1 - A15 Line:	<u>0.065</u>	inches	from Panel Center:	<u>2.340</u> inches
S.G. #16 Above A1 - A15 Line:	<u>c/l</u>	inches	from Panel Center:	<u>2.320</u> inches
S.G. #17 Above A1 - A15 Line:	<u>0.035</u>	inches	from Panel Center:	<u>2.260</u> inches
S.G. #18 Above A1 - A15 Line:	<u>c/l</u>	inches	from Panel Center:	<u>2.200</u> inches
S.G. #19 Above A1 - A15 Line:	<u>0.018</u>	inches	from Panel Center:	<u>6.620</u> inches
S.G. #20 Above A1 - A15 Line:	<u>c/l</u>	inches	from Panel Center:	<u>6.700</u> inches
S.G. #21 Below H1 - H15 Line:	<u>1.000</u>	inches	from Panel Center:	<u>6.780</u> inches
S.G. #22 Below H1 - H15 Line:	<u>0.995</u>	inches	from Panel Center:	<u>6.760</u> inches
S.G. #23 Below H1 - H15 Line:	<u>1.000</u>	inches	from Panel Center:	<u>6.700</u> inches
S.G. #24 Below H1 - H15 Line:	<u>1.000</u>	inches	from Panel Center:	<u>6.720</u> inches

Measurements Taken By: J. Vannorsdall & L. Mack

Top Skin Width @ Grips:	<u>22.035</u>	inches	
Top Skin Width @ Splice:	<u>22.055</u>	inches	
Top Skin Length (Left):	<u>          </u>	inches	
Top Skin Length (Right):	<u>          </u>	inches	
Bottom Skin Width @ Grips:	<u>22.008</u>	inches	
Bottom Skin Width @ Splice:	<u>22.035</u>	inches	
Bottom Skin Length (Left):	<u>          </u>	inches	
Bottom Skin Length (Right):	<u>          </u>	inches	
A1 - B1 Measurement:	<u>0.870</u>	inches	A1 - F1 Measurement: <u>3.735</u> inches
A15 - B29 Measurement:	<u>0.823</u>	inches	A15 - F28 Measurement: <u>3.717</u> inches
A1 - C1 Measurement:	<u>1.492</u>	inches	A1 - G1 Measurement: <u>4.359</u> inches
A15 - C28 Measurement:	<u>1.463</u>	inches	A15 - G29 Measurement: <u>4.337</u> inches
A1 - D1 Measurement:	<u>2.103</u>	inches	A1 - H1 Measurement: <u>5.250</u> inches
A15 - D29 Measurement:	<u>2.078</u>	inches	A15 - H15 Measurement: <u>5.182</u> inches
A1 - E1 Measurement:	<u>3.128</u>	inches	
A15 - E29 Measurement:	<u>3.081</u>	inches	
S.G. #1 Above A1 - A15 Line:	<u>1.000</u>	inches	from Panel Center: <u>6.735</u> inches
S.G. #2 Above A1 - A15 Line:	<u>0.970</u>	inches	from Panel Center: <u>6.700</u> inches
S.G. #3 Above A1 - A15 Line:	<u>          </u>	inches	from Panel Center: <u>          </u> inches
S.G. #4 Above A1 - A15 Line:	<u>          </u>	inches	from Panel Center: <u>          </u> inches
S.G. #5 Above A1 - A15 Line:	<u>          </u>	inches	from Panel Center: <u>          </u> inches
S.G. #6 Above A1 - A15 Line:	<u>          </u>	inches	from Panel Center: <u>          </u> inches
S.G. #7 Above A1 - A15 Line:	<u>          </u>	inches	from Panel Center: <u>          </u> inches
S.G. #8 Above A1 - A15 Line:	<u>          </u>	inches	from Panel Center: <u>          </u> inches
S.G. #9 Above A1 - A15 Line:	<u>          </u>	inches	from Panel Center: <u>          </u> inches
S.G. #10 Above A1 - A15 Line:	<u>          </u>	inches	from Panel Center: <u>          </u> inches
S.G. #11 Above A1 - A15 Line:	<u>1.020</u>	inches	from Panel Center: <u>6.760</u> inches
S.G. #12 Above A1 - A15 Line:	<u>1.039</u>	inches	from Panel Center: <u>6.775</u> inches
S.G. #13 Above A1 - A15 Line:	<u>          </u>	inches	from Panel Center: <u>          </u> inches
S.G. #14 Above A1 - A15 Line:	<u>          </u>	inches	from Panel Center: <u>          </u> inches
S.G. #15 Above A1 - A15 Line:	<u>          </u>	inches	from Panel Center: <u>          </u> inches
S.G. #16 Above A1 - A15 Line:	<u>          </u>	inches	from Panel Center: <u>          </u> inches
S.G. #17 Above A1 - A15 Line:	<u>          </u>	inches	from Panel Center: <u>          </u> inches
S.G. #18 Above A1 - A15 Line:	<u>          </u>	inches	from Panel Center: <u>          </u> inches
S.G. #19 Above A1 - A15 Line:	<u>          </u>	inches	from Panel Center: <u>          </u> inches
S.G. #20 Above A1 - A15 Line:	<u>          </u>	inches	from Panel Center: <u>          </u> inches
S.G. #21 Below H1 - H15 Line:	<u>1.000</u>	inches	from Panel Center: <u>6.735</u> inches
S.G. #22 Below H1 - H15 Line:	<u>0.972</u>	inches	from Panel Center: <u>6.700</u> inches
S.G. #23 Below H1 - H15 Line:	<u>1.000</u>	inches	from Panel Center: <u>6.770</u> inches
S.G. #24 Below H1 - H15 Line:	<u>1.000</u>	inches	from Panel Center: <u>6.775</u> inches

Measurements Taken By: J. Vannorsdall & L. Mack

Top Skin Width @ Grips:	<u>22.035</u>	inches		
Top Skin Width @ Splice:	<u>22.055</u>	inches		
Top Skin Length (Left):	<u>22.100</u>	inches		
Top Skin Length (Right):	<u>22.100</u>	inches		
Bottom Skin Width @ Grips:	<u>22.020</u>	inches		
Bottom Skin Width @ Splice:	<u>22.006</u>	inches		
Bottom Skin Length (Left):	<u>22.240</u>	inches		
Bottom Skin Length (Right):	<u>22.300</u>	inches		
A1 - B1 Measurement:	<u>0.847</u>	inches	A1 - F1 Measurement:	<u>3.746</u> inches
A15 - B29 Measurement:	<u>0.925</u>	inches	A15 - F28 Measurement:	<u>3.775</u> inches
A1 - C1 Measurement:	<u>1.470</u>	inches	A1 - G1 Measurement:	<u>4.333</u> inches
A15 - C28 Measurement:	<u>1.546</u>	inches	A15 - G29 Measurement:	<u>4.400</u> inches
A1 - D1 Measurement:	<u>2.095</u>	inches	A1 - H1 Measurement:	<u>5.217</u> inches
A15 - D29 Measurement:	<u>2.160</u>	inches	A15 - H15 Measurement:	<u>5.230</u> inches
A1 - E1 Measurement:	<u>3.090</u>	inches		
A15 - E29 Measurement:	<u>3.150</u>	inches		
S.G. #1 Above A1 - A15 Line:	<u>0.960</u>	inches	from Panel Center:	<u>2.750</u> inches
S.G. #2 Above A1 - A15 Line:	<u>1.000</u>	inches	from Panel Center:	<u>6.720</u> inches
S.G. #3 Above A1 - A15 Line:		inches	from Panel Center:	
S.G. #4 Above A1 - A15 Line:		inches	from Panel Center:	
S.G. #5 Above A1 - A15 Line:		inches	from Panel Center:	
S.G. #6 Above A1 - A15 Line:		inches	from Panel Center:	
S.G. #7 Above A1 - A15 Line:		inches	from Panel Center:	
S.G. #8 Above A1 - A15 Line:		inches	from Panel Center:	
S.G. #9 Above A1 - A15 Line:		inches	from Panel Center:	
S.G. #10 Above A1 - A15 Line:		inches	from Panel Center:	
S.G. #11 Above A1 - A15 Line:	<u>0.926</u>	inches	from Panel Center:	<u>6.740</u> inches
S.G. #12 Above A1 - A15 Line:	<u>0.957</u>	inches	from Panel Center:	<u>6.700</u> inches
S.G. #13 Above A1 - A15 Line:		inches	from Panel Center:	
S.G. #14 Above A1 - A15 Line:		inches	from Panel Center:	
S.G. #15 Above A1 - A15 Line:		inches	from Panel Center:	
S.G. #16 Above A1 - A15 Line:		inches	from Panel Center:	
S.G. #17 Above A1 - A15 Line:		inches	from Panel Center:	
S.G. #18 Above A1 - A15 Line:		inches	from Panel Center:	
S.G. #19 Above A1 - A15 Line:		inches	from Panel Center:	
S.G. #20 Above A1 - A15 Line:		inches	from Panel Center:	
S.G. #21 Below H1 - H15 Line:	<u>1.019</u>	inches	from Panel Center:	<u>6.780</u> inches
S.G. #22 Below H1 - H15 Line:	<u>1.080</u>	inches	from Panel Center:	<u>6.735</u> inches
S.G. #23 Below H1 - H15 Line:	<u>1.059</u>	inches	from Panel Center:	<u>6.750</u> inches
S.G. #24 Below H1 - H15 Line:	<u>1.021</u>	inches	from Panel Center:	<u>6.730</u> inches


Measurements Taken By: J. Vannorsdall

Top Skin Width @ Grips:	<u>22.000</u>	inches		
Top Skin Width @ Splice:	<u>22.010</u>	inches		
Top Skin Length (Left):	<u>22.200</u>	inches		
Top Skin Length (Right):	<u>22.140</u>	inches		
Bottom Skin Width @ Grips:	<u>22.029</u>	inches		
Bottom Skin Width @ Splice:	<u>22.050</u>	inches		
Bottom Skin Length (Left):	<u>22.100</u>	inches		
Bottom Skin Length (Right):	<u>22.140</u>	inches		
A1 - B1 Measurement:	<u>0.875</u>	inches	A1 - F1 Measurement:	<u>3.750</u> inches
A15 - B29 Measurement:	<u>0.860</u>	inches	A15 - F28 Measurement:	<u>3.740</u> inches
A1 - C1 Measurement:	<u>1.500</u>	inches	A1 - G1 Measurement:	<u>4.491</u> inches
A15 - C28 Measurement:	<u>1.480</u>	inches	A15 - G29 Measurement:	<u>4.385</u> inches
A1 - D1 Measurement:	<u>2.150</u>	inches	A1 - H1 Measurement:	<u>5.265</u> inches
A15 - D29 Measurement:	<u>2.120</u>	inches	A15 - H15 Measurement:	<u>5.250</u> inches
A1 - E1 Measurement:	<u>3.150</u>	inches		
A15 - E29 Measurement:	<u>3.110</u>	inches		
S.G. #1 Above A1 - A15 Line:	<u>0.975</u>	inches	from Panel Center:	<u>6.760</u> inches
S.G. #2 Above A1 - A15 Line:	<u>1.000</u>	inches	from Panel Center:	<u>6.800</u> inches
S.G. #3 Above A1 - A15 Line:		inches	from Panel Center:	
S.G. #4 Above A1 - A15 Line:		inches	from Panel Center:	
S.G. #5 Above A1 - A15 Line:		inches	from Panel Center:	
S.G. #6 Above A1 - A15 Line:		inches	from Panel Center:	
S.G. #7 Above A1 - A15 Line:		inches	from Panel Center:	
S.G. #8 Above A1 - A15 Line:		inches	from Panel Center:	
S.G. #9 Above A1 - A15 Line:		inches	from Panel Center:	
S.G. #10 Above A1 - A15 Line:		inches	from Panel Center:	
S.G. #11 Above A1 - A15 Line:	<u>1.038</u>	inches	from Panel Center:	<u>6.700</u> inches
S.G. #12 Above A1 - A15 Line:	<u>1.000</u>	inches	from Panel Center:	<u>6.780</u> inches
S.G. #13 Above A1 - A15 Line:		inches	from Panel Center:	
S.G. #14 Above A1 - A15 Line:		inches	from Panel Center:	
S.G. #15 Above A1 - A15 Line:		inches	from Panel Center:	
S.G. #16 Above A1 - A15 Line:		inches	from Panel Center:	
S.G. #17 Above A1 - A15 Line:		inches	from Panel Center:	
S.G. #18 Above A1 - A15 Line:		inches	from Panel Center:	
S.G. #19 Above A1 - A15 Line:		inches	from Panel Center:	
S.G. #20 Above A1 - A15 Line:		inches	from Panel Center:	
S.G. #21 Below H1 - H15 Line:	<u>1.030</u>	inches	from Panel Center:	<u>6.780</u> inches
S.G. #22 Below H1 - H15 Line:	<u>0.970</u>	inches	from Panel Center:	<u>6.780</u> inches
S.G. #23 Below H1 - H15 Line:	<u>0.975</u>	inches	from Panel Center:	<u>6.730</u> inches
S.G. #24 Below H1 - H15 Line:	<u>1.000</u>	inches	from Panel Center:	<u>6.780</u> inches

## Appendix C Reconstructed Crack History Data

The following tables include all the data obtained during the fractographic investigation of all fracture surfaces for which marker bands could be detected. The  $\mu$  and  $\sigma$  symbols represent the mean and standard deviation of the "y" coordinate which is the distance from the faying surface to the crack front in the thickness direction. Crack length and "y" are in mm and  $dc_1/dN$  is mm/cycle. The average  $c_1$  crack length is used in calculating  $dc_1/dN$ ; however, raw  $c_1$  data is listed below. The crack naming convention is as follows:

3C14R


 Hole Side (Left or Right)  
 Hole Number (left to right)  
 Rivet Row  
 EIFS Specimen Number

3C14R					3C17R				
Groups	y	Cycles	c1	dc1/dN	Groups	y	Cycles	c1	dc1/dN
10	0.12	147660	0.16	2.39E-05	10	0.16	116020	0.34	1.32E-05
4	0.19	151420	0.25	4.07E-05	6	0.12	123320	0.43	1.17E-05
6	0.11	154960	0.40	6.72E-06	4	0.15	130950	0.52	1.36E-05
10	0.30	158830	0.42	5.37E-05	10	0.12	138360	0.62	9.32E-06
4	0.16	162590	0.63		6	0.16	145660	0.69	9.04E-06
$\mu =$	0.17				4	0.19	153290	0.76	1.19E-05
$\sigma =$	0.07				10	0.16	160700	0.85	1.23E-05
					6	0.21	168000	0.94	3.45E-05
					fracture	0.25	170000	1.01	
					$\mu =$	0.17			
					$\sigma =$	0.04			

3D13R					3D15L				
Groups	y	Cycles	c1	dc1/dN	Groups	y	Cycles	c1	dc1/dN
4	0.155	157860	0.20	8.23E-06	10	0.16	91810	0.27	1.65E-05
6					4	0.23	95570	0.33	2.71E-05
10	0.159	165270	0.26	1.33E-05	6	0.26	99110	0.43	2.07E-05
4	0.184	169030	0.31	3.09E-06	10	0.28	102980	0.51	1.86E-05
fracture		170000	0.32		4	0.29	106740	0.58	2.66E-05
$\mu =$	0.12				6	0.26	110280	0.67	2.22E-05
$\sigma =$	0.08				10	0.26	114150	0.76	2.69E-05
					4	0.26	117910	0.86	2.01E-05
					6	0.34	121450	0.93	2.95E-05
					10	0.32	125320	1.04	2.31E-05
					4	0.39	129080	1.13	3.53E-05
					6	0.32	132620	1.25	3.80E-05
					10	0.31	136490	1.40	3.48E-05
					4	0.33	140250	1.53	4.41E-05
					6	0.37	143790	1.69	4.99E-05
					10	0.35	147660	1.88	6.25E-05
					4	0.41	151420	2.12	7.23E-05
					6	0.42	154960	2.37	5.62E-05
					4	0.17	162590	2.80	7.09E-05
					10	0.32	170000	3.33	
					$\mu =$	0.30			
					$\sigma =$	0.07			

3D15L				
Groups	y	Cycles	c1	dc1/dN
10	0.105	98290	0.298	1.09E-05
4		102050		
6		105590		
10	0.277	109460	0.420	3.09E-05
4	0.194	113220	0.536	1.75E-05
6	0.248	116760	0.598	2.04E-05
10	0.336	120630	0.677	3.06E-05
4	0.238	124390	0.792	2.06E-05
6	0.326	127930	0.865	2.33E-05
10	0.388	131800	0.955	4.10E-05
4	0.255	135560	1.109	1.95E-05
6	0.438	139100	1.178	3.80E-05
10	0.401	142970	1.325	4.47E-05
4	0.402	146730	1.493	3.90E-05
6	0.505	150270	1.631	4.60E-05
10	0.476	154140	1.809	6.38E-05
4	0.413	157900	2.049	7.88E-05
6	0.410	161440	2.328	1.04E-04
10	0.354	165310	2.731	1.51E-04
4	0.308	169070	3.297	1.73E-04
fracture		170000	3.458	
μ = 0.30				
σ = 0.14				

4C9R					4C10R				
Groups	y	Cycles	c1	dc1/dN	Groups	y	Cycles	c1	dc1/dN
4	0.06	138250	0.057	2.18E-05	10?	0.21	-18,470	0.249	2.71E-05
6?	0.07	141790	0.134	9.56E-06	4?	0.15	-14,710	0.351	6.78E-06
10	0.10	145660	0.171	1.97E-05	6	0.23	-11,170	0.375	1.55E-05
4	0.17	149420	0.245	1.86E-05	10	0.28	-7,300	0.435	2.66E-05
6	0.15	152960	0.311	3.10E-05	4	0.24	-3,540	0.535	6.97E-07
10	0.22	156830	0.431	1.89E-05	fracture	0.26	170,000	0.656	
4	0.24	160590	0.502	2.94E-05	μ = 0.23				
6	0.22	164130	0.606	2.58E-05	σ = 0.05				
10	0.30	168000	0.706	8.40E-05					
fracture	0.37	170000	0.874						
μ = 0.19									
σ = 0.10									

4C11R					4C12R				
Groups	y	Cycles	c1	dc1/dN	Groups	y	Cycles	c1	dc1/dN
10	0.16	127020	0.065	3.43E-06	4	0.16	145,660	0.160	9.89E-06
10	0.20	135190	0.093	3.30E-06	6	0.24	149,200	0.195	2.71E-05
10	0.23	143360	0.120	1.18E-05	10	0.25	153,070	0.300	3.01E-05
10	0.29	151530	0.216	2.39E-06	4	0.18	156,830	0.413	1.33E-05
4	0.20	155290	0.225	1.50E-05	6	0.25	160,370	0.460	3.44E-05
6	0.19	158830	0.278	3.44E-05	10	0.22	164,240	0.593	1.78E-05
10	0.07	162700	0.411	9.57E-06	4	0.28	168,000	0.660	2.30E-05
4	0.17	166460	0.447	9.60E-06	fracture	0.29	170,000	0.706	
6	0.16	170000	0.481		μ = 0.23				
μ = 0.18					σ = 0.04				
σ = 0.06									

7A6L					7A6R				
Groups	y	Cycles	c1	dc1/dN	Groups	y	Cycles	c1	dc1/dN
6	0.34	80200	0.67	3.21E-05	10	0.23	28500	0.09	2.84E-05
10	0.45	82070	0.73	3.33E-05	4	0.20	30260	0.14	1.30E-05
4					6	0.22	31800	0.16	2.67E-05
6	0.46	85370	0.84	1.60E-05	10	0.19	33670	0.21	1.52E-05
10	0.43	87240	0.87	1.70E-05	4				
4	0.35	89000	0.90	6.49E-06	6	0.22	36970	0.26	3.21E-05
6	0.26	90540	0.91	1.07E-05	10	0.20	38840	0.32	1.52E-05
10	0.28	92410	0.93	2.12E-05	4				
4					6	0.24	42140	0.37	2.14E-05
6	0.35	95710	1.00	1.07E-05	10	0.22	44010	0.41	1.70E-05
10	0.58	97580	1.02	4.55E-05	4	0.25	45770	0.44	-2.9E-05
4	0.71	99340	1.10	3.90E-05	6				
6	0.60	100880	1.16	2.67E-05	10	0.10	49180	0.34	2.27E-05
10	0.70	102750	1.21	5.11E-05	4	0.05	50940	0.38	1.95E-05
4	0.52	104510	1.30	3.90E-05	6	0.09	52480	0.41	2.14E-05
6	0.32	106050	1.36	4.28E-05	10	0.10	54350	0.45	2.27E-05
10	0.49	107920	1.44	3.41E-05	4	0.12	56110	0.49	3.25E-05
4	0.33	109680	1.50	1.30E-05	6	0.05	57650	0.54	1.93E-05
6	0.51	111220	1.52	2.67E-05	10				
10	0.52	113090	1.57	3.98E-05	4				
4	0.45	114850	1.64	3.25E-05	6	0.09	62820	0.64	2.14E-05
6	0.48	116390	1.69	2.67E-05	10	0.10	64690	0.68	1.82E-05
10	0.47	118260	1.74	2.84E-05	4				
4	0.54	120020	1.79	2.60E-05	6	0.09	67990	0.74	1.60E-05
6	0.54	121560	1.83	3.74E-05	10	0.11	69860	0.77	1.70E-05
10	0.54	123430	1.90	3.41E-05	4	0.10	71620	0.80	3.90E-05
4	0.56	125190	1.96	6.49E-05	6	0.15	73160	0.86	4.28E-05
6	0.23	126730	2.06	3.21E-05	10	0.23	75030	0.94	2.84E-05
10	0.28	128600	2.12	3.41E-05	4	0.23	76790	0.99	3.90E-05
4	0.37	130360	2.18	3.25E-05	6	0.29	78330	1.05	2.14E-05
6	0.57	131900	2.23	4.28E-05	10	0.09	80200	1.09	2.27E-05
10	0.55	133770	2.31	3.98E-05	4	0.08	81960	1.13	3.25E-05
4	0.58	135530	2.38	5.84E-05	6	0.08	83500	1.18	2.14E-05
6	0.39	137070	2.47	4.81E-05	10	0.13	85370	1.22	1.82E-05
10	0.37	138940	2.56	5.11E-05	4				
4	0.27	140700	2.65	6.49E-05	6	0.18	88670	1.28	2.14E-05
6	0.30	142240	2.75	8.56E-05	10	0.19	90540	1.32	1.14E-05
10	0.19	144110	2.91	5.11E-05	4	0.25	92300	1.34	1.95E-05
4	0.23	145870	3.00	7.79E-05	6	0.30	93840	1.37	1.07E-05
6	0.27	147410	3.12		10	0.34	95710	1.39	1.14E-05
					4	0.38	97470	1.41	2.35E-05
					10				
$\mu =$	0.43				4				
$\sigma =$	0.14				6	0.37	100880	1.49	1.21E-05



7A7L					7A6R (cont.)				
Groups	y	Cycles	c1	dc1/dN	Groups	y	Cycles	c1	dc1/dN
6	0.28	93840	1.06	2.15E-05	10	0.46	104180	1.53	1.6E-05
10	0.24	95710	1.10	1.82E-05	4	0.46	106050	1.56	1.7E-05
4					6	0.45	107810	1.59	2.6E-05
6	0.18	99010	1.16	2.68E-05	10	0.54	109350	1.63	2.14E-05
10	0.07	100880	1.21	3.04E-05	4	0.53	111220	1.67	1.7E-05
4					6	0.55	112980	1.7	3.25E-05
6	0.28	104180	1.31	3.22E-05	10	0.50	114520	1.75	1.6E-05
10	0.36	106050	1.37	2.85E-05	4	0.48	116390	1.78	3.94E-05
4	0.37	107810	1.42	2.06E-05	6				
6					10	0.41	119690	1.91	1.07E-05
10	0.40	111220	1.50	1.7E-05	4	0.47	121560	1.93	4.55E-05
4	0.47	112980	1.53	2.61E-05	6	0.43	123320	2.01	3.9E-05
6	0.50	114520	1.57	1.61E-05	10	0.36	124860	2.07	3.74E-05
10	0.47	116390	1.60	1.52E-05	4	0.30	126730	2.14	2.84E-05
4					6	0.32	128490	2.19	3.25E-05
6	0.52	119690	1.65	2.68E-05	10	0.35	130030	2.24	2.67E-05
10	0.31	121560	1.70	5.70E-06	4	0.33	131900	2.29	2.27E-05
4	0.37	123320	1.71	2.61E-05	6	0.36	133660	2.33	4.55E-05
6	0.39	124860	1.75	2.15E-05	10	0.35	135200	2.4	4.81E-05
10	0.42	126730	1.79	9.12E-06	4	0.30	137070	2.49	4.55E-05
4	0.46	128490	1.82		6	0.26	138830	2.57	5.19E-05
6	0.37	130030	1.82	2.15E-05	10	0.19	140370	2.65	4.81E-05
10	0.40	131900	1.86	2.85E-05	4	0.26	142240	2.74	5.11E-05
4	0.39	133660	1.91	3.26E-05	6	0.24	144000	2.83	3.9E-05
6	0.28	135200	1.96	2.68E-05	10	0.35	145540	2.89	6.42E-05
10	0.34	137070	2.01	2.85E-05	4	0.55	147410	3.01	
4	0.34	138830	2.06	3.26E-05					
6	0.38	140370	2.11	2.68E-05	$\mu =$	0.27			
10	0.38	142240	2.16	2.28E-05	$\sigma =$	0.14			
4	0.40	144000	2.20	3.91E-05					
6	0.39	145540	2.26	3.76E-05					
10	0.38	147410	2.33						
	$\mu =$	0.36							
	$\sigma =$	0.10							

7A7R					7A8L				
Groups	y	Cycles	c1	dc1/dN	Groups	y	Cycles	c1	dc1/dN
4	0.18	71730	0.23	1.52E-05	10	0.54	126730	0.38	2.20E-05
6					4				
10	0.19	75030	0.28	1.60E-05	6	0.57	130360	0.46	3.90E-05
4	0.25	76900	0.31	2.12E-05	10	0.51	131900	0.52	1.65E-05
6					4				
10	0.26	80200	0.38	2.20E-05	6	0.46	135530	0.58	2.60E-05
4					10	0.47	137070	0.62	1.65E-05
6	0.25	83830	0.46	1.95E-05	4				
10	0.22	85370	0.49	2.14E-05	6	0.13	140700	0.68	1.95E-05
4	0.21	87240	0.53	1.70E-05	10	0.18	142240	0.71	1.60E-05
6	0.21	89000	0.56	1.95E-05	4	0.16	144110	0.74	1.70E-05
10	0.21	90540	0.59	1.60E-05	6	0.13	145870	0.77	2.60E-05
4	0.22	92410	0.62	2.27E-05	10	0.08	147410	0.81	
6	0.20	94170	0.66	9.67E-06					
10					$\mu =$	0.32			
4					$\sigma =$	0.20			
6	0.21	99340	0.71	1.95E-05					
10	0.13	100880	0.74	2.14E-05					
4	0.15	102750	0.78	2.27E-05					
6	0.13	104510	0.82	3.25E-05					
10	0.18	106050	0.87	2.14E-05					
4	0.22	107920	0.91	1.15E-05					
6									
10									
4									
6	0.21	114850	0.99	1.95E-05					
10	0.36	116390	1.02	1.93E-05					
4									
6	0.35	120020	1.09	1.95E-05					
10	0.35	121560	1.12	5.35E-06					
4	0.26	123430	1.13	1.14E-05					
6	0.29	125190	1.15	4.55E-05					
10	0.32	126730	1.22	1.07E-05					
4	0.35	128600	1.24	1.70E-05					
6	0.38	130360	1.27	5.87E-06					
10	0.39	131900	1.29						
4	0.43	133770	1.29	2.84E-05					
6	0.42	135530	1.34	1.30E-05					
10	0.44	137070	1.36	2.67E-05					
4	0.45	138940	1.41	2.27E-05					
6	0.38	140700	1.45	-1.30E-05					
10	0.31	142240	1.43	8.02E-05					
4	0.33	144110	1.58	2.84E-05					
6	0.25	145870	1.63	4.55E-05					
10	0.33	147410	1.70						
$\mu =$	0.28								
$\sigma =$	0.09								

7A12R					7A13R				
Groups	y	Cycles	c1	dc1/dN	Groups	y	Cycles	c1	dc1/dN
6	0.25	57760	0.23	3.41E-05	10	0.03	57650	0.18	2.15E-05
10	0.19	59520	0.29	2.68E-05	4	0.08	59520	0.22	1.96E-05
4	0.22	61390	0.34	1.95E-05	6	0.06	61060	0.25	2.29E-05
6	0.24	62930	0.37	2.28E-05	10	0.07	62820	0.29	1.08E-05
10	0.25	64690	0.41	1.61E-05	4	0.04	64690	0.31	1.96E-05
4	0.24	66560	0.44	1.95E-05	6	0.04	66230	0.34	2.86E-05
6	0.24	68100	0.47	1.14E-05	10	0.07	67990	0.39	1.61E-05
10	0.24	69860	0.49	1.61E-05	4	0.08	69860	0.42	1.31E-05
4	0.24	71730	0.52	2.60E-05	6	0.07	71400	0.44	2.29E-05
6	0.20	73270	0.56	1.14E-05	10	0.08	73160	0.48	5.84E-06
10	0.26	75030	0.58	1.47E-05	4				
4					6				
6	0.25	78440	0.63	1.14E-05	10	0.06	78330	0.51	5.38E-06
10	0.28	80200	0.65	2.14E-05	4	0.08	80200	0.52	1.83E-05
4	0.28	82070	0.69	1.95E-05	6				
6	0.28	83610	0.72	2.28E-05	10	0.13	83500	0.58	1.08E-05
10	0.31	85370	0.76	5.35E-06	4	0.11	85370	0.60	1.31E-05
4	0.38	87240	0.77	1.95E-05	6	0.11	86910	0.62	1.14E-05
6	0.40	88780	0.80	2.28E-05	10	0.11	88670	0.64	9.73E-06
10	0.33	90540	0.84	1.76E-05	4				
4					6				
6	0.34	93950	0.90	2.28E-05	10	0.11	93840	0.69	2.69E-05
10	0.33	95710	0.94	1.61E-05	4	0.14	95710	0.74	1.96E-05
4	0.36	97580	0.97	1.52E-05	6	0.14	97250	0.78	2.29E-05
6					10	0.13	99010	0.82	1.61E-05
10	0.40	100880	1.02	2.14E-05	4	0.13	100880	0.85	1.53E-05
4	0.38	102750	1.06	2.60E-05	6				
6	0.38	104290	1.10	5.12E-05	10	0.14	104180	0.90	1.18E-05
10	0.33	106050	1.19	3.75E-05	4				
4	0.28	107920	1.26	1.95E-05	6	0.12	107590	0.94	1.14E-05
6	0.30	109460	1.29	1.71E-05	10	0.12	109350	0.96	1.08E-05
10	0.34	111220	1.32	3.21E-05	4	0.11	111220	0.98	1.96E-05
4	0.33	113090	1.38	2.60E-05	6	0.12	112760	1.01	1.72E-05
6	0.36	114630	1.42	2.84E-05	10	0.14	114520	1.04	1.61E-05
10	0.36	116390	1.47	3.75E-05	4	0.13	116390	1.07	1.96E-05
4	0.33	118260	1.54	2.60E-05	6	0.13	117930	1.10	1.72E-05
6	0.38	119800	1.58	3.41E-05	10	0.12	119690	1.13	1.61E-05
10	0.43	121560	1.64	1.61E-05	4	0.13	121560	1.16	1.83E-05
4	0.54	123430	1.67	3.25E-05	6				
6	0.58	124970	1.72	3.98E-05	10	0.13	124860	1.22	2.15E-05
10	0.63	126730	1.79	4.82E-05	4	0.13	126730	1.26	2.75E-05
4	0.64	128600	1.88	5.20E-05	6				
6	0.70	130140	1.96	5.12E-05	10	0.04	130030	1.35	4.31E-05
10	0.77	131900	2.05	6.43E-05	4	0.01	131900	1.43	2.75E-05
4	0.80	133770	2.17	3.25E-05	6				
6	0.91	135310	2.22	7.96E-05	10	0.01	135200	1.52	2.66E-05
10	0.97	137070	2.36	-2.14E-05	4				
4	0.68	138940	2.32	1.52E-05	6	0.05	138610	1.61	3.43E-05
6	0.59	140480	2.37		10	0.07	140370	1.67	3.23E-05
10	0.58	142240	2.37	1.66E-04	4	0.09	142240	1.73	6.54E-05
4	0.66	144110	2.68	1.56E-04	6	0.07	143780	1.83	9.15E-05
6	0.65	145650	2.92	2.05E-04	10	0.09	145540	1.99	1.18E-04
10	0.34	147410	3.28		4	0.02	147410	2.21	
$\mu = 0.42$					$\mu = 0.09$				
$\sigma = 0.19$					$\sigma = 0.04$				

7A14L					7A14R				
Groups	y	Cycles	c1	dc1/dN	Groups	y	Cycles	c1	dc1/dN
4	0.58	66560	0.83	3.90E-05	4	0.07	40710	0.12	6.50E-06
6	0.58	68100	0.89	2.84E-05	6	0.07	42250	0.13	1.14E-05
10	0.75	69860	0.94	1.52E-05	10	0.07	44010	0.15	7.11E-06
4					4				
6					6				
10					10				
4					4	0.12	51050	0.20	1.30E-05
6	0.75	78440	1.07	3.98E-05	6	0.12	52590	0.22	1.71E-05
10	0.75	80200	1.14	2.32E-05	10	0.17	54350	0.25	1.61E-05
4					4	0.15	56220	0.28	1.82E-05
6					6				
10	0.80	85370	1.26	1.76E-05	10	0.18	59520	0.34	2.35E-05
4					4				
6	0.84	88780	1.32	3.41E-05	6	0.19	62930	0.42	1.71E-05
10	0.82	90540	1.38	2.05E-05	10	0.22	64690	0.45	2.14E-05
4					4	0.2	66560	0.49	1.95E-05
6	0.72	93950	1.45	2.27E-05	6	0.23	68100	0.52	2.27E-05
10	0.72	95710	1.49	3.52E-05	10	0.22	69860	0.56	3.23E-05
4					4				
6	0.68	99120	1.61	1.71E-05	6	0.13	73270	0.67	2.27E-05
10	0.50	100880	1.64	4.28E-05	10	0.16	75030	0.71	1.61E-05
4	0.45	102750	1.72	1.30E-05	4	0.15	76900	0.74	3.25E-05
6	0.45	104290	1.74	2.27E-05	6	0.12	78440	0.79	2.27E-05
10	0.47	106050	1.78	1.60E-05	10	0.12	80200	0.83	2.68E-05
4	0.50	107920	1.81	2.12E-05	4	0.1	82070	0.88	2.60E-05
6					6	0.12	83610	0.92	3.41E-05
10	0.60	111220	1.88	2.14E-05	10	0.07	85370	0.98	2.05E-05
4	0.63	113090	1.92	3.25E-05	4				
6	0.61	114630	1.97	3.41E-05	6	0.1	88780	1.05	2.27E-05
10	0.64	116390	2.03	2.14E-05	10	0.1	90540	1.09	2.14E-05
4	0.68	118260	2.07	2.60E-05	4	0.12	92410	1.13	2.60E-05
6	0.72	119800	2.11	3.98E-05	6	0.1	93950	1.17	1.71E-05
10	0.70	121560	2.18	3.21E-05	10	0.12	95710	1.20	3.21E-05
4	0.72	123430	2.24	5.20E-05	4	0.11	97580	1.26	3.25E-05
6	0.71	124970	2.32	5.12E-05	6	0.06	99120	1.31	1.71E-05
10	0.66	126730	2.41	5.35E-05	10	0.08	100880	1.34	2.14E-05
4	0.59	128600	2.51	1.30E-05	4	0.09	102750	1.38	3.25E-05
6	0.77	130140	2.53	5.68E-05	6	0.09	104290	1.43	2.84E-05
10	0.74	131900	2.63	5.88E-05	10	0.11	106050	1.48	2.14E-05
4	0.69	133770	2.74	1.95E-05	4	0.099	107920	1.52	2.60E-05
6	0.84	135310	2.77	5.12E-05	6	0.12	109460	1.56	2.27E-05
10	0.89	137070	2.86	5.88E-05	10	0.08	111220	1.60	2.68E-05
4	0.90	138940	2.97	9.74E-05	4	0.07	113090	1.65	1.95E-05
6	0.85	140480	3.12	7.96E-05	6	0.07	114630	1.68	2.27E-05
10	0.84	142240	3.26	7.49E-05	10	0.15	116390	1.72	2.68E-05
4	0.84	144110	3.40	1.17E-04	4	0.16	118260	1.77	3.25E-05
6	0.83	145650	3.58	1.19E-04	6	0.22	119800	1.82	2.84E-05
10	0.85	147410	3.79		10	0.24	121560	1.87	2.64E-05
					4				
	$\mu =$	0.70			6	0.26	124970	1.96	1.71E-05
	$\sigma =$	0.13			10	0.3	126730	1.99	4.82E-05
					4	0.21	128600	2.08	4.55E-05
					6	0.26	130140	2.15	3.98E-05
					10	0.26	131900	2.22	3.21E-05
					4	0.25	133770	2.28	5.85E-05
					6	0.2	135310	2.37	3.41E-05
					10	0.27	137070	2.43	4.82E-05
					4	0.27	138940	2.52	5.20E-05
					6	0.32	140480	2.60	6.82E-05
					10	0.25	142240	2.72	7.49E-05
					4	0.28	144110	2.86	1.10E-04
					6	0.26	145650	3.03	1.14E-04
					10	0.26	147410	3.23	
						$\mu =$	0.16		
						$\sigma =$	0.074195		



7A16R					7A17L				
Groups	y	Cycles	c1	dc1/dN	Groups	y	Cycles	c1	dc1/dN
6	0.13	104290	0.02	1.75E-05	6	0.11	78440	0.32	1.65E-05
10	0.18	106050	0.05	7.93E-06	10				
4					4	0.18	82070	0.38	1.95E-05
6					6	0.18	83610	0.41	1.70E-05
10	0.14	111220	0.09	1.64E-05	10	0.19	85370	0.44	1.07E-05
4	0.15	113090	0.12	1.55E-05	4	0.20	87240	0.46	1.95E-05
6					6	0.22	88780	0.49	2.27E-05
10	0.07	116390	0.17	1.64E-05	10	0.22	90540	0.53	1.60E-05
4	0.11	118260	0.21	1.33E-05	4	0.22	92410	0.56	1.95E-05
6	0.11	119800	0.23	1.75E-05	6	0.19	93950	0.59	2.84E-05
10		121560	0.26	1.10E-05	10	0.21	95710	0.64	1.07E-05
4		123430	0.28	2.00E-05	4	0.22	97580	0.66	2.12E-05
6	0.01	124970	0.31	1.75E-05	6				
10		126730	0.34	1.64E-05	10	0.20	100880	0.73	1.07E-05
4	0.01	128600	0.37	5.33E-05	4	0.19	102750	0.75	2.60E-05
6	0.03	130140	0.45	1.75E-05	6	0.23	104290	0.79	2.84E-05
10	0.04	131900	0.48	1.20E-05	10	0.12	106050	0.84	1.60E-05
4					4	0.12	107920	0.87	3.25E-05
6	0.04	135310	0.52	1.17E-05	6	0.12	109460	0.92	2.27E-05
10	0.05	137070	0.54	9.02E-06	10	0.18	111220	0.96	3.21E-05
4					4	0.18	113090	1.02	3.25E-05
6	0.10	140480	0.57	2.33E-05	6	0.16	114630	1.07	3.41E-05
10	0.05	142240	0.62	2.19E-05	10	0.23	116390	1.13	3.21E-05
4	0.07	144110	0.66		4	0.28	118260	1.19	5.20E-05
<div> <div>μ = 0.07</div> <div>σ = 0.06</div> </div>					6	0.22	119800	1.27	4.55E-05
					10	0.23	121560	1.35	4.28E-05
					4	0.29	123430	1.43	4.55E-05
					6	0.35	124970	1.50	5.11E-05
					10	0.35	126730	1.59	4.28E-05
					4	0.40	128600	1.67	5.84E-05
					6	0.35	130140	1.76	5.11E-05
					10	0.37	131900	1.85	5.35E-05
					4	0.43	133770	1.95	7.14E-05
					6	0.32	135310	2.06	6.25E-05
					10	0.40	137070	2.17	5.88E-05
					4	0.33	138940	2.28	7.14E-05
					6	0.43	140480	2.39	7.39E-05
					10	0.48	142240	2.52	7.49E-05
					4	0.54	144110	2.66	8.44E-05
					6	0.52	145650	2.79	8.52E-05
					10	0.43	147410	2.94	
					<div> <div>μ = 0.27</div> <div>σ = 0.12</div> </div>				

7A17R					7A17R (cont.)				
Groups	y	Cycles	c1	dc1/dN	Groups	y	Cycles	c1	dc1/dN
10	0.06	23,330	0.14	2.14E-05	6	0.12	93,950	1.28	1.72E-05
4					10	0.12	95,710	1.31	1.62E-05
6					4	0.12	97,580	1.34	2.62E-05
10	0.06	28,500	0.25	1.62E-05	6	0.15	99,120	1.38	1.15E-05
4	0.04	30,370	0.28	1.96E-05	10	0.07	100,880	1.40	1.77E-05
6	0.02	31,910	0.31	1.15E-05	4				
10	0.03	33,670	0.33	2.16E-05	6	0.01	104,290	1.46	2.86E-05
4	0.02	35,540	0.37	1.53E-05	10	0.09	106,050	1.51	2.69E-05
6					4	0.17	107,920	1.56	1.31E-05
10	0.04	38,840	0.42	2.69E-05	6	0.07	109,460	1.58	3.44E-05
4	0.01	40,710	0.47	6.54E-06	10	0.10	111,220	1.64	2.16E-05
6	0.01	42,250	0.48	1.15E-05	4	0.17	113,090	1.68	1.96E-05
10	0.04	44,010	0.50	8.87E-06	6	0.07	114,630	1.71	2.29E-05
4					10	0.06	116,390	1.75	2.16E-05
6	0.08	47,420	0.53	2.29E-05	4	0.08	118,260	1.79	3.27E-05
10	0.10	49,180	0.57	1.62E-05	6	0.08	119,800	1.84	3.44E-05
4	0.10	51,050	0.60	1.96E-05	10	0.08	121,560	1.90	3.77E-05
6	0.10	52,590	0.63	1.72E-05	4	0.11	123,430	1.98	3.27E-05
10	0.10	54,350	0.67	1.08E-05	6	0.18	124,970	2.03	4.01E-05
4	0.11	56,220	0.69	1.31E-05	10	0.10	126,730	2.10	3.77E-05
6	0.11	57,760	0.71	1.66E-05	4	0.10	128,600	2.17	3.93E-05
10					6		130,140	2.23	4.58E-05
4					10		131,900	2.31	4.31E-05
6					4	0.02	133,770	2.39	5.24E-05
10					6	0.02	135,310	2.47	4.58E-05
4					10	0.03	137,070	2.55	6.47E-05
6	0.19	68,100	0.88	1.72E-05	4	0.02	138,940	2.67	6.54E-05
10	0.14	69,860	0.91	1.56E-05	6	0.01	140,480	2.77	7.44E-05
4					10	0.01	142,240	2.90	7.01E-05
6					4	0.02	144,110	3.03	
10	0.20	75,030	0.99	1.62E-05	$\mu = 0.09$ $\sigma = 0.065145$				
4	0.19	76,900	1.02	1.96E-05					
6	0.17	78,440	1.05	1.72E-05					
10	0.23	80,200	1.08	1.62E-05					
4	0.23	82,070	1.11	1.31E-05					
6	0.20	83,610	1.13	1.72E-05					
10	0.19	85,370	1.16	1.48E-05					
4									
6	0.17	88,780	1.21	1.72E-05					
10	0.15	90,540	1.24	1.18E-05					
4									

8A10L					8A10R				
Groups	y	Cycles	c1	dc1/dN	Groups	y	Cycles	c1	dc1/dN
4	0.206	65340	0.292	5.03E-05	6	0.286	65340	0.222	5.78E-05
6	0.026	67210	0.386	2.09E-05	10	0.232	67210	0.33	2.33E-05
10	0.222	68970	0.38		4		68970		
4	0.036	70510	0.455	9.88E-06	6	0.158	70510	0.407	9.09E-06
6	0.154	72380	0.448		10	0.149	72380	0.424	1.82E-05
10	0.255	74140	0.441		4		74140		
4		75680			6		75680		
6		77550			10	-0.028	77550	0.518	2.44E-05
10	0.298	79310	0.451		4	0.120	79310	0.561	2.14E-05
4		80850			6	-0.061	80850	0.594	1.20E-05
6		82720			10		82720		
10	0.226	84480	0.593	7.14E-06	4		84480		
4	0.230	86020	0.604		6	0.201	86020	0.656	2.57E-05
6	0.345	87890	0.555		10	0.523	87890	0.507	
10	0.255	89650	0.639	2.46E-05	4		89650		
4		91190			6	0.260	91190	0.789	1.50E-05
6	0.061	93060	0.723	1.12E-05	10	0.313	93060	0.817	1.82E-05
10	0.408	94820	0.658		4		94820		
4		96360			6	0.320	96360	0.877	2.75E-05
6	0.091	98230	0.781	1.99E-05	10		98230		
10	0.080	99990	0.816	4.90E-05	4	0.226	99990	0.977	5.32E-05
4		101530			6	0.118	101530	1.059	1.07E-06
6	0.076	103400	0.983	5.40E-05	10	0.243	103400	1.061	4.18E-05
10	-0.115	105160	1.078	4.81E-05	4		105160		
4		106700			6	0.330	106700	1.199	4.06E-05
6	0.276	108570	1.242	8.52E-05	10	0.341	108570	1.275	5.09E-05
10	0.122	110330	1.392	6.17E-05	4		110330		
4	0.179	111870	1.487	8.56E-05	6	0.262	111870	1.443	2.57E-05
6	0.081	113740	1.647	5.63E-05	10	0.379	113740	1.491	7.79E-05
10	0.225	115500	1.746	9.55E-05	4		115500		
4	0.145	117040	1.893	7.97E-05	6	0.515	117040	1.748	4.06E-05
6	0.285	118910	2.042	9.09E-05	10	0.365	118910	1.824	7.58E-05
10	0.247	120670	2.202	1.41E-04	4		120670		
4	0.185	122210	2.419	1.08E-04	6	0.236	122210	2.074	9.89E-05
6	0.055	124080	2.621	1.44E-04	10	0.101	124080	2.259	8.13E-05
10	0.038	125840	2.875	2.15E-04	4	0.259	125840	2.402	1.66E-04
4	0.314	127380	3.206	1.91E-04	6	0.409	127380	2.658	2.71E-04
6	0.322	129250	3.563	5.32E-04	10	0.341	129250	3.164	1.03E-03
fracture		130000	3.962		fracture		130000	3.936	
$\mu =$	0.140				$\mu =$	0.174			
$\sigma =$	0.127				$\sigma =$	0.166			

8A19L				
Groups	y	Cycles	c1	dc1/dN
6	0.070	122210	0.53	1.25E-04
10	0.095	124080	0.764	1.53E-04
4	0.183	125840	1.033	2.01E-04
6	0.122	127380	1.343	2.06E-04
10	0.308	129250	1.728	4.44E-03
fracture		130000	5.06	
$\mu =$	0.156			
$\sigma =$	0.095			



9A5L					9A5R				
Groups	y	Cycles	c1	dc1/dN	Groups	y	Cycles	c1	dc1/dN
10	0.299	481850	1.116	7.29E-05	6	0.139	468510	0.391	-2.23E-05
4	0.296	485610	1.390	1.11E-04	10	0.342	470480	0.347	2.93E-05
6	0.176	489150	1.744	1.41E-04	4		474240		
10	0.305	493020	2.211	4.48E-06	6	0.303	477780	0.561	6.19E-05
fracture		498063	3.000		10	0.096	479750	0.683	1.74E-05
$\mu =$	0.269				4		483510		
$\sigma =$	0.062				6	0.107	487050	0.810	1.38E-04
					10	0.125	489020	1.081	5.82E-05
					4	0.054	492780	1.300	1.02E-04
					6	0.233	496320	1.661	1.27E-04
					fracture		498063	1.882	
					$\mu =$	0.140			
					$\sigma =$	0.118			

10F5R					10F6L				
Groups	y	Cycles	c1	dc1/dN	Groups	y	Cycles	c1	dc1/dN
10	0.200	119760	0.148	2.05E-05	6	0.116	126010	0.321	1.42E-05
4	0.144	123520	0.225	1.50E-05	10	0.167	129880	0.376	2.13E-05
6	0.134	127060	0.278	8.79E-06	4	0.228	133640	0.456	2.60E-05
10	0.141	130930	0.312	1.22E-05	6	0.222	137180	0.548	2.45E-05
4	0.137	134690	0.358	1.30E-05	10	0.201	141050	0.643	2.42E-05
6	0.178	138230	0.404	1.58E-05	4	0.126	144810	0.734	2.85E-05
10	0.091	142100	0.465	1.65E-05	6	0.195	148350	0.835	5.40E-05
4	0.074	145860	0.527	1.67E-05	10	0.226	152220	1.044	8.09E-05
6	0.173	149400	0.586	4.16E-05	4	0.227	155980	1.348	1.21E-04
10	0.192	153270	0.747	8.83E-05	6	0.146	159520	1.777	1.63E-04
4	0.077	157030	1.079		10	0.241	163390	2.407	
$\mu =$	0.140				$\mu =$	0.190			
$\sigma =$	0.044				$\sigma =$	0.045			

10F6R					10F7L				
Groups	y	Cycles	c1	dc1/dN	Groups	y	Cycles	c1	dc1/dN
4	0.099	122470	0.228	2.66E-05	10	0.152	129880	0.252	1.88E-05
6	0.066	126010	0.322	2.35E-05	6	0.146	137180	0.389	2.09E-05
10	0.097	129880	0.413	3.40E-05	10	0.125	141050	0.47	1.86E-05
6	0.112	137180	0.661	4.50E-05	4	0.122	144810	0.54	3.25E-05
10	0.097	141050	0.835	4.55E-05	6	0.189	148350	0.655	7.13E-05
4	0.065	144810	1.006	6.50E-05	10	0.182	152220	0.931	9.57E-05
6	0.063	148350	1.236	8.35E-05	4	0.188	155980	1.291	1.56E-04
10	0.112	152220	1.559	1.24E-04	6	0.142	159520	1.843	2.05E-04
4	0.058	155980	2.024	1.62E-04	10	0.218	163390	2.637	
6	0.186	159520	2.597	2.22E-04	$\mu =$	0.163			
10	0.166	163390	3.457		$\sigma =$	0.033			
$\mu =$	0.102								
$\sigma =$	0.042								

10F7R					10F8L				
Groups	y	Cycles	c1	dc1/dN	Groups	y	Cycles	c1	dc1/dN
10	0.211	143950	0.482	4.79E-05	10	0.136	88200	0.145	8.20E-06
4	0.254	147710	0.662	7.60E-05	10	0.136	96370	0.212	1.14E-05
6	0.209	151250	0.931	1.24E-04	4	0.108	100130	0.255	1.01E-05
10	0.208	154220	1.298	2.01E-04	10	0.131	107540	0.330	1.04E-05
4	0.223	157980	2.053		4	0.113	111300	0.369	1.36E-05
					6	0.118	114840	0.417	7.24E-06
					10	0.132	118710	0.445	9.04E-06
					4	0.139	122470	0.479	9.04E-06
					6	0.166	126010	0.511	1.55E-05
					10	0.137	129880	0.571	1.20E-05
					4	0.179	133640	0.616	1.53E-05
					6	0.100	137180	0.670	1.50E-05
					10	0.173	141050	0.728	2.31E-05
					4	0.087	144810	0.815	2.46E-05
					6	0.206	148350	0.902	2.84E-05
					10	0.180	152220	1.012	4.18E-05
					4	0.186	155980	1.169	4.75E-05
					6	0.203	159520	1.337	9.66E-05
					10	0.226	163390	1.711	

11F6L					11F6R				
Groups	y	Cycles	c1	dc1/dN	Groups	y	Cycles	c1	dc1/dN
10	0.234	127590	0.527	3.15E-06	10	0.003	106250	0.673	1.38E-05
4		131350			4		110010		
6	0.731	134890	0.550	1.23E-04	6		113550		
10	0.424	138760	1.026	8.91E-05	10	0.301	117420	0.827	6.16E-06
4	0.289	142520	1.361	1.26E-04	4		121180		
6	0.219	146060	1.806	1.69E-04	6	0.294	124720	0.872	3.85E-05
10	0.258	149930	2.460		10	0.095	128590	1.021	2.82E-05
fracture		154827			4	0.197	132350	1.127	1.58E-05
$\mu =$	0.308				6	0.559	135890	1.183	7.96E-05
$\sigma =$	0.225				10	0.163	139760	1.491	1.16E-04
					4	0.214	143520	1.929	1.62E-04
					6	0.375	147060	2.501	
					fracture		154287		
					$\mu =$	0.161			
					$\sigma =$	0.195			

11F7L					11F7R				
Groups	y	Cycles	c1	dc1/dN	Groups	y	Cycles	c1	dc1/dN
10	0.377	128590	0.491	1.68E-05	10	0.318	127590	0.483	3.83E-05
4	0.673	132350	0.554	1.13E-04	4	0.341	131350	0.627	1.07E-05
6	0.233	135890	0.954	7.67E-05	6	0.662	134890	0.665	1.07E-04
10	0.263	139760	1.251	1.05E-04	10	0.318	138760	1.081	9.95E-05
4	0.336	143520	1.645	1.53E-04	4	0.634	142520	1.455	1.29E-04
6	0.29	147060	2.185	1.48E-05	6	0.532	146060	1.913	1.83E-04
fracture		154827	2.300		10	0.714	149930	2.622	1.55E-04
$\mu =$	0.362				fracture		154297	3.300	
$\sigma =$	0.161				$\mu =$	0.503			
					$\sigma =$	0.174			

11F8L					11F8R				
Groups	y	Cycles	c1	dc1/dN	Groups	y	Cycles	c1	dc1/dN
10	0.217	128590	0.393	2.56E-05	10	0.19	127590	0.163	4.23E-05
4		132350			4	0.283	131350	0.322	6.89E-05
6	0.226	135890	0.580	1.86E-05	6	0.132	134890	0.566	5.89E-05
10	0.409	139760	0.652	5.98E-05	10	0.187	138760	0.794	6.33E-05
4	0.269	143520	0.877	7.54E-05	4	0.354	142520	1.032	7.37E-05
6	0.27	147060	1.144		6	0.277	146060	1.293	9.04E-05
fracture		154287			10	0.261	149930	1.643	2.23E-05
$\mu =$	0.232				fracture		154287	1.740	
$\sigma =$	0.133				$\mu =$	0.241			
					$\sigma =$	0.075			

11F9R					11F10R				
Groups	y	Cycles	c1	dc1/dN	Groups	y	Cycles	c1	dc1/dN
6	0.196	124720	0.584	8.50E-05	6	0.178	123720	0.477	7.73E-05
10	0.29	128590	0.913	7.61E-05	10	0.28	127590	0.776	7.74E-05
4	0.388	132350	1.199	8.62E-05	4	0.344	131350	1.067	7.40E-05
6	0.445	135890	1.504	1.48E-04	6	0.142	134890	1.329	7.44E-05
10	0.844	139760	2.075	1.47E-04	10	0.293	138760	1.617	7.21E-05
4	0.439	143520	2.627	1.58E-04	4	0.195	142520	1.888	8.84E-05
6	0.096	147060	3.185		6	0.217	146060	2.201	9.15E-05
					10	0.144	149930	2.555	5.00E-05
					fracture		154827	2.800	
$\mu =$	0.385				$\mu =$	0.224			
$\sigma =$	0.240				$\sigma =$	0.074			

15E2R					15E11R				
Flights	y	Cycles	c1	dc1/dN	Flights	y	Cycles	c1	dc1/dN
20	0.08	171287	0.40	2.02E-05	18	0.26	154155	0.71	4.09E-05
21	0.09	179853	0.57	1.93E-05	19	0.21	162721	1.06	4.33E-05
22	0.18	188419	0.74	2.69E-05	20	0.15	171287	1.43	4.73E-05
23	0.21	196985	0.97	3.39E-05	21	0.15	179853	1.84	4.89E-05
24	0.24	205551	1.26	3.56E-05	22	0.15	188419	2.26	6.19E-05
25	0.29	214117	1.56	6.70E-05	23	0.18	196985	2.79	7.72E-05
25.5	0.00	218484	1.86		24	0.14	205551	3.45	9.97E-05
					25	0.25	214117	4.30	1.03E-04
					25.5	0.00	218484	4.75	
$\mu =$	0.16				$\mu =$	0.17			
$\sigma =$	0.10				$\sigma =$	0.08			

15E16L					15E16R				
Flights	y	Cycles	c1	dc1/dN	Flights	y	Cycles	c1	dc1/dN
19	0.27	162721	0.28	1.49E-05	13	0.40	111325	0.12	1.61E-05
20	0.24	171287	0.41	1.81E-05	14	0.32	119891	0.26	1.76E-05
21	0.25	179853	0.56	1.85E-05	15	0.31	128457	0.41	2.10E-05
22	0.31	188419	0.72	3.09E-05	16	0.39	137023	0.59	2.63E-05
23	0.27	196985	0.99	3.28E-05	17	0.32	145589	0.82	2.12E-05
24	0.17	205551	1.27	5.64E-05	18	0.43	154155	1.00	2.97E-05
25	0.05	214117	1.75	1.07E-04	19	0.43	162721	1.25	3.87E-05
25.5	0.00	218484	2.22		20	0.39	171287	1.58	4.43E-05
					21	0.21	179853	1.96	5.13E-05
					22	0.19	188419	2.40	6.75E-05
					23	0.24	196985	2.98	8.00E-05
					24	0.20	205551	3.67	1.05E-04
					25	0.23	214117	4.57	1.49E-04
					25.5	0.00	218484	5.22	
$\mu =$	0.20				$\mu =$	0.31			
$\sigma =$	0.11				$\sigma =$	0.12			

15E20L					15E26R				
Flights	y	Cycles	c1	dc1/dN	Flights	y	Cycles	c1	dc1/dN
16	0.28	137023	0.43	1.93E-05	19	0.23	162721	0.65	4.02E-05
18	0.18	154155	0.76	3.35E-05	20	0.23	171287	1.00	4.50E-05
19	0.20	162721	1.05	3.54E-05	21	0.23	179853	1.38	5.83E-05
20	0.38	171287	1.35	4.24E-05	22	0.25	188419	1.88	6.77E-05
21	0.42	179853	1.72	6.65E-05	23	0.25	196985	2.46	1.00E-04
22	0.26	188419	2.29	7.88E-05	24	0.19	205551	3.32	1.07E-04
23	0.26	196985	2.96	1.13E-04	25	0.24	214117	4.23	1.47E-04
24	0.31	205551	3.93	1.63E-04	25.5	0.00	218484	4.87	
25	0.31	214117	5.33	2.29E-04					
25.5	0.00	218484	6.33						
$\mu = 0.29$					$\mu = 0.23$				
$\sigma = 0.08$					$\sigma = 0.02$				

15E28R				
Flights	y	Cycles	c1	dc1/dN
23	0.22	196985	0.44	3.11E-05
24	0.18	205551	0.70	4.29E-05
25	0.23	214117	1.07	1.11E-04
25.5	0.00	218484	1.56	7.12E-06
$\mu = 0.16$				
$\sigma = 0.11$				

## Appendix D SEM Fractographs of Fracture Surfaces

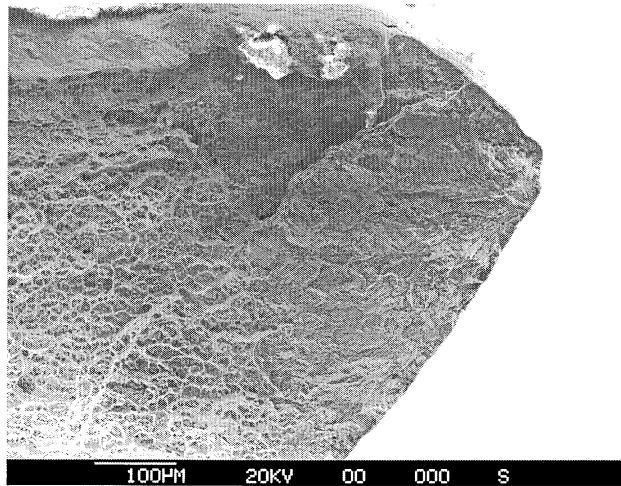


Figure 120 3C9R



Figure 121 3C12R

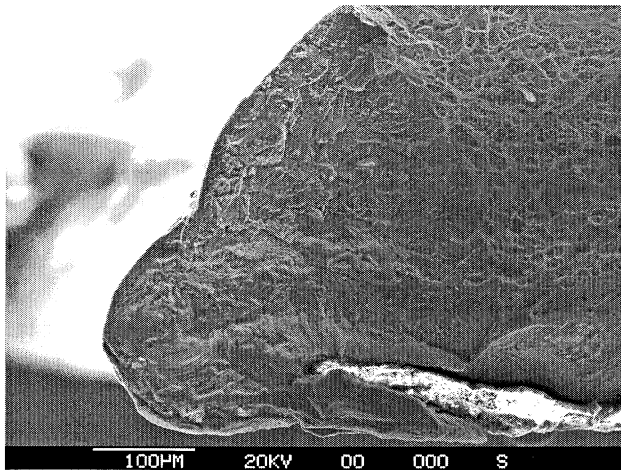


Figure 122 3C12R Nucleation Site

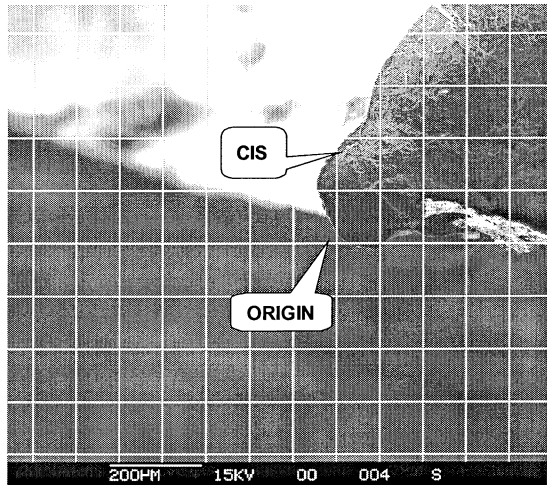


Figure 123 3C12R Nucleation Site

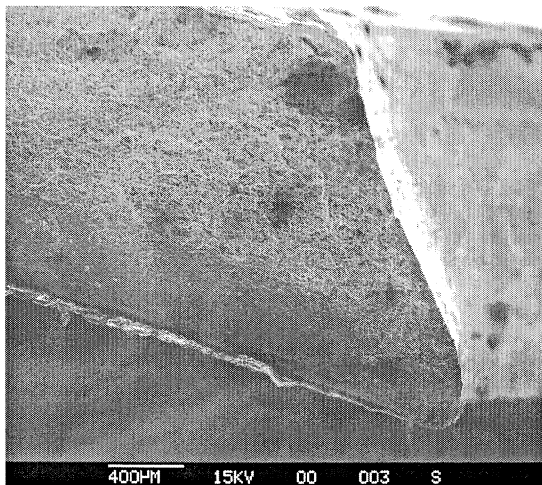


Figure 124 3C14L

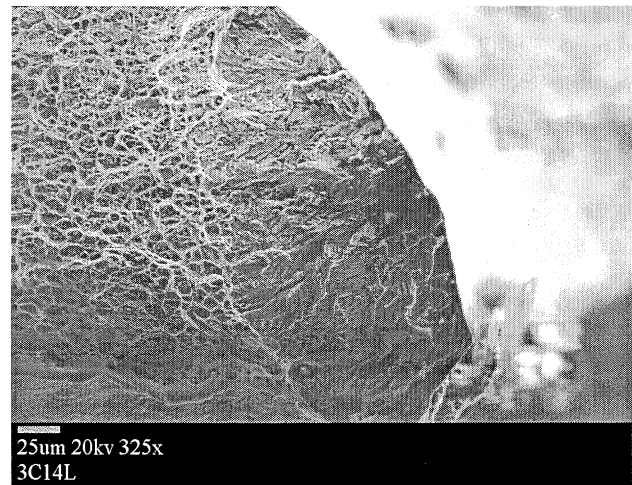


Figure 125 3C14L Nucleation Site

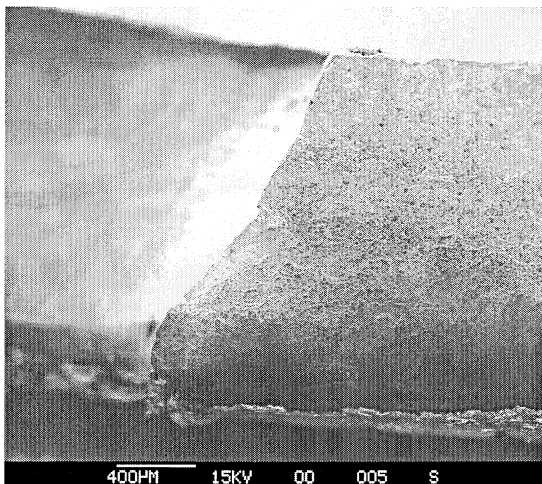


Figure 126 3C17R

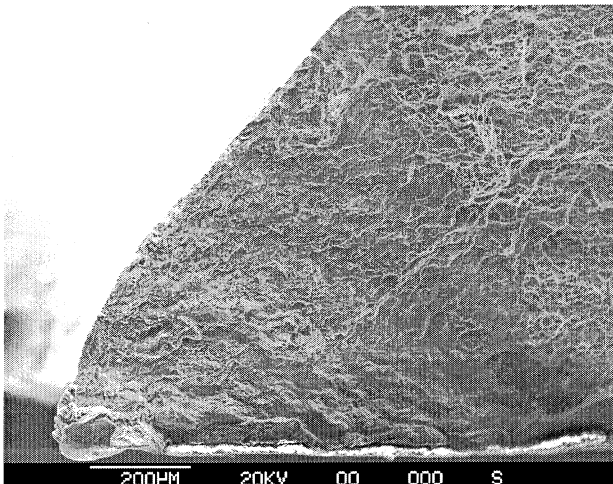


Figure 127 3C17R

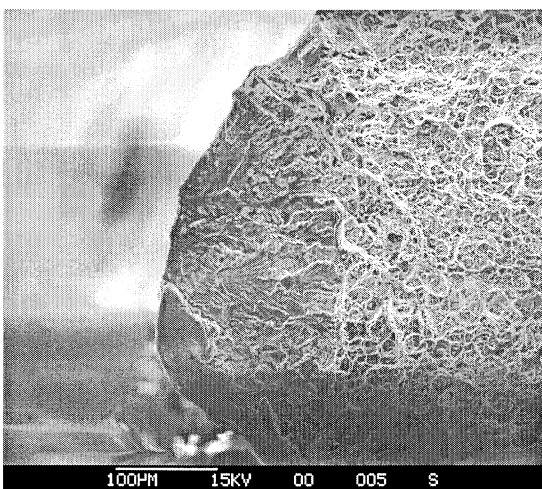


Figure 128 3C17R Nucleation Site

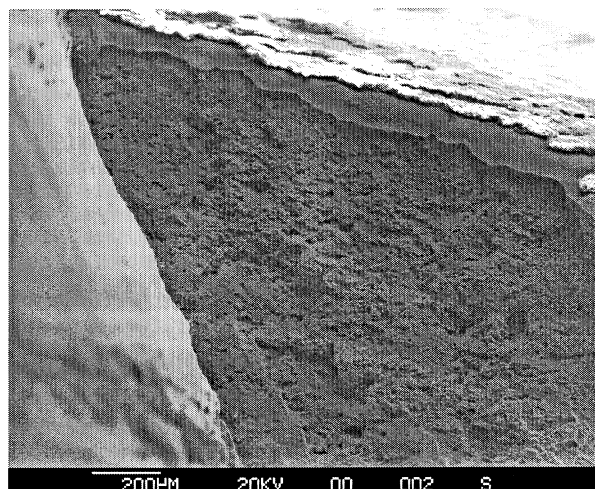


Figure 129 3C18L

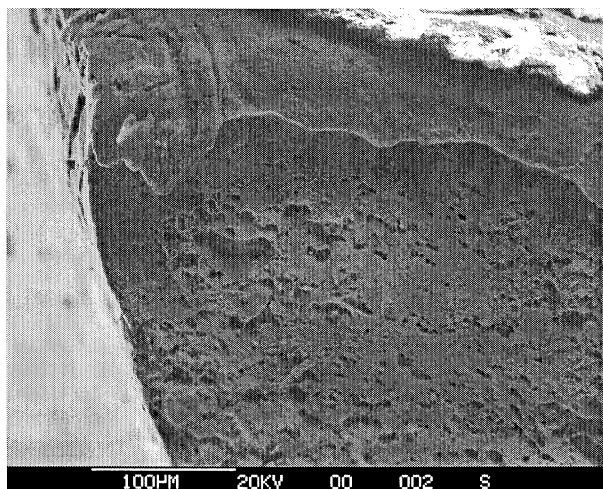


Figure 130 3C18L

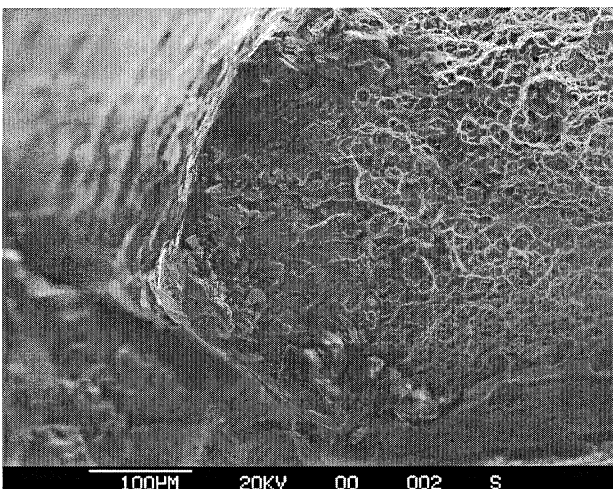


Figure 131 3C18R



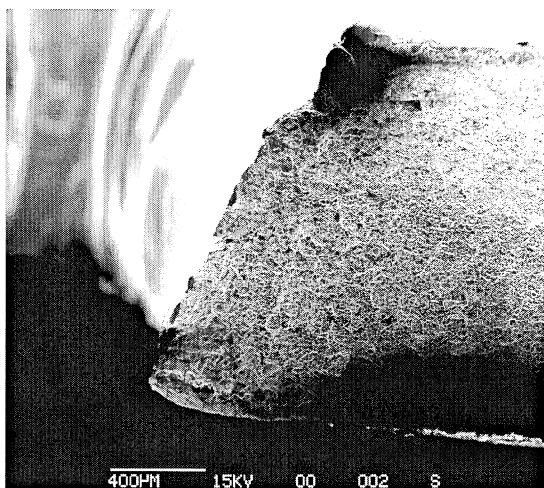


Figure 132 3D11R

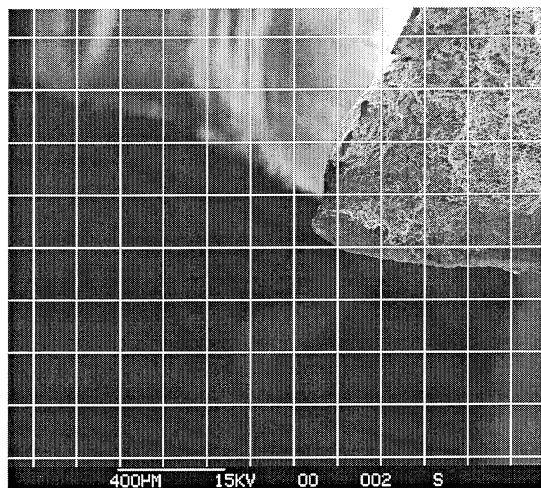


Figure 133 3D11R

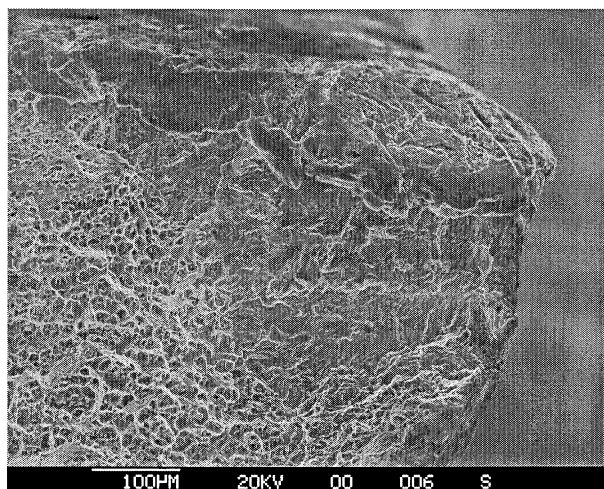


Figure 134 3D11R Nucleation Site

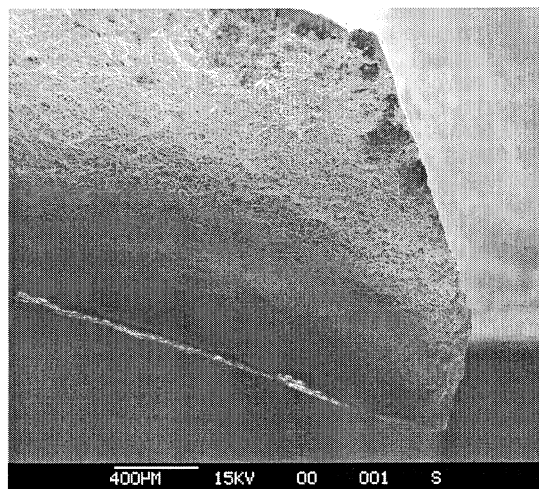


Figure 135 3D12L

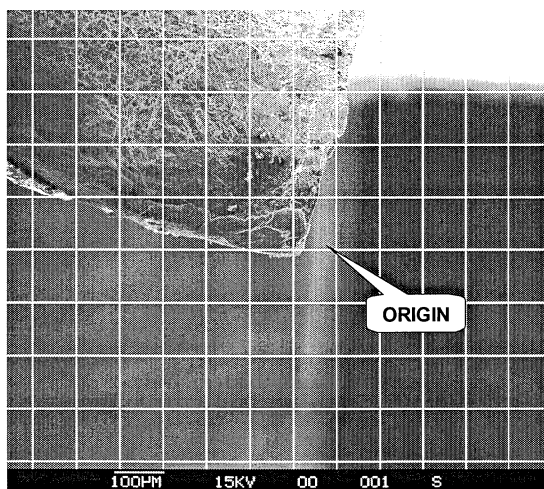


Figure 136 3D12L

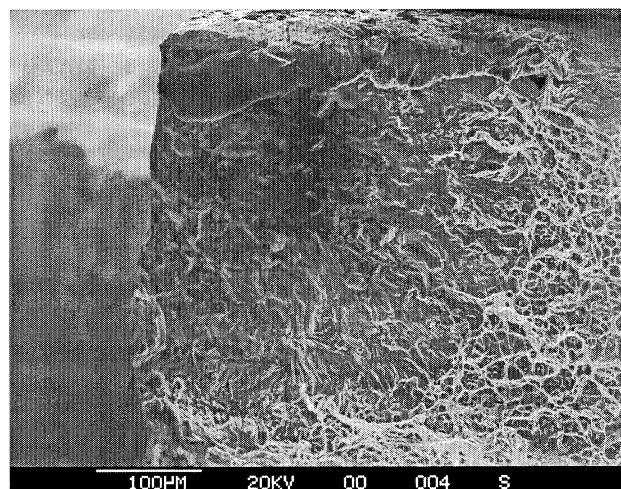


Figure 137 3D12L Nucleation Site



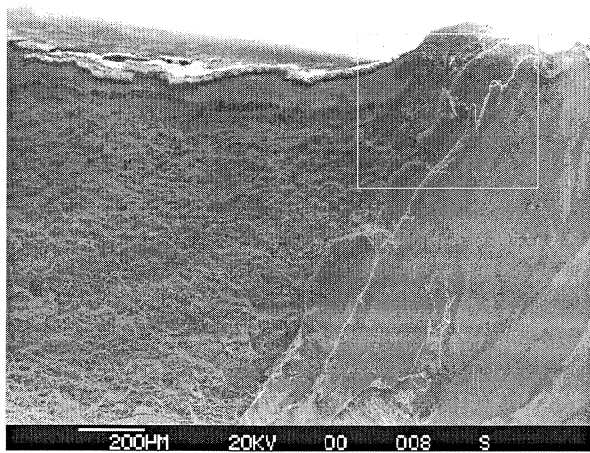


Figure 138 3D12R

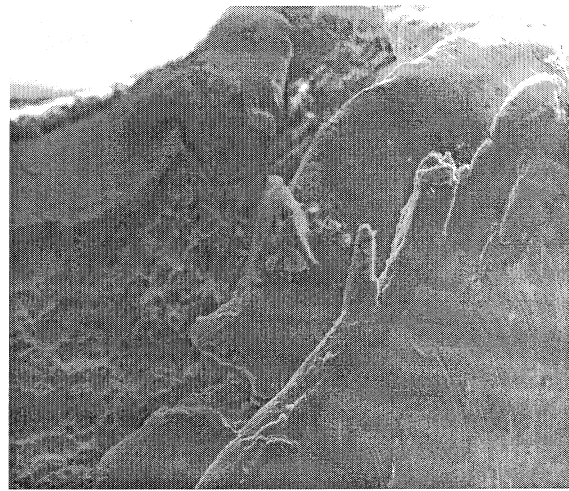


Figure 139 3D12R

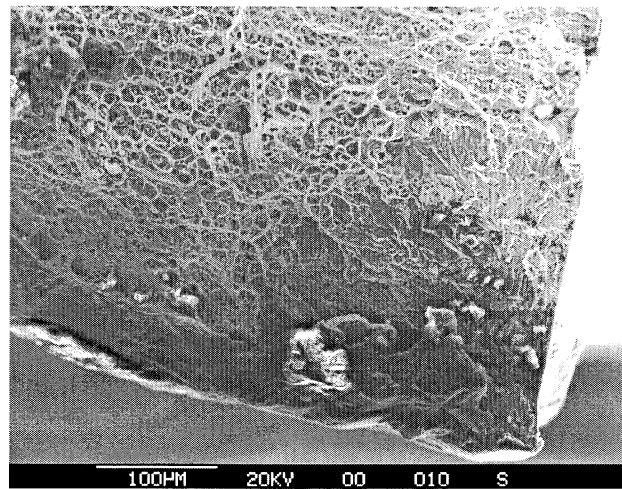


Figure 140 3D13L

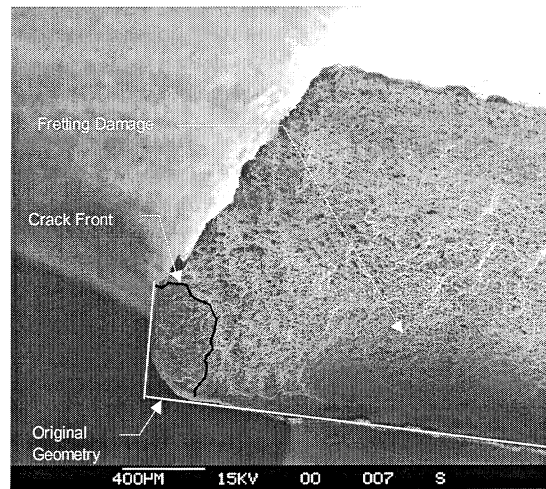


Figure 141 3D13R

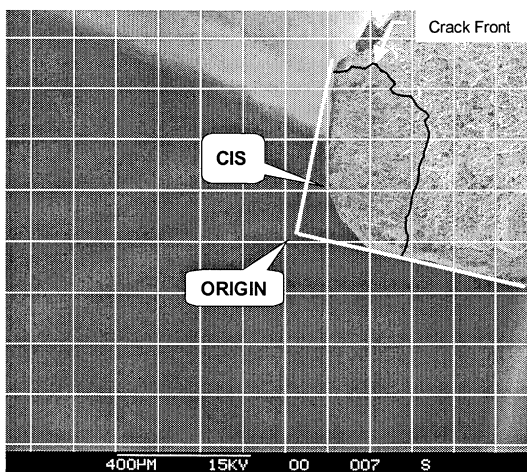


Figure 142 3D13R

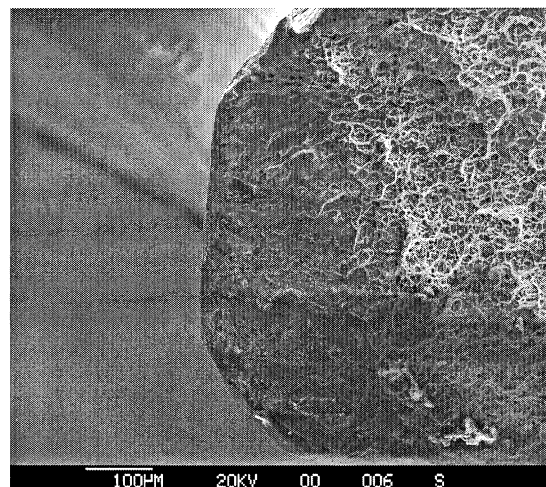


Figure 143 3D13R Nucleation Site

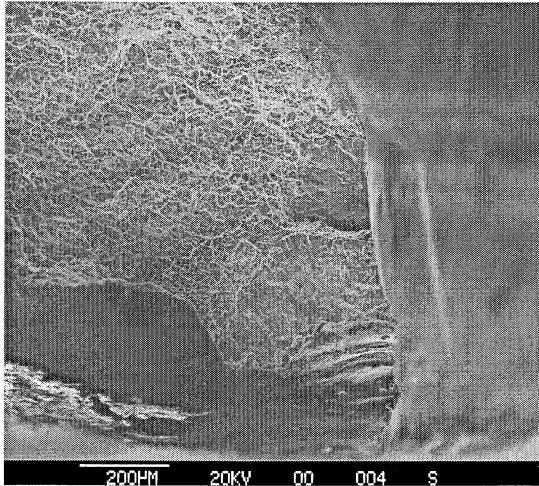


Figure 144 3D14L

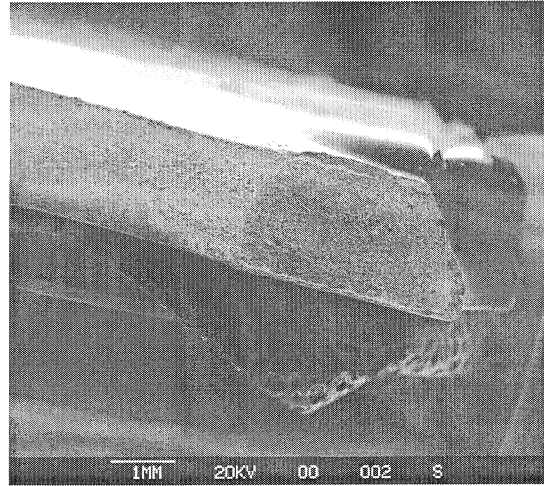


Figure 145 3D15L

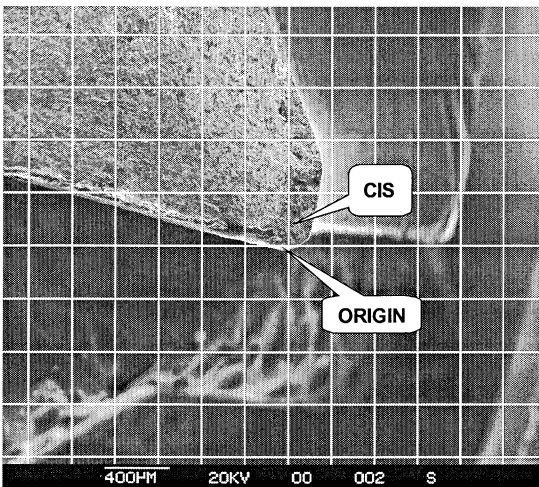


Figure 146 3D15L

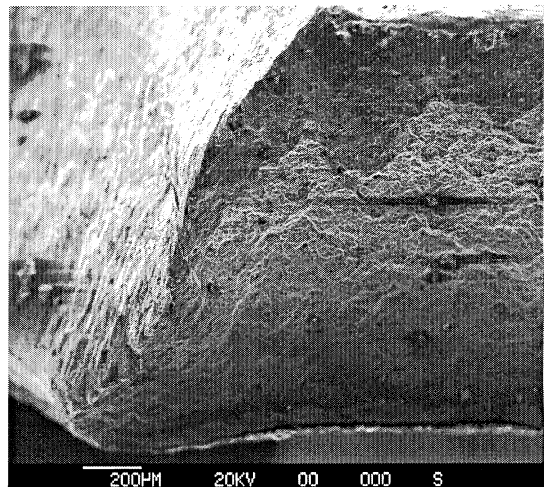


Figure 147 4A13L

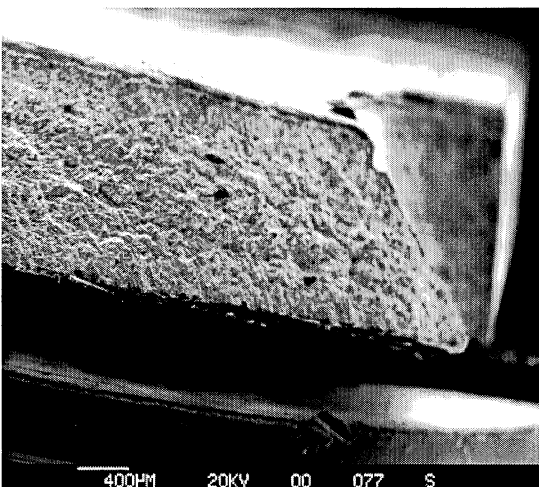


Figure 148 4C2L

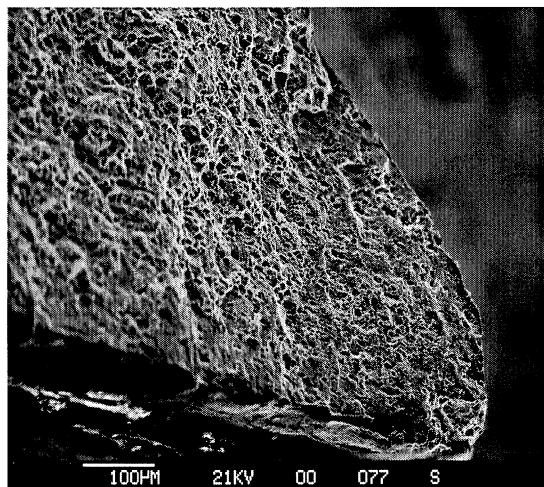


Figure 149 4C2L Nucleation Site



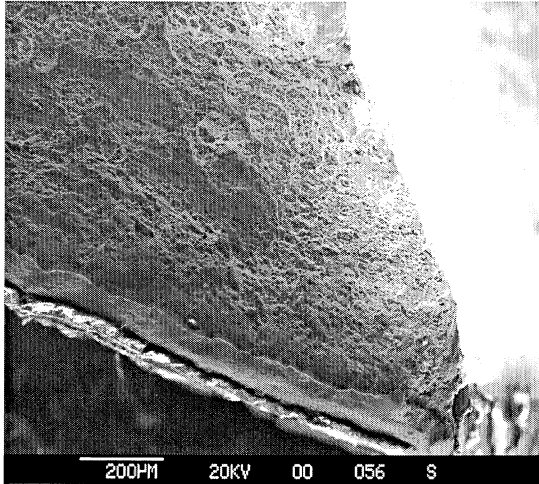


Figure 150 4C3L

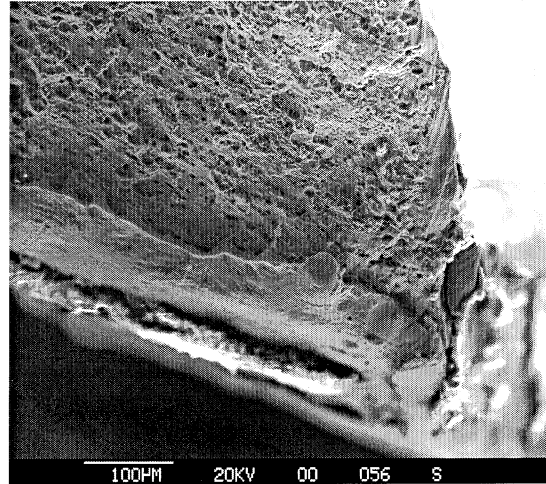


Figure 151 4C3L Nucleation Site

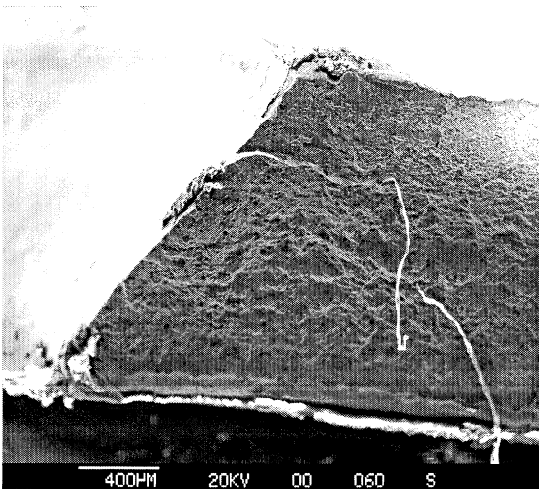


Figure 152 4C3R

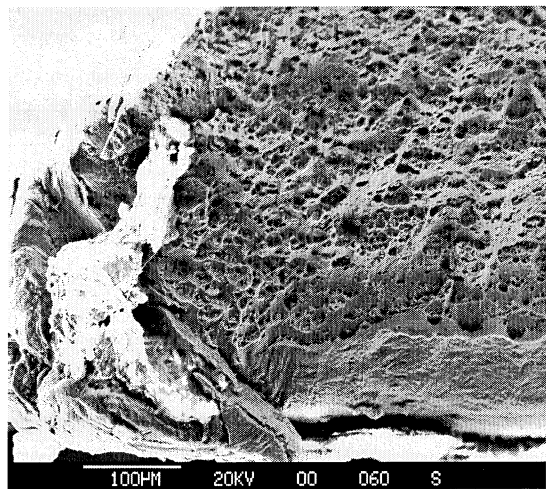


Figure 153 4C3R Nucleation Site



Figure 154 4C4L

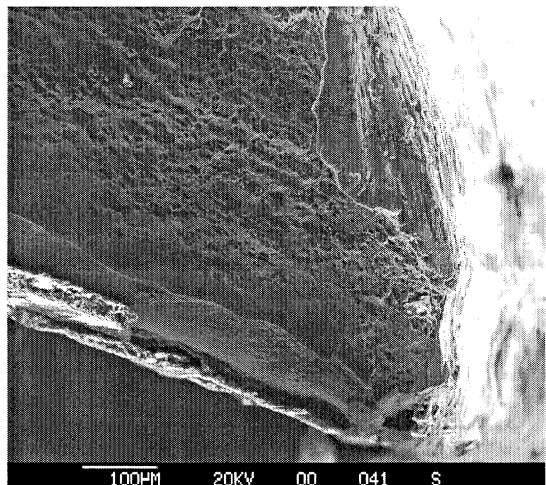


Figure 155 4C4L Nucleation Site

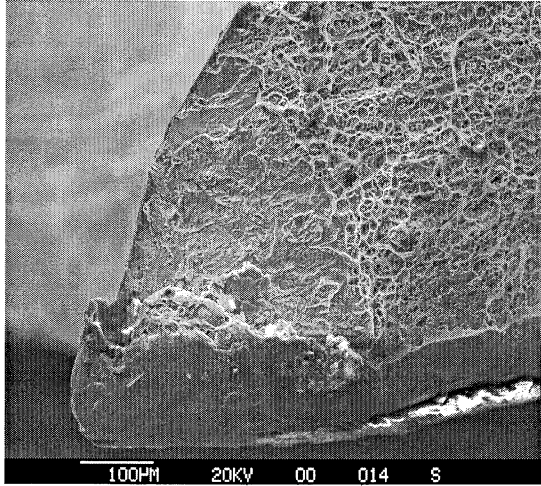


Figure 156 4C4R

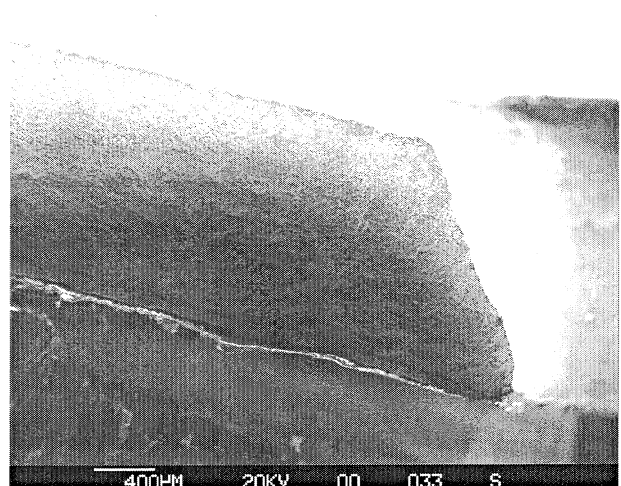


Figure 157 4C5L

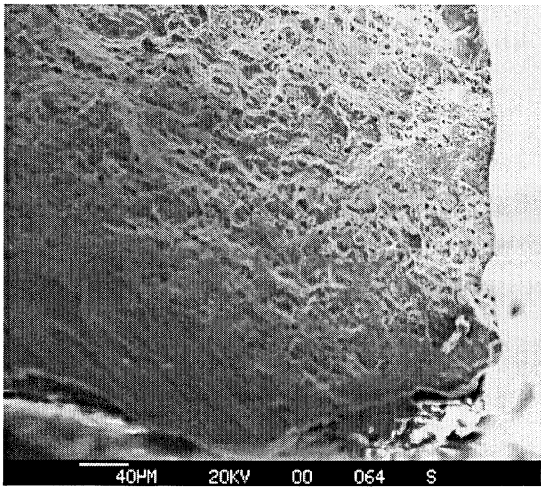


Figure 158 4C5L Nucleation Site

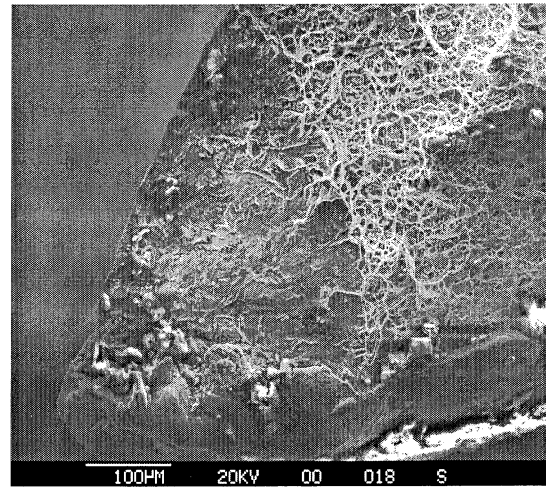


Figure 159 4C5R

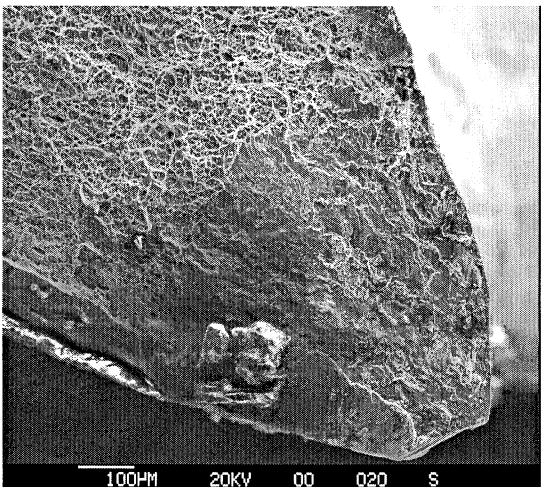


Figure 160 4C6L

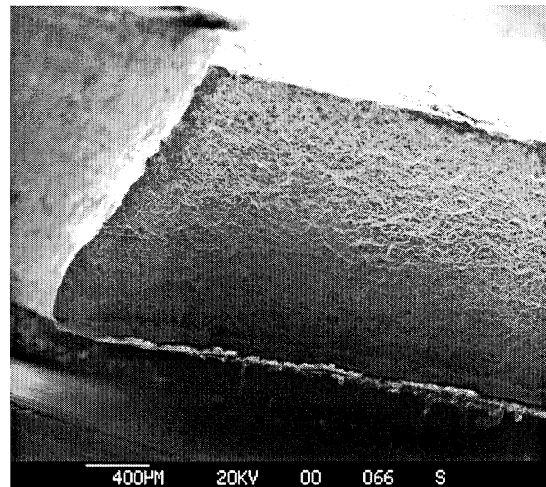


Figure 161 4C6R

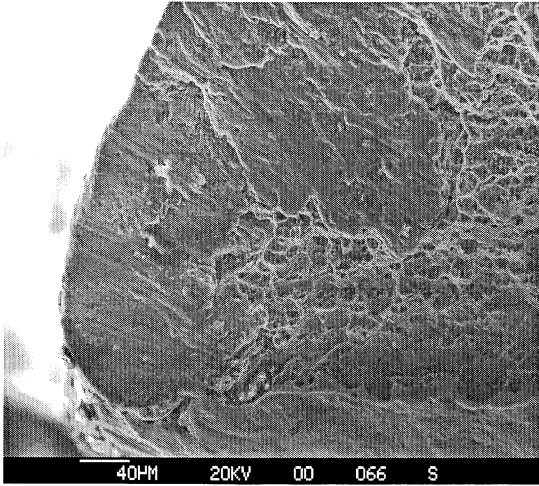


Figure 162 4C6R Nucleation Site

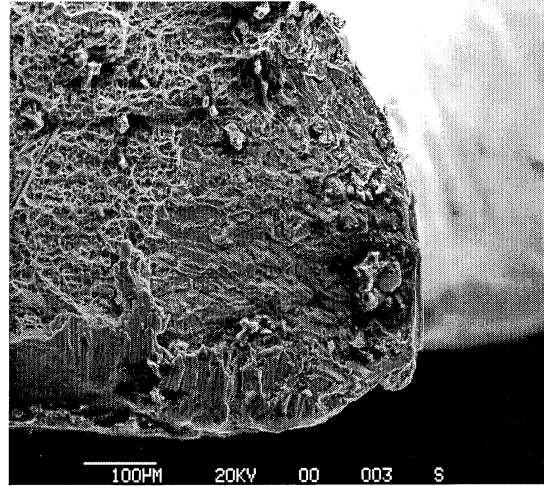


Figure 163 4C7L

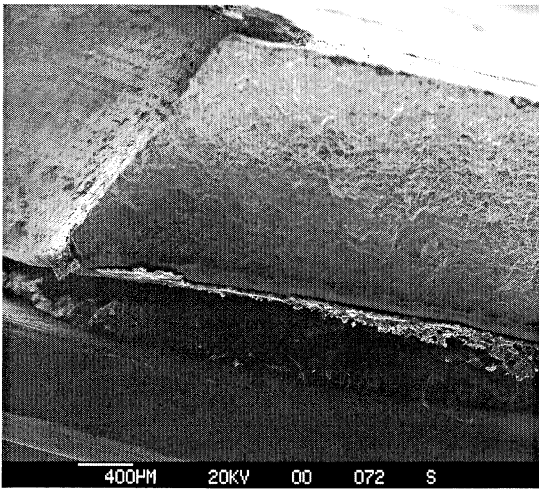


Figure 164 4C7R

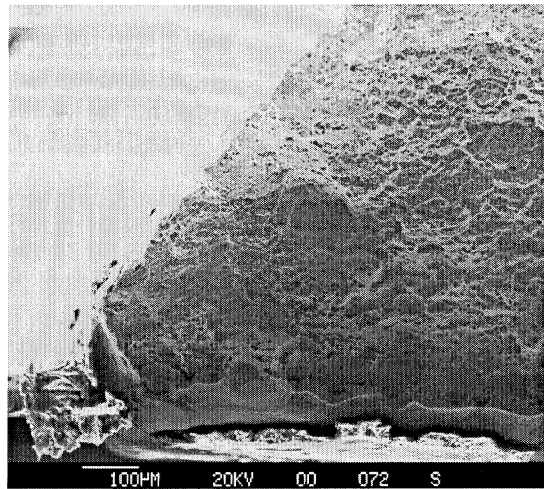


Figure 165 4C7R Nucleation Site

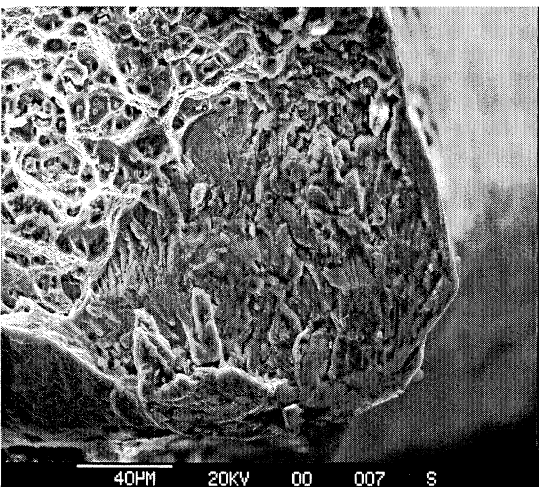


Figure 166 4C8L

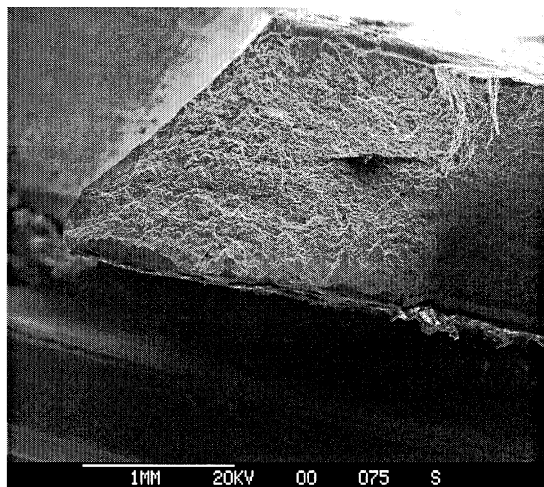


Figure 167 4C8R



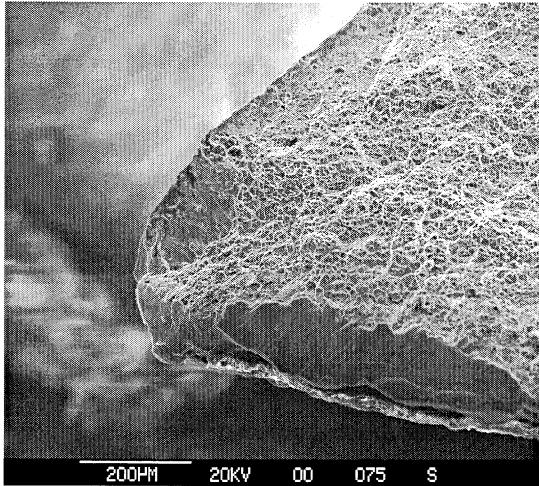


Figure 168 4C8R Nucleation Site

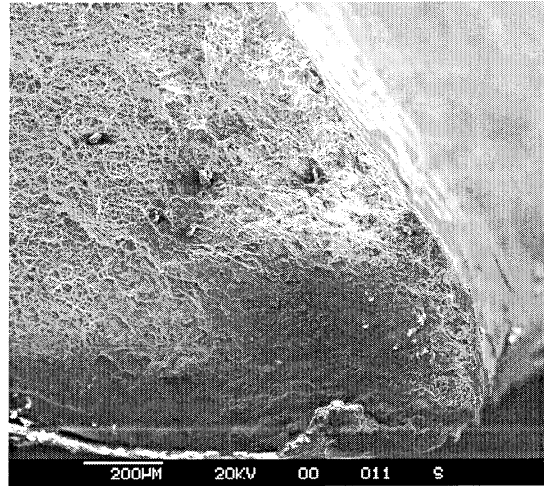


Figure 169 4C9L

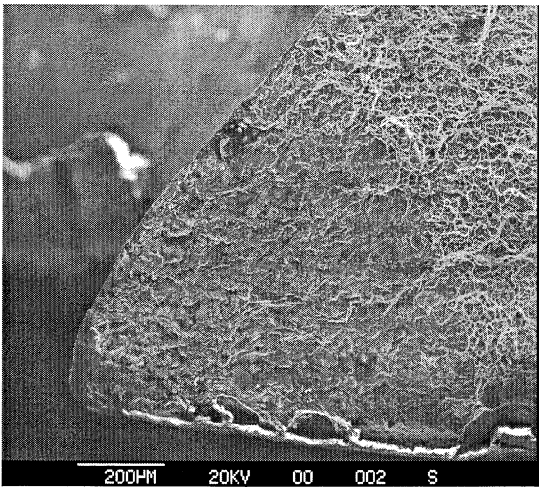


Figure 170 4C9R

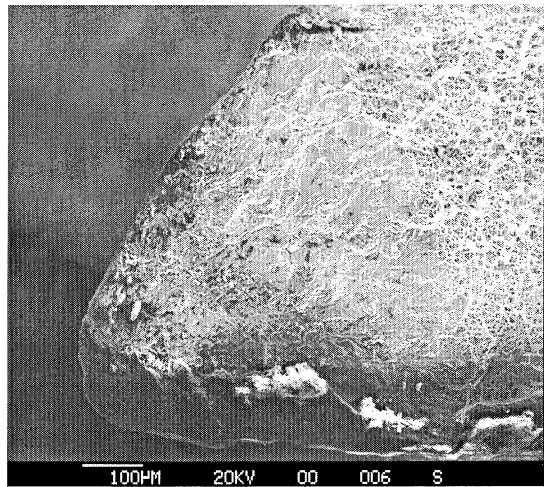


Figure 171 4C10R

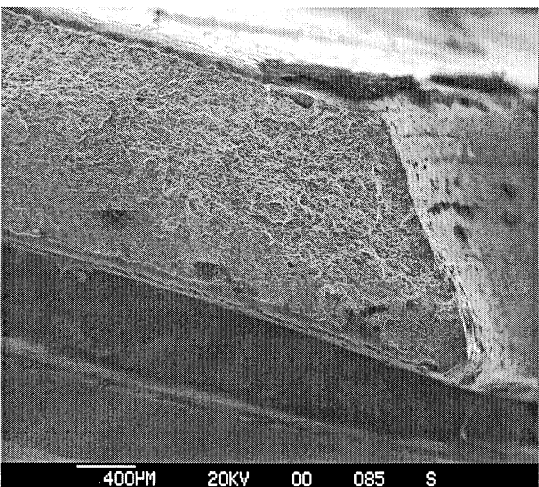


Figure 172 4C11L

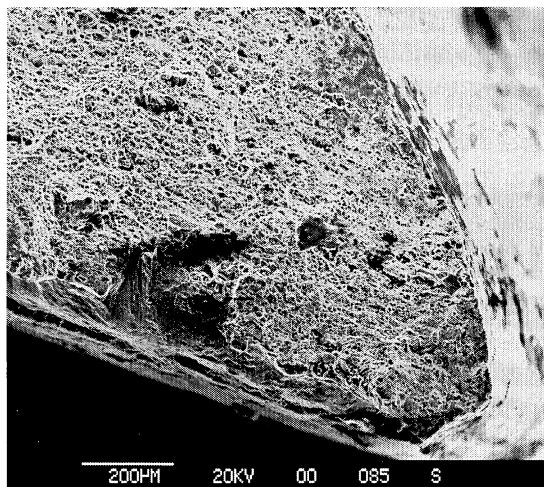


Figure 173 4C11L Nucleation Site

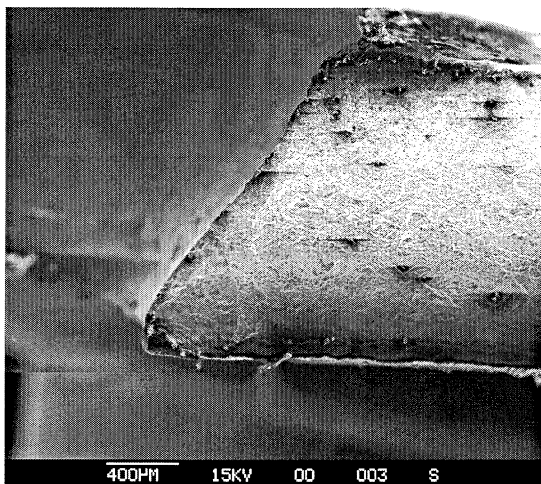


Figure 174 4C11R

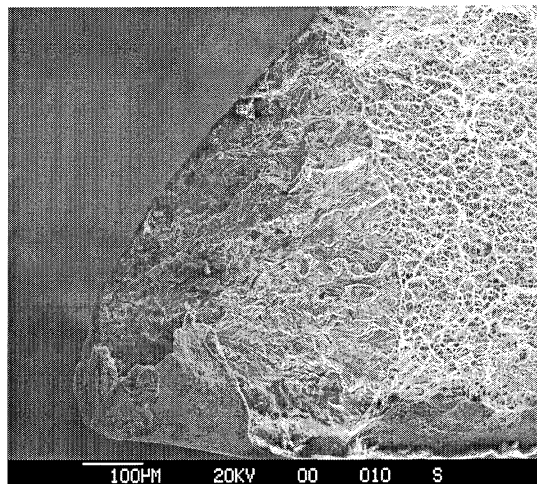


Figure 175 4C11R Nucleation Site

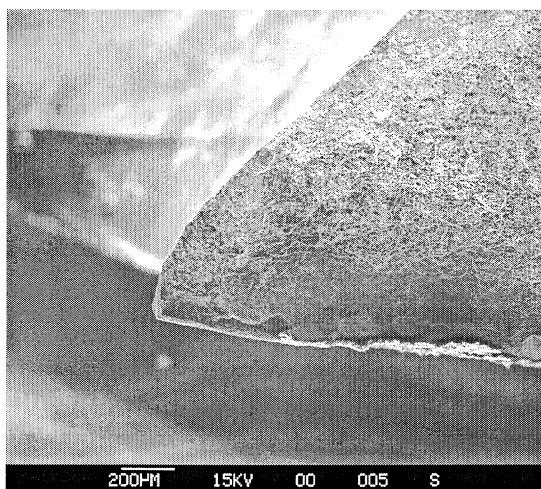


Figure 176 4C12R

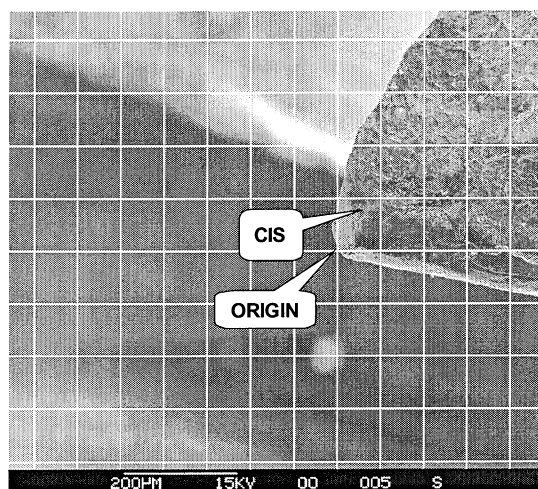


Figure 177 4C12R

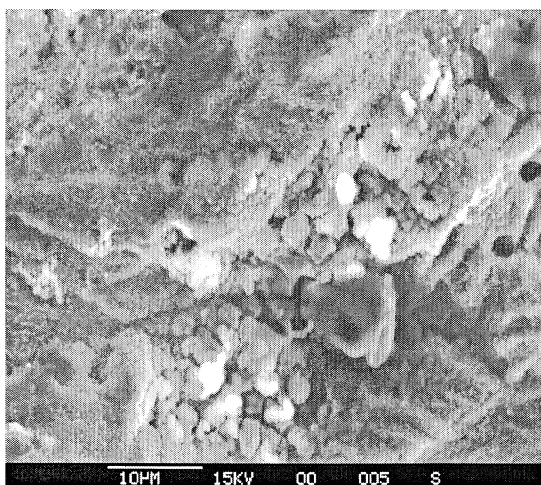


Figure 178 Corrosion on 4C12R

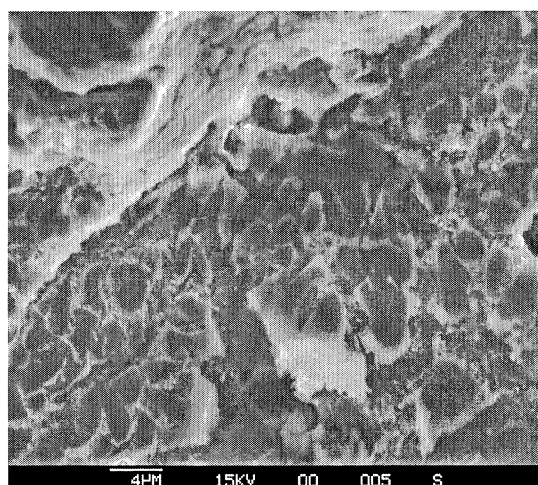


Figure 179 Corrosion on 4C12R



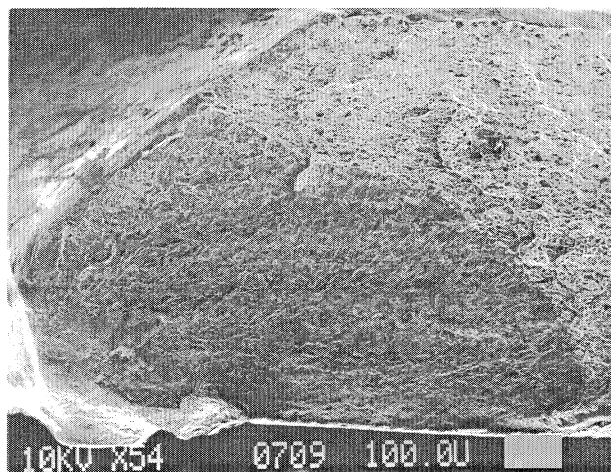


Figure 180 7A4R

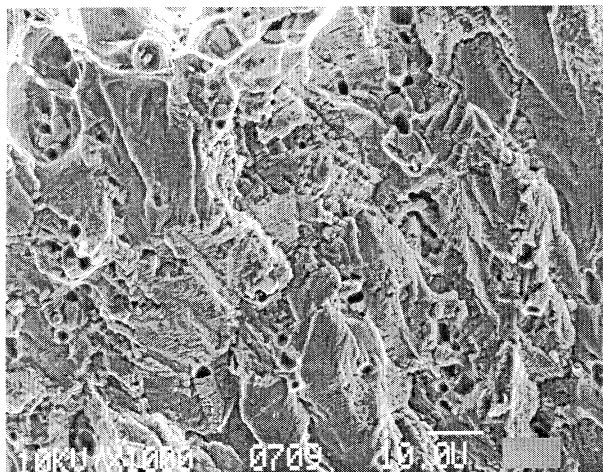


Figure 181 7A4R Marker Bands



Figure 182 7A6L

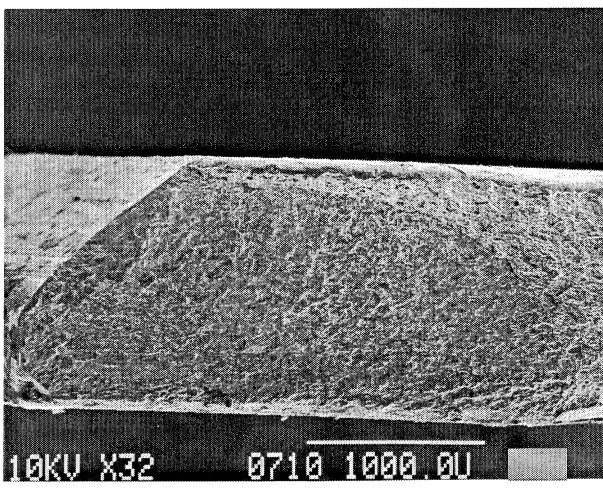


Figure 183 7A6R

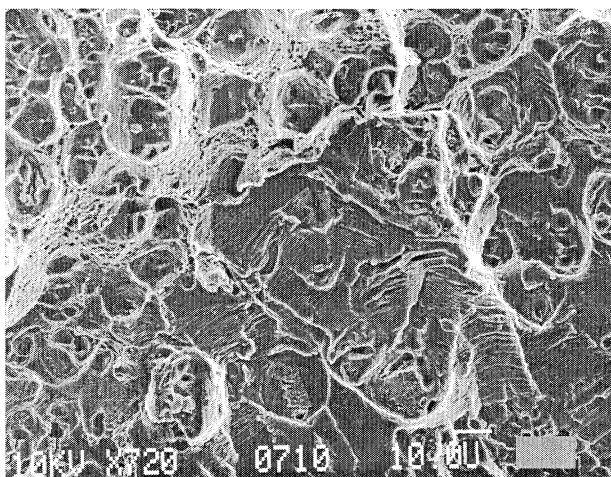


Figure 184 7A6R Marker Bands

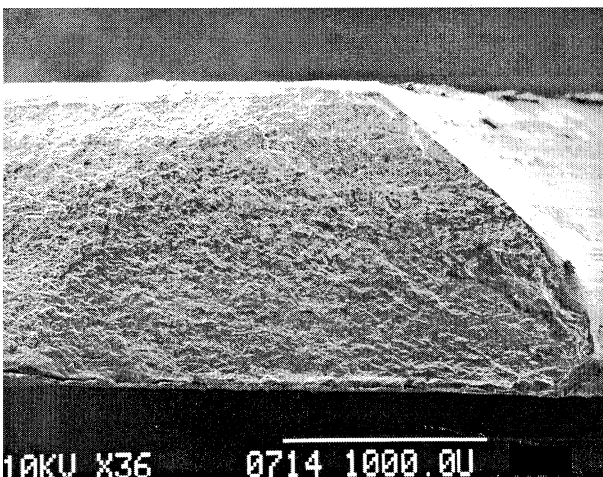


Figure 185 7A7L



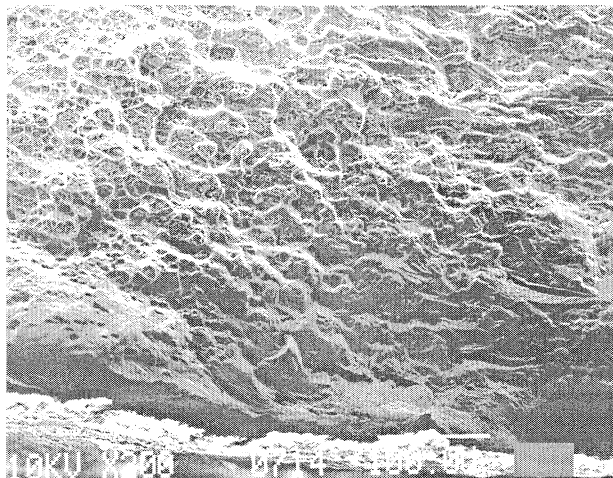


Figure 186 7A7L Nucleation Site

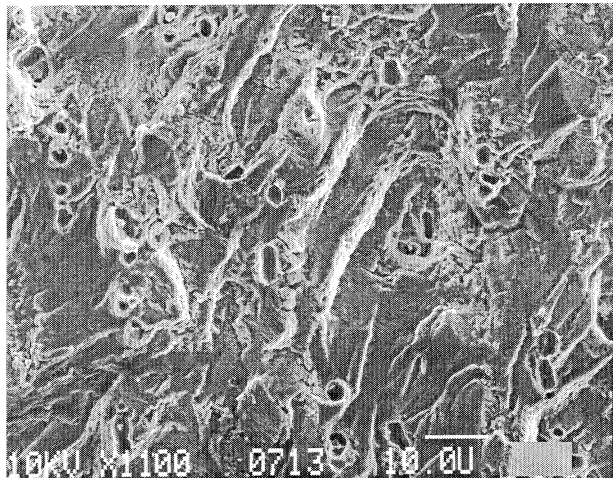


Figure 187 7A7L Marker Bands

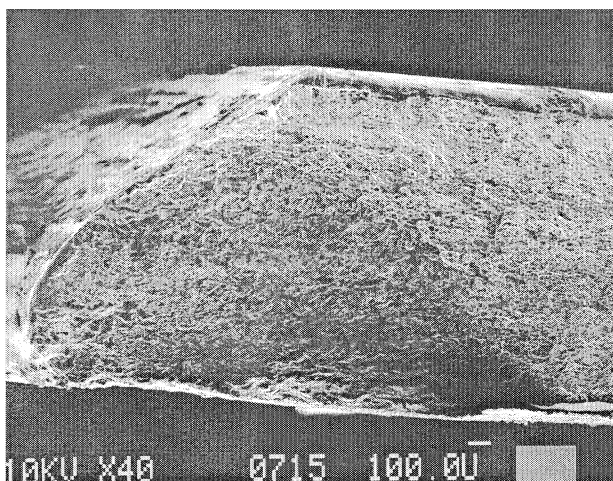


Figure 188 7A7R

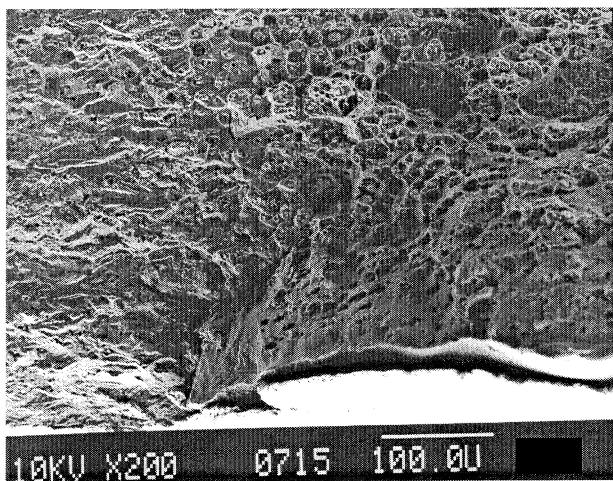


Figure 189 7A7R Nucleation Site

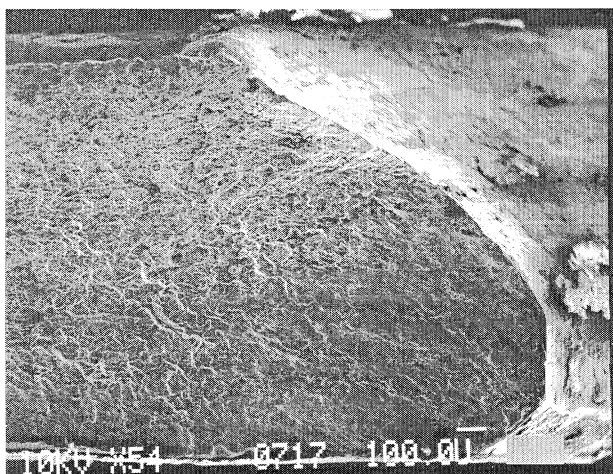


Figure 190 7A8L

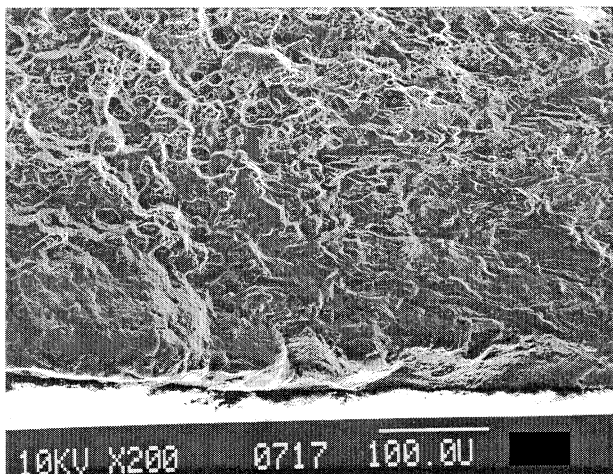


Figure 191 7A8L Nucleation Site

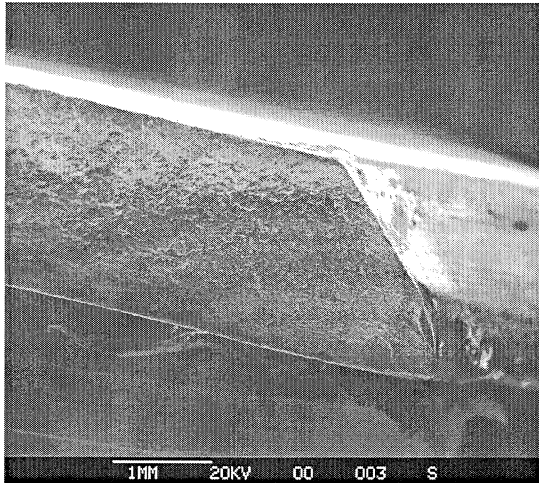


Figure 192 7A10L

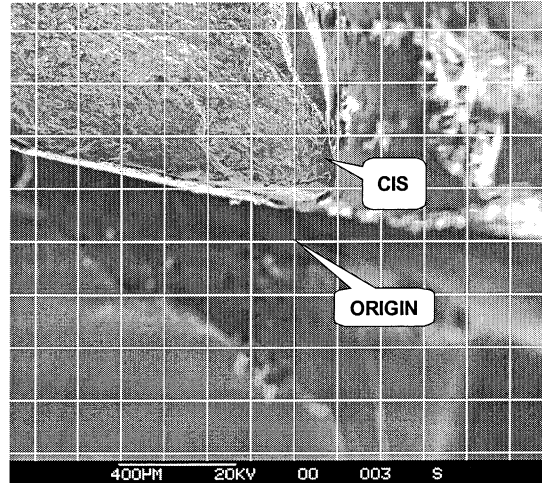


Figure 193 7A10L

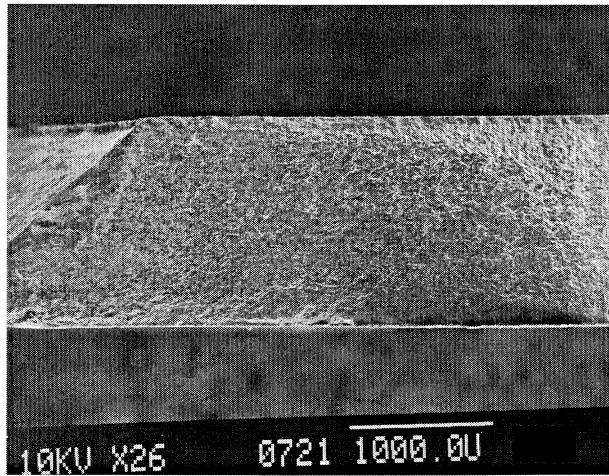


Figure 194 7A12R

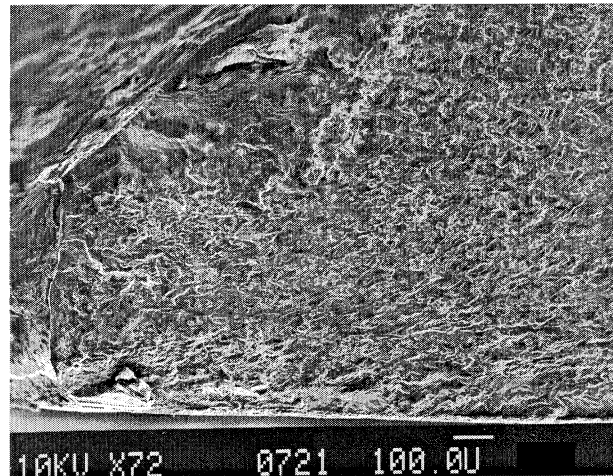


Figure 195 7A12R Nucleation Site, Macro View

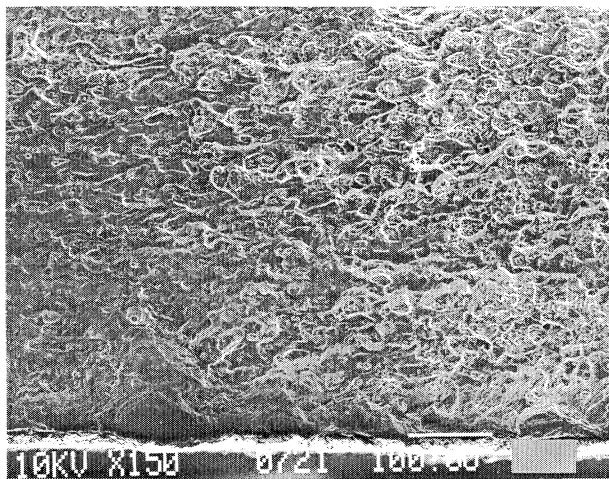


Figure 196 7A12R Nucleation Site

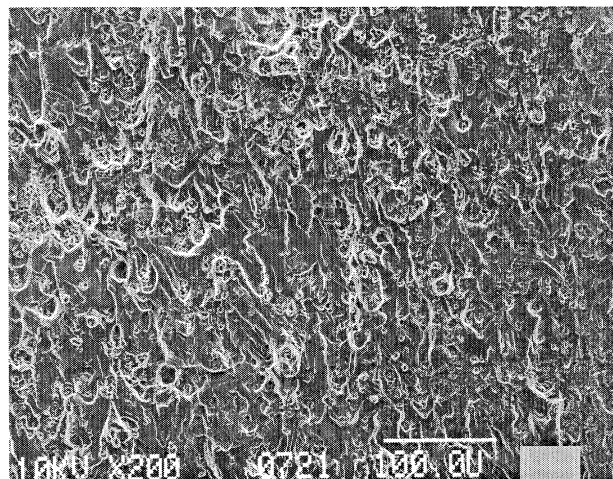


Figure 197 7A12R Marker Bands



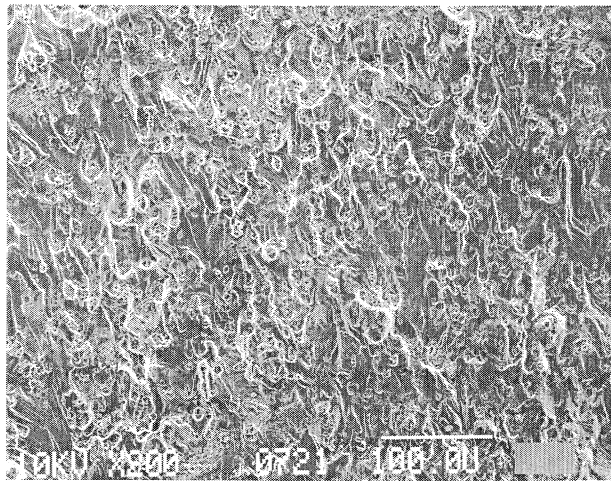


Figure 198 7A12R Marker Bands

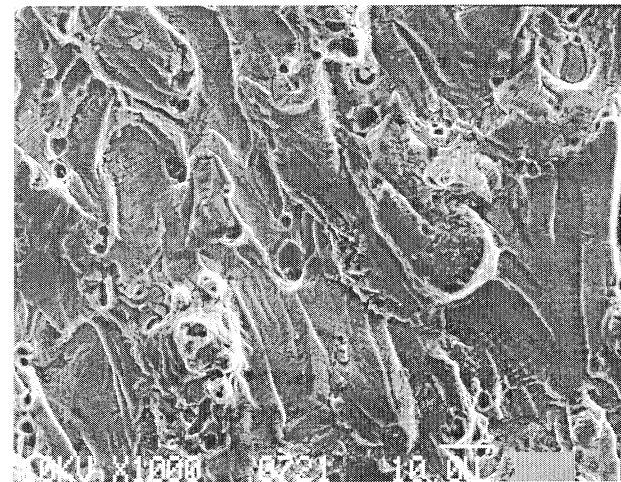


Figure 199 7A12R Marker Bands

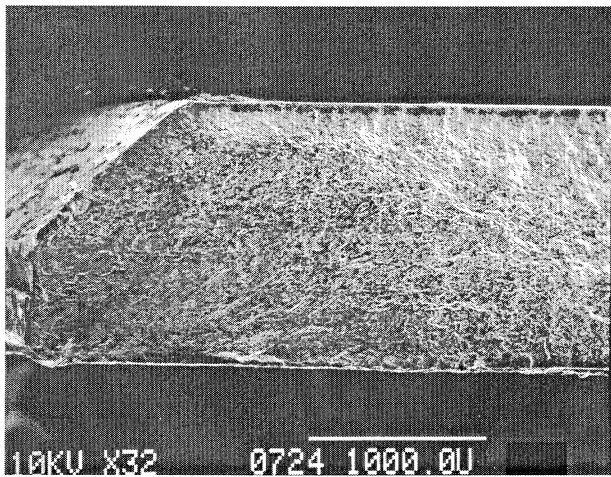


Figure 200 7A13R

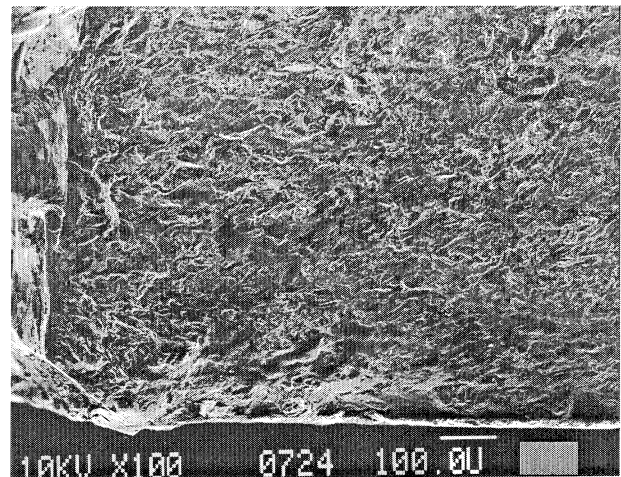


Figure 201 7A13R Nucleation Site, Macro View

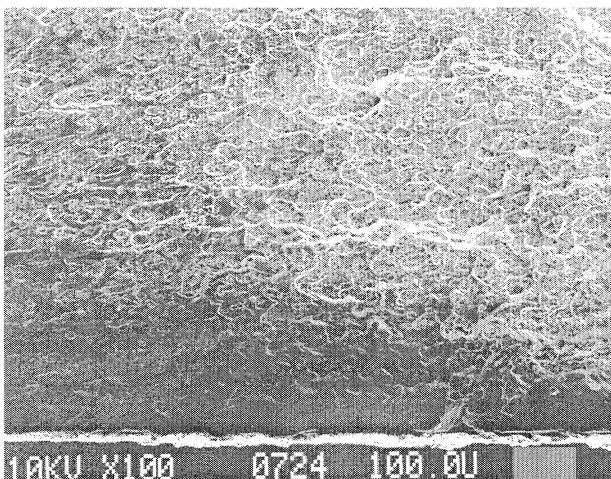


Figure 202 7A13R Nucleation Site

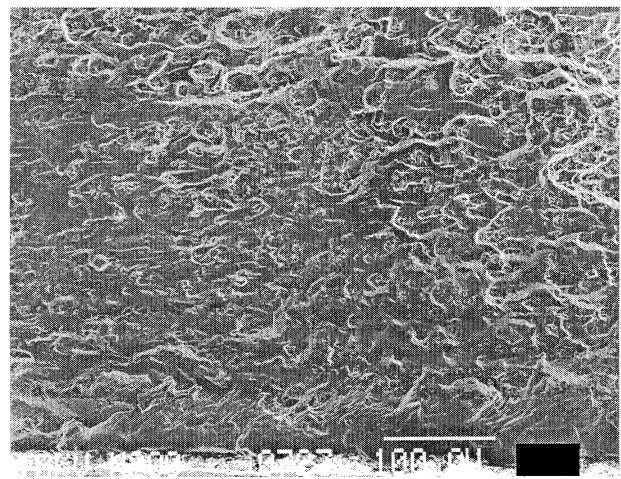


Figure 203 7A13R Marker Bands

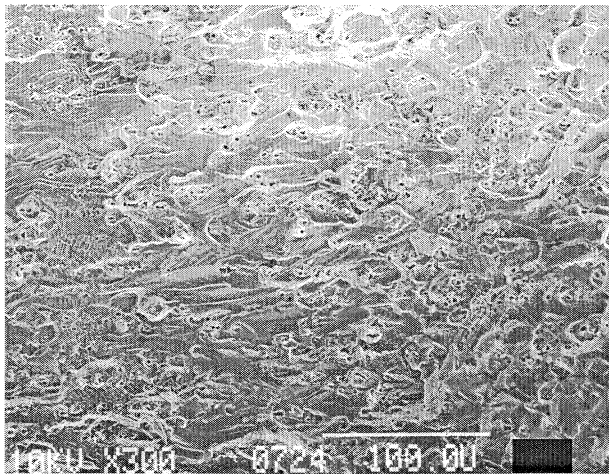


Figure 204 7A13R Marker Bands

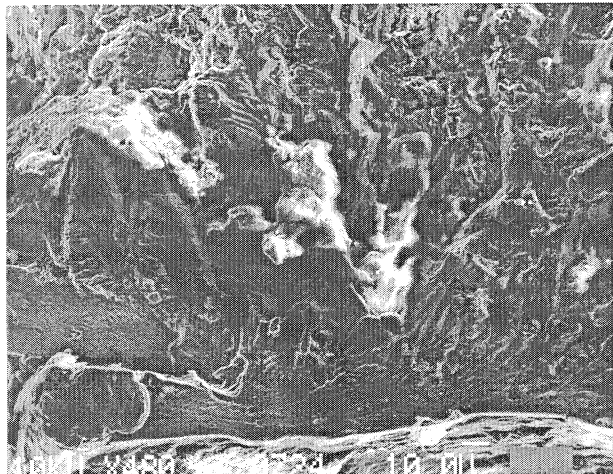


Figure 205 7A13R Marker Bands

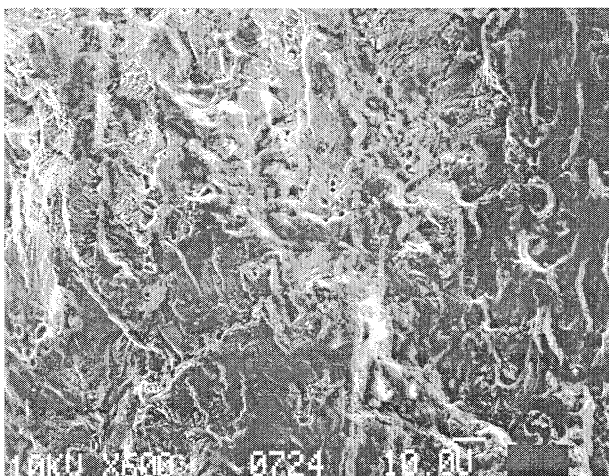


Figure 206 7A13R Marker Bands

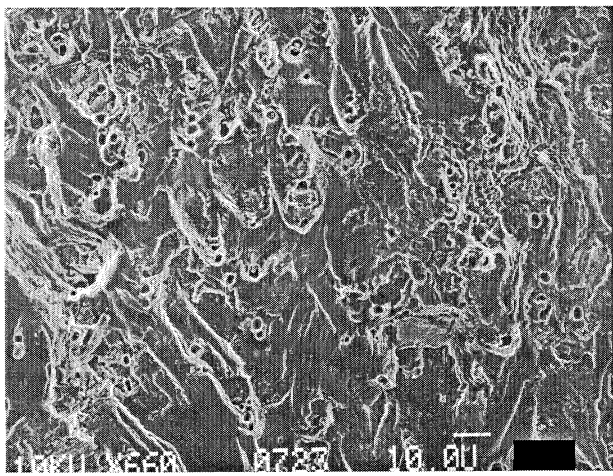


Figure 207 7A13R Marker Bands

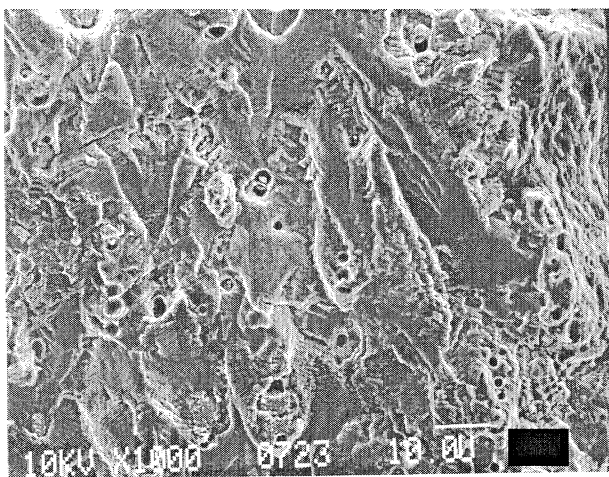


Figure 208 7A13R Marker Bands

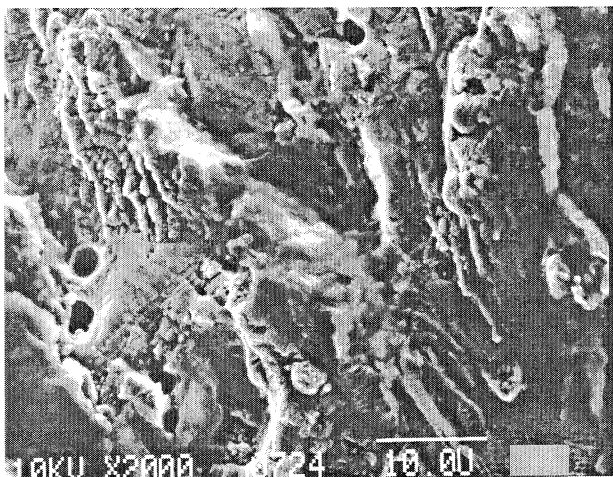


Figure 209 7A13R Marker Bands



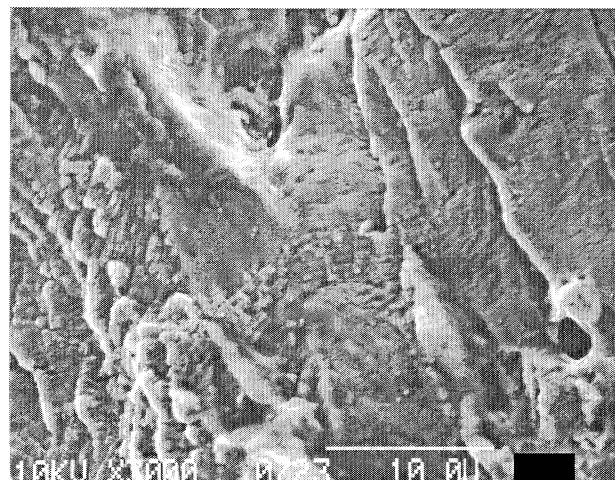


Figure 210 7A13R Marker Bands

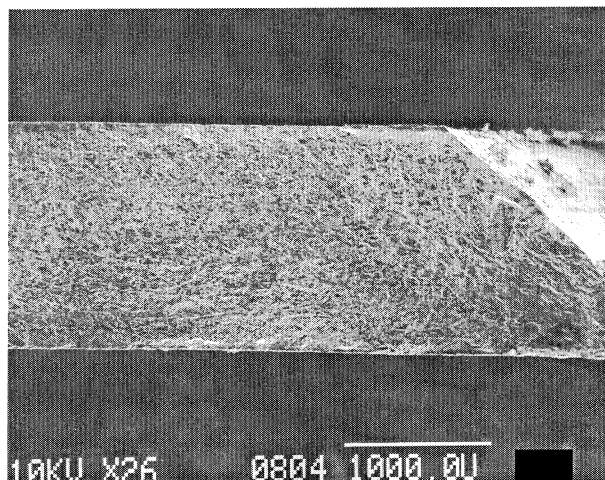


Figure 211 7A14L

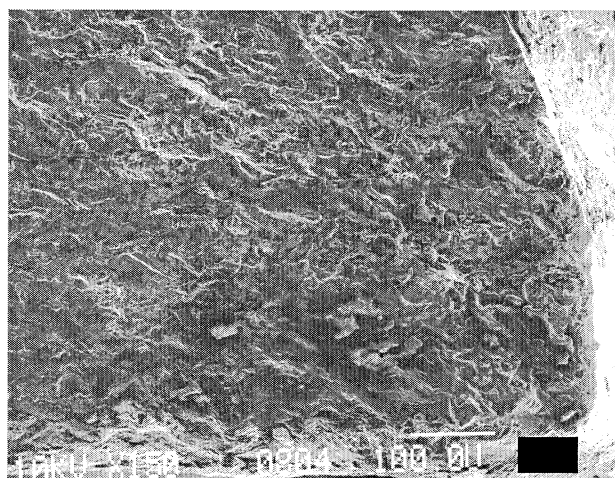


Figure 212 7A14L Nucleation Site

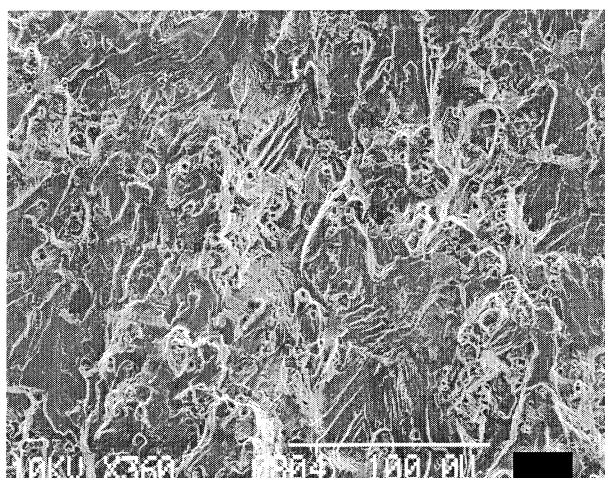


Figure 213 7A14L Marker Bands

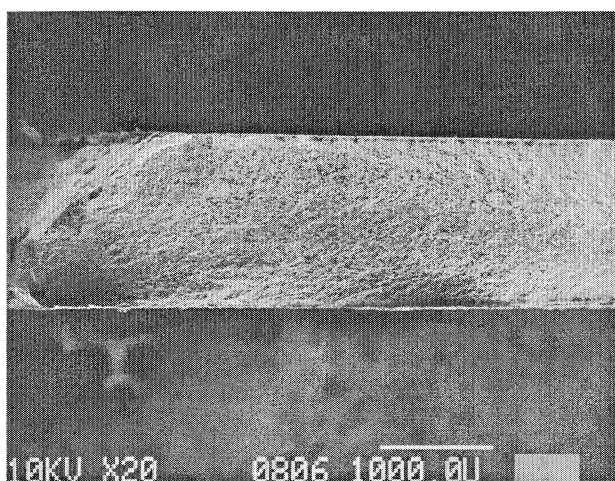


Figure 214 7A14R

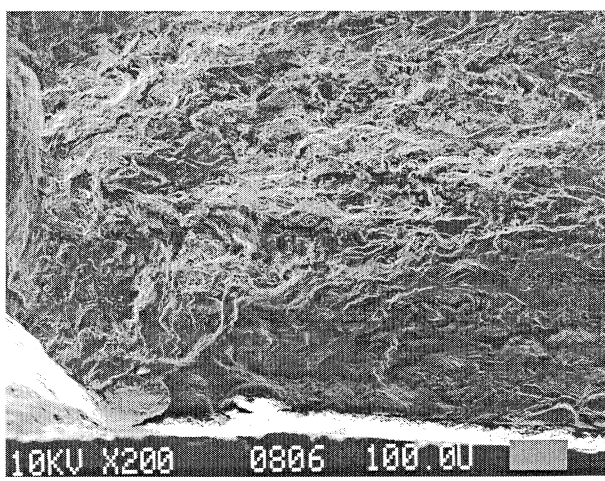


Figure 215 7A14R Nucleation Site

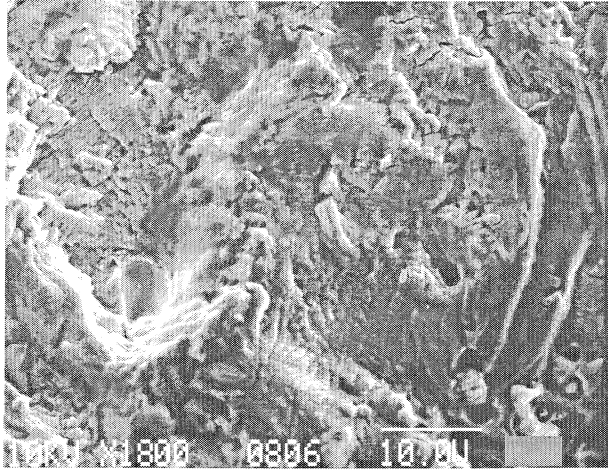


Figure 216 7A14R Marker Bands

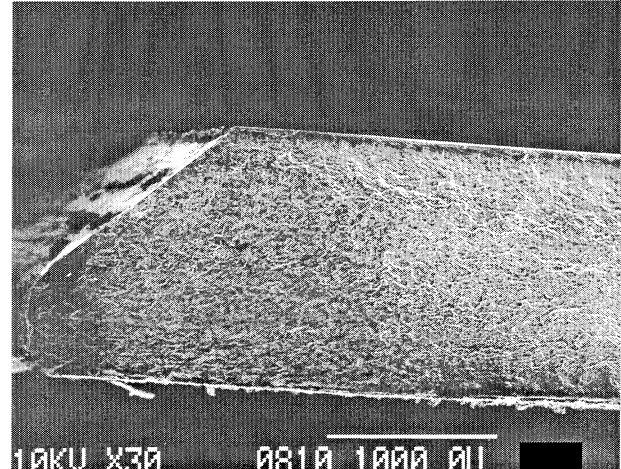


Figure 217 7A15R

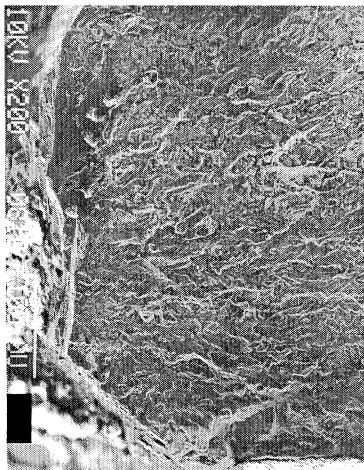


Figure 218 7A15R Nucleation Site

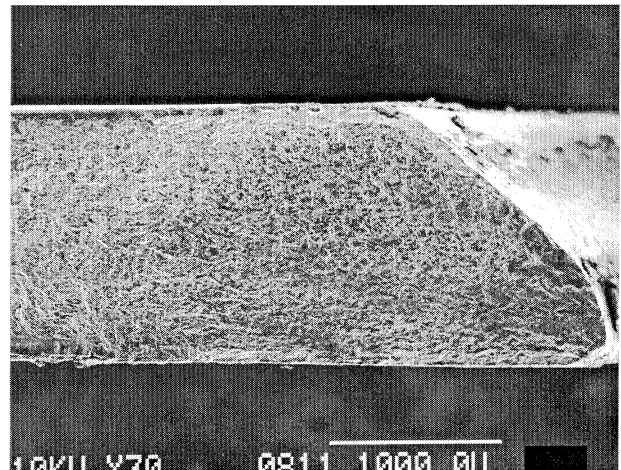


Figure 219 7A16L

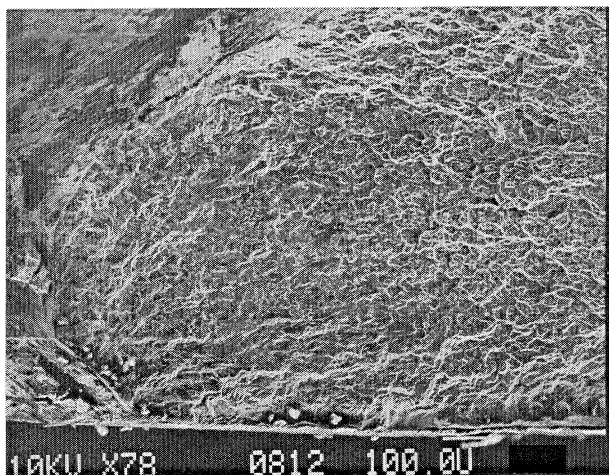


Figure 220 7A16R

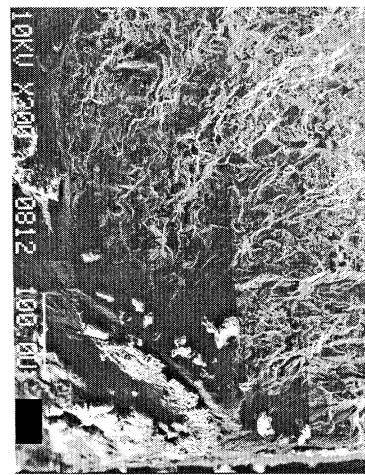


Figure 221 7A16R Nucleation Site



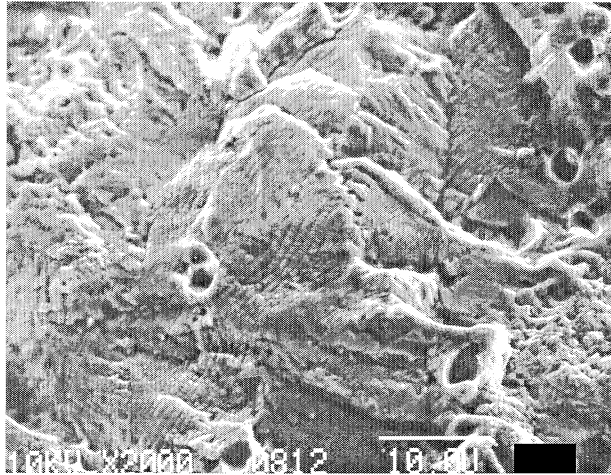


Figure 222 7A16R Marker Bands

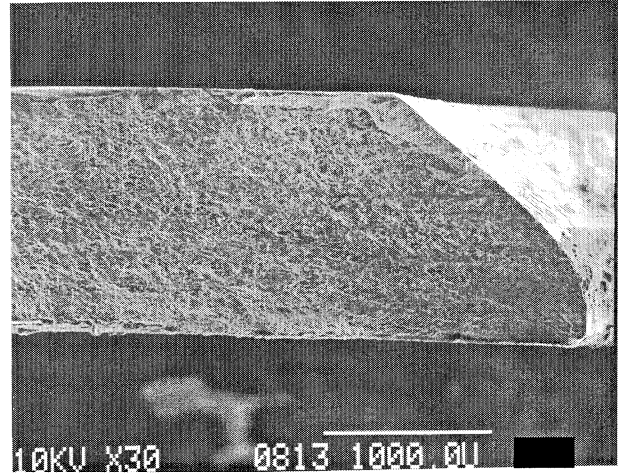


Figure 223 7A17L

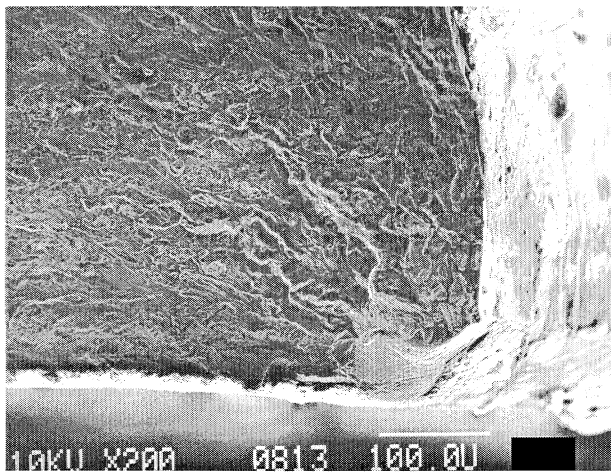


Figure 224 7A17L Nucleation Site

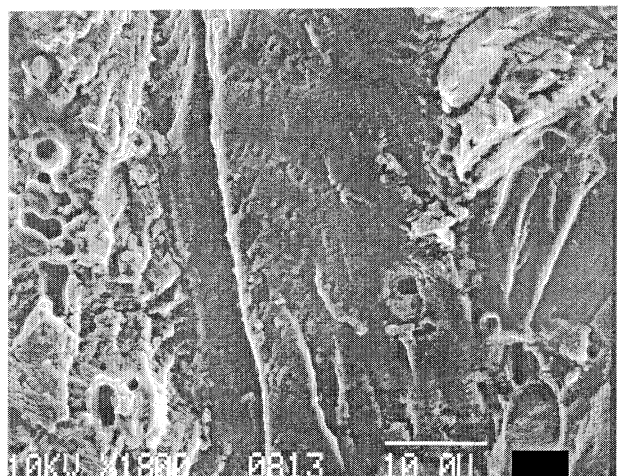


Figure 225 7A17L Marker Bands

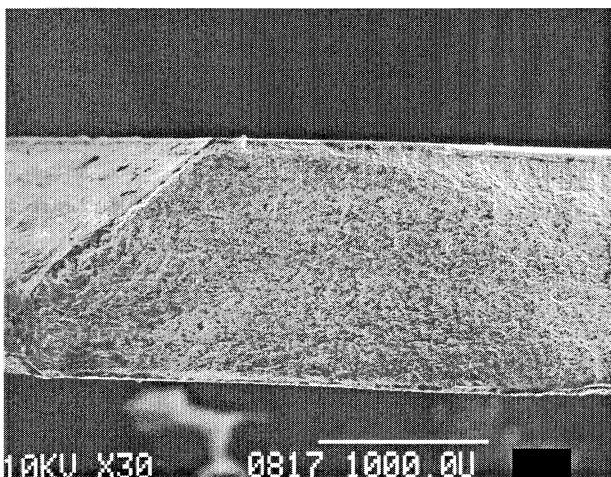


Figure 226 7A17R

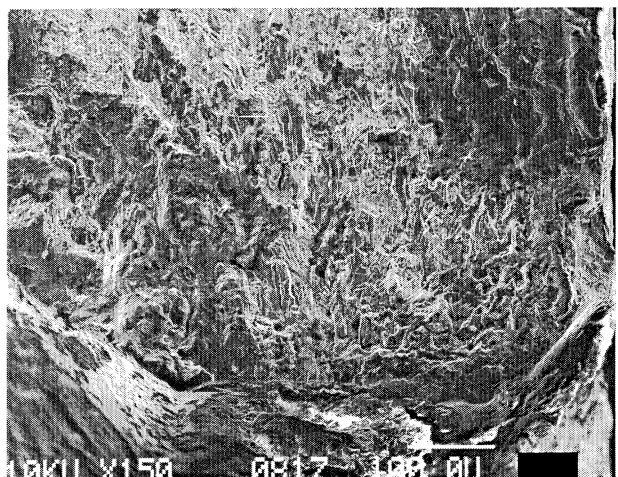


Figure 227 7A17R Nucleation Site

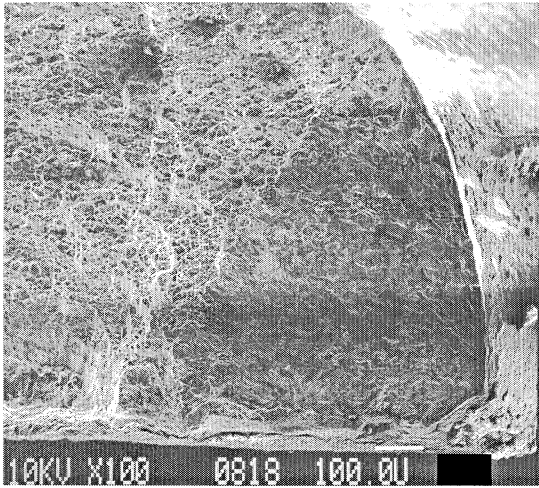


Figure 228 8A4L

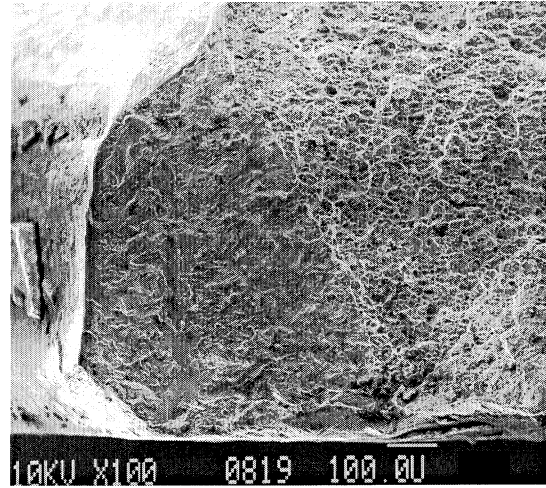


Figure 229 8A4R

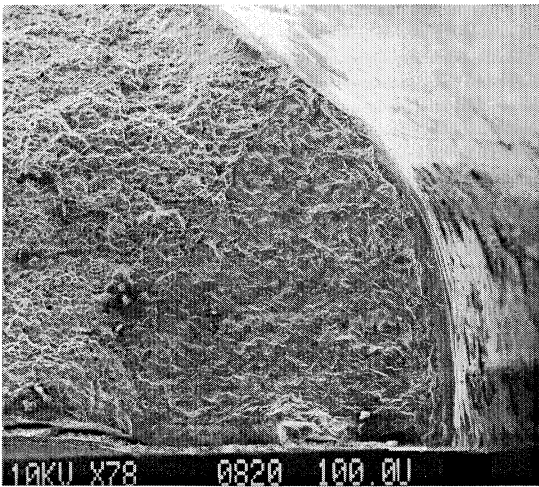


Figure 230 8A5L

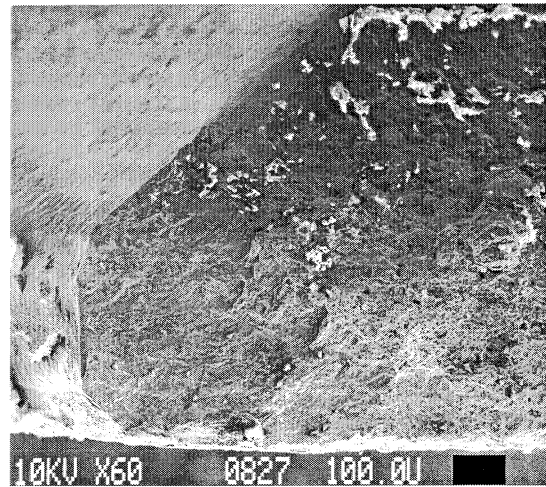


Figure 231 8A5R

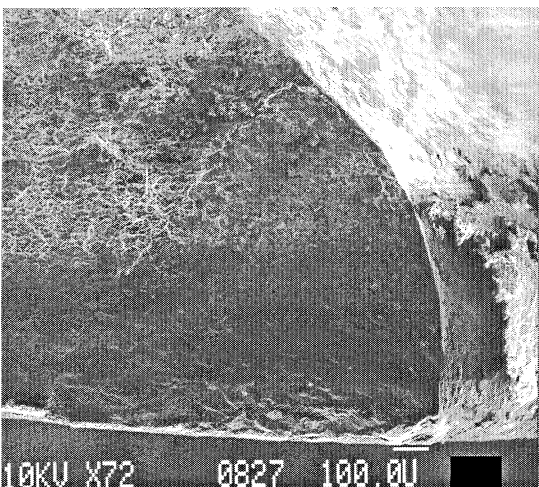


Figure 232 8A6L

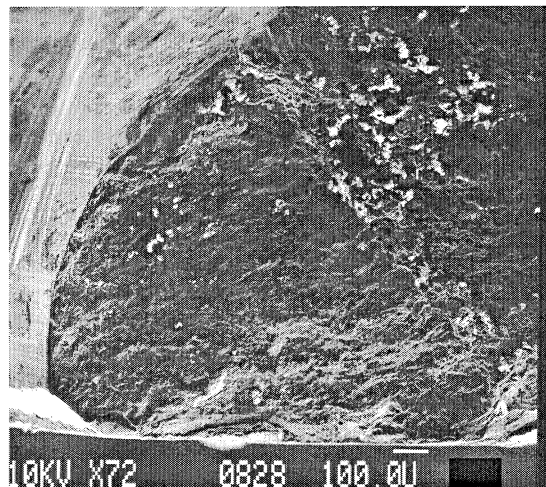


Figure 233 8A6R



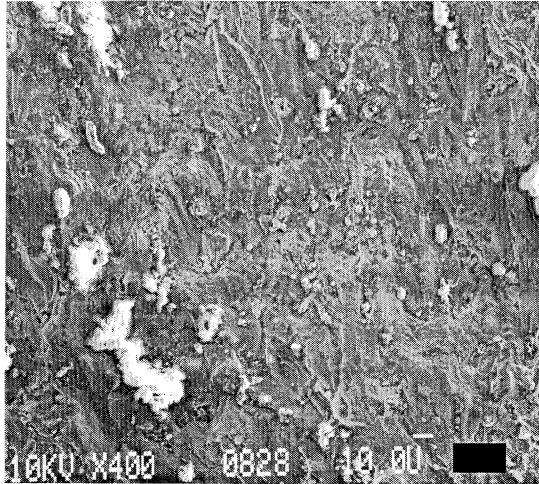


Figure 234 8A6R Close-up

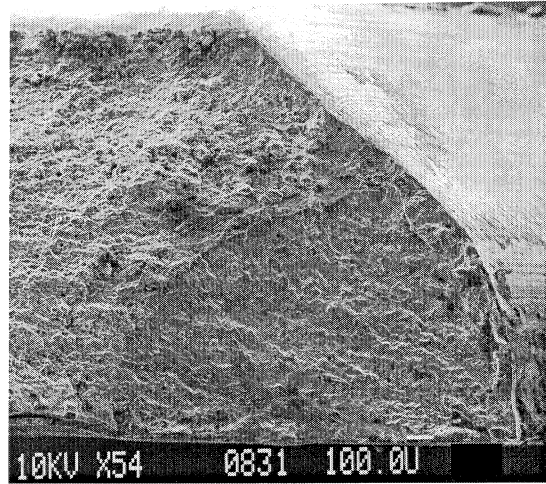


Figure 235 8A7L

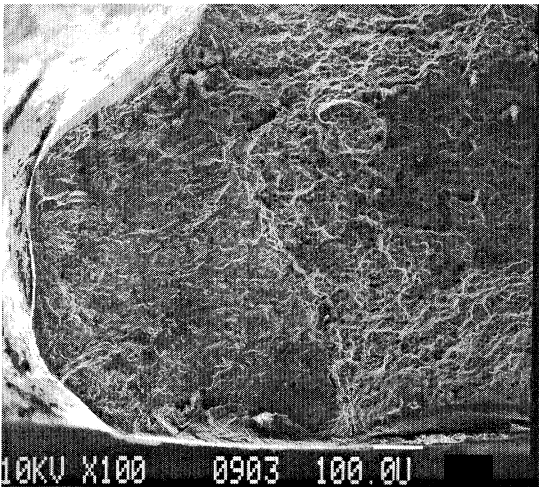


Figure 236 8A7R

Intentionally Left Blank

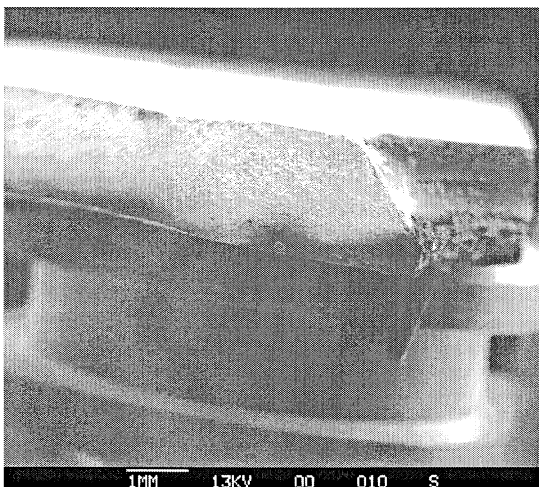


Figure 237 8A10L

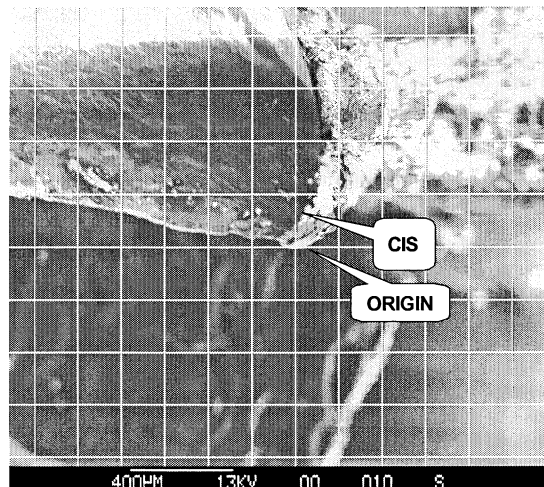


Figure 238 8A10L Nucleation Site

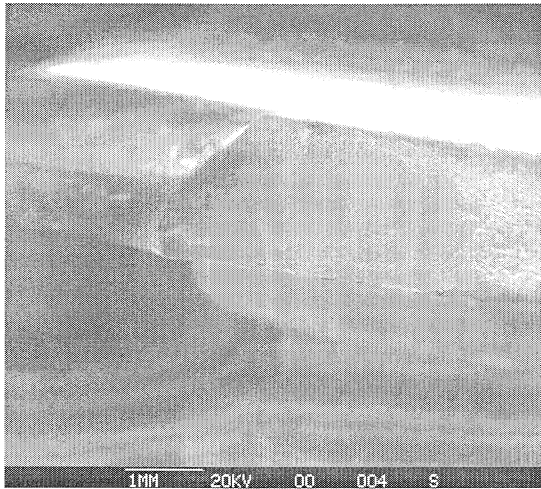


Figure 239 8A10R

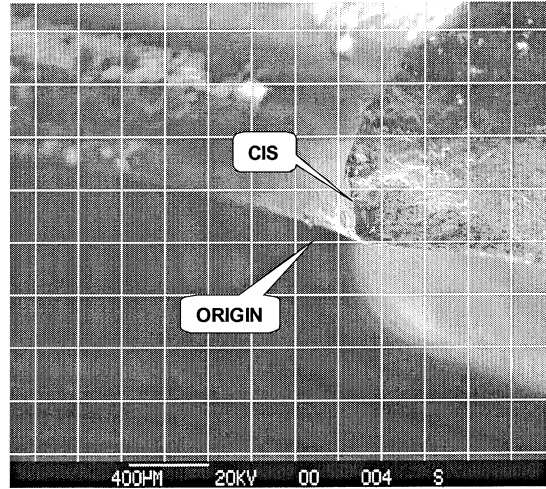


Figure 240 8A10R Nucleation Site

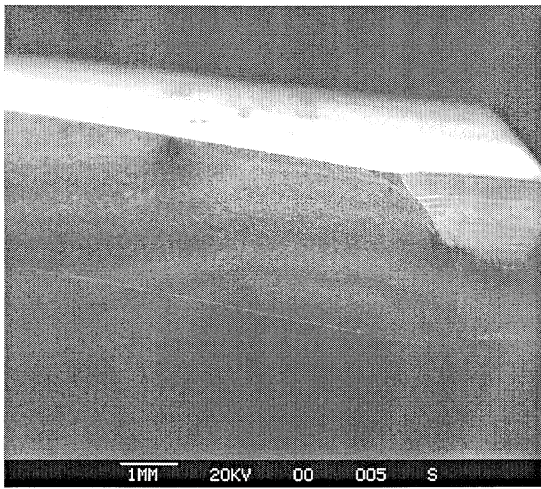


Figure 241 9A5L

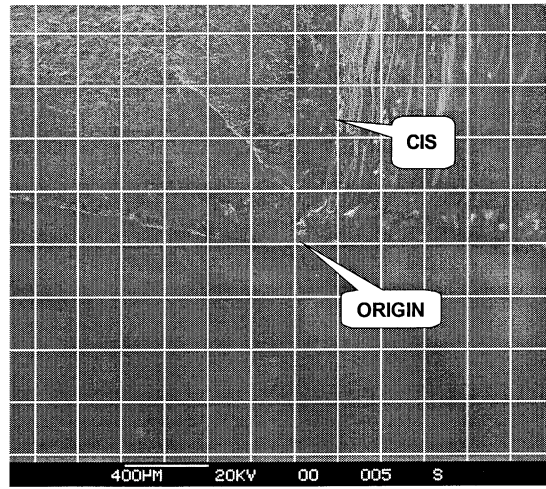


Figure 242 9A5L Nucleation Site

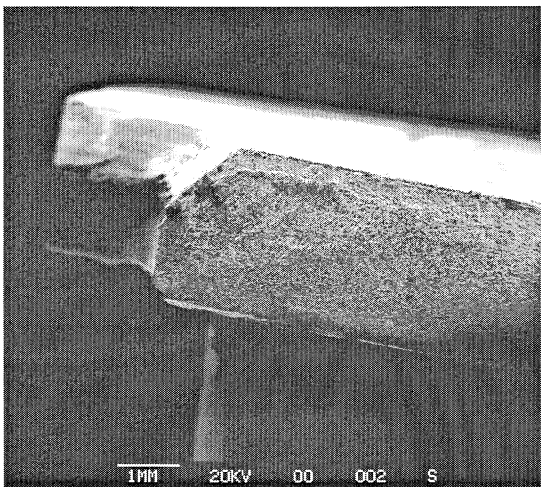


Figure 243 9A5R

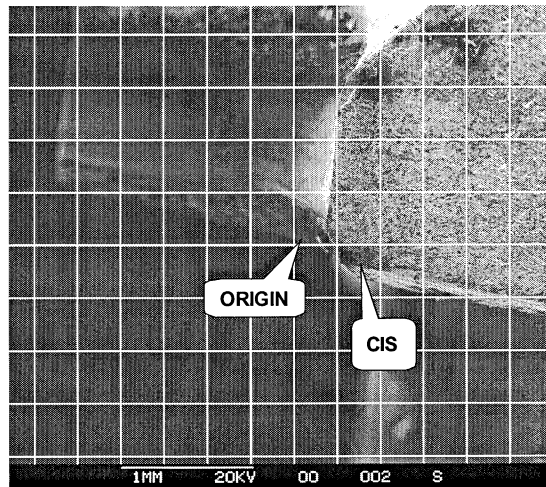


Figure 244 9A5R Nucleation Site



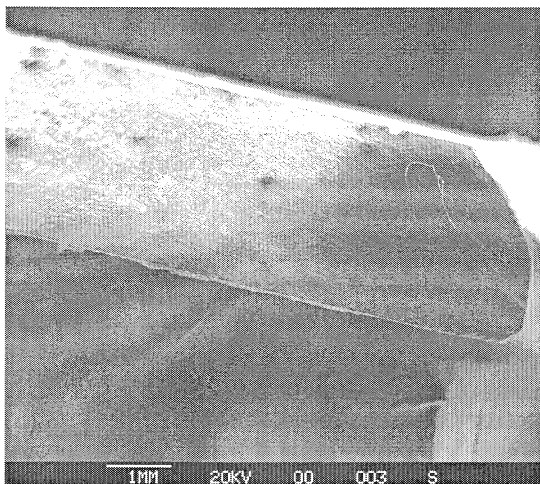


Figure 245 10F6R

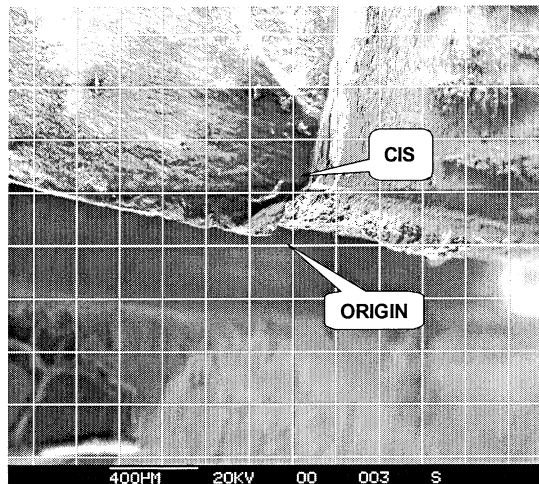


Figure 246 10F6R Nucleation Site

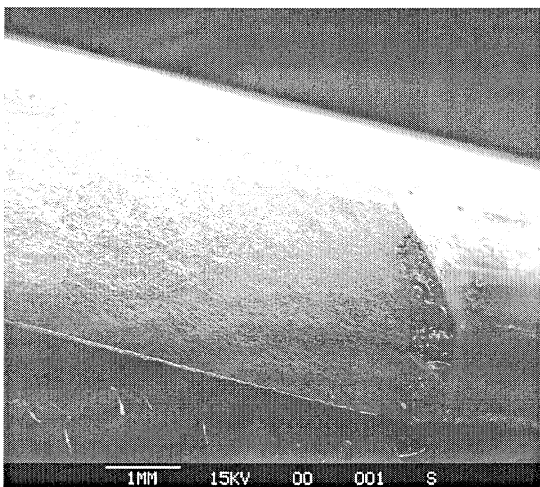


Figure 247 10F7R

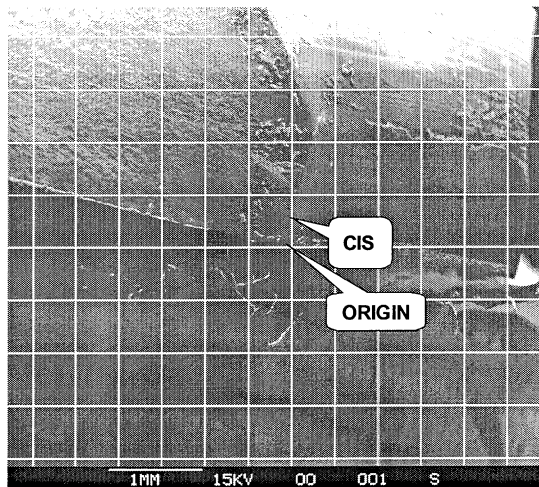


Figure 248 10F7R Nucleation Site

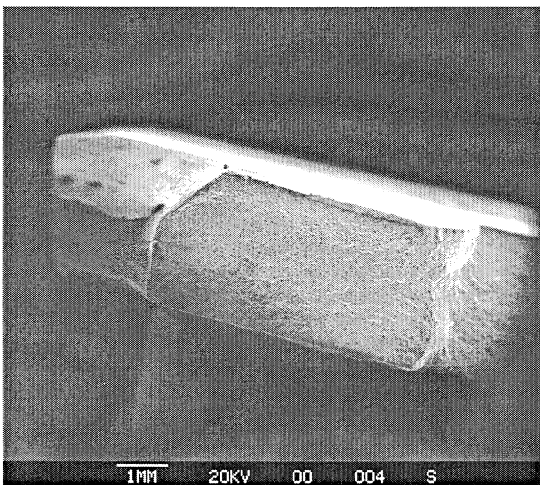


Figure 249 10F8L

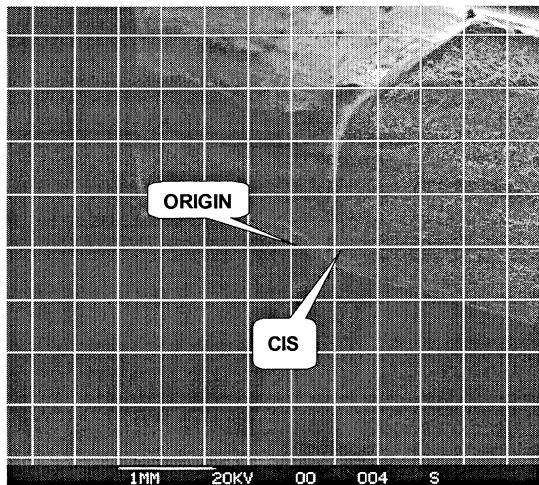


Figure 250 10F8L Nucleation Site

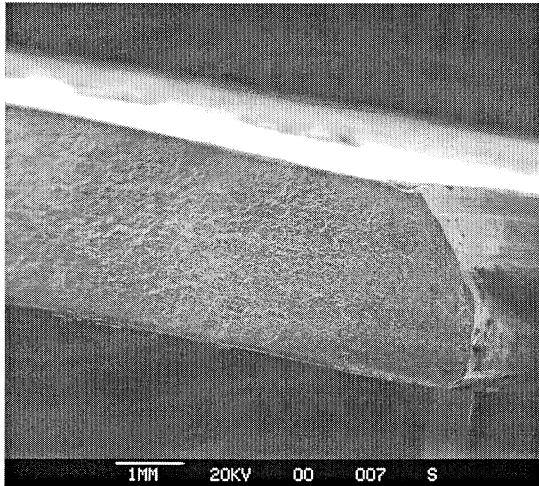


Figure 251 10F8R

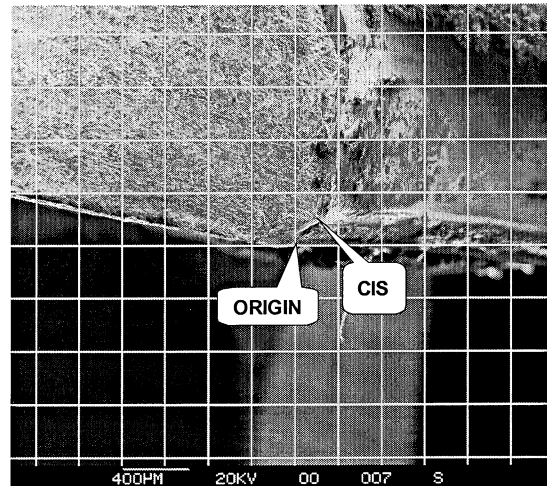


Figure 252 10F8R

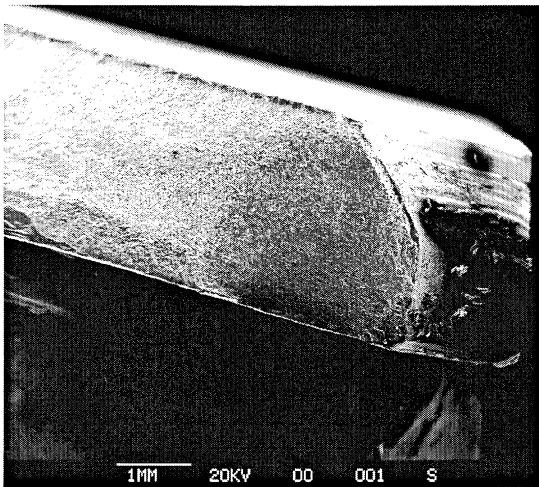


Figure 253 10F10R

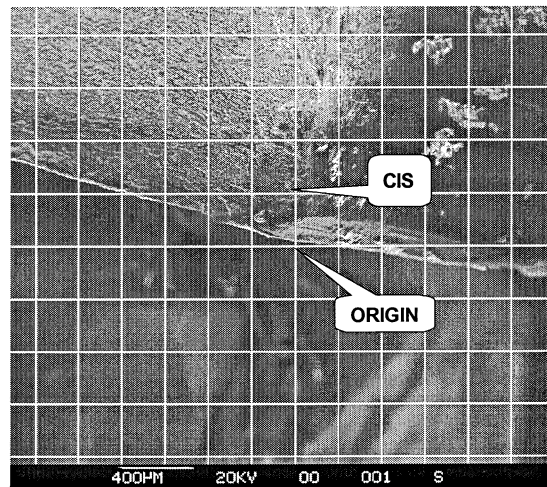


Figure 254 10F10R Nucleation Site

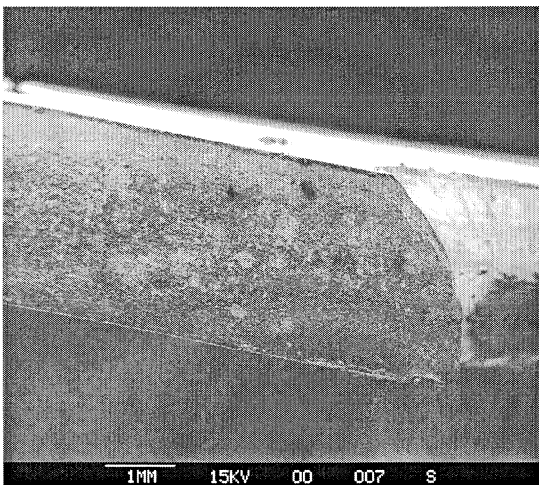


Figure 255 11F6L

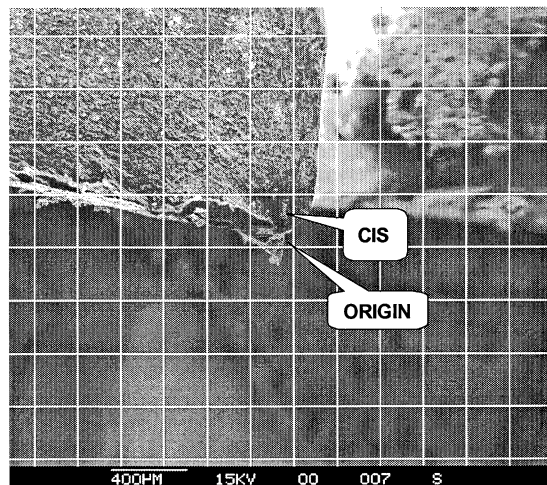


Figure 256 11F6L Nucleation Site



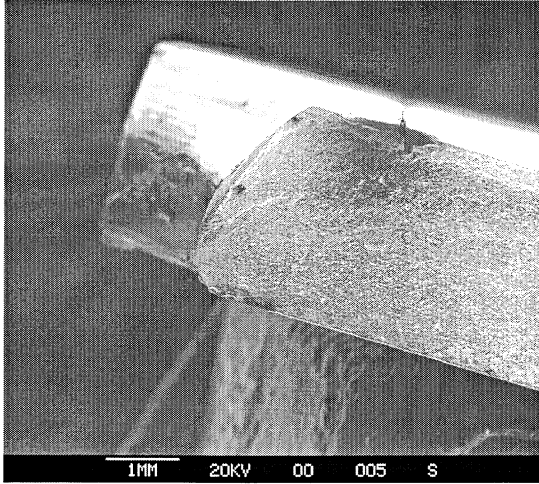


Figure 257 11F6R

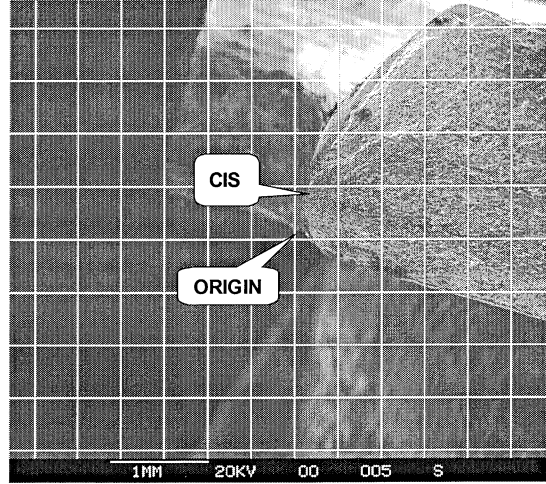


Figure 258 11F6R Nucleation Site

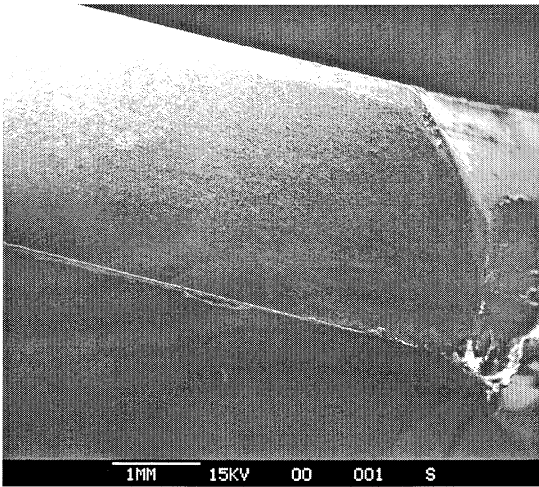


Figure 259 11F7L

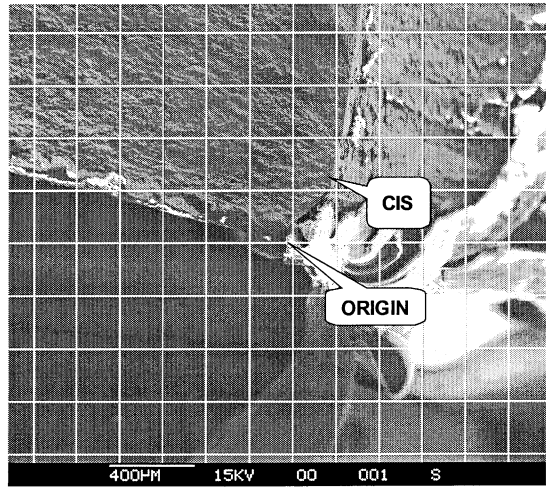


Figure 260 11F7L Nucleation Site

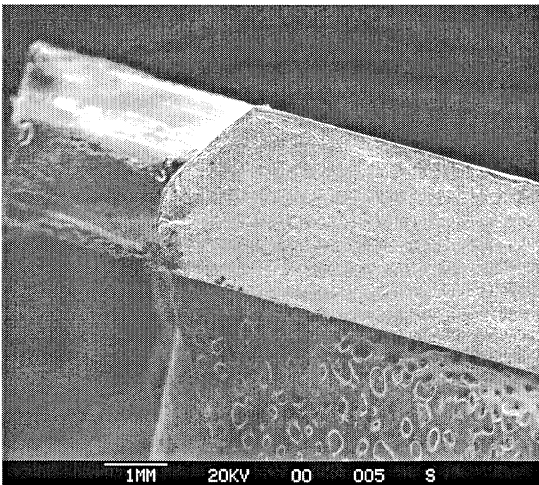


Figure 261 11F7R

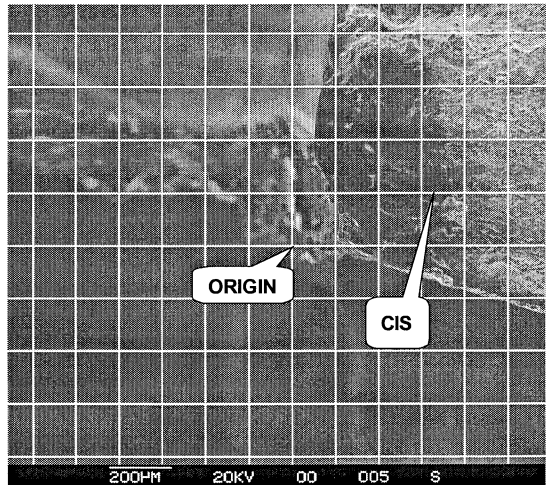


Figure 262 11F7R Nucleation Site

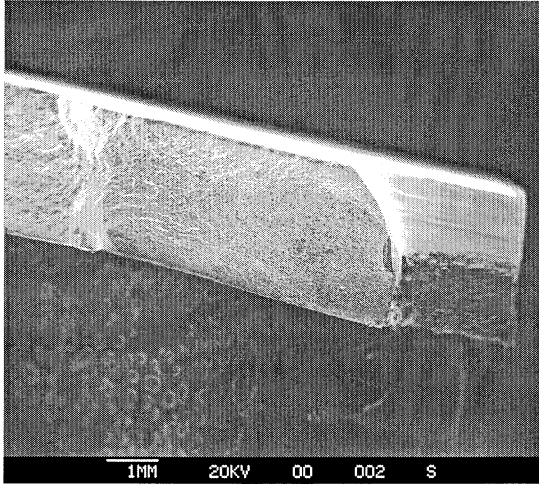


Figure 263 11F8L

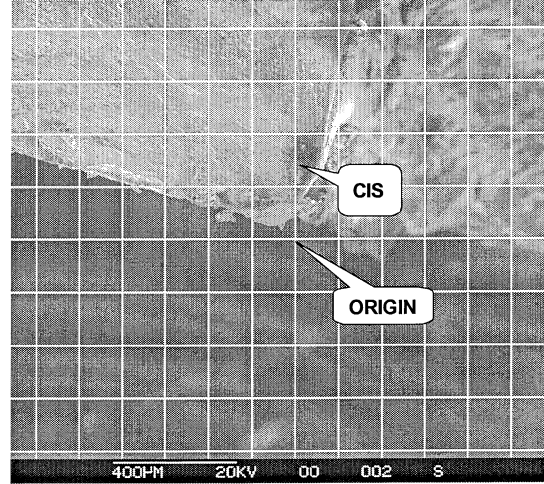


Figure 264 11F8L Nucleation Site

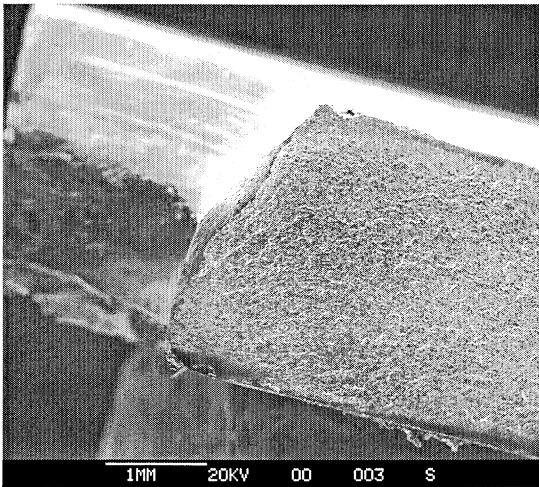


Figure 265 11F8R

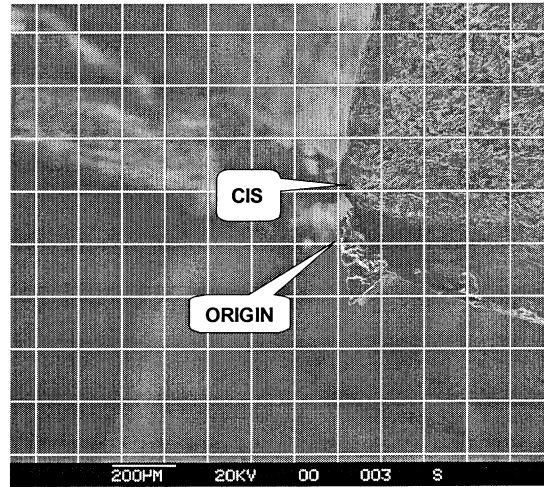


Figure 266 11F8R Nucleation Site

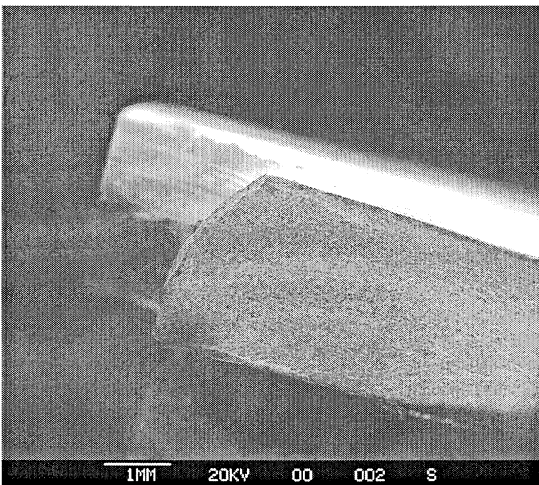


Figure 267 11F9R

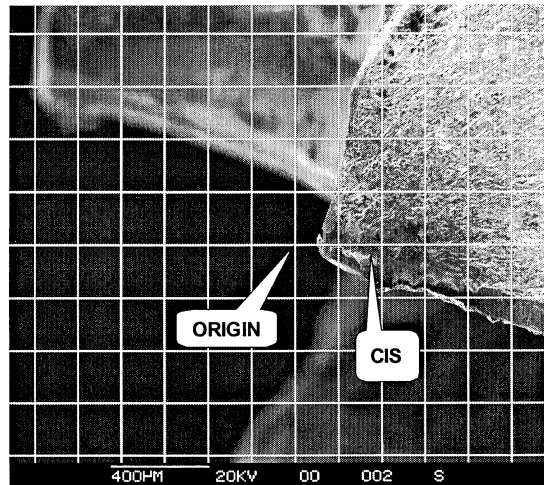


Figure 268 11F9R Nucleation Site

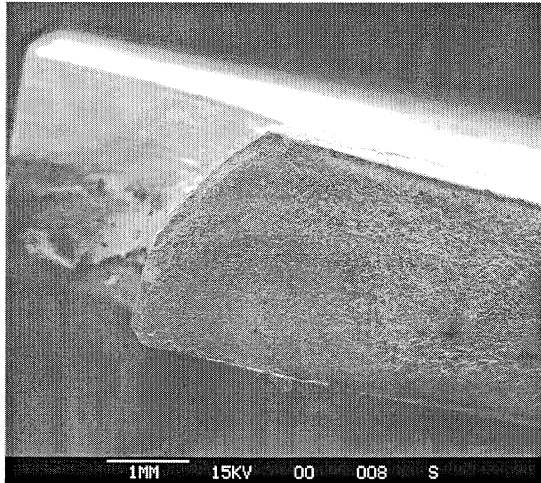


Figure 269 11F10R

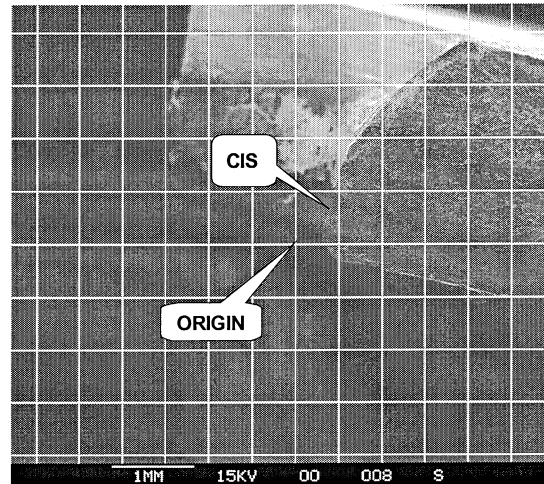


Figure 270 11F10R Nucleation Site

Space Intentional Left Blank



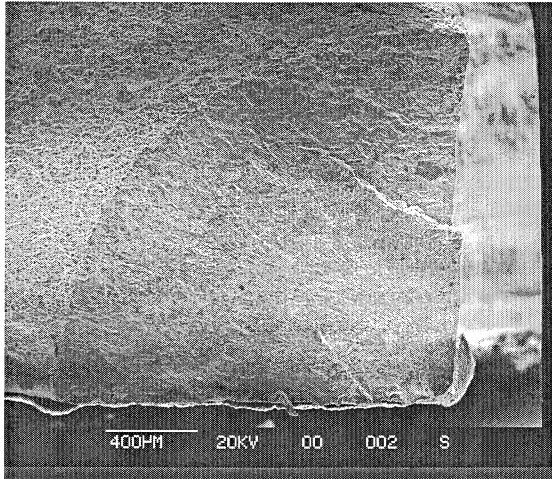


Figure 271 15E2R

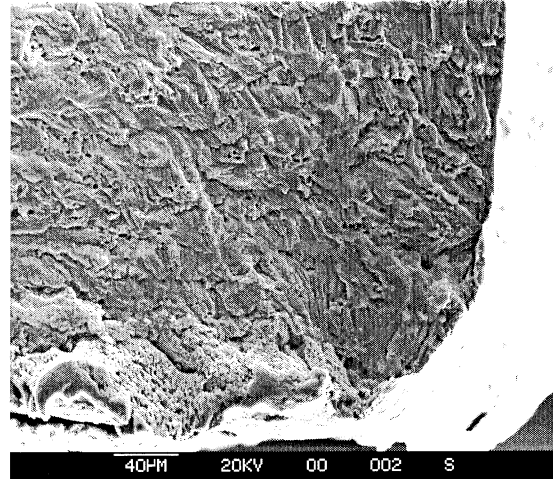


Figure 272 15E2R Nucleation Site

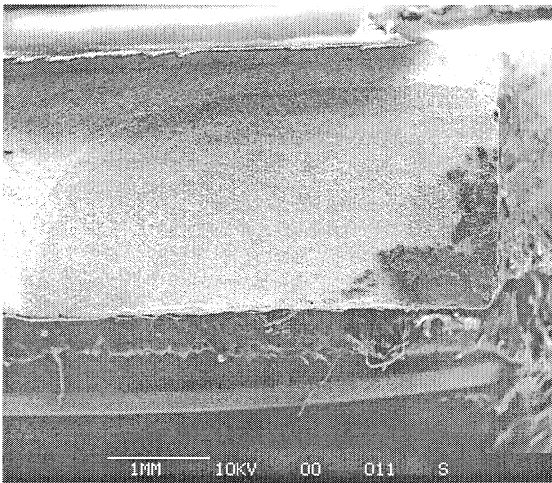


Figure 273 15E11R

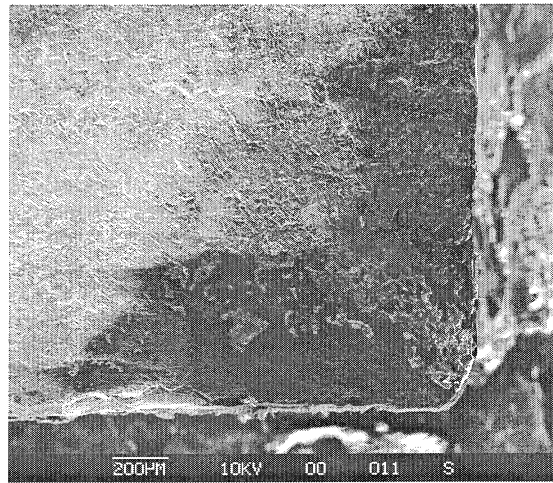


Figure 274 15E11R Nucleation Site

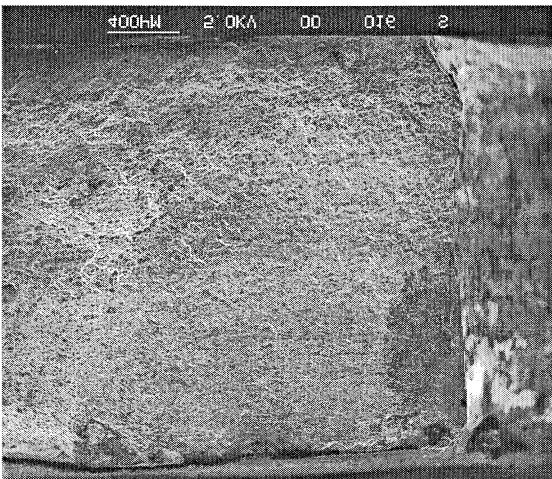


Figure 275 15E16L

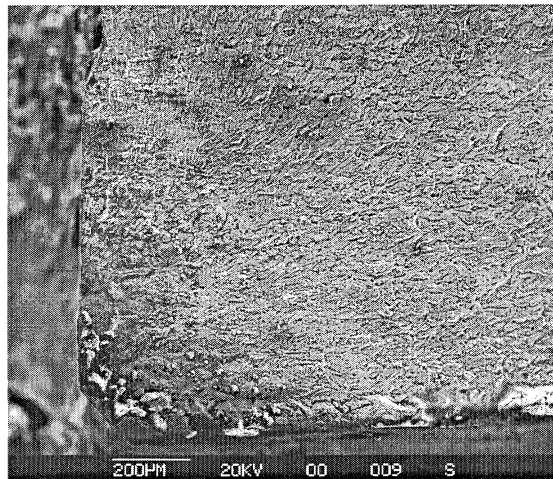


Figure 276 15E16L Nucleation Site



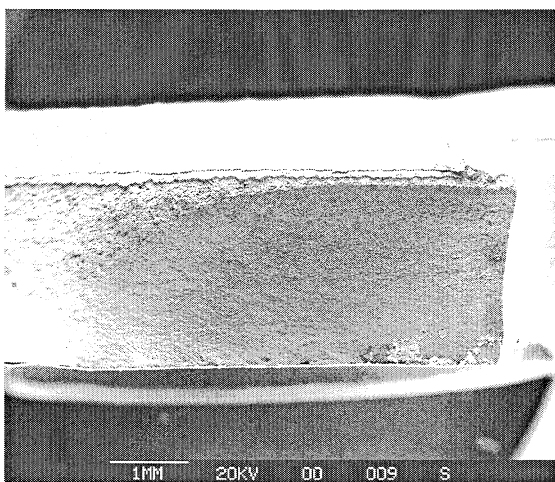


Figure 277 15E16R

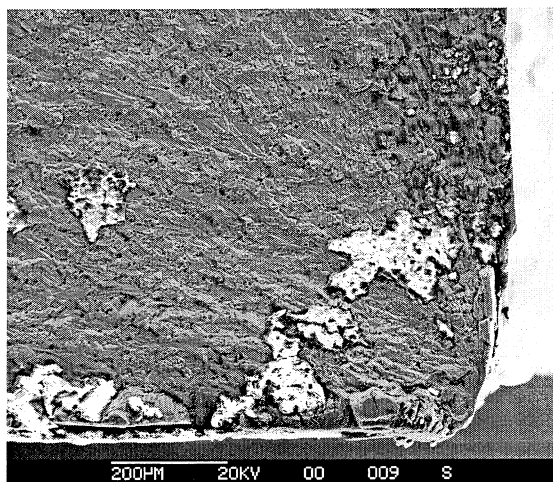


Figure 278 15E16R Nucleation Site

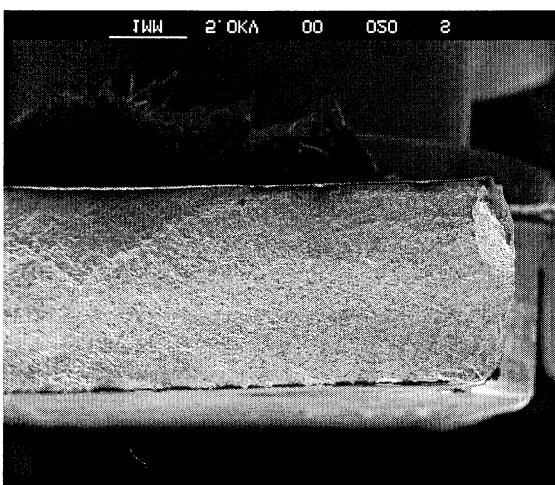


Figure 279 15E20L

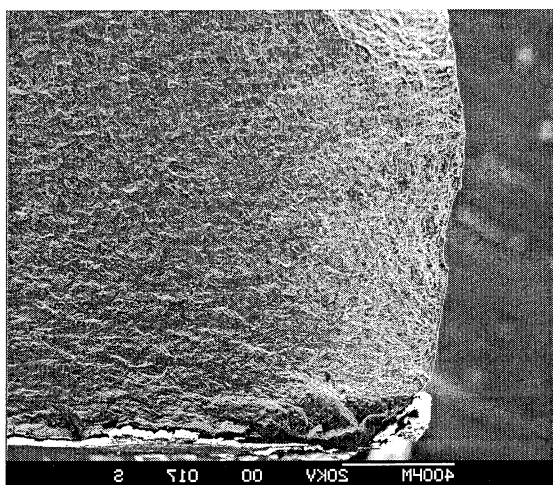


Figure 280 15E20L Nucleation Site

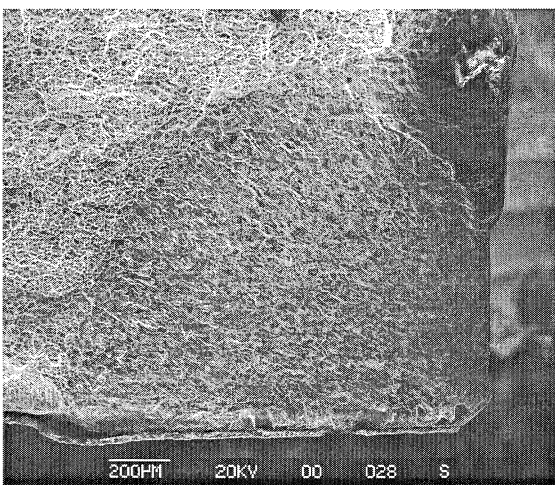


Figure 281 15E28R

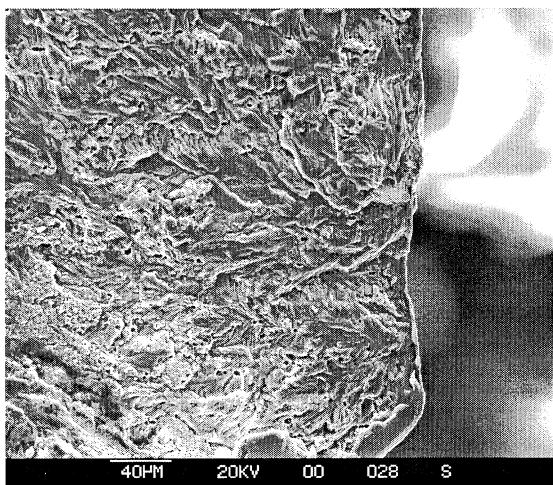


Figure 282 15E28R Nucleation Site

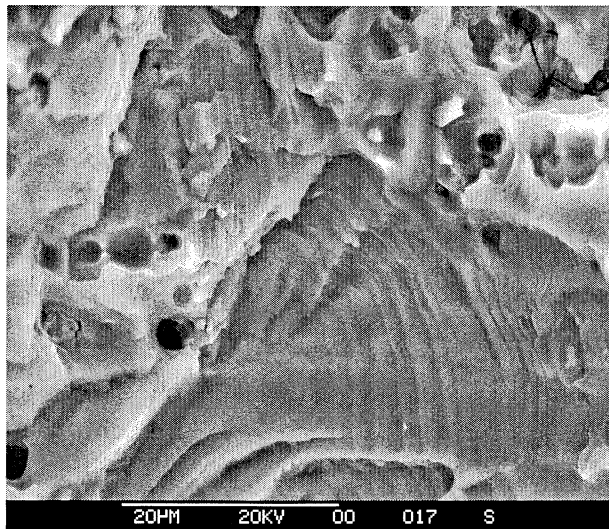


Figure 283 15E20L Marker Bands

Space Intentionally Left Blank

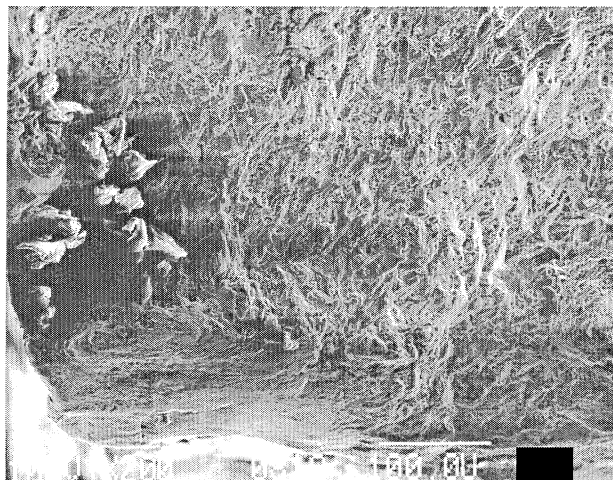


Figure 284 No Cleaning

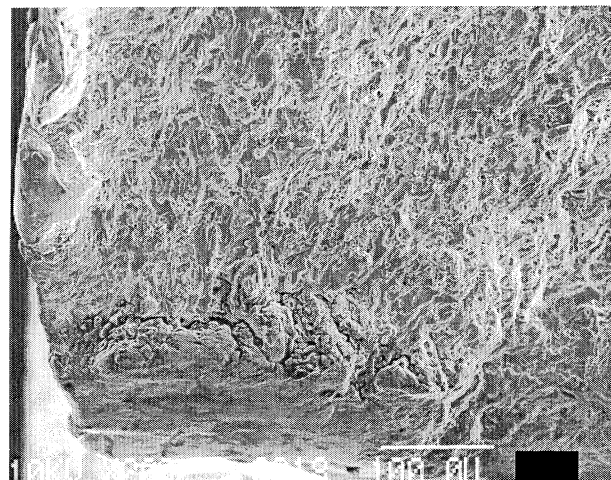


Figure 285 1 Minute 2% MicroClean™, Sonicate

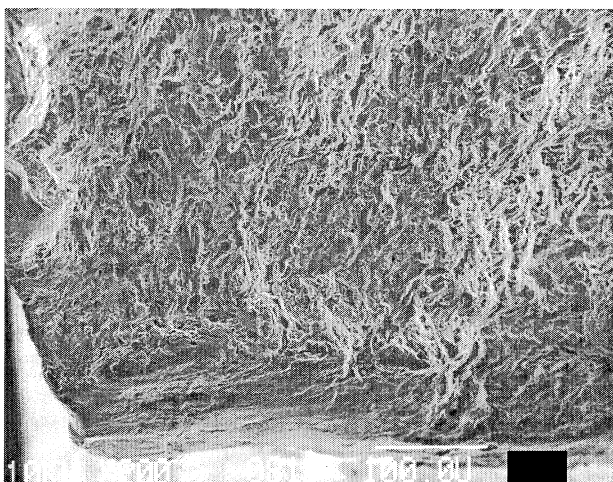


Figure 286 5 Minute 2% MicroClean™, Sonicate

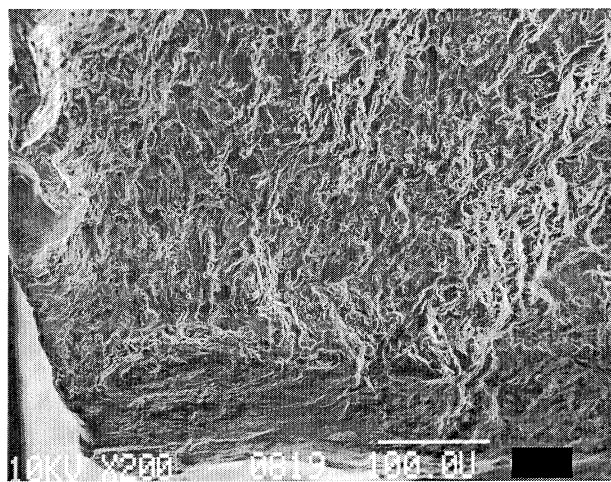


Figure 287 25 Minute 2% MicroClean™, Sonicate

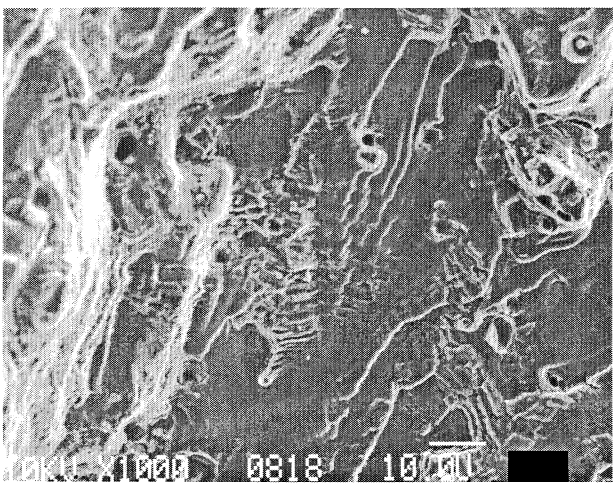


Figure 288 No Cleaning

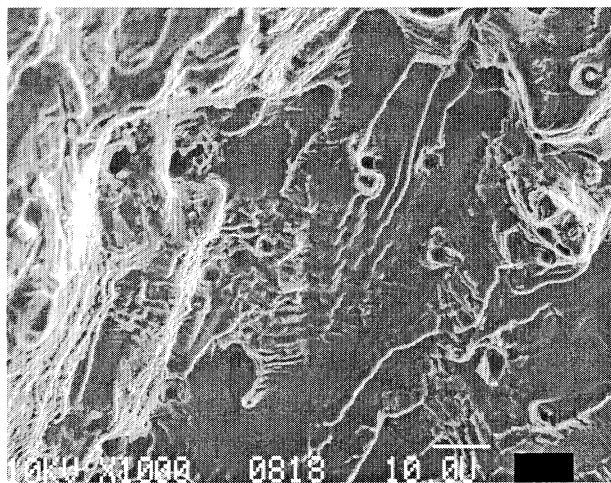


Figure 289 1 Minute 2% MicroClean™, Sonicate



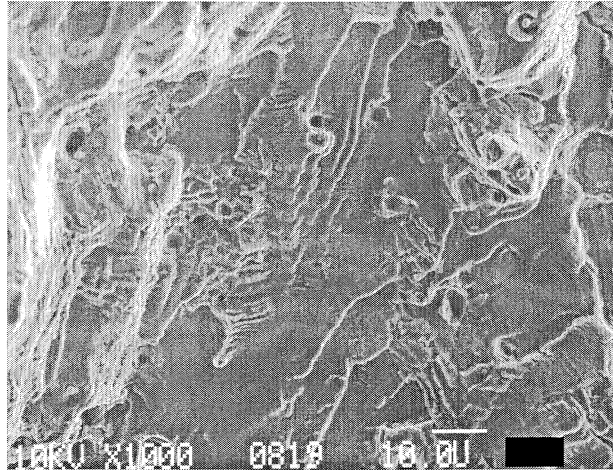


Figure 290 5 Minute 2% MicroClean™, Sonicate



Figure 291 25 Minute 2% MicroClean™, Sonicate

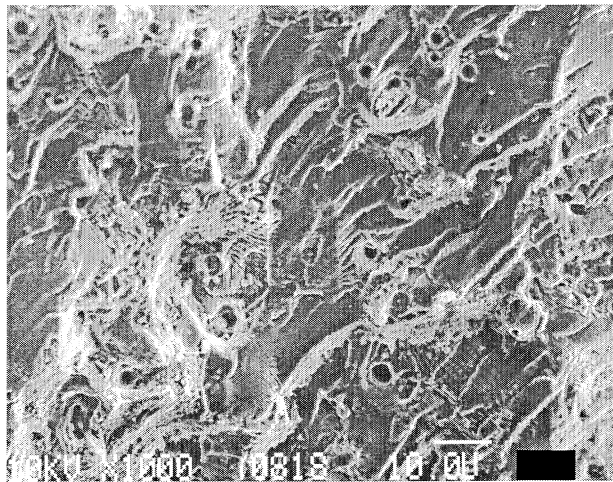


Figure 292 No Cleaning

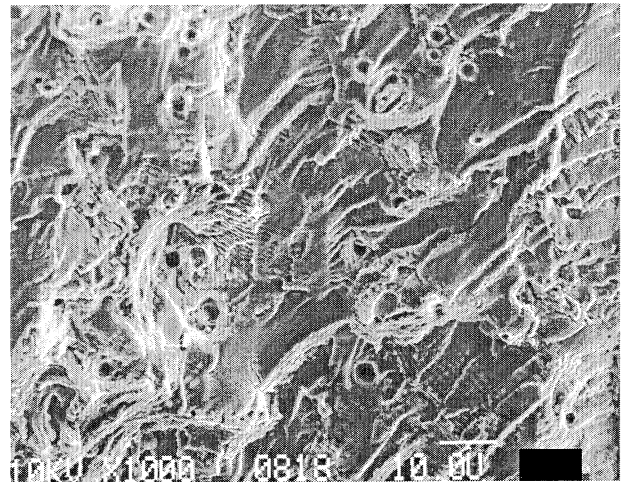


Figure 293 1 Minute 2% MicroClean™, Sonicate

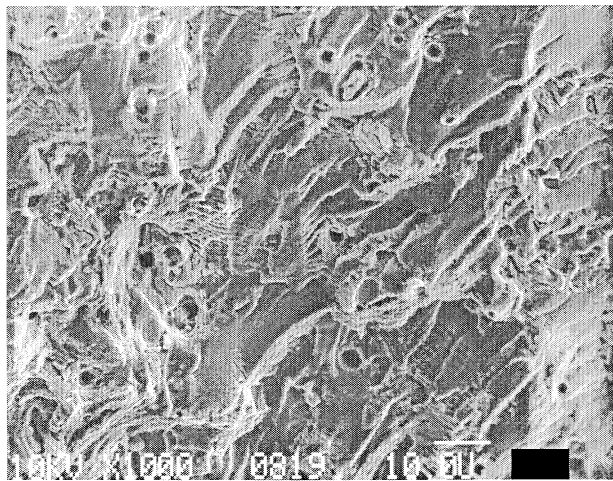


Figure 294 5 Minute 2% MicroClean™, Sonicate

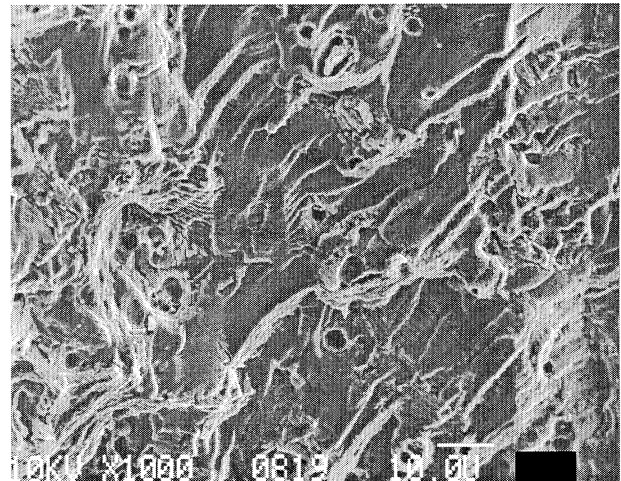


Figure 295 25 Minute 2% MicroClean™, Sonicate

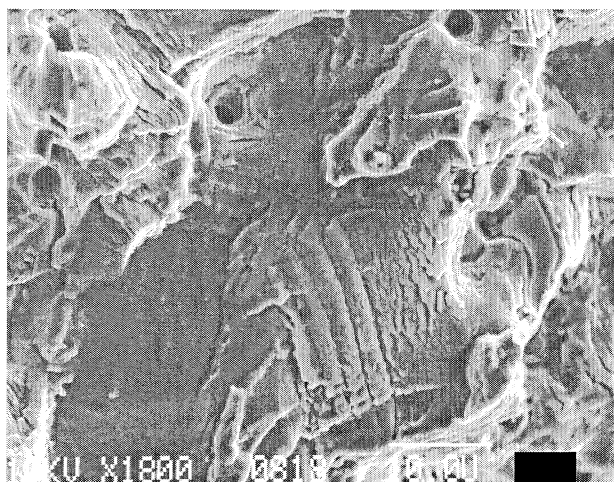


Figure 296 1 Minute 2% MicroClean™, Sonicate

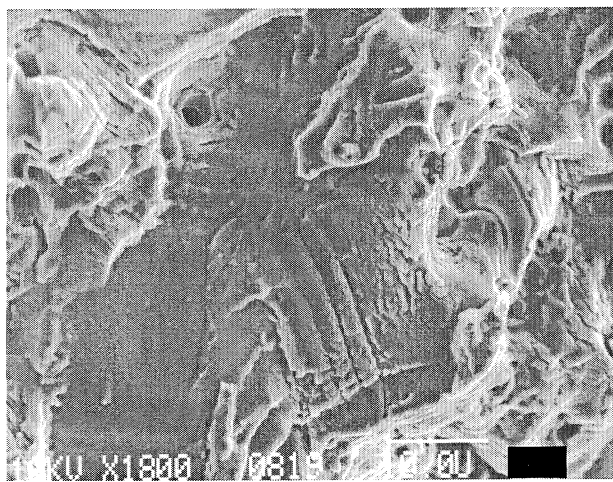


Figure 297 5 Minute 2% MicroClean™, Sonicate

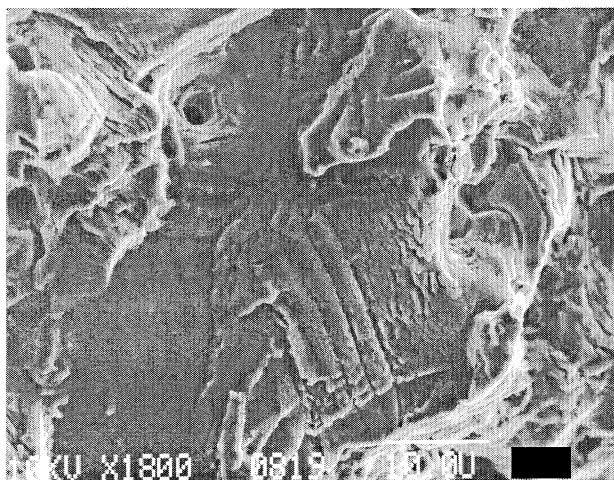


Figure 298 25 Minute 2% MicroClean™, Sonicate

## Appendix E Rotating Self-Nulling Eddy Current Probe System Data

In the tables that follow, the rivet row designation is in accordance with Appendix C. Eddy current equipment calibration standards were used to establish the sensitivity level for the inspection of the different panel configurations. Electrical discharge machined notches; 0.030, 0.040, 0.050, and 0.075 in. in length are machined into the 2024-T3 skins, which are 0.063" (standard A) and 0.084" (standard B).

EIFS-3 ZB118853-1				
Cycles	Row A	Row C	Row D	Standard
90,000	No cracks	No crack	No cracks	B .050 - 52 .075 - 26 A .050 - 34 .075 - 81
100,000	No cracks	No cracks	No cracks	B .050 - 59 .075 - 35 A .050 - 33 .075 - 105
110,000	No cracks	No cracks	No cracks	B .050 - 52 .075 - 33 A .050 - 38 .075 - 126
120,000	No cracks	No cracks	No cracks	B .050 - 57 B .075 - 29 A .050 - 49 A .075 - 124
130,000	No cracks	No cracks	No cracks	B .050 - 64 .075 - 23 A .050 - 42 .075 - 122
140,000	No cracks	C4 21 C14 17+ C16 16+	No cracks	B .050 - 59 .075 - 28 A .050 - 43 .075 - 128
150,000	No cracks	C4 = 17 C14 = 17 C16 = 30 C17 = 17	No cracks	B .050 - 59 B .075 - 36 A .050 - 44 A .075 - 132
160,000	No cracks	C4 = 16 C14 = 22 C16 = 23 C17 = 17 C21 = 20	D15 = 139	B .050 - 63 .075 - 40 A .050 - 48 .075 - 127
170,000	No cracks	C4 = 21 C14 = 22 C15 = 17 C16 = 27 C17 = 22	D15=165 @ -1.7  150 @ + 1.9	B .050 - 54 B .075 - 34 A .050 - 48 A .075 - 124

EIFS-4 ZB118853-1				
Cycles	Row A	Row C	Row D	Standard
60,000	No Cracks	C 24-31	No Cracks	A .050 44 .075 129 B .050 65 .075 33
80,000	No Cracks	C 14-25 C 24-41	No Cracks	A .050-39 .075-121 B .050-63 .075-32
90,000	No Cracks	C8-17 C14-30 C17-23 C24-42	No Cracks	A .050-40 .075-123 B .050-56 .075-36
100,000	No Cracks	C13-21 C14-35 C17-20 C21-23 C24-43	No Cracks	A .050-45 .075-122 B .050-65 .075-38
110,000	No Cracks	C13-27 C14-41 C17-24 C19-20 C20-18 C21-25 C24-52	No Cracks	A .050-39 .075-124 B .050-53 .075-31
120,000	No Cracks	C13-40 C14-58 C16-17 C17-32 C18-19 C19-37 C20-26 C21-47 C22-18 C23-17 C24-75	No Cracks	A .050-46 .075-144 B .050-56 .075-33
130,000	No Cracks	C13-40 C14-58 C16-28 C17-34 C18-18 C19-52 C20-22 C21-52 C22-24 C23-20 C24-71 C25-18	No Cracks	A .050-50 .075-128 B .050-47 .075-43
140,000	No Cracks	C9-17 C13-52 C14-65 C15-22 C16-38 C17-41 C19-52 C20-25 C21-52 C22-28 C23-37 C24-79 C25-22	D11-19	A .050-44 .075-143 B .050-45 .075-40

EIFS-4 ZB118853-1				
Cycles	Row A	Row C	Row D	Standard
150,000	A15-19	C9-20 C13-53 C14-73 C15-29 C16-55 C17-49 C19-63 C20-27 C21-60 C22-29 C23-34 C24-82 C25-30	D11-18	A .050-42 .075-140 B .050-43 .075-34
160,000	A15-51	C9-28 C13-48 C14-64 C15-32 C16-53 C17-46 C19-63 C20-25 C21-61 C22-32 C23-41 C24-78 C25-28	D11-19	A .050-41 .075-131 B .050-58 .075-39
170,000	A15-142	C9-22 C13-59 C14-67 C15-42 C16-58 C17-48 C19-65 C20-26 C21-67 C22-44 C23-48 C24-81 C25-22	D11-19	A .050-43 .075-127 B .050-57 .075-35

EIFS-9 ZB118853-503							
Cycles	1st Row A	1st Row F	2nd Row A	2nd Row F	Row B	Row E	Standard
60,000	No Cracks	No Cracks	No Cracks	No Cracks	No Cracks	No Cracks	A .050=79 .075=211 B .050=66 .075=154
80,000	No Cracks	No Cracks	No Cracks	No Cracks	No Cracks	No Cracks	A .050=81 .075=217 B .050=65 .075=160
100,000	No Cracks	No Cracks	No Cracks	No Cracks	No Cracks	No Cracks	A .050=82 .075=220 B .050=63 .075=162
120,000	A2=24	No Cracks	A2=1.8	No Cracks	No Cracks	No Cracks	A .050=87 .075=218 B .050=72 .075=176
130,000	A2=34	No Cracks	A2=2.2	No Cracks	No Cracks	No Cracks	A .050=84 .075=226 B .050=64 .075=143
140,000	A2=40	No Cracks	A2=3.5	No Cracks	No Cracks	No Cracks	A .050=82 .075=222 B .050=68 .075=150
150,000	A2=55	No Cracks	A2=6.2	No Cracks	No Cracks	No Cracks	A .050=83 .075=214 B .050=62 .075=148
160,000	A2=80	No Cracks	A2=9.3	No Cracks	No Cracks	No Cracks	A .050=78 .075=196 B .050=60 .075=145
170,000	A2=142	No Cracks	A2=11.2		No Cracks	No Cracks	A .050=79 .075=210 B .050=60 .075=159
180,000	A2=223	No Cracks	A2=19.7	No Cracks	No Cracks	No Cracks	A .050=76 .075=204 B .050=62 .075=150
190,000	A2=233	No Cracks	A2=29.9	No Cracks	No Cracks	No Cracks	A .050=77 .075=216 B .050=62 .075=150
200,000	A2=255	F1=18	A2=31.1	No Cracks	No Cracks	No Cracks	A .050=81 .075=221 B .050=66 .075=154
210,000	A2=262	F1=21	A2=38.7	No Cracks	No Cracks	No Cracks	A .050=88 .075=225 B .050=67 .075=168
220,000	A2=278	F1=19	A2=43	No Cracks	No Cracks	No Cracks	A .050=82 .075=221 B .050=70 .075=166
230,000	A2=304	F1=18	A2=36.9	No Cracks	No Cracks	No Cracks	A .050=80 .075=212 B .050=66 .075=160
240,000	A2=305	F1=15	A2=39.8	No Cracks	No Cracks	No Cracks	A .050=81 .075=201 B .050=58 .075=151

EIFS-9 ZB118853-503							
Cycles	1st Row A	1st Row F	2nd Row A	2nd Row F	Row B	Row E	Stan
250,000	A2=320	F1=16 F13=17	A2=46.1	F13=1.8	No Cracks	No Cracks	A
260,000	A1=283 A2=300	F1=16 F13=19	A1=36.5 A2=40.6	F+3=2.6	No Cracks	No Cracks	A B
Removed Edge Crac,000s at 259,601 cycles							
270,000	No Cracks	No Cracks	No Cracks	No Cracks	No Cracks	No Cracks	A B
290,000	No Cracks	No Cracks	No Cracks	No Cracks	No Cracks	No Cracks	A B
310,000	No Cracks	No Cracks	No Cracks	No Cracks	No Cracks	No Cracks	A B
330,000	No Cracks	No Cracks	No Cracks	No Cracks	No Cracks	No Cracks	A B
350,000	A3=64	No Cracks	A3=4.6	No Cracks	No Cracks	No Cracks	A B
370,000	A3=62	No Cracks	A3=4.8	No Cracks	No Cracks	No Cracks	A B
Cut Upper/Lower Sheets into DogBone							
390,000	A3=62	No Cracks	A3=4.9	No Cracks	No Cracks	No Cracks	A B
410,000	A3=65	No Cracks	A3=5.2	No Cracks	No Cracks	No Cracks	A B
430,000	A3=70	No Cracks	A3=5.2	No Cracks	No Cracks	No Cracks	A B
450,000	A3=63	No Cracks	A3=7.4	No Cracks	No Cracks	No Cracks	A B
467,000	A3=65 A5=21	No Cracks	A3=5.5 A5=1.6	No Cracks	Not Checked	Not Checked	A
472,000	A3=69 A5=33	No Cracks	A3=5.3 A5=3.7				A
480,000	A3=72 A5=120		A3=5.3 A5=11.6	No Cracks			A
490,000	A3=61 A5=298	No Cracks	A3=5.4 A5=35.8				A



EIFS-10 ZB118853-503							
Cycles	1st Row "A"	1st Row "F"	2nd Row "A"	2nd Row "F"	Row "B"	Row "E"	Standard
32,000	No Cracks	No Cracks	No Cracks	No Cracks	No Cracks	No Cracks	A .050=87 .075=164 B .050=63 .075=155
32,000 Dogbone	A1=11 A2=38 C A12=15 C A13=10 A3=4 A11=1	F1=31C F2=16 C F12=7 F13=32 C F3=5 F11=5	A1=1.7C A2=1.6 C A12=1.2 C A13=1.4 C A3=0.5 A11=0.2	F1=1.4 C F2=2.5 C F12=2.2 C F13=6.0 C F3=0+F59.5 F11=.4	No Cracks	No Cracks	A .050=83 .075=220 B .050=54 .075=154
42,000	A1=10 A2=41 C A12=20 C A13=8	F1=24 C F2=46 C F12=30 C F13=25 C	A2=2.7 C A12=2.7 C	F2=2.3 C F12=3.5 C			A .050=100 .075=255 B .050=51 .075=135
62,000	A1=14 A2=53 C A12=21 C A13=13	F1=24 C F2=48 C F12=33 C F13=34 C	A2=4.6 C A12=2.3 C A13=	F1=1.3 C F2=2.3 C F12=3.0 C F8=5.7 C	No Cracks	No Cracks	A .050=81 .075=216 B .050=62 .075=161
72,000	A1=10 A2=40 C A12=19 C A13=10	F1=20 C F2=42 C F12=31 C F13=34 C	A1=28.8 C A2=3.0 C A12=2.6 C A13=	F1=1.3 C F2=2.4 C F12=3.0 C F13=4.7 C	No Cracks	No Cracks	A .050=79 .075=205 B .050=52 .075=154
82,000	A1=11 A2=40 A12=21 A13=10	F1=21 F2=38 F12=27 F13=33	A1= A2=2.3 C A12=2.9 C A13=	F1=1.3 C F2=2.3 C F12=2.8 C F13=6.4 C	No Cracks	No Cracks	A .050=83 .075=221 B .050=73 .075=156
92,000	A1=10 A2=48 C A12=19 C A13=8	F1=26 C F2=38 C F12=26 C F13=30 C	A1= A2=2.7 C A12=2.5 C A13=	F1=1.2 C F2=2.4 C F12=3.2 C F13=6.6 C	No Cracks	E22 Border	A .050=87 .075=213 B .050=63 .075=157
112,000	A1=8 A2=48 C A12=18 C A13=7	F1=26 C F2=38 C F12=29 C F13=31 C	A1= A2=3.3 C A12=2.4 C A13=	F1=1.3 C F2=2.5 C F12=3.2 C F13=5.4 C	B1=15 B17=15 B19=15 B20=16 B23=16 B24=21 B26=20	E7=15 E8=16 E9=19 E10=18 E11=15 E12=16 E18=19 E19=17 E20=16 E22=15	A .050=85 .075=224 B .050=68 .075=164
122,000	A1=10 A2=38 A12=24 A13=6	F1=22 F2=41 F12=26 F13=25	A1= A2=1.5 A12=2.8 A13=	F1=1.4 F2=2.2 F12=2.6 F13=6.8	No Cracks	No Cracks	A .050=81 .075=212 B .050=65 .075=158
142,000	A1=8 A2=37 A12=19 A13=9	F1=25 F2=39 F12=32 F13=32	A1= A2=2.2 A12=2.5 A13=	F1=1.5 F2=2.2 F12=3.4 F13=5.9	No Cracks	No Cracks	A .050=88 .075=220 B .050=68 .075=167
162,000	A1=10 A2=40 A12=21 A13=8	F1=20 F2=38 F12=28 F13=25	A1= A2=2.4 A12=2.4 A13=	F1=1.5 F2=1.8 F12=2.9 F13=5.8	No Cracks	No Cracks	A .050=81 .075=212 B .050=63 .075=154

EIFS-11 ZB 118853-503							
Cycles	1st Row "A"	1st Row "F"	2nd Row "A"	2nd Row "F"	Row B	Row E	Standard
	A1=4	F1=12	A1=1.5	F1=1.1	B1=21	E2=20	A .050=89
	A13=24	F13=34	A2=0.1	F2=0.6	B2=21	E3=19	.075=238
		F2=10	A12=3.2	F12=1.3	B3=22	E4=20	B .050=70
	A2=9	F12=44	A13=2.4	F13=1.9	B6=18	E5=21	.075=174
	A12=28				B7=22	E6=16	
					B8=18	E7=21	
					B9=17	E8=18	
					B10=20	E9=18	
					B11=20	E10=18	
					B12=20	E11=18	
					B13=20	E12=22	
					B14=22	E13=20	
					B15=21	E14=17	
					B16=17	E15=23	
					B17=20	E16=18	
					B18=21	E17=20	
					B19=25	E18=21	
					B20=19	E19=17	
					B21=17	E20=23	
					B22=20	E21=22	
					B25=21	E22=18	
					B26=21	E23=18	
					B27=17	E24=17	
50,000	A1-26	F1-24	A1-1.8	F1-1.2	B2-18	E7-16	A .050=89
	A12-19	F2-39	A2-0.4	F2-2.7	B3-23	E8-17	.075=230
	A12-26	F12-53	A12-2.2	F12-2.3	B5-16	E9-18	B .050=68
	A13-35	F13-31	A13-2.1	F13-3.4	B6-15	F10-15	.075=180
					B7-16	F11-15	
					B8-16	E12-19	
					B9-17	E13-17	
					B10-17	E14-21	
					B11-18	E15-21	
					B12-21	E16-17	
					B13-16	E17-20	
					B14-22	E18-22	
					B15-18	E19-23	
					B16-16	E20-15	
					B17-18	E21-15	
					B18-21	E22-18	
					B19-19	E23-17	
					B20-20	E24-18	
					B21-18	E25	
					B22-18	E26-30	
					B23-21	E27-24	
					B24-24		
					B25-21		
					B26-18		
					B27-18		

(cont.)	EIFS-11 ZB 118853-503						
Cycles	1st Row "A"	1st Row "F"	2nd Row "A"	2nd Row "F"	Row B	Row E	Standard
75,000	A1=25 A2=18 A12=24 A13=40	F1=32 F2=45 F12=68 F13=32	A1=1.4 A2=1.1 A12=2.3 A13=1.9	F1=1.4 F2=1.6 F12=1.6 F13=3.0	No Cracks	No Cracks	A .050=83 .075=240 B .050=78 .075=187
100,000	A1-30 A2-12 A12-20 A13-42	F1-31 F2-57 F12-73 F13-32	A1-1.4 C A2-0.2 A12-1.8 C A13-2.0 C	F1-1.4 C F2-18 C F12-1.9 C F13-3.2 C	No Cracks	No Cracks	A .050=79 .075=212 B .050=65 .075=162
123987	A1- A2-38 A12-34 A13-	F1-54 F2- F12-78 F13-75	A1-6.2 A2-1.9 A12-2.9 A13-1.5	F1-2.0 F2-3.4 F12-2.5 F13-6.8	No Cracks	No Cracks	A .050=82 .075=219 B .050=68 .075=161
135,000	A1-10 A2=15 A12=13 A13=53	F1=23 F2=36 F6=80 F1=59 F12=19 F13=39	A1=1.4 A2=1.0 A12=1.6 A13=2.5	F6=6.4 F7=5.5 F9=1.2 F1=1.1 F2=1.3 F12=2.2 F13=3.1			A .050=91 .075=225 B .050=66 .075=162
145,000	A1=9 A2=13 A12=13 A13=58	F1=29 F2=23 F12=23 F13=40 F6=341 F7=369 F9=71 F10=42	A1=1.5 A2=1.0 A12=1.7 A13=2.7	F6=36 F7=32 F9=6.0 F10=4.1 F1=1.8 F2=1.6 F12=2.1 F13=2.1		E12=20	A .050=91 .075=236 B .050=65 .075=172

EIFS-12 ZB 118853-503								
Cycles	1st Row "A"	1st Row "F"	2nd Row "A"	2nd Row "F"	Row "B"	Row "E"		Standard
50K	A1=50 A2=31 A12=62 A13=54	F1=27 F2=47 F12=58 F13=69	A1=3.7 A2=2.3 A12=2.9 A13=4.2	F1=3.7 F2=4.1 F12=2.6 F13=5.4	B12=21 B17=21 B19=19 B24=22 B27=18	E3=19 E4=18 E5=23 E7=20 E8=23 E9=20 E13=18 E14=18 E15=18 E16=22 E17=24 E20=23 E21=21 E22=19 E25=19 E26=24 E27=16		A .050=91 B .075=221 B .050=70 B .075=167
75K	A1=52 A2=22 A12=54 A13=54	F1=22 F2=41 F12=51 F13=69	A1=3.6 A2=2.6 A12=3.0 A13=4.0	F1=3.6 F2=4.0 F12=2.8 F13=5.3		E20=18		A .050=83 A .075=234 B .050=75 B .075=168
100K	A1=46 A2=27 A12=56 A13=49	F1=31 F2=42 F12=58 F13=68	A1=4.0 A2=3.1 A12=2.7 A13=4.5	F1=4.1 F2=3.8 F12=3.1 F13=5.3	B26=28 B27=23	E3=26 E4=20 E5=20 E6=27 E7=20 E9=24 E10=28 E11=25 E12=24 E13=18 E18=23 E23=24		A .050=93 B .075=245 B .050=67 B .075=162
125K	A1-4.5 A2-3.1 A12-60 A13-55	F1-35 F2-50 F12-57 F13-69	A1-3.3 A2-2.5 A12-2.4 A13-4.0	F1-3.5 F2-4.0 F13-3.2 F13-4.8	6-21 10-25 11-16 12-18 19-18 20-17 21-19 26-18	E1=24 E2=22 E3=19 E4=21 E5=23 E6=16 E7=21 E8=30 E9=17 E10=27 E11=21 E12=18 E13=24	E14-19 E15-17 E16-18 E17-24 E18-17 E19-25 E20-18 E21-20 E22-17 E23-16 E24-24	A .050=85 B .075=223 B .050=68 B .075=166
150K	A1-50 A2-30 A12-54 A13-55	F1-31 F2-46 F12-50 F13-69	A1-3.5 A2-2.4 A12-2.1 A13-3.9	F1-3.9 F2-3.8 F12-4.3 F13-5.3	No Cracks	No Cracks		A .050-80 B .075-220 B .050-67 B .075-159
175K	A1-52 A2-30 A12-39 A13-52 A8-59	F1-30 F2-44 F12-49 F13-65	A1-4.1 A2-2.8 A12-2.3 A13-3.8 A8-5.4	F1-3.8 F2-4.0 F12-3.6 F13-5.6	No Cracks	No Cracks		A .050-83 B .075-213 B .050-67 B .075-162
185K	A1-53 A2-29 A12-32 A13-55 A4-281	F1-32 F2-48 F12-44 F13-63	A1-3.2 A2-2.7 A12-1.8 A13-3.9 A7-1.2 A8-30.2	F1-4.1 F2-3.5 F12-3.1 F13-5.3				A .050-82 B .075-222 B .050 B .075
195K	A1-44 A2-32 A12-36 A13-53 A8-310	F1-32 F2-45 F12-48 F13-65						A .050-82 B .075-222
205K	A1-49 A2-38 A12-39 A13-53 A7-19	F1-37 F2-45 F12-44 F13-76	A8-298					A .050-79 B .075-206

EIFS-13 ZB118853-505					
Cycles	Row "A"	Row "B"	Row "G"	Row "11"	Standard
100,000	No Crack	No Crack	No Crack	No Crack	B .050=45 .075=131 A .050=60 .075=73
125,000	No Crack	No Crack	No Crack	No Crack	A .050-42 .075-132 B .050-59 .075-70
150,000	No Crack	No Crack	No Crack	No Crack	A .050-37 .075-130 B .050-55 .075-76
175,000	No Crack	No Crack	No Crack	No Crack	A .050-42 .075-135 B .050-54 .075-69
200,000	A4-17	No Crack	No Crack	No Crack	A .050-39 .075-139 B .050-58 .075-72
210,000	A4-17	No Crack	No Crack	No Crack	A .050-40 .075-136 B .050-55 .075-76
220,000	A3-22 A4-30 A5-15	No Crack	No Crack	On verge of crack	A .050-45 .075-137 B .050-62 .075-66
230,000	A3-22 A4-27 A5	No Crack	No Crack	H12-19	A .050-42 .075-133 B .050-51 .075-74
240,000	A3-30 A4-35 A5-16	No Crack	No Crack	H12-19 H13-15	A .050-40 .075-131 B .050-52 .075-71
250,000	A3-37 A4-35 A5-17	No Crack	No Crack	H12-22 H13-18	A .050-43 .075-130 B .050-55 .075-71
260,000	A3-36 A4-36 A5-17	No Crack	No Crack	H12-24 H13-20	A .050-41 .075-136 B .050-57 .075-75
270,000	A3-39 A4-41 A5-20	No Crack	No Crack	H12-27 H13-22	A .050-40 .075-137 B .050-56 .075-70
280,000	A3-46 A4-42 A5-21	No Crack	No Crack	H12-28 H13-25	A .050-41 .075-142 B .050-62 .075-74
290,000	A3-51 A4-49 A5-21	No Crack	No Crack	H3-19 H12-30 H13-26	A .050-40 .075-137 B .050-57 .075-77
300,000	A3-56 A4-60 A5-21	No Crack	No Crack	H3-32 H4-15 H12-34 H13-28	A .050-45 .075-133 B .050-54 .075-77

EIFS-14 ZB118853-505							
Cycles	Row "A"	Row "B"	Row "G"	Row "H"	Row "D"	Row "E"	Standard
75,000	No Crack	No Crack	No Crack	No Crack	No Crack	No Crack	A .050=38 .075=137 B .050=63 .075=68
150,000	No Crack	No Crack	No Crack	No Crack	No Crack	No Crack	A .050=41 .075=129 B .050=56 .075=73
225,000	A3=15 A12=32	B20=28 B22=26 B24=22	No Crack	No Crack	No Crack	No Crack	A .050=43 .075=132 B .050=56 .075=76
240,000	A3=25 A12=54	B20=32 B22=31 B24=20	G16=18	No Crack	No Crack	No Crack	A .050=42 .075=140 B .050=57 .075=76
255,000	A3=28 A5=15 A8=19 A9=18 A12=60	B5=17 B24=31 B10=19 B16=15 B20=40 B22=32	G16=21 G18=20	No Crack	No Crack	No Crack	A .050=39 .075=137 B .050=54 .075=75
270,000	A5=36 A10=2 A5=21 A12=7 A7=18 A13=2 A8=33 A9=24	B5=23 B24=38 B10=27 B16=19 B20=43 B22=41	G16=29 G18=31 G19=25	No Crack	No Crack	No Crack	A .050=39 .075=132 B .050=61 .075=71

EIFS-15 ZB118853-505							
Cycles	Row "A"	Row "B"	Row "G"	Row "H"	Row "D"	Row "E"	Standard
75,000	No Crack	No Crack	G2=15	H4=27	No Crack	No Crack	A .050=42 .075=138 B .050=58 .075=75
150,000	No Crack	No Crack	G2=27	H4=28	No Crack	No Crack	A .050=45 .075=139 B .050=58 .075=70
217,500	No Crack	No Crack	G2=35	H3=18 H4=28 H8=29 H12=32 H13=24	No Crack	No Crack	A .050=43 .075=139 B .050=58 .075=73

## Appendix F EIFS Iteration Routine, Visual Basic for Applications

```

Public WithEvents mAfgrow As Afgrow.Application
Public prefs As PredictPreferences
Public user_beta As UserDefinedBeta
Public table_lookup As TabularLookupMaterial
Public i As Integer
Public j As Integer
Public k As Integer
Dim AArray(2) As Double
Dim CArray(2) As Double
Dim BaArray(2, 2) As Double
Dim BcArray(2, 2) As Double
Dim BTable(5, 1) As Double
Dim KTable(22, 3) As Double 'must be exact size
Dim BTable(24, 2) As Double 'must be exact size
Dim middle As Variant
Dim SpectrumFile As String
Dim beta_result As Integer
Public ai As Double
Public ci As Double
Public TOL As Double
Public c1stop As Double
Public cyclestop As Long
Public IterationControl As Integer
Public rerun As Boolean
Dim NewRun As Boolean
Dim Count As Integer
Dim Sheet As Worksheet
Dim answer As Boolean
Dim retard As Boolean

Private Sub CommandButton1_Click()
i = CInt(StartBox.Text)
CurrentBox.Text = CStr(i)
'Set startup variables
rerun = Sheet1.Cells(2, 12)
ai = Sheet1.Cells(i, 3)
ci = Sheet1.Cells(i, 4)
c1stop = Sheet1.Cells(i, 8)
cyclestop = Sheet1.Cells(i, 9)
'Call mAfgrow.PredictPreferences.SetPropagationLimits(True, True, , , c1stop, cyclestop)
mAfgrow.PredictPreferences.SetPropagationLimits True, True, , , c1stop, cyclestop
mAfgrow.PredictPreferences.bCycleByCycleBetaCalc = True
mAfgrow.PredictPreferences.nTransitionAt = KlcTransition
mAfgrow.PredictPreferences.bOutputToPlotFile = True
mAfgrow.PredictPreferences.SetOutputIntervals SpectrumCyclicIncrement, 1000
Call Run
End Sub

Public Sub Run()
mAfgrow.SMF = Sheet1.Cells(i, 2)
mAfgrow.CrackLengthA = ai

```

```

mAfgrow.CrackLengthC = ci
Sheet1.Cells(i, 3) = ai
Sheet1.Cells(i, 4) = ci
retard = Sheet1.Cells(2, 13)
If retard = True Then
    Call mAfgrow.SetRetardation(RetardClosureModel, 0.375, True)
End If
mAfgrow.PredictPreferences.sOutputPlotFileName = Sheet1.Cells(i, 12)
On Error Resume Next
Set Sheet = ThisWorkbook.Worksheets(CStr(i - 5))
If Err.Number <> 0 Then
    Set Sheet = ThisWorkbook.Sheets.Add(, ThisWorkbook.Sheets(i - 3))
    Sheet.Name = CStr(i - 5)
End If
ThisWorkbook.Worksheets("Results").Activate
NewRun = True
answer = mAfgrow.RunPredict
End Sub

Private Sub mAfgrow_PredictFinished(ByVal result As Integer, ByVal dblCycles As Double, ByVal
dblKc As Double, ByVal dblKa As Double, ByVal dblKct As Double, ByVal dbIC As Double, ByVal
dblA As Double, ByVal dblCt As Double)
Dim inc As Double
Dim high As Boolean
Sheet1.Cells(i, 5) = dbIC
Sheet1.Cells(i, 6) = dblCycles

If result = 0 Then
    Sheet1.Cells(i, 26) = "Completed Normally"
ElseIf result = 1 Then
    Sheet1.Cells(i, 26) = "After one pass of the spectrum, growth was less than 1.0e-13 Program
halted"
ElseIf result = 2 Then
    Sheet1.Cells(i, 26) = "Maximum Number of passes exceeded"
ElseIf result = 3 Then
    Sheet1.Cells(i, 26) = "Maximum crack length exceeded "
ElseIf result = 4 Then
    Sheet1.Cells(i, 26) = "Maximum cycle count exceeded "
ElseIf result = 10 Then
    Sheet1.Cells(i, 26) = "No Spectrum file specified... Can not Predict"
ElseIf result = 11 Then
    Sheet1.Cells(i, 26) = "Beta table has zero length... Can not Predict"
ElseIf result = 12 Then
    Sheet1.Cells(i, 26) = "Repair patch applied and initiation on... Can not Predict! "
ElseIf result = 13 Then
    Sheet1.Cells(i, 26) = "Initiation is not allowed with this model. Can not Predict! "
ElseIf result = 14 Then
    Sheet1.Cells(i, 26) = "NASGRO equation Rhi value is to large"
ElseIf result = 20 Then
    Sheet1.Cells(i, 26) = "Wrong geometry for an oblique crack"
ElseIf result = 21 Then
    Sheet1.Cells(i, 26) = "The initial crack length in the thickness direction is greater than the input
thickness. Check data.."
ElseIf result = 22 Then
    Sheet1.Cells(i, 26) = "Error in spectrum file(s)"
ElseIf result = 23 Then

```



```

Sheet1.Cells(i, 26) = "Unable to open plotfile"
Elseif result = 24 Then
    Sheet1.Cells(i, 26) = "Error in Initiation. Predict stopped"
Elseif result = 25 Then
    Sheet1.Cells(i, 26) = "The number of cycles to initiation is greater than 2.e+9. Predict stopped"
Elseif result = 26 Then
    Sheet1.Cells(i, 26) = "Not enough memory to allocate spectrum"
Elseif result = 27 Then
    Sheet1.Cells(i, 26) = "Only a BLOCKED spectrum may have more than one (1) cycle per stress level"
Elseif result = 28 Then
    Sheet1.Cells(i, 26) = "Program termination by user"
Elseif result = -1 Then
    Sheet1.Cells(i, 26) = "Unknown Error"
End If

```

```

high = True
inc = -ci / 2

```

```

IterationControl = 2 '0 = Crack length, 1 = Cycles, 2 = Both crack length and cycles
If IterationControl = 2 Then 'Crack Length and Cycles Control Iteration
    If ((Abs(dblC - c1stop) < (0.02 * c1stop)) And (Abs(dblCycles - cyclestop) < (0.02 * cyclestop)))
    Then
        i = i + 1
        Sheet.Cells(1, 7) = Count
        If rerun = False Then
            Sheet1.Cells(i - 1, 3) = ai
            Sheet1.Cells(i - 1, 4) = ci
        Else
            ai = Sheet1.Cells(i, 3)
            ci = Sheet1.Cells(i, 4)
        End If
        c1stop = Sheet1.Cells(i, 8)
        cyclestop = Sheet1.Cells(i, 9)
        Call mAfgrow.PredictPreferences.SetPropagationLimits(True, True, , , c1stop, cyclestop)
        mAfgrow.PredictPreferences.bCycleByCycleBetaCalc = True
        Elseif (dblC < c1stop Or dblCycles > cyclestop) Then
            If (c1stop > 0.08) Then
                ai = ai * 1.0001
                ci = ci * 1.0001
            Else
                ai = ai * 1.001
                ci = ci * 1.001
            End If
        Elseif (dblC > c1stop Or dblCycles < cyclestop) Then
            If (c1stop > 0.08) Then
                ai = ai / 1.0001
                ci = ci / 1.0001
            Else
                ai = ai / 1.001
                ci = ci / 1.001
            End If
        End If
        Do While (Abs((c1stop - dblC)) > 0.0001 And Abs((cyclestop - dblCycles) > 100))
        ' If (Abs(inc) < 0.00001) Then
        '     Exit Do
    End If

```

```

' End If
' ai = ai + inc
' ci = ci + inc
' c1stop = Sheet1.Cells(i, 8)
' cyclestop = Sheet1.Cells(i, 9)
' Call mAfgrow.PredictPreferences.SetPropagationLimits(True, True, , , , c1stop, cyclestop)
' mAfgrow.PredictPreferences.bCycleByCycleBetaCalc = True
' If ((Not high) And (c1stop > dblC) Or (cyclestop > dblCycle)) Then
'     inc = -0.5 * inc
'     high = True
' End If
' If ((high) And (c1stop < dblC) Or (cyclestop < dblCycle)) Then
'     inc = -0.5 * inc
'     high = False
' End If

ElseIf IterationControl = 0 Then 'Crack Length Controls Iteration
    If (dblC < (c1stop + TOL) And dblC > (c1stop - TOL)) Then
        Sheet.Cells(1, 7) = Count
        i = i + 1
        If rerun = False Then
            Sheet1.Cells(i - 1, 3) = ai
            Sheet1.Cells(i - 1, 4) = ci
        Else
            ai = Sheet1.Cells(i, 3)
            ci = Sheet1.Cells(i, 4)
        End If
        c1stop = Sheet1.Cells(i, 8)
        cyclestop = Sheet1.Cells(i, 9)
        Call mAfgrow.PredictPreferences.SetPropagationLimits(True, False, , , , c1stop, cyclestop)
        mAfgrow.PredictPreferences.bCycleByCycleBetaCalc = True
    ElseIf dblC < (c1stop - TOL) Then
        ai = ai * 1.1
        ci = ci * 1.1
    ElseIf dblC > (c1stop + TOL) Then
        ai = ai / 1.1
        ci = ci / 1.1
    End If

Else 'Cycles Controls Iteration
    If (dblCycles < (cyclestop + 100) And dblCycles > (cyclestop - 100)) Then
        Sheet.Cells(1, 7) = Count
        i = i + 1
        If rerun = False Then
            Sheet1.Cells(i - 1, 3) = ai
            Sheet1.Cells(i - 1, 4) = ci
        Else
            ai = Sheet1.Cells(i, 3)
            ci = Sheet1.Cells(i, 4)
        End If
        c1stop = Sheet1.Cells(i, 8)
        cyclestop = Sheet1.Cells(i, 9)
        Call mAfgrow.PredictPreferences.SetPropagationLimits(False, True, , , , c1stop, cyclestop)
        mAfgrow.PredictPreferences.bCycleByCycleBetaCalc = True
    ElseIf dblCycles < (cyclestop + 100) Then
        ai = ai / 1.1
        ci = ci / 1.1
    End If
End If

```

```

        ElseIf dblCycles > (cyclestop - 100) Then
            ai = ai * 1.1
            ci = ci * 1.1
        End If
    End If
    If Sheet1.Cells(i, 2) > 0 Then
        CurrentBox.Text = CStr(i)
        Call Run
    Else:
        answer = mAfgrow.Quit
        Set mAfgrow = Nothing
        Unload UserForm1
    End If
End Sub
Private Sub CommandButton2_Click()
    j = 6
    Do While Sheet1.Cells(j, 2) > 0
        Sheet1.Cells(j + 1, 3) = 0
        Sheet1.Cells(j + 1, 4) = 0
        Sheet1.Cells(j, 5) = 0
        Sheet1.Cells(j, 6) = 0
        Sheet1.Cells(j, 26) = " "
        j = j + 1
    Loop
End Sub
Private Sub CommandButton3_Click()
    answer = mAfgrow.Quit
    Set mAfgrow = Nothing
    Unload UserForm1
End Sub
Private Sub mAfgrow_PredictInfo(ByVal Model As Long, ByVal dStress As Double, ByVal
dRStress As Double, ByVal dCycles As Double, ByVal dPass As Long, ByVal iOutputInfo1 As
Object, ByVal iOutputInfo2 As Object, ByVal iOutputInfo3 As Object, ByVal iOutputInfo4 As
Object)
    Dim iOutput1 As Afgrow.OutputInfoInt
    Dim iOutput2 As Afgrow.OutputInfoInt
    Set iOutput1 = iOutputInfo1
    If Model < 2000 Then Set iOutput2 = iOutputInfo2
    If NewRun = True Then
        j = 1
        Do While ((j < 500) Or (Sheet.Cells(j + 1, 1) = " "))
            Sheet.Cells(j + 1, 1) = " "
            Sheet.Cells(j + 1, 2) = " "
            Sheet.Cells(j + 1, 3) = " "
            Sheet.Cells(j + 1, 4) = " "
            Sheet.Cells(j + 1, 5) = " "
            j = j + 1
        Loop
        Count = 0
        'Header information
        Sheet.Cells(1, 1) = "Cycles"
        Sheet.Cells(1, 2) = "c-tip"
        Sheet.Cells(1, 3) = "c-tip beta"
        If Model < 2000 Then
            Sheet.Cells(1, 4) = "a-tip"
            Sheet.Cells(1, 5) = "a-tip beta"
        End If
    End If
End Sub

```

```

    End If
    Sheet.Cells(1, 6) = "Count"
End If
NewRun = False
Count = Count + 1
Sheet.Cells(Count + 1, 1) = dCycles
Sheet.Cells(Count + 1, 2) = iOutput1.dCrackLength
Sheet.Cells(Count + 1, 3) = iOutput1.dBeta
If Model < 2000 Then
    Sheet.Cells(Count + 1, 4) = iOutput2.dCrackLength
    Sheet.Cells(Count + 1, 5) = iOutput2.dBeta
End If
Set iOutput1 = Nothing
End Sub

Private Sub UserForm_Activate()
Dim k As Integer
Dim W As Double
Dim t As Double
Dim D As Double
Dim Tension As Double
Dim Bending As Double
Dim Bearing As Double
Dim UseBetaCorrection As Boolean

TOL = 0.0001

'Spectrum
SpectrumFile = Sheet1.Cells(3, 2)
'SpectrumFile = "D:\Analysis\AFGROW\10-4-6 Marker.sp3"
Set mAfgrow = CreateObject("Afgrow.Application")
answer = mAfgrow.OpenSpectrumFile(SpectrumFile)
'Material Model
Set table_lookup = mAfgrow.SetTabularLookupMaterial
'Crack Case
mAfgrow.Model = aDoubleCornerAtHole
W = Sheet1.Cells(2, 2)
t = Sheet1.Cells(2, 3)
D = Sheet1.Cells(2, 4)
Call mAfgrow.SetCrackedPlateWithHoleProp(W, t, D)
'Loads
Tension = Sheet1.Cells(2, 5)
Bending = Sheet1.Cells(2, 6)
Bearing = Sheet1.Cells(2, 7)
Call mAfgrow.SetLoad(Tension, Bending, Bearing)
Call mAfgrow.SetTransitionToOblique
'Miscellaneous
mAfgrow.Visible = False

'Read in the Beta Correction Factors
UseBetaCorrection = Sheet1.Cells(2, 10)
If (UseBetaCorrection = True) Then
    mAfgrow.BetaCorrection.bUseBetaCorrection = True
    mAfgrow.BetaCorrection.nTypeOfData = BetaCorrectionFactors
    k = 0
    Do While k < 25

```

```

    BTable(k, 0) = Sheet2.Cells(4 + k, 2)
    BTable(k, 1) = Sheet2.Cells(4 + k, 3)
    BTable(k, 2) = Sheet2.Cells(4 + k, 4)
    k = k + 1
Loop
middle = BTable
mAfgraw.BetaCorrection.aBetaCorrectionData = middle
End If
'Set the crack growth rate data using tabular look-up
k = 0
Do While k < 4
j = 0
Do While j < 23
If (k = 0 And j = 0) Then
    KTable(j, k) = 0#
Else
    KTable(j, k) = Sheet3.Cells(j + 2, k + 2)
End If
j = j + 1
Loop
k = k + 1
Loop
table_lookup.sMaterialName = Sheet3.Cells(2, 6)
Dim kVar As Variant
kVar = KTable
Call table_lookup.SetData(kVar, Sheet3.Cells(8, 7), Sheet3.Cells(8, 6), Sheet3.Cells(5, 7),
Sheet3.Cells(5, 6), Sheet3.Cells(8, 9))
table_lookup.dKc = Sheet3.Cells(5, 8)
table_lookup.dKlc = Sheet3.Cells(5, 9)
table_lookup.dPoissonsRatio = Sheet3.Cells(5, 10)
table_lookup.dThermalEx = Sheet3.Cells(8, 8)
table_lookup.dYield = Sheet3.Cells(8, 10)
table_lookup.dYoungModulus = Sheet3.Cells(8, 11)
End Sub

```





